Novel Tandem Catalytic Routes Towards Middle- to Long-Chain Alcohols as Synthetic-Fuel Additives

Von der Fakultät für Mathematik, Informatik und Naturwissenschaften der RWTH Aachen University zur Erlangung des akademischen Grades eines Doktors der Naturwissenschaften genehmigte Dissertation

vorgelegt von

Thorsten Rösler, M.Sc.

aus

Bergkamen, Deutschland

Berichter:

Univ.-Prof. Dr. rer. nat. Walter Leitner
Univ.-Prof. Dr. rer. nat. Marcel Liauw

Tag der mündlichen Prüfung: *2. Februar 2024*

"Humanity stands ... before a great problem of finding new raw materials and new sources of energy that shall never become exhausted. In the meantime, we must not waste what we have, but must leave as much as possible for coming generations."

Svante Arrhenius
Winner of the Nobel Prize in Chemistry, 1903

Diese Dissertation wurde im Zeitraum zwischen April 2018 und Oktober 2022 in der Abteilung für Molekulare Katalyse am MAX-PLANCK-INSTITUT FÜR CHEMISCHE ENERGIEKONVERSION (MPI-CEC) in Mülheim an der Ruhr unter Betreuung von PROF. DR. WALTER LEITNER angefertigt.

Danksagung

Wie es im Leben aber auch in der Wissenschaft üblich ist, gab es während der Erschaffung dieser Arbeit Höhen und Tiefen. Da beides unweigerlich miteinander verknüft ist, ist es umso wichtiger Menschen in seinem Leben zu haben, die die das eine zusammen feiern und dabei helfen das andere zu überwinden.

Ich bin dankbar, dass ich in den letzten Jahren Menschen um mich hatte, die dies sowohl im privaten als auch im wissenschaftlichen Bereich zu tun wussten.

Im wissenschaftlichen Bereich danke ich **Prof. Dr. Walter Leitner** für die Erschaffung eines großartigen Arbeitsumfelds, sowie für seine zielweisenden Ideen die Grundlage für wesentliche Teile dieser Arbeit waren.

Weiterhin danke ich **PD. Dr. Andreas Vorholt** für seine Geduld, sein Vertrauen und die zahlreichen Arbeitsstunden, die er während meiner Betreuung investiert hat und die es mir erlaubten mich stets weiterzuentwickeln.

Ich danke meinen Studenten, die ich während meiner Zeit betreuen und mit denen ich zahlreiche positive Erfahrungen sammeln durfte. Zu nennen sind hier**: Kira Ehmann**, **Sebastian Obst**, **Maurice Belleflamme** und **Janek Betting**.

Schließlich danke ich auch **allen** anderen **Arbeitskreis Mitgliedern**, die ich hier nicht aufzählen kann, welche aber für ein außerordentlich angenehmes Arbeitsklima verantwortlich waren.

Im privaten danke ich **meinen Eltern** die mich schon während des Studiums aber auch danach unterstützt haben und im Wesentlichen dafür verantwortlich sind, dass ich stets verfolgen konnte was mich begeistert.

Ich danke meinen Brüdern, **Hendrik Rösler** und **Jonas Rösler**, die auch immer fester Bestandteil in meinem Leben waren sowie meinen Freunden, die zusammen einen Großteil der Arbeit leisten mussten, mich durch alle Phasen dieser Doktorarbeit zu unterstützen.

Abstract

Man-made climate change poses unprecedented challenges to our society. To overcome this, timely and fundamental changes to our networks for resources and energy are necessary. In particular, the switch from fossil-based fuels to renewable fuels in the transport sector has proven to be a challenge during recent years. Synthetic fuels based on renewables are one opportunity to substitute fossil fuels in a comparatively short time frame. Fischer-Tropsch synthesis plays a key role in this. Fischer Tropsch synthesis enables the generation of mixtures of saturated and unsaturated hydrocarbons from carbon monoxide and hydrogen (synthesis gas). Various ways of producing synthesis gas from renewable resources have already been established. The hydrocarbon mixtures produced in this way show astonishing similarities to existing fuels from fossil sources and, after a few adjustments, can be used in the currently circulating fleet of internal combustion engines. During recent years, the modification of synthetic fuels by the addition of alcohols has proven advantageous. Medium to longer chain alcohols can reduce emissions without significantly affecting the energy density of the fuel. However, in order to produce these alcohols on the required scale and in a resource-efficient way, highly efficient synthetic routes are needed.

In this work, two concepts for the synthesis of medium to longer chain alcohols based on unsaturated hydrocarbons from the Fischer Tropsch process are investigated. The first approach investigates the reductive hydroformylation of terminal olefins to alcohols. For this, novel rhodium/amine catalysts are used. Rhodiumin combination with tertiary amines are known for their hydrogenation activity in this reaction. Nevertheless, ther are comparatively little studies about them so far. The amine concentration, the carbon monoxide partial pressure and the electronic and steric properties of the amine were found to be critical parameters for the hydrogenation activity of the catalysts. By optimising of the the reaction parameters and integrating the solvent and the amine in a single molecule, in the forms of amine-functionalised polyethylene glycols, a highly active and selective reaction system was developed (TOF 280 h^{-1}). Spectroscopic analysis of rhodium species in the reaction solution revealed that a sensitive equilibrium between different anionic rhodium cluster species exists. Under reaction conditions, when using triethylamine, the mononuclear rhodium species $[HNEt_3]^+[Rh(CO)_4]^-$ was identified as the major species. After further investigations of hydride species under reaction conditions and with the support of computational chemistry, an equilibrium was postulated for the formation of $[HRhNEt_3(CO)_3]$ from $[HNEt_3]^+[Rh(CO)_4]^-$. Finally, a recycling concept for the extraction of product alcohols using supercritical CO_2 was developed. High-molecular and amine-functionalised polyethylene glycol derivatives, synthesised especially for this purpose, were used as the staionary phase during this process. In addition, a reactor setup was developed for extraction under supercritical conditions. Hence, it was possible to recycle the catalyst over a number of nine recycling runs without any noticeable loss of activity or selectivity. Over the duration of all nine experiments combined, a leaching of the rhodium catalyst of <0.1 % was determined.

The second concept presented in this work investigates the tandem catalytic combination of a highly olefin selective Fischer-Tropsch catalyst and a highly active cobalt/phosphorus-based hydroformylation catalyst in a One-Pot approach. This allows for the direct conversion of

synthesis gas to paraffin/alcohol mixtures. After few experiments, this concept proved to be highly efficient. Alcohol selectivities of more than 50%, related to the generated hydrocarbons, with a simultaneously high carbon monoxide conversion and a low selectivity to methane and CO_2 were achieved. Herby, the intrinsic advantage of this approach, of keeping the catalytic centres for the reactions separate but in close special proximity to each other was demonstrated. Intercepting *in situ* generated olefins by the molecular hydroformylation catalyst allowed for alcohol selectivities far above the theoretical olefin selectivity of the Fischer-Tropsch catalyst. Investigations of the yield-time profile revealed that an initial deposition of the molecular cobalt catalyst occurs until an equilibrium is established. After about 20 hours the catalytic system is stable and no deactivation was observed for either catalyst up to a period of 72 hours. Overall, alcohol selectivities of up to 60% were achieved with carbon monoxide conversions above 50%. This represents a novelty in the research on transition metal catalysed synthesis gas to alcohol approaches. This novel concept allows for the direct conversion of synthesis gas to a mixture of saturated hydrocarbons and alcohols, as a potential synthetic fuel precursor.

Kurzfassung

Der menschengemachte Klimawandel stellt unsere Gesellschaft vor nie da gewesene Herausforderungen. Um diesen zu bewältigen sind zeitnahe und grundlegende Änderungen an unseren Netzwerken für Ressourcen und Energie notwendig. Insbesondere die Umstellung von fossilen auf erneuerbare Energieträger im Transportsektor hat sich während der letzten Jahre als Herausforderung dargestellt. Eine Möglichkeit fossile Treibstoffe vergleichsweise zeitnah zu substituieren stellen synthetische Kraftstoffe auf Basis nachwachsender Rohstoffe dar. Eine zentrale Rolle kommt dabei der Fischer-Tropsch-Synthese zu. Die Fischer-Tropsch-Synthese ermöglicht die Generierung von Mischungen an gesättigten und ungesättigten Kohlenwasserstoffen aus Kohlenmonoxid und Wasserstoff (Synthese Gas). Für die Herstellung von Synthese Gas aus erneuerbaren Ressourcen sind bereits verschiedene Wege erforscht. Die dabei erzeugten Kohlenwasserstoffe zeigen erstaunliche Ähnlichkeiten zu bestehenden Brennstoffen aus fossilen Energieträgern und lassen sich nach wenigen Anpassungen in den derzeit zirkulierenden Verbrennungsmotoren einsetzen. In den letzten Jahren hat sich die Modifikation synthetischer Kraftstoffe durch die Zugabe von Alkoholen als vorteilhaft erwiesen. Mittel bis längerkettige Alkohole können den Schadstoffausstoß verringern ohne dabei die Energiedichte des Kraftstoffs maßgeblich zu beeinträchtigen. Um diese Alkohole in dem benötigten Ausmaß und ressourceneffizient herzustellen sind jedoch hocheffiziente Synthese Wege nötig.

In dieser Arbeit werden zwei Konzepte für die Synthese von mittel- bis längerkettigen Alkoholen auf Basis von ungesättigten Kohlenwasserstoffen aus dem Fischer-Tropsch-Prozess untersucht. Der erste Ansatz befasst sich mit der reduktiven Hydroformylierung von endständigen Olefinen zu Alkoholen. Dabei werden neuartige Rhodium/Amin-Katalysatoren eingesetzt. Rhodium in Kombination mit tertiären Aminen ist für seine Hydrierleistung in dieser Reaktion bekannt. Dennoch sind bisher vergleichsweise wenig Studien dazu bekannt. Als entscheidende Parameter für die Hydrieraktivität der untersuchten Katalysatoren wurden die Aminkonzentration, der Kohlenmonoxid Partialdruck und die elektronischen sowie sterischen Eigenschaften des Amins identifiziert. Durch Optimierung der Reaktionsparameter und die Integration von Lösemittel und Amin in einem einzigen Molekül, in Form von Amin- funktionalisierten Polyethylenglykolen, wurde ein hoch aktives und selektives Reaktionssystem entwickelt (TOF 280 h^{-1}). Die spektroskopische Untersuchung von Rhodium-Spezies in der Reaktionslösung zeigte dabei, dass ein sensibles Gleichgewicht zwischen verschiedenen anionischen Rhodium-Cluster Spezies existiert. Unter Reaktionsbedingungen wurde, unter Verwendung von Triethylamin, die mononukleare Rhodium Spezies $[HNEt_3]^+[Rh(CO)_4]^-$ als gleichgewichtsbestimmend identifiziert. Nach weiteren Untersuchen von Hydridspezies unter Reaktionsbedingungen und mit Unterstützung computerchemischer Berechnungen wurde die Bildung von $[HRhNEt_3(CO)_3]$ aus $[HNEt_3]^+[Rh(CO)_4]^-$ postuliert. Letztendlich wurde mit Hilfe der gesammelten Erkenntnisse ein Recyclingkonzept für die Extraktion von Produktalkoholen mit Hilfe von überkritischem CO_2 entwickelt. Dabei wurden speziell synthetisierte hochmolekulare und aminfunktionalisierte Polyethylenglykol-Derivate als stationäre Phase eingesetz. Zusätzlich wurde ein Reaktor-Setup für die Extraktion unter überkritischen Bedingungen entwickelt. Dadurch war es möglich den Katalysator über eine Anzahl von neun Versuchen zu recyclen ohne sichtlichen Aktivitäts- oder Selektivitätsverlust. Über die Dauer der neun Versuche wurde ein Leaching des Rhodium-Katalysators von <0.1 % erreicht.

Das zweite in dieser Arbeit vorgestellte Konzept untersucht die tandem katalytische Kombination eines Olefin selektiven Fischer-Tropsch Katalysators und eines hochaktiven Cobalt/Phophor basierten Hydroformylierungskatalysators in einem Reaktionsansatz. Dies erlaubt die direkte Umwandlung von Synthese Gas zu Paraffin/Alkohol Gemischen. Bereits nach wenigen Untersuchungen erwies sich dieses Konzept als hoch effizient. Alkoholselektivitäten von über 50%, bezogen auf die generierten Kohlenstoffe, bei gleichzeitig hohem Kohlenmonoxid Umsatz und geringer Selektivität zu Methan und CO_2 wurden erzielt. Hierbei hat sich der intrinsische Vorteil dieses Ansatzes, die katalytischen Zentren der beiden Reaktionen zwar zu trennen allerdings in unmittelbarer räumlicher Nähe zu halten gezeigt. Durch abfangen *in situ* generierter Olefine durch den molekularen Hydroformylierungs Katalysator konnten Alkoholselektivitäten weit über der theoretischen Olefin Selektivität des Fischer-Tropsch Katalysators erzielt werden. Untersuchungen des Umsatz-Zeit Profils haben gezeigt dass ein anfängliches Ablagern des molekularen Cobalt Katalysators stattfindet bis sich ein Gleichgewicht bildet. Nach circa 20 Stunden ist das katalytische System stabil und es konnte keine Deaktivierung für einen der beiden Katalysatoren bis zu einem Zeitraum von 72 Stunden beobachtet werden. Insgesamt konnten Alkohol Selektivitäten von bis zu 60% bei Kohlenstoffumsätzen über 50% erzielt werden. Dies stellt ein Novum in der Forschung zur Übergangsmetall katalysierten Umwandlung von Synthese Gas zu Alkoholen dar. Dieses neuartige Konzept erlaubt die direkte Umwandlung von Synthesegas zu einem Gemisch aus gesättigten Kohlenwasserstoffen und Alkoholen, als potentieller Vorläufer eines synthetischen Kraftstoffgemisches.

Table of Contents

List of Abbreviations

α	Chain Growth Propability
δ_D	Dispersion Forces
δ_H	Hydrogen Bonding Contribution
δ_P	Dipole-Dipole Interactions
2-PrOH	Isopropanole
AOm	Mesoporous Alumina Oxide
AOmM	Meso/ macroporous Alumina Oxide
acac	Acetylacetonate
ASF	Anderson-Schulz-Florey
BET	Brunauer-Emmett-Teller
BPR	Back-Pressure-Regulator
BTL	Biomass-To-Liquid
COD	1,5-Cyclooctadiene
cPC	Cyclic propylenecarbonate
CTY	Carbon Time Yield
DFT	Density Functional Theory
DimCarb	Dimethylammonium Dimethylcarbamate
E	Absolute Electronic Energy
E_A	Activation Energy
EDS	Energy-Dispersive-X-ray Spectroscopy
EU	European Union
FIB	Focused Ion Beam
FID	Flame Ionization Detector
FT	Fischer-Tropsch
FTIR	Fourier Transformation Infrared
G	Gibbs Energy
GC	Gaschromatography
HAADF	High-Angle-Annular-Dark-Field
HMBC	Hetronuclear Multiple Bond Coherence
HPLC	High-Pressure-Liquid-Chromatography
Hyfo	Hydroformylation
ICP	Inductively-Coupled-Plasma
IPCC	Intergovernmental Panel on Climate Change
IR	Infrared
[Cat.]	Catalyst
L	Monodentate Ligand
L∩L	Bidentate Ligand
l:b	Linear-to-Branched ratio
LPO	Low Pressure Oxo
MeCN	Acetonitrile

M:L	Metal-to-Ligand ratio
M:N	Metal-to-Amine (Nitrogen) ratio
MS	Mass Spectrometry
MW	Molecular Weight
nbd	2,5-Norbornadiene
NEt_3	Triethylamine
NMR	Nuclear Magnetic Resonance
p	Pressure (synthesis gas)
PEG	Poly Ethylene Glycole
pK_a	Acid strength (negative decadic logarithm of the acid constant)
PNP	Bis(triphenylphosphine)iminium
ppb	Parts Per Billion
ppm	Parts Per Million
PTL	Power-To-Liquid
PV	Pore Volume
*q*NMR	Quantitative-Nuclear-Resonance-Spectroscopy
REDIFUEL	Robust and efficient processes and technologies for drop in renewable fuels for road transport
ROI	Region of Interest
rpm	Revolutions Per Minute
RT	Room Temperature
S	Selectivity
sc	Supercritical
SEM	Scanning Electron Microscopy
STEM	Scanning-Transmission-Electron-Microscopy
t_{ret}	Retention Time
T	Temperature
TCD	Thermal-Conductivity-Detector
TEA	Triethylamine
TetraEG	Tetraethylene glycole
TEG	Triethylene glycole
TEP	TOLMAN Electronic Parameter
TGA	Thermo-Gravimetric-Analysis
TMS	Tetramethylsilan
TOF	Turn Over Frequency
TOF-MS	Time-Of-Flight Mass-Spectrometry
TON	Turn-Over-Number
TPG	Tripropylene glycole
TPP	Triphenylphosphine
TPPTS	Sodium Triphenylphosphinetrisulfonat
TTON	Total-Turn-Over-Number

UCC	Union Carbide Corporation
VE	Valence Electron
WGSR	Water-Gas-Shift-Reaction
X	Conversion
Y	Yield
ZPE	Zero Point Vibrational Energy
θ	Cone Angle

1 Introduction

The human made climate crisis is probably the biggest challenge humanity has had to face since its existence. Since 1880 the average surface temperature has risen by 1.04 °C (Figure 1). Every year between 2013 and 2021 rank among the 10 warmest since the beginning of recording.[1,2] The most recent world climate record by the IPCC (Intergovernmental Panel on Climate Change) calls for immediate action before the so called "point of no return" is reached at which point the climate change can no longer be stopped by human measures.

While this is a multidimensional problem which must be addressed by all areas of society, ranging from politics and economics up to public acceptance and everyday life, natural sciences play a key role as "problem solver" and as driving force behind the majority of innovations targeted at fighting climate change.[3]

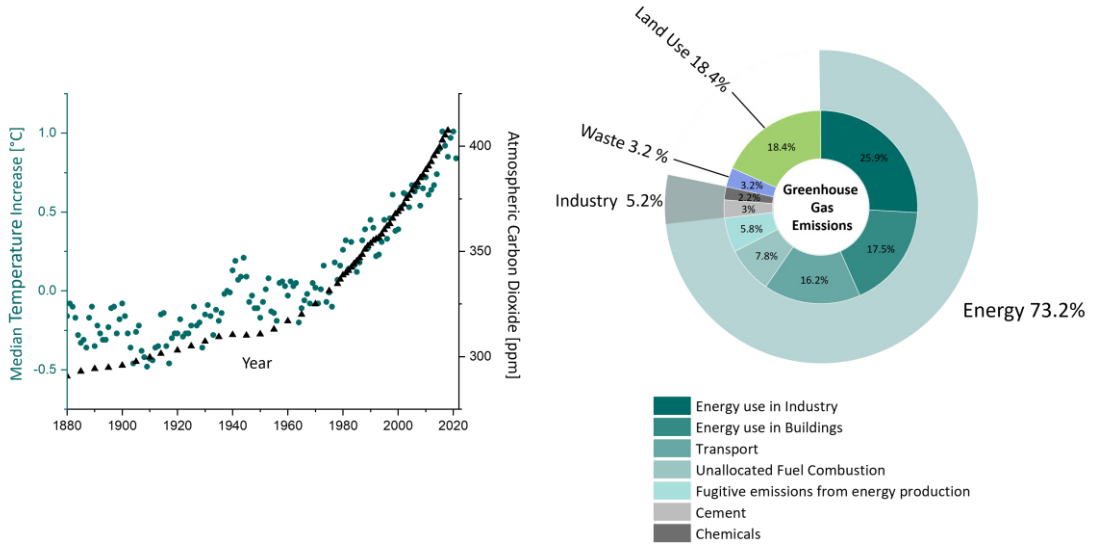

Figure 1: Global increase of median temperature and CO_2 concentration from 1880 until today, adapted from [4],[5] (left) and sources of greenhouse gas emissions in 2020, adapted from [6] (right).

One of the most pressing challenges is the change from a fossil-based value chain to one which is based on renewable energy and resources.[7,8] The extensive use of fossil energy and fossil-based hydrocarbons as building blocks in our chemical value chain is the main reason for the increasing concentration of carbon in our ecosphere. Since the start of the industrialization in the 18th century, the concentration of CO_2 in our atmosphere has risen more than 30% from 280 ppm to 418 ppm (Figure 1). The rise of CO_2 emissions can be directly correlated to the global temperature increase. It is uncontroversial that the greenhouse gas effect of CO_2 is one of the main driving forces behind the global warming.[9]

While some of the fossil resources are used as building blocks in our chemical value chain, the overwhelming majority is used to generate energy from fossil fuels e.g. in power plants, private households and in the transport sector. Over 73% of all greenhouse gas emissions can be tracked

back to the generation of energy from fossil fuels (Figure 1).[6] Therefore, the biggest contribution to fighting climate change must be made in the energy sector.

As the foundation for a sustainable energy sector, which will work independent from fossil fuels, the generation and storage of renewable energy which can be supplied to the existing power grid is necessary (Figure 2).[10]

While this concept works to supply stationary facilities, the substitution of fossil fuels in the transport sector poses additional challenges. The European Union (EU) strongly focuses on the electrification of the transport sector. This makes substantial changes in the existing infrastructure and an exchange of the existing transportation fleet with electrified vehicles necessary. The declared goal of the EU is to replace conventional combustion engine cars with electrified vehicles by 50% untill 2030.[11]

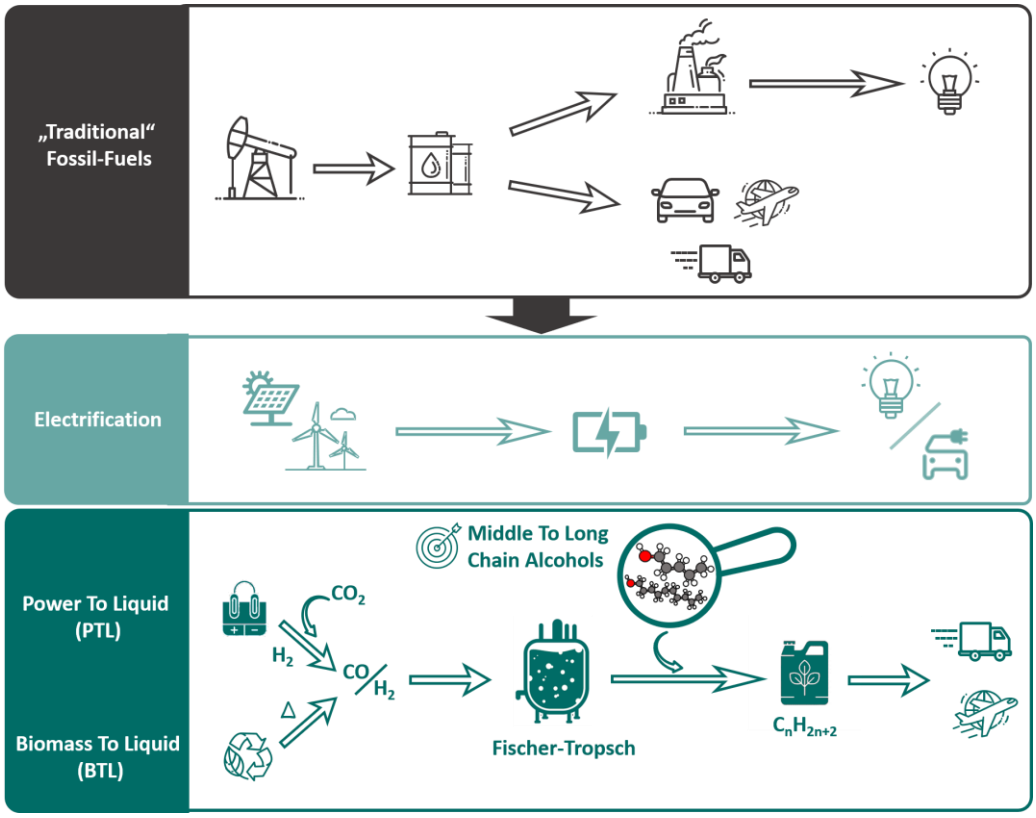

Figure 2: Concepts for the change from a fossil-based energy sector to a sustainable energy sector.

At the time of writing, the share of electric cars in new registrations is about 11%.[12] Electrification of the private automotive sector is a long-term goal but will not be feasible within few years. In addition, even though electrification will be possible for the fleet of private cars, important parts of the mobile transport sector, such as long-distance shipping, road and aerial transport, cannot be electrified within the foreseeable future.[13,14]

A solution, which offers to be a short- to mid-term transition technology in the existing fleet of private cars and a substitution of fossil fuels in long distance transport, is the application of

synthetic-fuels (syn-fuels) in conventional combustion engines. Syn-fuels can be designed as so called “drop in” fuels which are usable in the existing fleet of private cars and would allow a fast defossilization, in unison with offering long-term alternatives for long distance transport applications. While the EU, over long periods of time, strictly focused on the electrification of the mobile sector, those technologies are highly complementary.

Different concepts for the production of Syn-fuels have been developed. Among them, Biomass-To-Liquid (BTL) and Power-To-Liquid (PTL) approaches based on the generation of synthesis gas from either electroloysis or waste biomass gasification and subsequent transformation of synthesis gas to hydrocarbons using the Fischer-Tropsch process (Figure 2).[15–20] From the Fischer-Tropsch reaction hydrocarbon mixtures are obtained which exhibit similar properties to currently used diesel fuels. After downstream processing (e.g. hydrotreating) those could be applicable in the current fleet of combustion engines.

During the last decade, the beneficial effect of alcohols as fuel additives in those concepts moved into the focus of the scientific community.[8,16,21–23] By adding oxygen, alcohols can help to significantly reduce the emission of pollutants like NO_x, soot emissions and, to a lesser degree, CO_2 during the combustion of synthetic fuels. Especially middle to long chain alcohols, like *n*-octanol, offer a good compromise of energy density and reduction of emissions.[22,23] Yet, current industrial processes for the production of middle to long chain alcohols are targeted at the use of alcohols as intermediate chemicals and not as fuels. To produce middle to long chain alcohols as fuel additives, highly efficient transformation protocols are needed. For this, the use of tandem catalysis offers a versatile tool to combine catalytic reactions and develop highly energy and resource efficient processes.

An example for a BTL concept, which investigated the production of alcohols from Fischer-Tropsch cuts and their direct application as fuel additives, is the EU funded REDIFUEL (Robust and Efficient processes and technologies for Drop In renewable FUELs) project.[24] The REDIFUEL project and the research related to it has been an inspiration for a lot of the presented work and will be discussed in the following section.

2 Theoretical Background

In the following chapter, the theoretical background about topics discussed in this work will be summarized. In the frame of this work, it is only possible to give a general overview of the different topics. For specific topics, relevant for the discussion, an overview about current literature is given and the metrics which will be used in the course of this work are explained.

2.1 The Concept of the REDIFUEL Process for the Generation of a Second-Generation Bio-Synthetic-Fuel

REDIFUEL is an EU funded project aiming at developing a process for the production of synthetic fuels based on the use of synthesis gas generated from renewable resources and was funded from 2018 to 2022. The majority of the work presented in the following is connected to the REDIFUEL project.

The goal of the REDIFUEL project was to produce a synthetic diesel fuel which is compliant with the EN590 regulation for diesel fuels, applicable in the current fleet of combustion engine vehicles and which shows enhanced combustion characteristics. To achieve this, a concept based on three major process steps was envisioned (Figure 3).

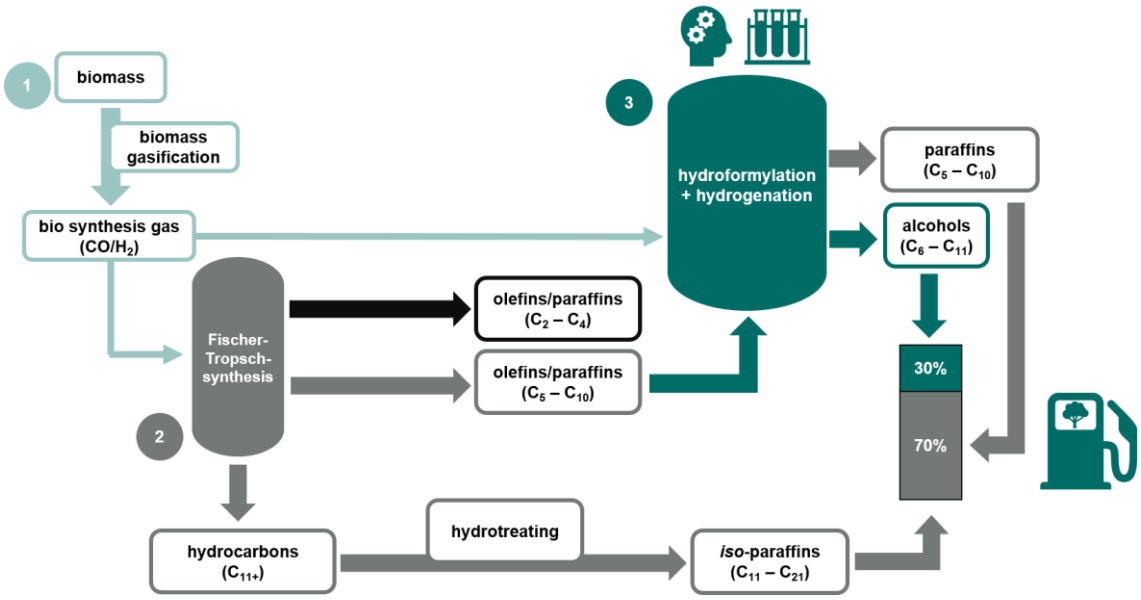

Figure 3: Concept of the three step process scheme envisioned in the REDIFUEL project (Grant Agreement no. 817612).[24]

As renewable biomass resource, different waste biomass products such as wood chips from the woodworking industry, straw wastes from the agriculture sector and ultimately organic wastes from private households are envisioned. The use of bio waste mass as a resource is intended to prevent competition with food production. Within the framework of the project, wood chips have been used as model biomass waste. In a first step, this biowaste is gasified (steam

reforming) to carbon monoxide and synthesis gas and subsequently purified (Process step one in Figure 3). The resulting synthesis gas mixture has a CO:H_2 composition of roughly 1:2 and can be used as substrate for the Fischer-Tropsch reaction in the next process step (process step two in Figure 3). The Fischer-Tropsch reaction assembles carbon monoxide and hydrogen to paraffins and olefins. Within the Fischer-Tropsch step, a cobalt-based Fischer-Tropsch catalyst with exceptional selectivity towards olefinic products is used. After the Fischer-Tropsch step, the resulting hydrocarbon mixture is fractionized *via* distillation into three cuts. The low boiling C_2-C_4 fraction cannot be used as fuel component in the current fleet of combustion engines and is sold to other applications. The C_{11+} fraction of high boiling Fischer-Tropsch products is blended to the final fuel mixture after a hydrotreatment step. Hydrotreating of the high boiling Fischer-Tropsch hydrocarbons is necessary to hydrogenate olefins and convert linear paraffins to branched paraffins which are necessary to fulfill the specifications of diesel fuels according to the EN590 regulation. Those branched C_{11+} paraffins will make up about 70% of the final fuel mixture.

The biggest fraction of C_5-C_{10} containing olefins and paraffins is further refined in the third process step (process step 3 in Figure 3). In this step, olefins in the C_5-C_{10} range are converted to alcohols *via* a sequence of hydroformylation and hydrogenation reactions. For this upgrading, the whole mixture of paraffins and olefins is used as the substrate mixture.

Finally, after upgrading of C_5-C_{10} olefins to C_6-C_{11} alcohols, the resulting C_5-C_{11} paraffin/alcohol mixture is blended with the C_{11}-C_{21} paraffin mixture coming from the hydrotreating step, resulting in a mixture of paraffins and alcohols with an alcohol share targeted at 30% as the final “drop in” bio-synthetic-fuel.

During the REDIFUEL project, two separate catalytic systems have been investigated for the reductive hydroformylation step (process step three in Figure 3) in our group. The first one is a two-step process based on the sequence of hydroformylation and hydrogenation reactions the former of which was conducted in a biphasic liquid/liquid solvent system. Due to an established catalyst recycling concepts for the two-step process in liquid-liquid biphasic media, it has been chosen as the final option to convert the C_5-C_{10} substrate mixture in a miniplant setup within the time limit of the project. In a recent publication our group reported about this two-step process, in which a complex Fischer-Tropsch product mixture was successfully converted *via* the hydroformylation reaction in biphasic-biphasic liquid media for the first time.[25]

The second reaction system, investigated as a part of the REDIFUEL project, is the direct conversion of olefins to alcohols using rhodium/tertiary amine catalysts for the reductive hydroformylation of middle to long chain olefins. The results of this approach will be presented in this work (chapter 4.1 - 4.2). It should be noted though that parts of this work have been investigated after the ending of the REDIFUEL project.

Inspired by the REDIFUEL project a third approach for the synthesis of paraffin alcohol mixtures will be presented in this work (chapter 4.3). The integration of the Fischer-Tropsch synthesis and the reductive hydroformylation reaction in a One-Pot approach for the direct conversion of synthesis gas to paraffin/alcohol mixtures. Effectively combining the process steps two and three displayed in Figure 3. Although this idea has not been envisioned in the initial proposal of the project, it evolved during it and is therefore a direct consequence of the REDIFUEL project.
Since the second and third process step of the REDIFUEL project, namely the Fischer-Tropsch synthesis and the (reductive) hydroformylation reaction, are an integral part of the tandem catalytic concepts presented in this work, they will be discussed in detail in the upcoming chapters after a short introduction to catalysis.

2.2 Catalysis – Definition and Metrics

The importance of catalysis cannot be overestimated both in our chemical industry as well as in nature. Over 80% of all chemical products are produced by catalytic processes. Catalysts are used to reduce emissions in vehicles and industrial exhaust gases. Furthermore, most fundamental processes of life are catalyzed by enzymes.[26,27]
As defined by W. Ostwald, a catalyst is a substance which influences the speed of the reaction but is not changed or consumed during the reaction.[28] A catalyst enables new reaction pathways which offer a lower energy barrier. By doing so, they can increase the reaction speed or enable reactions which are otherwise inaccessible or only accessible under harsh conditions. It is important to note, that a catalyst only influences the kinetics of a reaction and not the thermodynamics, meaning the equilibrium of a reaction is not changed directly by the catalyst.[29]
The new pathway offered by the catalyst consists of one or more rearrangement steps. The exact sequence of those steps is often visualized as a catalytic cycle in which reaction partners enter and leave the cycle. Some important metrics to describe the performance of a catalyst have been established over the years, which will be used throughout this work.[26]
Although a catalyst is theoretically not changed or consumed during the reaction, every catalyst sooner or later deactivates or decomposes, e.g by thermal decomposition, blocking of reactive sites by catalyst poisons or leaching of the catalyst. The number of catalytic cycles a catalyst conducted during a reaction can be expressed as the amount of product produced during those reactions ($n(\mathrm{product})$; with n =amount of substance) divided by the amount of catalyst ($n(\mathrm{catalyst})$). This is known as the Turn-Over-Number (TON; Equation 1).

$$\mathrm{TON} = \frac{n(\mathrm{product})}{n(\mathrm{catalyst})} \qquad (1)$$

In literature the TON is sometimes still mistakenly used synonymous to the TOF, which will be explained later is this chapter. This is misleading since the TON does not resemble a catalytic activity. However, the TON can be used to express the stability or robustness of a catalytic system. In catalyst recycling experiments it is common practice to use the the Total-Turn-Over-Number (TTON) for this. E.g., in a series of recycling experiments the TTON resembles the sum total of all TON´s over the course of the experiments (Equation 2; N= number of recycling experiments). In an ideal case, the TTON resemples how many catalytic cycles can be achieved until deactivation of the catalyst occurs. Since this can not always be determined, the TTON can also be used to express how many catalytic have been achieved without deactivation of the catalyst.

$$\mathrm{TTON} = \sum_0^N \mathrm{TON} \qquad (2)$$

To express the catalytic activity of the catalyst, the Turn-Over-Frequency (TOF) is used which can be derived from the Turn-Over-Number by multiplying the amount of catalyst ($n(\mathrm{catalyst})$) with the reaction time (t) needed to produce a certain amount of product (Equation 3). The TOF can be read as catalytic cycles a catalyst executes per hour of reaction time.

$$\mathrm{TOF} = \frac{n(\mathrm{product})}{n(\mathrm{catalyst})\cdot t} \qquad (3)$$

It should be noted that the TOF changes with the concentration of the reactants. A vastly different TOF is gained when measured at 10% conversion compared to the TOF at 90% conversion of a reaction. It is topic of frequent discussion under which conditions the TOF should be determined in order to make it a comparable unit to other catalytic systems or if the TOF is a reliable unit of measure for the catalytic activity at all.[30] To this date there is no uniform practice in literature to determine the TOF. Nevertheless, it should be kept in mind that the TOF is not a unit to describe the universal activity of a catalyst for a specific reaction but is an expression of the average activity under the given reaction conditions.

2.2.1 Homogeneous and Heterogeneous Transition Metal Catalysis

Catalysts are differentiated based on the nature of the catalytically active species. While in nature enzymes are used as catalysts for biological processes, in the chemical industry most processes are catalyzed by transition metal catalysts. These can be differentiated into homogeneous and heterogeneous catalysts, depending on the state of aggregation of the catalyst during the reaction/catalytic cycle. While this work focuses on the application of homogeneous catalysts, both types of transition metal catalysts have been used in this work.

To this date the production of about 80% of all chemical goods involve heterogeneous transition metal catalyzed processes.[31] The defining characteristic of heterogeneously catalyzed reactions is that the catalyst has a different state of aggregation than the substrates. In most cases this means the catalyst is a solid while substrates/products are liquid or gaseous. The reaction proceeds at the surface of the heterogeneous catalyst material. Often times, the reaction only proceeds at specific catalytic centers of the catalyst surface (e.g. on surface edges or steps). Hence, some of the catalytic metal is inside of the solid bulk and not accessible for the reactants. Only parts of the catalytic material is active for the catalytic reaction at all times. To increase the metal specific catalytic activity, often catalyst support materials are used. They make up the bulk of the solid material and are loaded with the catalytically active metal. It should be noted though, that the support can have a significant influence on the catalyst, e.g. by electron transfer between the support and the catalyst metal.[32] Furthermore, to increase the catalytically surface area, heterogeneous catalysts are applied as porous materials. The diffusion of reactants and heat in and out of the pores is often a limiting factor for heterogeneous catalysts. Optimizing the hierarchical structure of the porous materials is important to optimize the activity and selectivity of heterogeneous catalysts.[33]

The physical separation of the catalyst and the reactants/products allows for an easy recycling of the catalyst after the reaction simply by separating the different phases of catalyst and substrates/products. This easy and cost-effective separation of the heterogeneous catalysts is the main reason for their dominance in large scale applications. In contrast to heterogeneous catalysts, homogeneous transition metal catalysts are molecular complexes which are dissolved in the reaction medium together with substrates and products. A molecular catalyst consists of a central metal atom to which so called ligands are bound *via* coordinative bonds. Together, the ligands make up the inner coordination sphere of the catalyst. Ligands, substrated and products can leave or enter the coordination sphere during the catalytic cycle. Together with the active metal, the coordination sphere of a catalysts dictates the activity and selectivity of a catalyst. The coordination sphere under given conditions is well defined, which allows for a selective modification to steer the activity or selectivity of a homogeneous catalyst. In addition, every

metal center is active for the catalytic reaction because the molecular catalyst is dissolved in the reaction medium. Therefore, homogeneous catalysts usually achieve a high metal specific activity and a high selectivity when they are optimized for a specific reaction. Because they allow for a high catalytic activity and, more important, selectivity, homogeneous catalysts are frecuently applied in the production of pharmaceuticals or other fine chemicals.[34]

One of the downsides often associated with homogeneous catalysts is directly connected to its upsides. As homogeneous catalysts are dissolved in the reaction medium, a greater effort has to be invested to separate them from the substrates and products after the reaction. The separation of a homogeneous catalyst from the reaction mixture is a mandatory part of every homogeneously catalyzed process, especially since rare and expensive metals are used as catalysts.[26]

Numerous concepts for the recycling of homogeneous catalysts have been developed over the years. Due to their integral part of homogeneous catalysis research in general but also in this work in particular, these shall be shortly discussed in the following.

2.2.2 Recycling Strategies for Homogeneous Transition Metal Catalysts

While there exist numerous concepts for the recycling of homogeneous catalysts, this chapter will primarily focus on the general concepts of selected methods, which have been chosen as the most important ones in the context of this work. To narrow the field of recycling techniques, only transition metal complexes are considered in this context. For a more detailed overview of homogeneous catalyst recycling strategies I refer to several reviews published about the topic, among them a short review published by myself about the recycling in aqueous multiphase media.[35–42]

The goal of homogeneous catalyst recycling concepts is the resource and energy efficient separation of the catalyst from the products while keeping the loss of catalyst metal (leaching) low. During the last two decades, the separation by immobilization of the molecular catalyst on a support material and the separation in liquid/liquid or related multiphase media have moved into the focus as concepts for the recycling of homogeneous catalysts.

The immobilization of homogeneous catalysts, sometimes referred to as “heterogenization”, is often viewed as the combination of the beneficial characteristics of homogeneous and heterogeneous catalysis: A high metal specific activity and well-defined molecular catalytically active sites, coupled with the easy separation of solid catalysts. The goal of this methodology is to coordinatively bind a molecular catalyst to a solid support material. By a coordination of the molecular metal catalyst to a solid surface, the catalyst is effectively immobilized and can be separated much like heterogeneous catalysts simply by separating the catalyst immobilized on the support from the product phase (Figure 4). Several applications, such as the use of

phosphorus (ligand) modified polymers, have been reported in literature.[43,44] As the success of separation relates to the strength of the coordinative binding to the support, more advanced approaches report the use of multidentate binding sites in order to decrease leaching of the catalyst into the liquid phase or the use of ionic phases which are immobilized on a support in order to immobilize the catalyst.[43,45–47]

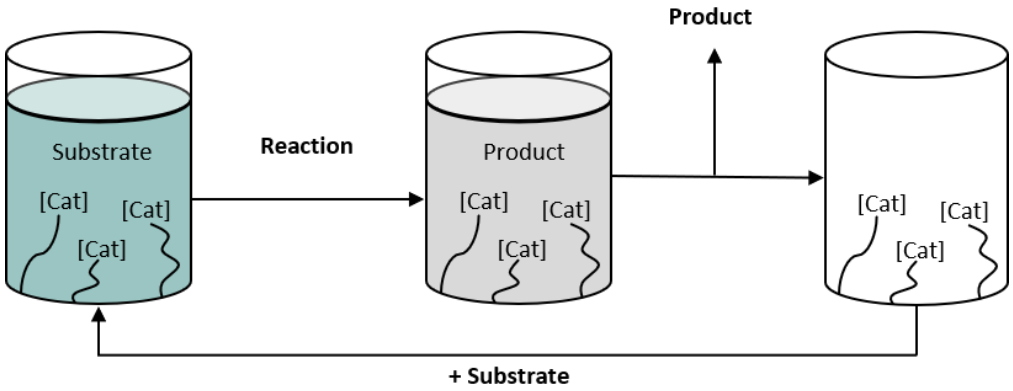

Figure 4: Schematic recycling concept for the immobilization of molecular catalysts on heterogeneous supports.

More recently the investigation of modified isolated single catalytic sites has moved into focus, blurring the boundaries between heterogeneous and homogeneous catalysis.[48] Although the immobilization of homogeneous catalysts on heterogeneous supports is one of the most intensively studied recycling concepts for homogeneous catalysts, with impressive examples about their success in laboratory scale, there have been critical concerns about the feasibility of this approach for industrial processes.[49] Probably the most well-known recycling concept is the use of liquid/liquid biphasic media to recycle homogeneous transition metal catalysts. In this approach, the catalyst and the products are dissolved in different phases. Separation of the catalyst can be achieved by decanting of the product phase from the catalyst phase.[40]

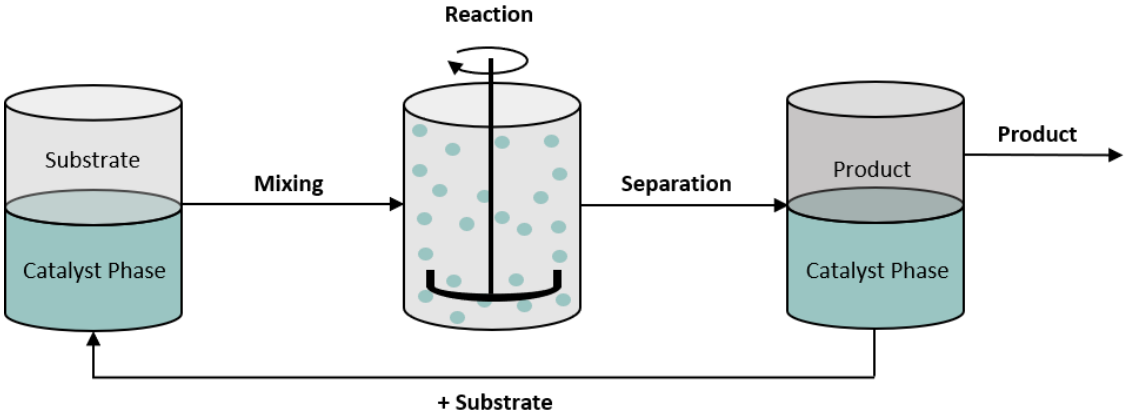

Figure 5: Schematic recycling concept for liquid/liquid biphasic recycling of homogeneous catalysts.[35]

There are several approaches to this technique based on the phase in which the catalyst is dissolved, the nature of the phases and the phase behavior during the reaction. Prominent

examples for this are the Shell-Higher-Olefin-Process (SHOP) for the production of linear alpha olefins by ethen oligomerization and the Ruhr-Chemie-Rhône-Poulenc process for the hydroformylation of propene to butanal.

The SHOP process was developed in laboratorys of the Shell company under leadership of Wilhelm Keim in 1977. Starting from ethene, linear alpha olefins of various chain length can be produced *via* a sequence of oligomerization, isomerization and methathesis reactions. For the oligomerization reaction nickel complexes coordinated by bidentate phosphino keto/carboxylate ligands are used. The resulting hydrophilic nickel catalyst is solved in a polar solvent (e.g. butanediol) during the reaction. While ethen shows acceptable solubility in polar solvents, longer chain alkenes, produced during the oligomerization reaction, are basically insoluble and separate as a second organic phase. After the reaction, product and catalyst phase are transferred into a phase settler. Products can be simply decanted from the catalyst phase and the catalyst phase is transferred back into the reactor. Up until today, more than one million tons of alkenes per year are generated by the SHOP process.[50,51]

Nevertheless, the largest scale industrial process for this liquid/liquid catalyst recycling technique is the Ruhr-Chemie-Rhône-Poulenc process. This process is used for the hydroformylation of propene to butanal (the hydroformylation reaction will be discussed in detail in chapter 2.3). While the catalyst in this process is highly hydrophilic, due to its sulfonated and highly water-soluble phosphine ligands (TPPTS), the products and substrates separate into a second organic phase, which is insoluble with the aqueous catalyst phase. During the reaction, the catalyst and substrate are brought together by increasing the surface area between the two liquid phases through intensive stirring. Additionally, propene is soluble in water to a lesser degree. After the reaction, the products can be removed by decanting the product phase. This recycling technique has been optimized over the years to reduce the rhodium catalyst leaching as low as <1 ppb.[52]

Different variations of this concept have been developed over the years. Surfactant[53] or cyclodextrine[54–57] modified liquids increase the surface area or substrate concentration in the catalyst phase. Another concept, so called Thermomorphic-Solvent-Systems (TMS), use thermoresponsive reaction mixtures which are monophasic at reaction temperature but can be switched to a biphasic reaction mixture after the reaction simply by a temperature decrease.[41,58,59]

A highly interesting approach is the use of supercritical carbon dioxide (*sc*CO_2) as a secondary product phase. The critical point of carbon dioxide is at comparatively mild conditions of T_c = 31 °C and p_c = 73.15 bar. In addition, *sc*CO_2 is non-flammable, nontoxic, highly abundant and can be separated from products after the reaction simply by reducing the pressure.[60,61] One example for a big scale application of such a concept is the decaffeination of coffee beans.[62,63]

The recycling of homogeneous transition metal catalysts by extracting product alcohols in a *sc*CO_2 phase has been proven for several different reactions like hydrogenation[64–72], oxidation[73], hydrovynilation[46], metathesis[74,75] and hydroformylation[76–81] reactions. One of the main benefits of *sc*CO_2 is that the polarity can be adjusted with the temperature and pressure to exhibit characteristics resembling solvent properties ranging from *n*-pentane to pyridine.[82,83] Usually polar solvents are used as catalyst phase which show limited solubility with *sc*CO_2 under most conditions. Commonly applied solvents for the catalyst phase are water, ionic liquids or polyethylene glycol (PEG). An impressive example for the recycling of a rhodium catalyst in the hydroformylation of various linear olefins has been reported by our group. By functionalization of PEG_{750} with triphenylphosphine (TPP) groups a very effective immobilization of the rhodium catalyst in the stationary TPP functionalized PEG phase was achieved. During the recycling of the catalyst a TTON of >11000 was achieved.[78]

Besides the mentioned recycling strategies for homogeneous catalysts the distillation of products and the precipitation of molecular catalysts are still important recycling concepts in industry.[26,42] Since they are usually accompanied by high energy and/or resource investments and are not important in the context of this work, they shall not be further discussed here.

2.2.3 Tandem Catalysis

For the production of chemicals, often times several reaction steps are necessary. Between those reaction steps, intermediate products have to be separated and purified before they can be used in the next reaction step. Those separation and purification techniques are energy and resource intensive.[26] The integration of two or more catalytic reaction steps into a “One-Pot” reaction, in which the sequence of reactions is achieved without any intermediate separation is called a tandem reaction. The benefit of tandem reactions is, that complex products can be synthesized without any intermediate steps. Due to the previously mentioned downsides are eliminated that way, tandem catalyzed reactions can make processes economically and ecologically more efficient. ANASTAS and WARNER defined the twelve principles of “Green Chemistry” which are often used as a guideline towards more sustainable chemical processes.[84] By increasing the energy efficiency, preventing waste and supporting the use of catalysis, tandem catalytic reaction fulfill three of those twelve principles simultaneously. The replacement of existing processes with tandem catalytic reactions is therefore highly desirable. Tandem catalysis as defined by FOGG and SANTOS is separated into three subcategories based on the nature of the catalyst (Figure 6).[85] Orthogonal-tandem-catalysis describes the use of two more separate catalysts for the individual reaction steps. While this allows to optimize each

catalyst for the individual reaction steps, cross interactions between both catalysts and simultaneous recycling of two catalysts is often challenging.[86]

Assisted-tandem-catalysis is defined by using an external trigger which induces catalysis of the subsequent reaction step. This can be the simple adjustment of the reaction parameters, e.g. an increase of the reaction temperature, or the modification of the catalytic species, e.g. by adding a certain ligand during the reaction. This allows for the use of individual reaction conditions or catalytic species for each reaction step but increases the operational expense, because both reactions are not running consecutively and the subsequent reaction has to be triggered.

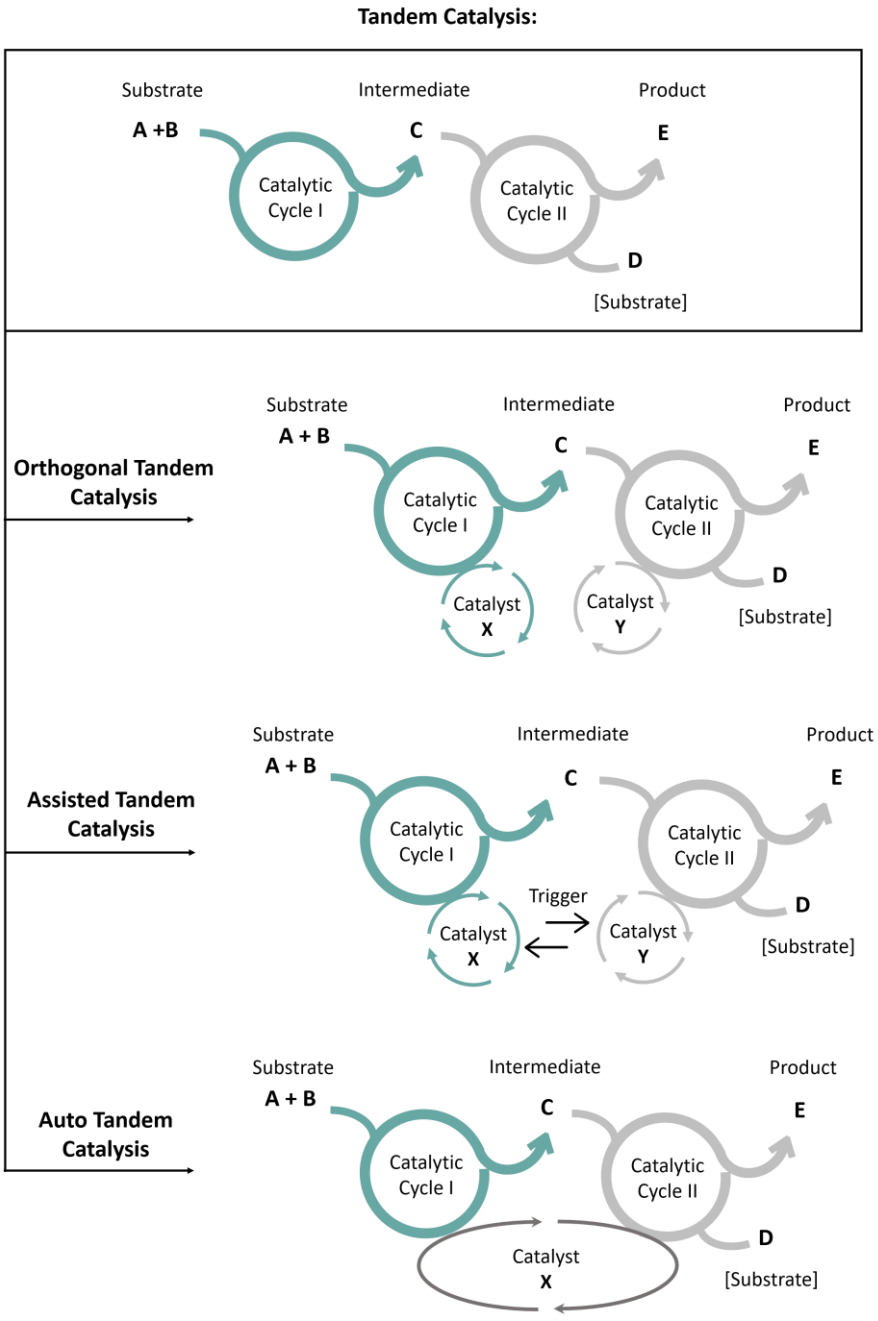

Figure 6: The three categories of tandem catalysis as defined by FOGG and SANTOS.[85]

Probably the most desirable form of tandem catalytic reactions, from an economic point of view, are auto-tandem-catalysed reaction systems. In auto-tandem catalytic reactions, both reaction steps are catalyzed with the same catalyst and under the same reaction conditions. They do not necessarily have to be catalyzed by the same catalytically active species, but no additional catalyst or trigger is required. Although this offers the least operational effort, the difficulty for this kind of tandem catalytic reaction lies in the development of such a system and in finding suitable reaction conditions, under which all reaction steps are efficiently catalyzed using a single catalyst.

In the context of this work, one of the main targets is to integrate reactions and make extensive use of tandem catalytic reaction systems.

2.3 The Hydroformylation Reaction

The hydroformylation reaction was discovered by Otto-Roelen by accident in 1938 during his research of redirecting ethylene streams together with ammonia in the Fischer-Tropsch reaction. He discovered the formation of propionaldimine, a condensation product of ammonia and propanal, in the product stream. He quickly concluded that that the formation of propanal from ethylene and synthesis gas is an independent side reaction not catalyzed by the Fischer-Tropsch reaction, but by molecular cobalt complexes which have been formed by leaching of surface cobalt from the Fischer-Tropsch catalyst into the reaction solution. He postulated that cobalt hydride species are responsible for this transformation and he was proven right a few years later.

Up until today, we know this reaction as the hydroformylation reaction and by now it developed to be the most important and largest scale homogeneously catalyzed process in the world with an annual production volume above 12 Mt/a.[87]

The hydroformylation describes the conversion of olefin double bonds with synthesis gas to aldehydes (Figure 7). Formally, a formyl group and a hydrogen atom are added to the double bond (hydro-formyl-ation). The addition of the formyl group at an α-olefin can proceed at both positions of the double bond. The resulting products are linear or branched aldehydes (*l:b*, also called *n*/*iso*-aldehydes).

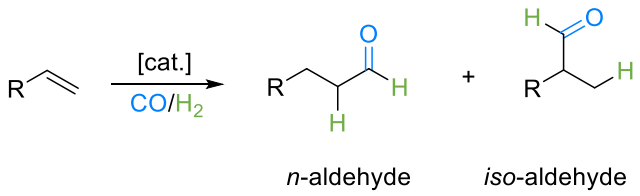

Figure 7: General reaction scheme for the hydroformylation reaction. Most common catalyst metals ([cat.]) include cobalt and rhodium.

Since the development of cobalt hydride carbonyls for this reaction, several generations of hydroformylation catalysts have been developed. Original cobalt catalysts are robust towards impurities and can be easily modified to obtain alcohols as products instead of aldehydes (reductive hydroformylation). However, cobalt catalysts usually require severe reaction conditions during the hydroformylation reaction (>90 bar, >150 °C). Just recently it was shown though that cobalt catalysts are also able to operate at milder reaction conditions.[88]

Several other metals have been investigated as catalysts for the hydroformylation reaction over the years. Among them iridium,[89–91] ruthenium[92–95] and iron[96,97] but most dominantly rhodium.[98] Until today, most cobalt-based processes have been replaced by rhodium-based ones. Some cobalt based processes are still operated for the conversion of higher chain length substrates, as for the production of alcohols from olefins generated in the SHOP process. The activity of

modern rhodium catalysts is roughly one thousand times higher in comparison to cobalt catalysts.[98] Additionally, rhodium-based processes can be operated at lower temperature and pressure ranges, which results in a massive energy saving during the process.

The main products produced by the hydroformylation reaction are propanal and butanal which are used as intermediates for alcohols or polymers. Aldehydes of different chain lengths are used as intermediates for a variety of chemical products like carboxylic acids, alcohols and amines, due to their easy functionalization. Today, the rhodium catalyzed hydroformylation reaction is probably the most intensively investigated homogeneously catalyzed reaction. Most commonly, rhodium is used in combination with phosphorus-based ligands. Although there are still discussions about the mechanism in some cases, a generally accepted catalytic cycle for the rhodium catalyzed hydroformylation reaction in combination with frequently used phosphine ligands is the so called Wilkinson´s dissociative mechanism, as displayed in Figure 8.[99]

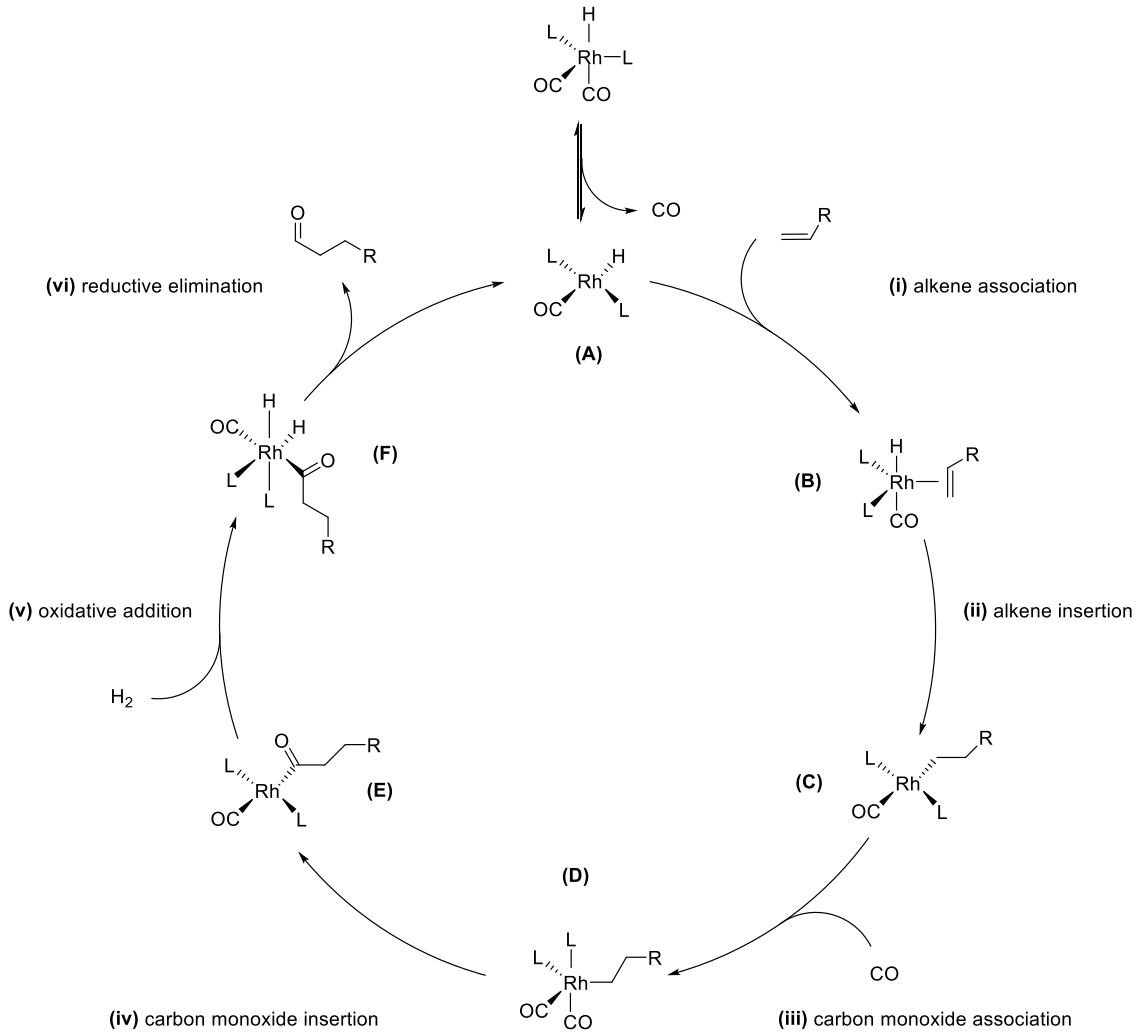

Figure 8: Catalytic cycle for the rhodium catalyzed hydroformylation reaction in combination with phosphine ligands as described by WILKINSON.[99] L = monodentate phosphine ligand (PPh_3 in WILKINSON´S original publication).

The general sequence of elemental reaction steps can be transferred to other types of ligands though. The active species for the hydroformylation reaction is formed from a penta-coordinated 18valence electron (VE) hydride complex after dissociation of a carbon monoxide (Figure 8, top). In the first step (**i**) an alkene associates to the 16 VE complex (**A**) to form a trigonal-bipyramidal 18VE complex (**B**). By inserting the alkene double bond into the rhodium hydrido bond (**ii**) a square planar 16VE complex (**C**) is formed. During the insertion step of the alkene, the regioselectivity of the product is decided. Hydride migration to the beta position leads to the linear product. When the hydride migrates to the alpha position the branched product is formed. After the alkene insertion, another carbon monoxide can associate (**iii**) to regain a trigonal-bipyramidal 18 VE complex (**D**). Carbon monoxide can now insert into the rhodium alkyl bond (**iv**) to form a rhodium acyl species (**E**). After an oxidative addition of dihydrogen (**v**) an octahedral dihydride complex is formed (**F**). Ultimately, the product is cleaved from the complex by a reductive elimination (**vi**) and the original 16 VE catalyticaly active species (**A**) is regained. Besides the desired pathway for the hydroformylation reaction several side reactions are possible (Figure 9).

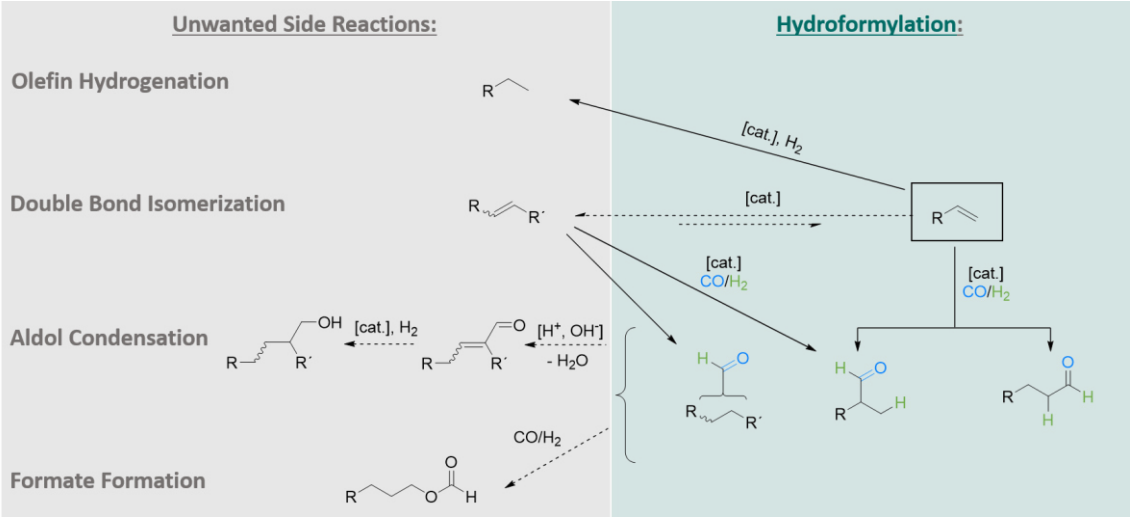

Figure 9: Side reactions in the hydroformylation reaction.

The isomerization of terminal olefins to internal double bonds is commonly observed. Although internal double bonds can often be converted to branched aldehydes and are not lost for the reaction, usually the hydroformylation of those substrates is sterically more demanding and proceeds with slower reaction rates compared to the conversion of terminal double bonds. Another common side reaction is the hydrogenation of the olefinic double bond to saturated alkanes. This is undesirable since alkanes are unreactive and an unwanted byproduct.[26] Less common, but possible when certain reaction conditions are met, is the aldol condensation of aldehydes to higher molecular aldehydes or alcohols and the formation of formates *via* a subsequent addition of carbon monoxide to aldehyde products.

2.3.1 The Reductive Hydroformylation Reaction

Another reaction which is often observed during the hydroformylation, especially when cobalt catlaysts are used, is the consecutive hydrogenation of aldehydes to alcohols. This reaction is referred to as reductive hydroformylation and is the tandem catalyzed sequence of the hydroformylation reaction and subsequent hydrogenation of intermediate aldehydes to alcohols as shown in Figure 10.

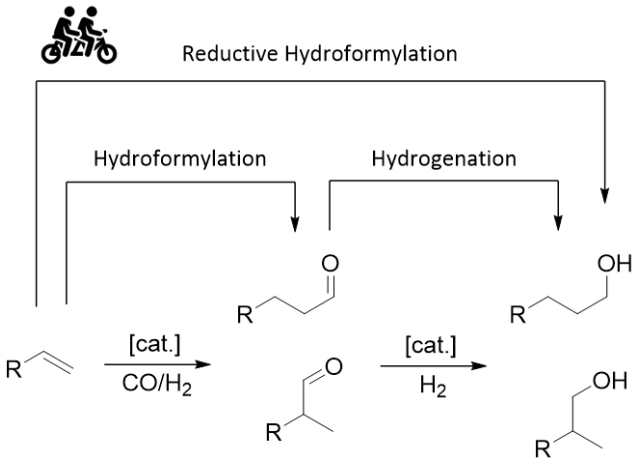

Figure 10: General reaction scheme for the reductive hydroformylation.

As alcohols are highly sought-after chemical products which are used as solvents, polymer precursors, detergents and food additives,[29,100] the direct conversion of olefins to alcohols has been a desirable reaction ever since the discovery of hydroformylation catalysts. Cobalt catalysts in combination with trialkylphosphine ligands are known to show an extraordinary activity for the hydrogenation step under certain reaction conditions. For example, Shell developed a process based on cobalt alkyl phosphine catalysts for the reductive hydroformylation of olefins to alcohols in the 1960s.[101] The activity for the hydrogenation step increases with the basicity of the trialkyphosphine ligand.[102,103]

Due to the great success of rhodium-based processes for the hydroformylation reaction and the usually low reactivity of cobalt catalysts for the hydrogenation step, a common pathway to produce middle to long chain alcohols is *via* two-step processes. Hence, using highly active rhodium catalysts for the hydroformylation reaction and hydrogenation of intermediate aldehydes over heterogeneous hydrogenation catalysts (e.g. nickel catalysts) afterwards.

Even though the direct production of alcohols from olefins in a one step reductive hydroformylation would be highly beneficical from an economical and ecological point of view, it is challenging to find catalytic systems which exhibit a catalytic activity for both reaction steps that can compete with modern two-step processes. The different requirements for the catalyst to catalyze both, the hydroformylation and hydrogenation step, and the competition between

aldehyde and olefin hydrogenation reaction remain the major challenges in this field. Several attempts to steer rhodium phosphorus catalysts to express a higher hydrogenation activity have been investigated with limited success.[100] To the best of my knowledge, the highest catalytic activity for rhodium-based catalysts has been achieved by the group of VOGT in an innovative approach in which the reaction was conducted "on water" using a rhodium/xantphos catalyst. During investigations of the reaction in time-resolved experiments a Turn-Over-Fruequency (TOF) of 220 h^{-1} was achieved.[104] More recently, several orthogonal tandem catalytic systems based on a rhodium catalyst for the hydroformylation step and a ruthenium catalyst for the hydrogenation step have been reported.[105–107] In those systems, higher catalytic activities can be achieved because each catalyst can be optimized towards the individual reaction step. Neverthless, two homogeneous catalysts pose additional challenges towards recycling and long-term stability of the catalytic system and are not suited for industrial processes. For a more detailed overview about catalytic systems investigated for the reductive hydroformylation reaction, I refer to an excellent review published by the group of FRANKE in 2015.[100]

2.3.2 The Reductive Hydroformylation Using Rhodium/Amine Catalysts

Besides the considerable scientific effort to improve the selectivity of rhodium catalysts in combination with phosphorus-based ligands to produce alcohols from olefins, up until today omly limited success was achieved. No catalytic system has been found which can compete with the activity of two-step processes as applied in industry.[100] In addition, phosphorous ligands are prone to several decompositions pathways such as oxidation, or hydrolysis.[36,108]

In contrary to phosphorus-based systems, tertiary amines as ligands are stable towards oxygen and other decomposition pathways and often highly cost efficient in comparison to phosphorus analogues. A remarkable increase in the hydrogenation activity for the reductive hydroformylation, using rhodium in combination with tertiary amines, has already been described in the 1970´s, but little effort has been made to further investigate these catalytic systems or to understand the underlying mechanisms ever since.

The application of tertiary amines in combination with rhodium for the conversion of 1-octene to nonanol has been first described by FELL in 1972 (Figure 11, (I)). Rhodium (III) oxide (Rh_2O_3) as a precursor in combination with methylpyrrolidin was investigated. It was found by FELL that a high amine concentration is beneficial for the hydrogenation step.[109]

In 1974 JUREWITZ elaborated on these findings and tested several monomeric tertiary amines such as a polymeric dimethylbenzylamine for the reductive hydroformylation of 1-hexene (Figure 11, (II)). JUREWICZ was also the first to attempt the characterization of the catalytic species by IR-spectroscopy. Based on this, he suggested the formation of (multinuclear) rhodium amine hydride complexes as active species.[110] A few years later, KANEDA investigated the activity of

several bidentate tertiary amines as additives together with $Rh_6(CO)_{16}$ in comparison to several benzylic and pyridinic amines as additives (Figure 11, (III)).[111]

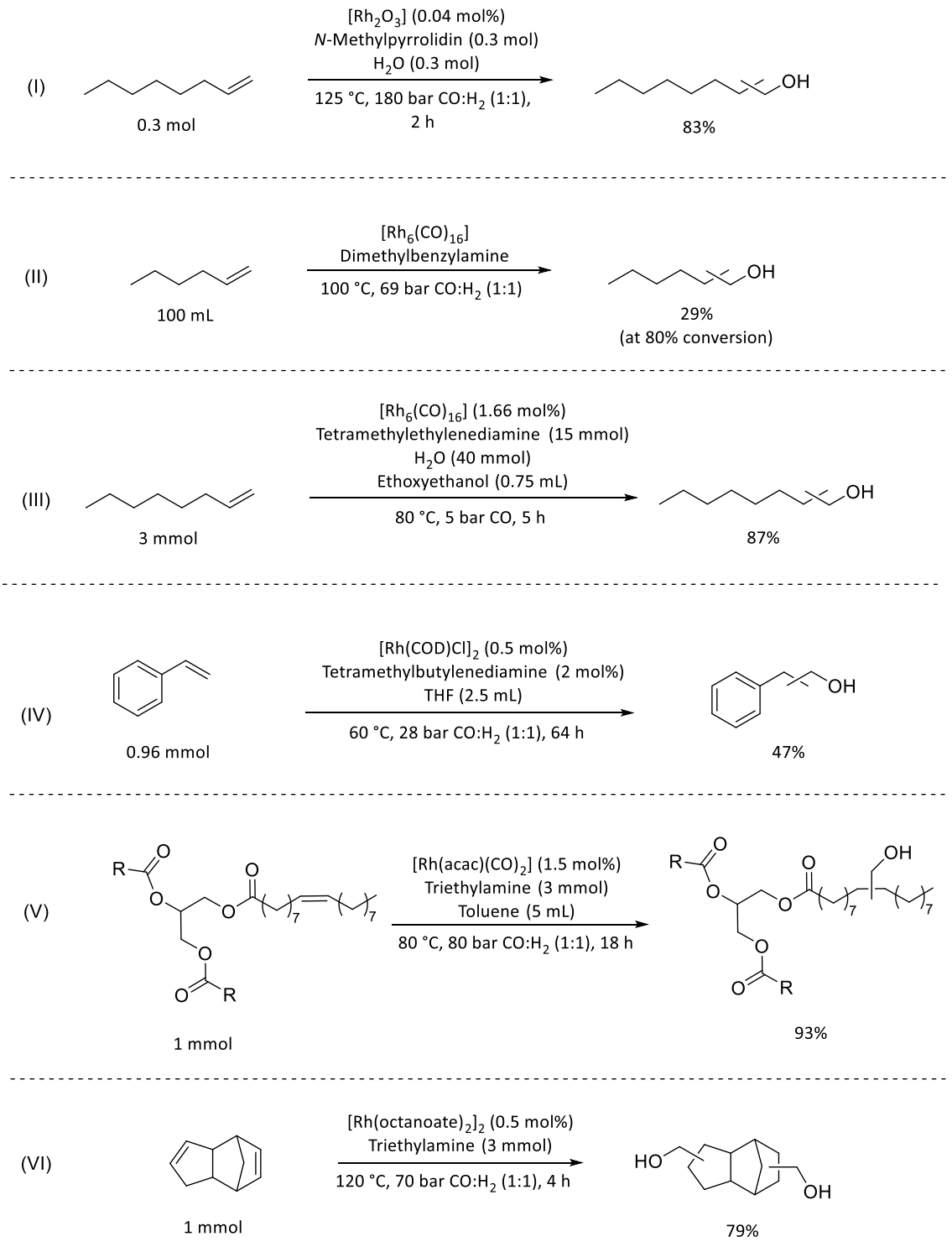

Figure 11: Catalytic systems based on rhodium in combination with teretiary amines for the reductive hydroformylation reaction published in literature.

Since then, no further results on this topic have been published up to 2012, when ALPER reported the reductive hydroformylation of styrene using a $[Rh(COD)Cl]_2$ precursor in combination with several monodentate and bidentate trialkylamines (Figure 11, (IV)). Interestingly, he found that

the reaction proceeds even under very mild conditions at room temperature, even though with a much lower activity. In a substrate scope several other aromatic susbtrates have been successfully converted.[112]

This new publication after more than 30 years shed new light on the application of tertiary amines as additives for the reductive hydroformylation. In 2016 HAPIOT reported about an interesting approach in which unsaturated vegetable oils were used as substrate in the reductive hydroformylation with [Rh(acac)$(CO)_2$] in combination with several simple trialkylamines such as triethylamine as the catalyst (Figure 11, (V)). The effect of several reaction parameters has been investigated and it was found that trialkylamines support the hydrogenation step while benzylic amines preferably achieve aldehydes as reaction products. This is in accordance with previous findings by KANEDA. Furthermore, it was suggested that the steric hindrance of the amine affects the catalytic activity, which would suggest that amines bind to rhodium during the catalytic cycle, even though this was not proven.[113]

At the same time, the group of VORHOLT investigated the combination of [Rh(octanoate$)_2]_2$ with triethylamine for the reductive hydroformylation of the industrially relevant dicyclopentadiene to the corresponding diol (Figure 11, (VI)). It was possible to scale the reaction to a reaction volume of 2 L and achieve an alcohol selectivity of 81 % at this scale. An attempt to run the reaction in neat triethylamine was not successful. Alcohols were obtained, but only at much higher catalyst loadings and reaction times.[114]

Even though the reductive hydroformylation using rhodium in combination with tertiary amines is known since the discovery by FELL in 1972, the previously described publications are the only ones known to date. Most of them describe the reaction in a purely phemonological approach, based on the variation and investigation of reaction parameters. Very little is known about the catalytic species or the reaction mechanism. Although it is generally assumed that the tertiary amine acts as ligand in those catalytic systems, this is by no means self evident, since tertiary amines are in general weakly binding ligands compared to carbon monoxide. Very little attempts have been made to surpass this phemonological approach and systematically investigate the influence of the tertiary amine on the hydrogenation activity or the nucelarity of the catalytic species.

2.4 The Fischer-Tropsch Reaction

The Fischer-Tropsch synthesis was discovered by Franz Fischer and Hans Tropsch in 1925 only about 50 m from the place of writing this sentence at the Kaiser-Wilhelm Institut für Kohlenforschung (nowadays Max-Planck-Institut für Kohlenforschung). During investigations on the process of coal gasification they noticed the conversion of synthesis gas to a mixture of saturated and unsaturated hydrocarbons with water as by product in the presence of iron or cobalt catalysts (Figure 12).[115]

$$n\ CO + (2n+1)\ H_2 \xrightarrow[-\ n\ H_2O]{[Fe];\ [Co]} C_nH_{2n+2} + C_nH_{2n}$$

Figure 12: Simplified reaction scheme of the Fischer-Tropsch reaction.

After further investigations, it was found that the Fischer-Tropsch reaction is an exothermic polymerization reaction which propagates the formation of hydrocarbon chains at the surface of heterogeneous metal catalysts.[115] The resulting hydrocarbon mixtures resemble the composition of current fossil-based fuels closely and can be used as a substitute after some refinement. The potential of this application was recognized immediately. Over the next years, the reaction gained immense attention, especially in Germany, as an effective way to produce liquid fuels from coal without the dependency on oil supplied from foreign countries. For example, shortly before the end of the second world war the estimated capacity of the liquid fuel production from the Fischer-Tropsch synthesis in Germany was 600 kta-^{1}.[116] After the end of the second world war, the industrial importance of the Fischer-Tropsch reaction was closely connected to the price of fossil fuels. Generally, the Fischer-Tropsch reaction was not able to compete with liquid fossil fuels at a cheap price rate. As such, over long periods of time the reaction was not considered industrially important, except in select countries like south Africa, in which large and cheap coal reserves and sanctions regarding crude oil because of the apartheid regime supported the production of fuels *via* the Fischer-Tropsch synthesis.[115] With the decreasing industrial importance of the Fischer-Tropsch reaction, its importance in the scientific community also decreased rapidly. Although the importance of the reaction shortly sparked after the first oil crisis in 1973, it decreased again afterwards.[115,117]

During recent years it has been becoming more and more obvious that we need to change our dependency on fossil fuels. As such, the Fischer-Tropsch reaction has regained attention in the scientific community as an effective way to produce sustainable liquid synthetic fuels from renewable resources. Especially during the last decade, the Fischer-Tropsch reaction has been recognized as one of the key technologies for a sustainable energy sector in the future.[18,118,119]

A search on Web of Science for publications including the Fischer-Tropsch reaction keyword

achieved 800 results for the years 2000 to 2005 and more than 3500 results for the years 2016-2022.[120] Before going into more detail regarding the products and selectivity of the Fischer-Tropsch reaction (chapter 2.4.2 to 2.4.3) some important metrics used to describe the Fischer-Tropsch reaction shall be explained in the following.

2.4.1 Metrics in Fischer-Tropsch Synthesis

Since the Fischer-Tropsch reaction is a polymerization reaction, the description of individual products is cumbersome and not expedient. Rather than individual products, product distributions and the resulting selectivity towards hydrocarbon fractions are used for the characterization of the reaction. These metrics will be used later in this chapter 2.4 and, more importantly, be used as the foundation for the analysis of the Fischer-Tropsch reaction investigated during this work (chapter 4.3).

As a baseline for further analysis of the selectivity of the Fsicher-Tropsch reaction, the product distribution curve of the different hydrocarbon products are used. The product distribution can be mathematically approximated with an Anderson-Florey-Schulz distribution (Figure 13).

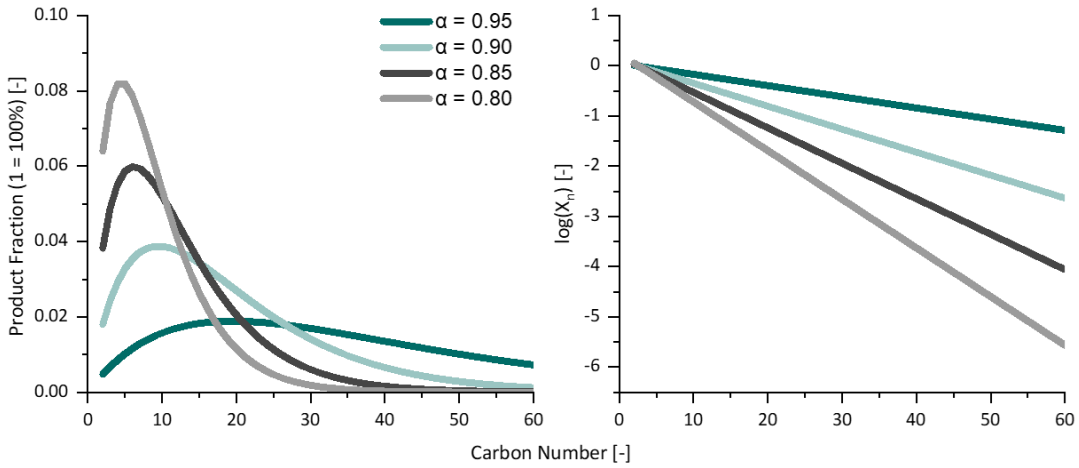

Figure 13: Anderson-Schulz-Florey (ASF) distribution and its linearization at different chain growth propagation (α) values.

Anderson, Florey and Schulz introduced a mathematical expression for polymerization reactions which can be used to determine the weight fraction of a product depending on their carbon number (Equation 4),

$$w_n = n \cdot (1 - \alpha)^2 \cdot \alpha^{n-1} \qquad (4)$$

where n is the carbon number and α the chain growth probability, which is defined as the likelihood of another chain propagation event compared to the likelihood of a chain elimination event at any point during the polymerization reaction.

The chain growth propability α can be determined by a linearization of the Anderson-Florey-Schulz-distribution in a logarythmic plot and can be calculated from the linearized function as displayed in Equation 5.

$$\log(x_n) = n \log \alpha + \log\left(\frac{1-\alpha}{\alpha}\right) = n \log \alpha + \text{constant} \quad (5)$$

Hydrocarbons produced *via* the general Fischer-Tropsch mechanism follow this mathematical distribution in very good approximation. Exceptions are methane and CO_2, since other mechanisms contribute to their generation.

As the product spectrum of the polymerization reaction follows this mathematical distribution, it can be used to calculate the contribution of missing hydrocarbons when the concentration of enough other products (=datapoints) to derive α with a good certainty are known. In scientific research this is commonly done for higher boiling hydrocarbons in the Fischer-Tropsch reaction which precipitate as waxes. To further characterize the Fischer-Tropsch mixture, the carbon selectivity for the CH_4 and CO_2 formation are commonly given together with the selectivity for representative fractions of the hydrocarbon product spectrum. Often it is separated into the selectivity for the C_2-C_5 fraction as a representation of low boiling and gaseous products (at ambient temperature), the selectivity towards C_5-C_{21} hydrocarbons as a representation of liquid medium to long chain hydrocarbons, and the C_{21+} fraction which are often referred to as waxes.

As means to estimate the catalytic activity in Fischer-Tropsch reactions, the metal specific time yield, in this case the cobalt-time-yield (CTY), is given. The CTY is calculated based on the consumed amount of synthesis gas ($M_{\text{consumed CO}}$) in a given time (t) and referred to the amount of metal in the Fischer-Tropsch catalyst (M_{cobalt}) as displayed in Equation 6.

$$\text{CTY} = \frac{M_{\text{consumed CO}}}{t \cdot M_{\text{cobalt}}} \quad (6)$$

The CTY can be compared to the Turn-Over-Fruequency, often given for molecular catalysts as means to describe the catalytic activity (chapter 2.2). Although in this case the conversion of the educt is used to describe the overall catalytic activity instead of the catalytic activity referred to a specific product.

2.4.2 Product Spectrum and Selectivity of the Fischer-Tropsch Reaction

The main products of the Fischer-Tropsch (FT) reaction are saturated and unsaturated hydrocarbons as displayed in Figure 12. Oxygenated side products are observed to a small degree. Most commonly, alcohols but also aldehydes and ketones can be observed under certain reaction conditions.[121] Although parts of the mechanism are still frequently discussed,[117,119] the most widely accepted "methylene" mechanism is displayed in Figure 14.[122] The fundamental reaction step for the formation of hydrocarbons is the stepwise addition of carbon monoxide and hydrogen to CH_2 units under water dissociation on the surface of the Fischer-Tropsch catalyst. In this case, the CH_2 groups are considered the "monomers" of the polymerization reaction. The chain propagation of the hydrocarbon chain occurs by an addition of further CH_2 groups on the Fischer-Tropsch surface.

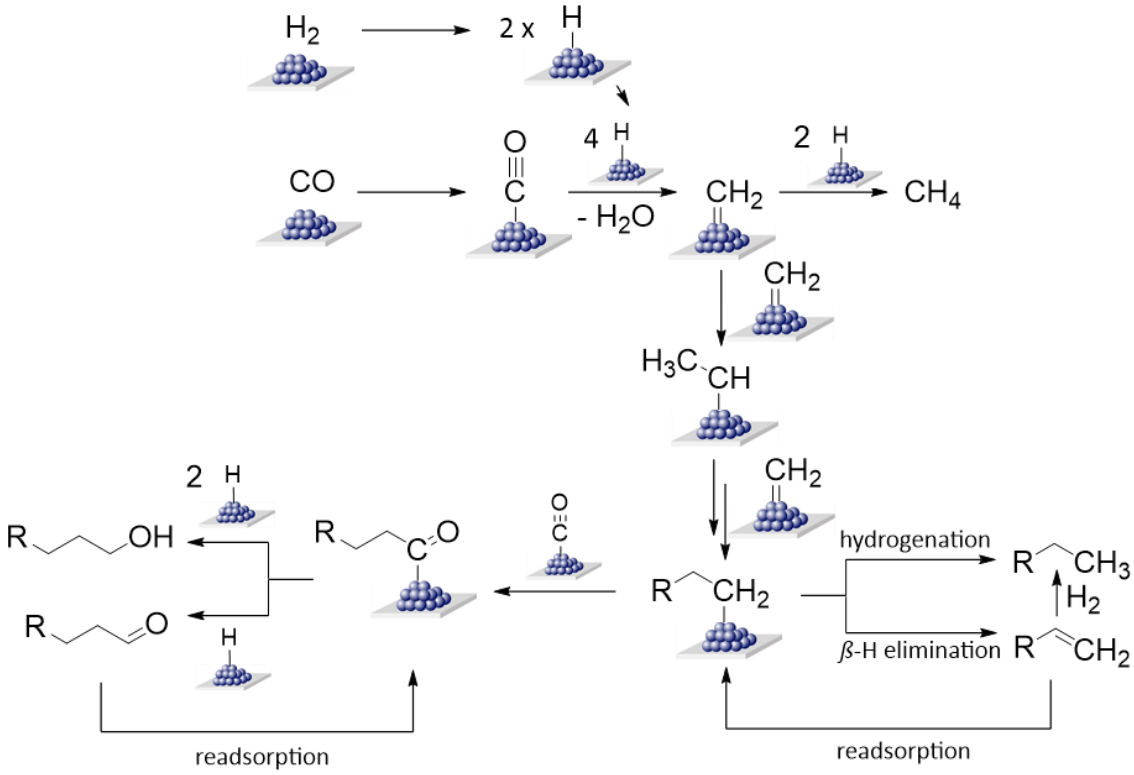

Figure 14: Illustration of the main surface reaction mechanisms during the Fischer-Tropsch reaction.

Chain elimination is achieved either by a hydrogenation of the surface bound CH_2 group to a CH_3 group and thereby a cleavage from the Fischer-Tropsch surface or by a transfer of a hydrogen atom at the beta position to the surface (*ß*-H-elimination). In this case, unsaturated terminal hydrocarbons are obtained as products. The likelihood of an elimination event and therefore the rate of chain growth propability (α; see chapter 2.4.1) can be influenced by the nature of the catalyst and the reaction conditions. Usually, the *ß*-H-elimination is the predominant pathway for chain elimination from the Fischer-Tropsch surface. Nevertheless, the reactive terminal olefin group can be reabsorbed at the Fischer-Tropsch surface and undergo further chain

propagation and ultimately chain elimination. Since in the elimination step, once more, hydrogenation or *ß*-H-elimination can occur, the final Fischer-Tropsch product spectrum usually contains mostly saturated hydrocarbons.[117]

The generation of oxygenated products is a side reaction of the Fischer-Tropsch reaction. One of the main mechanisms for their formation on the Fischer-Tropsch surface is displayed in Figure 14.[122] Beginning with the surface bound alkyl chain, an adsorbed carbon monoxide can be inserted into the alkyl chain instead of a CH_2 group. The surface bound oxygenate is likely to undergo a chain elimination event afterwards, in which case either an aldehyde or an alcohol is obtained as a product, depending on the amount of hydrogen atoms added during the chain elimination. Since resulting aldehydes can be reabsorbed, similarly to unsaturated hydrocarbons, usually alcohols are the main products ultimately received from this mechanism. Although the direct chain elimination is favored after insertion of carbon monoxide into the chain, in rare cases the chain propagation continues with insertion of another CH_2 group in which case ketones are gained as the product. Since this is generally not likely, this pathway is not displayed in Figure 14. Another widely accepted but less likely mechanism for the generation of alcohols is the addition of a hydroxyl group to the end of a surface bound CH_2 group or chain elimination by addition of a hydroxyl group as displayed in Figure 15.[123]

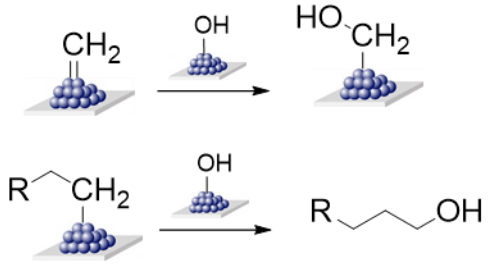

Figure 15: Alternative mechanisms for the formation of alcohols on the Fischer-Tropsch surface.

A mostly unwanted side reaction during the Fischer-Tropsch reaction is the hydrogenation of surface adsorbed CH_2 units. In this case, methane is cleaved from the Fischer-Tropsch surface as by product. A low methane selectivity is usually one of the goals for modern Fischer-Tropsch catalysts since methane is not considered a high value product. Another unwanted side reaction is the water gas shift reaction (WGSR) of carbon monoxide and water to form carbon dioxide and hydrogen. Carbon dioxide cannot be converted in the Fischer-Tropsch reaction.[122] Both carbon monoxide and methane therefore represent lost carbon for the reaction.

One of the main parameters which dictates the product spectrum of the Fischer-Tropsch reaction is the catalyst metal. Up until today, the two most important metals used for Fischer-Tropsch reactions are iron and cobalt catalysts as they have already been known since the discovery of the Fischer-Tropsch synthesis.[115] Both catalysts are still applied in industry to

this day. In terms of the product spectrum, both catalysts show a significant difference in selectivity. Iron catalysts are comparatively cheap. Their low hydrogenation activity usually results in a low methane production and the share of unsaturated hydrocarbons in their product spectrum is higher compared to cobalt catalysts. However, they show an increased activity for the Water-Gas-Shift-Reaction and thus, the CO_2 side production (usually >30 C%) is much higher than for cobalt catalysts. While this usually is an unwanted side reaction, it can be used in certain applications in which hydrogen starved synthesis gas is used as feedstock, e.g. synthesis gas from certain biomass feedstocks, to produce additional hydrogen *via* WSGR for the reaction. The cheap price of iron allows for high iron loadings (usually around 100 g iron per 25 g of support). To increase the stability of the catalyst, alkali promotors (0.5 w% - 1 w%), usually potassium, are added.[117] Compared to iron catalysts, cobalt catalysts generally have a higher catalytic activity for the Fischer-Tropsch reaction but are much more expensive. Because of their increased hydrogenation activity, they show a higher methane selectivity and a high selectivity towards saturated hydrocarbons. On the other hand, the WSGR activity is very low and the CO_2 selectivity is usually below 5%. Because of the comparatively high price of cobalt, much more effort is put into achieving a fine and even distribution of cobalt on the support and to reduce the amount of metal loading (down to 10 g Co per 100 g of support).[117]

Besides iron and cobalt, other catalytic metals have been investigated for the Fischer-Tropsch reaction. The most important ones are ruthenium and nickel-based catalysts, both showing a higher catalytic activity than the previously mentioned ones. The application of ruthenium is undesirable due to its high investment cost while nickel catalysts are even more active for the hydrogenation reaction which results in a high methane selectivity.[117] In Figure 16 exemplary logarithmic ASL distributions are displayed as reported by W. D. SHAFER for typical iron, cobalt and ruthenium Fischer-Tropsch catalysts.[124]

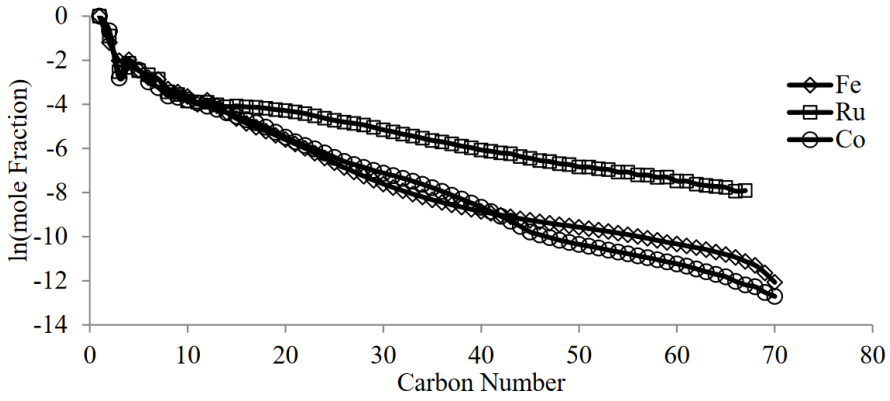

Figure 16: General Anderson-Florey-Schulz hydrocarbon distributions for iron, cobalt and ruthenium Fischer-Tropsch catalysts. As reported by W. D. SHAFER et al.[124]

Besides the metal catalyst, the selectivity of the reaction can be influenced by the reaction parameters, most importantly the reaction temperature.

In general, a higher reaction temperature promotes product mixtures with lower molecular weight products, while the selectivity to methane increases likewise and the deactivation of the catalyst due to cooking is increased. At lower temperatures, Fischer-Tropsch mixtures with a higher average molecular weight are produced. The importance of the temperature on the chain growth of the Fischer-Tropsch products leads to the distinction between two processes. The High Temperature Fischer-Tropsch process (HTFT) is used for the production of low molecular weight mixtures and is operated using iron catalysts at around 300-350 °C. The Low Temperature Fischer-Tropsch process (LFTF) is used for the production of for higher molecular weight mixtures and is operated at around 200-250 °C using iron or cobalt catalysts.[125,126] Figure 17 shows typical reaction conditions used during the HTFT and the LTFT process and the main products derived from the different processes.

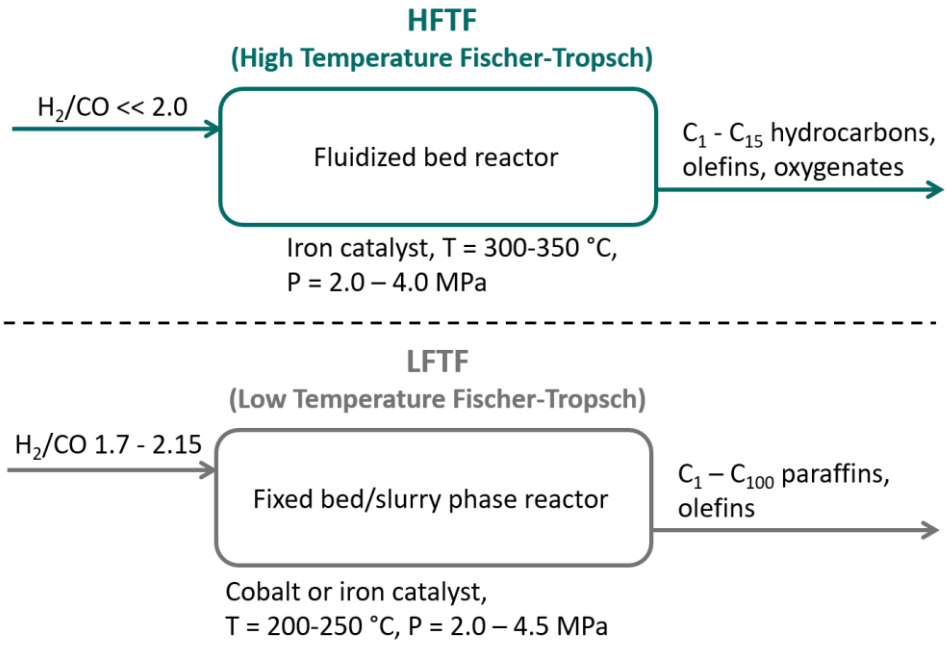

Figure 17: Comparison of the High Temperature Fischer-Tropsch process (HTFT) and the Low Temperature Fischer-Tropsch (LTFT) process. Adapted from BAE ET AL.[126]

While the HFTF process is usually carried out in fluidized bed reactors due to a better heat transfer from the exothermic reaction, LFTF process can be carried out as gas and liquid phase reactions in multitubular fixed bed or slurry phase reactors.[127,128]

2.4.3 Steering the Fischer-Tropsch Selectivity Towards Olefins or Alcohols

While the main product of saturated hydrocarbons contain a high energy density for the application of Fischer-Tropsch mixtures as fuels, it has often been attempted to influence the selectivity of the Fischer-Tropsch reaction towards more valuable products like unsaturated hydrocarbons.[117,129] Unsaturated double bonds offer an easy and flexible opportunity as platform chemicals for further functionalization, which is comparable to our current chemical value chain. Currently, olefins are mainly produced by catalytic cracking/reforming of fossil oil and gas or by ethylene oligomerization and stand right at the beginning of almost every chemical value chain.[130] Last but not least, during recent years the functionalization of Fischer-Tropsch cuts as fuel additives has gained increasing interest.[16,24,119] One of the main challenges for unsaturated hydrocarbons produced from Fischer-Tropsch reactions, which hinders a broader application, is that they are obtained only as a byproduct with saturated hydrocarbons. A lot of effort has been invested in so called Fischer-Tropsch to Olefin (FTO) processes over the years.[131] Most interesting for this approach are the low boiling olefinic products in the C_2-C_4 range. They can be separated easily and have a variety of applications, e.g. as precursors for monomers for polymerization reactions.[132] For this, iron-based catalysts are predestined since at higher temperature a bigger share of low molecular weight products is obtained. Under those conditions cobalt catalysts would produce large amounts of methane instead.[133]

While the FTO process for low molecular weight olefins works reasonably well, it is difficult to obtain higher molecular weight olefins in the C_{5+} region with sufficient efficiency. For higher molecular weight products, lower temperatures need to be used at which cobalt-based catalysts are beneficial due to their low WGSR activity. A higher chain growth is usually accompanied with a higher chance of a readsorption of olefins and therefore hydrogenation. On the other hand, when the hydrogenation activity is reduced, the chain growth of the catalyst is dampened. Some effort has been made in order to solve this problem as well.[134]

An interesting approach was reported by the group of FUJIMOTO who reported an olefin selectivity of up to 40% when using alkane solvents as reaction media.[135] The group of ZHONG reported Co_2C nanoprisms with a high density of exposed crystalline facets are able to achieve an olefin selectivity of up to 60% but unfortunately merely in the C_2-C_4 region due to a low chain growth probability.[136] The use of promotors in addition to cobalt has been investigated in an effort to steer the selectivity towards olefins. In 2016, the group of ZHAO reported the promotion of a cobalt catalyst with manganese to exhibit an olefin selectivity of up to 40% which has been almost three times higher than before. It was postulated that manganese blocks the catalytic sites responsible for the H_2 uptake and therefore creates a carbon rich surface.[137]

A very innovative approach has been reported by PRIETO ET AL. By tuning of the catalyst support with freeze casting, a structure of mesopores and micropores has been created.[134] While the overall surface area has not been significantly affected by this, the mesoporous structure of the catalyst allowed for a faster diffusion of hydrocarbon products out of the micropores in which reabsorption and hydrogenation is much more likely. After impregnation of the catalyst with cobalt, an olefin selectivity up to 50% has been achieved while maintaining a high chain growth propability and a low production of CO_2 and CH_4 side products.[118,138] Together with Dr. Prieto and Kai Jeske, an improved catalyst based on this concept has been developed for the direct conversion of synthesis gas to alcohols, presented in chapter 4.3 of this work.

Besides olefins, the direct production of alcohols through the Fischer-Tropsch synthesis is a long-held dream in Fischer-Tropsch research.[139] Even though alcohols are usually only a minor side product during Fischer-Tropsch synthesis, their direct generation from synthesis gas would be highly beneficial. Over the years, a variety of different approaches for the direct conversion of synthesis gas to alcohols with Fischer-Tropsch catalysts have been investigated. A very good overview is given in an article by the group of PÉREZ-RAMÍREZ.[139]

One of the earlierst reported approaches to shift the selectivity of Fischer-Tropsch synthesis towards alcohols is the doping of cobalt catalysts with lanthanum. In 1986, BARRAULT first published results in which an increase of the alcohol selectivity for commonly used cobalt catalysts with La_2O_3 was reported even though the overall catalytic activity was reduced by doping with lanthanum.[140]

Ever since, the dopping with lanthanum is propably the best-known method to shift the selectivity towards alcohols which has been investigated intensively. One of the more recent examples was published by the group of LU in 2009. The Fischer-Tropsch reaction of cobalt catalysts on activated carbon doped with La_2O_3 was investigated. Doping of the catalyst with 0.5 wt% La_2O_3 increased the selectivity towards middle to long chain alcohols in the range C_1-C_{18} from 22 C% to 39 C%.[141] The distribution of alcohols and hydrocarbons showed no difference for the chain growth probability in the case of the unpromoted cobalt catalyst, suggesting that both products are derived from the same surface mechanism. In contrast, when the catalyst is promoted with La_2O_3, the chain growth propability of alcohols is significantly lower (α = 0.58) than for hydrocarbons (α = 0.70). It was assumed that the difference in chain distribution is due to the generation of new active sites for the formation of alcohols. This was confirmed by XRD (X-Ray Diffraction) measurements which showed an increased concentration of Co_2C at the surface in presence of the lanthanum promotor.[141,142] Simultaniously, this example highlights a fundamental challenge that a lot of approaches to shift the selectivity of the Fischer-Tropsch reaction towards alcohols encounter: When increasing the activity for the formation of alcohols,

a decrease in chain growth propability is observed since the propability of elimination reactions is usually increased at the same time.

Based on the results by LU, the group of WANG investigated the role of the support in the formation of those Co_2C species and supported his experimental results with theoretical computations. It was found that in the presence of activated carbon the formation of Co_2C is increased while other more acidic supports inhibit it. A direct relation between the concentration of Co_2C and the alcohol selectivity is observed but at the same time Co_2C is unable to dissocate CO and therefore also partially deactivates the catalyst and lowers the overall catalytic activity for the Fischer-Tropsch reaction.[143]

A different approach to the commonly used doping with lanthanum was reported by the group of TOKUNAGA in 2013. The doping with alkali metals, most notably sodium, lead to an increase of the overall selectivity towards alcohols from 6% to 29% compared to the unpromoted catalyst, even though a decrease in the overall catalytic activity is observed as well.[123] The CO-conversion decreases from 73% to 53% in the case of the promoted catalyst. It was suggested that the addition of alakali metals increases the basicity of the Fischer-Tropsch surface and therefore increases the amount of surface hydroxy groups. From the fact that only linear alcohols have been observed, it was excluded that the increased selectivity towards alcohols is an effect of leached cobalt and a homogeneously catalyzed hydroformylation reaction.

3 Motivation

As previously mentioned, substantial changes to the consumption and generation of energy are necessary to fight climate change. Substitution of fossil fuels with alternatives based on renewable resources is highly sought after. For the substitution of fossil fuels in our current fleet of vehicles and in long-distance transport, synthetic fuels (syn-fuels) can make a crucial contribution. One of the inherent benefits of syn-fuels, is the possibility to tailor them to exhibit advantageous features. During the last decade, the beneficial effect of alcohols as fuel additives has moved into the focus of the scientific community.[16,21–23] By adding oxygen to the system, alcohols can help to significantly reduce the emission of pollutants like NO_x, sooth emissions and, to a lesser degree, CO_2. Especially middle to long chain alcohols, like *n*-octanol, offer a good compromise of energy density and emission reduction.[22,23]

To make medium to long chain alcohols accessible as fuel additives, energy and resource efficient routes for their production are needed. Currently, middle to long chain alcohols are produced mostly from olefins *via* a combination of hydroformylation and hydrogenation reactions (Figure 18, lower pathway).

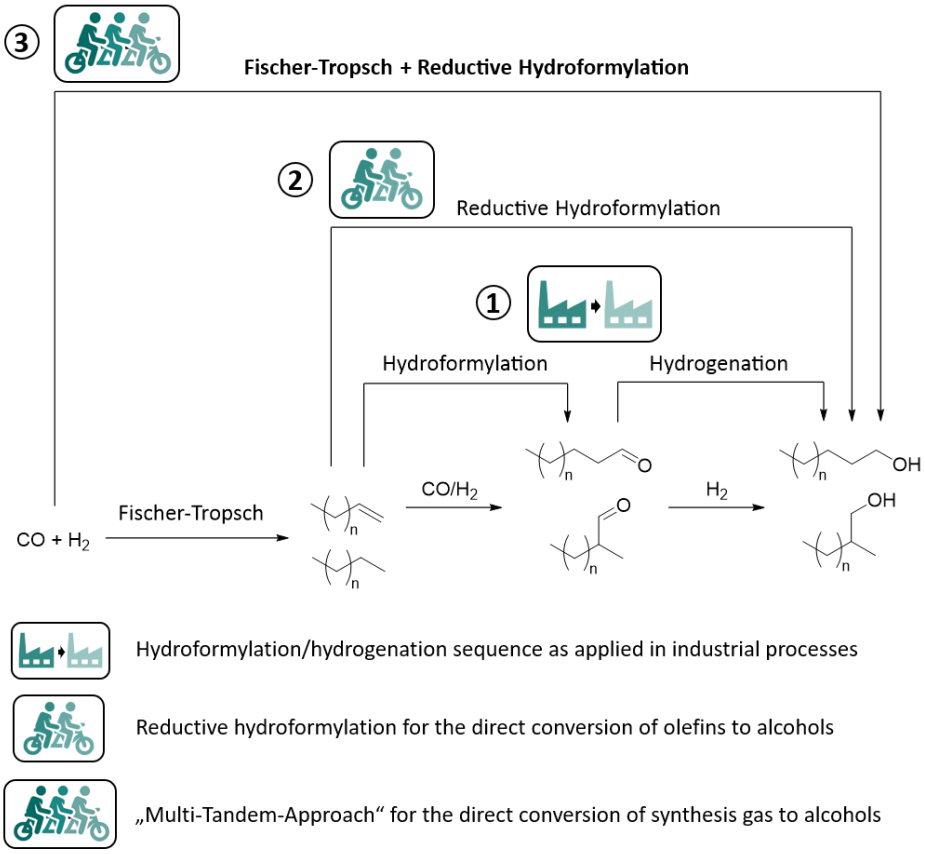

Figure 18: Tandem catalytic concepts for the synthesis of middle to long chain alcohols as bio-synthetic-fuel additives.

Furthermore, as aldehydes are produced on a much larger scale than the current demand of middle- to long-chain alcohols, there has been no reason to deviate from these two-step processes.[100] With the application as fuel additives, the dimension in which they would need to be produced changes drastically and requires highly cost-efficient transformation protocols.

One of those protocols is the tandem catalyzed sequence of hydroformylation and hydrogenation which is known as reductive hydroformylation (Figure 18, middle pathway). The reductive hydroformylation allows for the direct conversion of olefins to alcohols.[144] Intermediate separation and purification steps are obsolete.

Over time, several homogeneous catalytic systems based on rhodium in combination with phosphorus ligands have been investigated for the reductive hydroformylation with limited success.[100] Even though it seems that rhodium/phosphorus-based catalysts are not cut out for this reaction, the scientific community does seem to find it hard to deviate from them. As an alternative, homogeneous rhodium catalysts in combination with tertiary amines have shown an enhanced hydrogenation activity for said reaction. Although only few examples are reported in literature and the activity of those systems is still comparatively low, they offer a mostly undiscovered potential.[110,112–114] Additionally, tertiary amines do not suffer certain disadvantages of phosphorus-based ligands, like their vulnerability towards oxygenation or thermal decomposition.

In the first half of this work, the reductive hydroformylation of middle to long chain olefins using rhodium in combination with tertiary amines as catalysts shall be investigated. The goal is to gain a deeper understanding of those catalytic systems in terms of crucial reaction parameters for the hydrogenation activity and how the tertiary amine influences the formation of molecular rhodium species. Based on this information, a catalytic system, expressing an enhanced catalytic activity and selectivity, shall be developed. Finally, as the aim of this work is to give an outlook for potential industrial processes, a strategy for the recycling of those novel rhodium/amine catalysts shall be investigated.

The goal in this first approach is to highlight the potential of those catalytic systems for future processes envisioned for the production of medium to long chain alcohols.

As the second approach, a tandem catalytic system to synthesize alcohols directly from synthesis gas, by combining a heterogeneous Fischer-Tropsch catalyst with homogeneous reductive hydroformylation catalyst shall be investigated (Figure 18, upper pathway).

While the previously described attempt to produce alcohols directly from olefins already offers a significant improvement to current two-step processes, the direct synthesis of alcohols from synthesis gas is a long held dream in Fischer-Tropsch research.[139] Since this approach is highly innovative, the first challenge will be to find two different catalysts which are able to be catalytically active under the same reaction conditions. After that, fundamental understanding

of those kind of reaction systems must be gathered by answering questions like: How do the different catalysts interact with each other? Are the two catalysts stable over longer periods of time? And how can the selectivity of those catalytic systems be influenced? Gaining insights to those questions will be important to develop a tandem catalytic system, which is able to produce alcohol/paraffin mixtures from synthesis gas in high efficiency and whith a high and flexibile selectivity towards alcohols.

Although this approach poses many challenges, it would not only make medium- to long-chain alcohols easily accessible directly from synthesis gas, but would result in alcohol/paraffin mixtures which represent potential diesel fuel substitutes after very little downstream processing.

4 Results and Discussion

In this work two different approaches for the tandem catalytic synthesis of middle to long chain alcohols are described. The first two chapters will deal with the reductive hydroformylation of linear middle to long chain olefins to alcohols using novel rhodium/amine catalysts. Alcohols are gaining increasing attention as valuable fuel additives which inhibit soot and CO_2 emissions. The reductive hydroformylation to directly convert olefins to alcohols has the potential be a key technology in future BTL and PTX concepts to produce synthetic fuels.

Rhodium catalysts in combination with tertiary amines show enhanced hydrogenation activity for carbonyl double bonds and have been investigated as catalysts for this reaction. To show the potential of these kind of catalysts, the goal is not only to investigate and develop a catalytic system but to gain an understanding of the reaction on a molecular level and offer an effective concept for the recycling of the rhodium/amine catalyst (Figure 19).

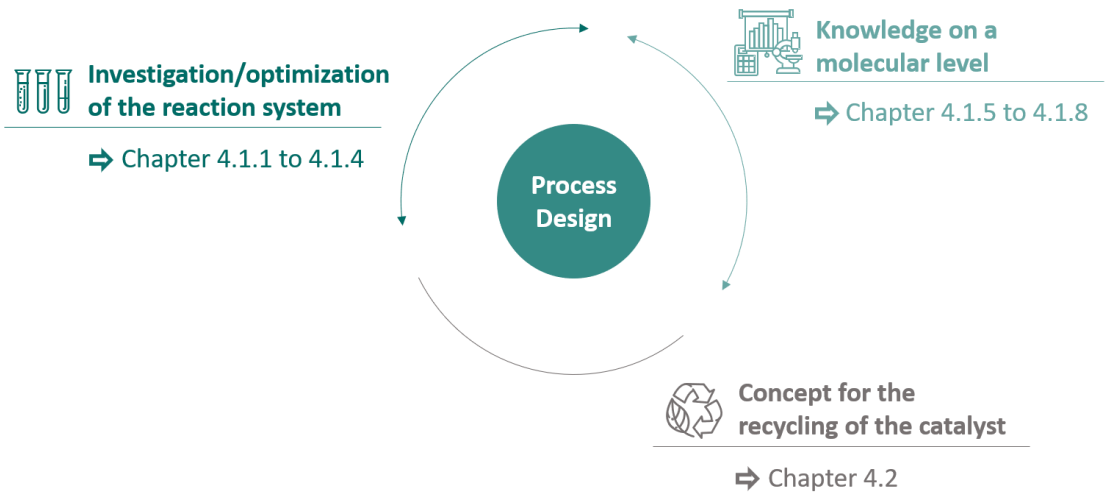

Figure 19: A concept for the development of an integrated process for the reductive hydroformylation of middle to long chain olefins using rhodium/amine catalysts.

4.1 Development and Optimization of a Reaction System for the Reductive Hydroformylation of 1-Octene using Rhodium/Amine Catalysts

At the start of the investigation of those catalytic systems, the reductive hydroformylation of 1-octene as a model substrate for middle to long chain alcohols was investigated. 1-Octene can be described as a medium chain alkene in the context of a typical chain length distribution of Fischer-Tropsch synthesis and similar alcohols have been described as possible fuel additives in literature.[22,23]

A general reaction scheme for the reductive hydroformylation of 1-octene, describing possible products and side products is displayed in Figure 20.

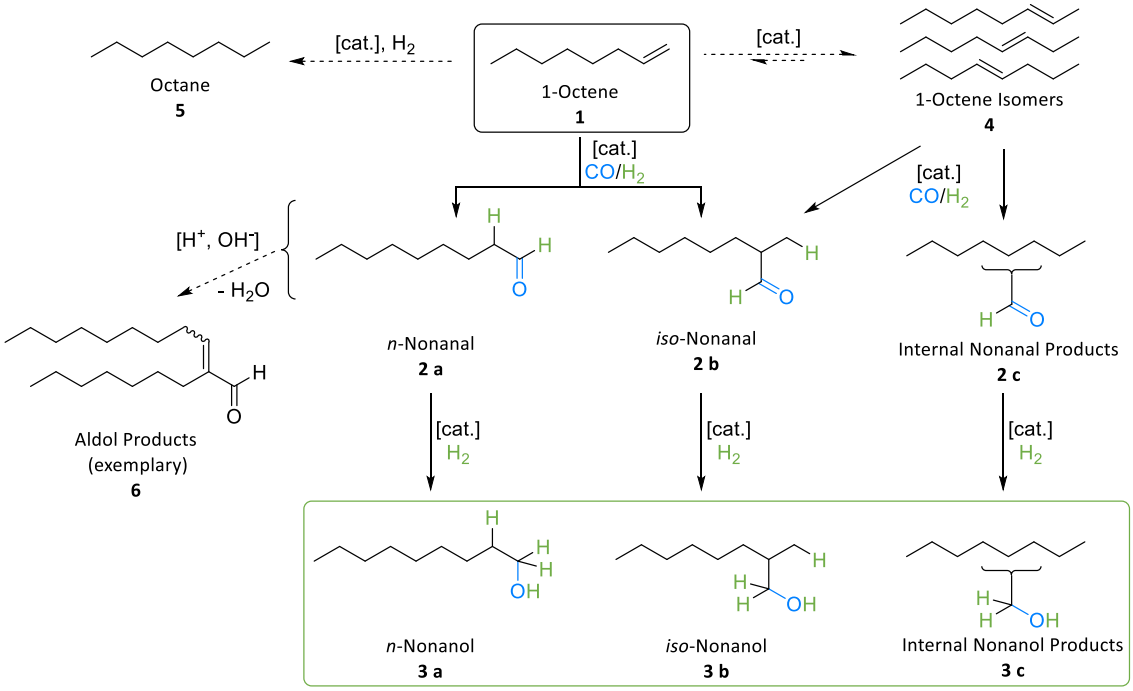

Figure 20: Reaction network for the reductive hydroformylation of 1-octene. Target products (alcohols) are marked in the green rectangle.

Starting from 1-Octene (1), the desired reaction is the hydroformylation to aldehydes (**2**). During the hydroformylation step, the formation of the linear (**2 a**) and branched (**2 b**) product is possible. The generation of the different products is determined during the addition of the alkene in the catalytic cycle (see chapter 2.3). One of the major parameters determining the selectivity between linear and branched products is the steric environment at the metal center in the active complex, which can be controlled by the geometry of the coordinating ligands.[26]

The catalytic hydrogenation of the intermediate aldehydes leads to the formation of linear (**3 a**) and branched alcohols (**3 b**) as the desired products. Controlling the stereoselectivity of the reaction towards high shares of linear aldehydes is often desired in industrial processes. As the

main application purpose for this system is the generation of alcohols as fuel additives, the regioselectivity is of minor importance and will not be discussed in detail in the following.

Commonly, the isomerization of the initial terminal 1-alkene to form isomers with an internal double bond (**5**) is observed. Although it is an equilibrium, the reverse reaction of isomers to the 1-alkene is less favored. Therefore the equilibrium lies on the side of internal akenes.[98] Internal alkenes can also undergo hydroformylation, which results in different internal hydroformylation products depending on the initial alkene (**2 b, 2 c**). As the hydroformylation of internal isomers and the reverse reaction of isomers to 1-octene is possible, they are not considered lost for the reaction but can be regarded as reactands themselves.

It should be noted that internal nonanal (**2 c**) and nonanol products (**3 c**), derived from the hydroformylation of internal octenes, are also called branched products of the reaction. In the following the term branched aldehyde/alcohol refers to the 1-methyl-aldehyde/alcohol product though (**2 b** and **3 b**), unless otherwise mentioned. Furthermore, for most experiments only the yield of **2 a+b** and **3 a+b** is given since further branched products (**2 c** and **3 c**) were not observed.

Besides the isomerization of the double bond, the hydrogenation to the saturated alkene (**4**) is possible. The hydrogenation of the alkene is often considered one of the major challenges of the reductive hydroformylation reaction. In general, the hydrogenation activity is required for the hydrogenation of aldehydes to alcohols but, on the down side, hydrogenation of the substrate to alkanes leads to side products which are and lost for any further reaction. A high selectivity for the hydrogenation of carbonyl double bonds is the most important parameter determining the overall selectivity of the reaction towards alcohols.

Finally, in the presence of Brønsted acids or bases, the formation of different aldol products is possible (exemplary product **6**). Since this has never occurred under the applied conditions, this side reaction is considered irrelevant for the reaction systems which will be discussed in the following.

All experiments have been conducted in 20 mL autoclave reactors if not stated otherwise. A detailed experimental procedure for high pressure experiments conducted in 10 mL to 20 mL autoclave reactors can be found in the experimental section in chapter 6.2.1. Quantitative analysis of the reaction compositions was conducted *via* GC-FID as discussed in chapter 6.3.1. For qualitative assignment of products, a combination of GC-MS and ^{1}H-NMR is used (chapter 6.3.1). All experiments displayed in graphical form can be found tabulated in the Appendix (chapter 10.2).

Parts of this chapter are published in:

T. Rösler; K. R. Ehmann; K. Köhnke; M. Leutzsch; N. Wessel; A. J. Vorholt; W. Leitner, “Reductive Hydroformylation with a Selective and Highly Active Rhodium Amine System”, *J. Catal.* **2021**, *400*, 234–243. DOI: 10.1016/j.jcat.2021.06.001.

Whereas authors contributed as follows (using CRediT standardized contribution descriptions):

T. Rösler:	Writing – original draft, investigation, methodology
K. Ehmann:	Investigation (masters thesis), methodology
K. Köhnke:	Investigation (DFT calculation)
M. Leutzsch:	Investigation (^{13}C- and *in situ* ^{1}H-NMR spectroscopy)
N. Wessel:	Investigation (*in situ* IR-spectroscopy)
A. J. Vorholt:	Methodology, supervision, writing – review and editing
W. Leitner:	Conceptualization, supervision, writing – review and editing

4.1.1 Screening of Different Rhodium- and Ruthenium-Based Catalyst Precursors

As a first step, a suitable combination of a catalyst precursor in combination with triethylamine as the tertiary amine additive has been investigated. Triethylamine was chosen as the amine additive during the first investigations because it is commonly used in literature about the rhodium/amine catalyzed reductive hydroformylation. Several rhodium precursors and two ruthenium precursors (for comparison) have been tested during the reductive hydroformylation of 1-octene.

Other reaction conditions have been chosen based on a publication by ALPER ET AL, describing the reductive hydroformylation of styrene with a rhodium/amine catalyst.[112] The reaction conditions are summarized in Table 1.

Table 1: Initial reaction parameters for investigation of the reductive hydroformylation with the rhodium/tertiary amine catalysts.

Parameter	
Educt	1-Octen (2,0 mmol)
Catalyst Concentration	2 mol%
Amine	NEt_3 (0,2 mmol)
Metal:Amine	1:5
Synthesis Gas	30 bar (CO/H_2 1:1)
Temperature	60 °C
Reaktion Time	8 h
Solvent	MeCN (2.34 g)

The results for six rhodium (I), one rhodium (III) and two ruthenium (II) precursors are displayed in Figure 21. The nature of the applied precursor shows a strong influence on the catalytic activity and selectivity of the reaction. When using the Rh (I) precursors $[Rh(COD)Cl]_2$ (**I**), $[RhCl(nbd)]_2$ (**II**), $[Rh(COD)_2]SbF_6$ (**III**) and $[Rh(acac)(CO)_2]$ (**VI**) alcohol yields (∑ **3 a** + **3 b**) between 81% and 64% are received, with $[RhCl(nbd)]_2$ (**II**) showing the highest activity. In comparison, $[Rh(C_2H_4)_2Cl]_2$ (**V**) and $[Rh(CO)_2Cl]_2$ (**VI**) show a high hydrogenation activity for the olefinic double bond and alkane side products (**4**) are dominating with yields of 35% and 30% respectively. The Rh(III) salt $RhCl_3 \cdot 3\ H_2O$ does seem to be active in the hydroformylation reaction, with 21% of aldehyde products obtained during the reaction, but rather unreactive for the hydrogenation step with only 3% alcohols gained during the reaction. A possible explanation for the low activity of the Rh(III) precursor compared to the tested Rh (I) precursors is that a reduction of Rh(III) to Rh(I) would be necessary prior to the the hydroformylation reaction (see chapter 2.3).

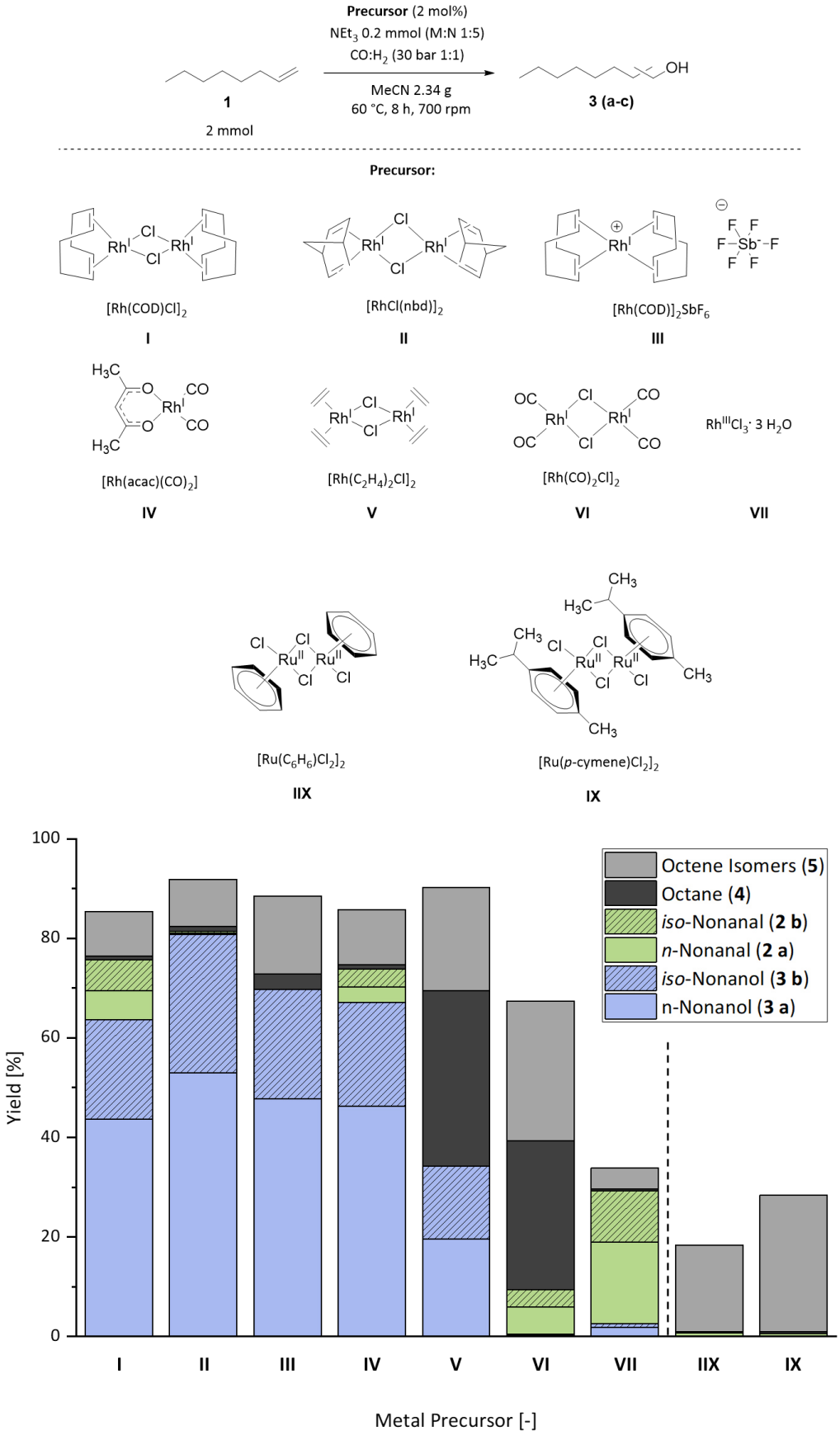

Figure 21: Screening of rhodium (**I - VII**) and ruthenium (**IIX – IX**) precursors in combination with triethylamine for the reductive hydroformylation of 1-octene. Quantitative/qualitative determination of product yields *via* GC-FID/GC-MS.

The two tested ruthenium precursors are both significantly less active for the hydroformylation reaction under the chosen reaction conditions and no products are received in significant amounts. While $[RhCl(nbd)]_2$ showed the highest activity, chloride is known to be corrosive and therefore not optimal considering the aim of developing processes with potential industrial application. $[Rh(acac)(CO)_2]$ shows a similar activity and was therefore chosen as the rhodium precursor for following studies.

During those first experiments, a comparatively low catalytic activity with a maximum Turn Over Frequency (TOF, see chapter 2.2) of 5 h^{-1} in case of $[RhCl(nbd)]_2$ was achieved. The goal during the following experiments was to increase the catalytic activity while maintaining a high selectivity towards alcohols. For this, the identification of important parameters and constraints when using rhodium/amine catalysts was necessary.

4.1.2 The Metal-to-Ligand Ratio as Crucial Parameter for the Hydrogenation Activity in the [Rh]/ Amine Catalyzed Reductive Hydroformylation

The ratio of the catalytic metal and the ligand coordinating to the metal center is known to significantly affect the catalytic activity and selectivity of catalyzed reactions. An excess of the ligand is usually necessary to shift the equilibrium towards coordinated catalytic species or to serve as reservoir when the ligand decomposes. On the other hand, a high excess can lead to blocking of catalytically active centers by over ligation. In scientific hydroformylation literature, using rhodium catalysts in combination with phosphorus ligands, commonly metal-to-ligand ratios between 1 to 1 and 1 to 10 are used.[26] Literature about rhodium/amine systems for the reductive hydroformylation hints that a much higher excess of the tertiary amine is needed.[112,114] A reasonable explanation is the lack of π-backbonding in the coordination of amines, which is much weaker compared to most other types of ligands and a high excess is needed to shift the equilibrium towards coordination of the amine. During the next experiments, the catalytic activity depending on the metal-to-amine ratio was investigated. Ratios between 1:2 and 1:400 have been tested (Figure 22). In general metal-to-ligand ratios above 1:5 are needed to support the hydrogenation of the aldehydes. At lower ratios of 1:2 less than 1% of alcohols (**3 a +b**) are generated, showing that almost no hydrogenation activity is observed even though aldehydes (15%, **2 a + b**) are present. Besides the severely hindered hydrogenation activity, the hydroformylation activity seems to also be reduced, with only 17% products (aldehydes and alcohols) being obtained. Furthermore, this indicates that the amine is not only involved in the formation of catalytically active species responsible for the hydrogenation, but also in the hydroformylation step.

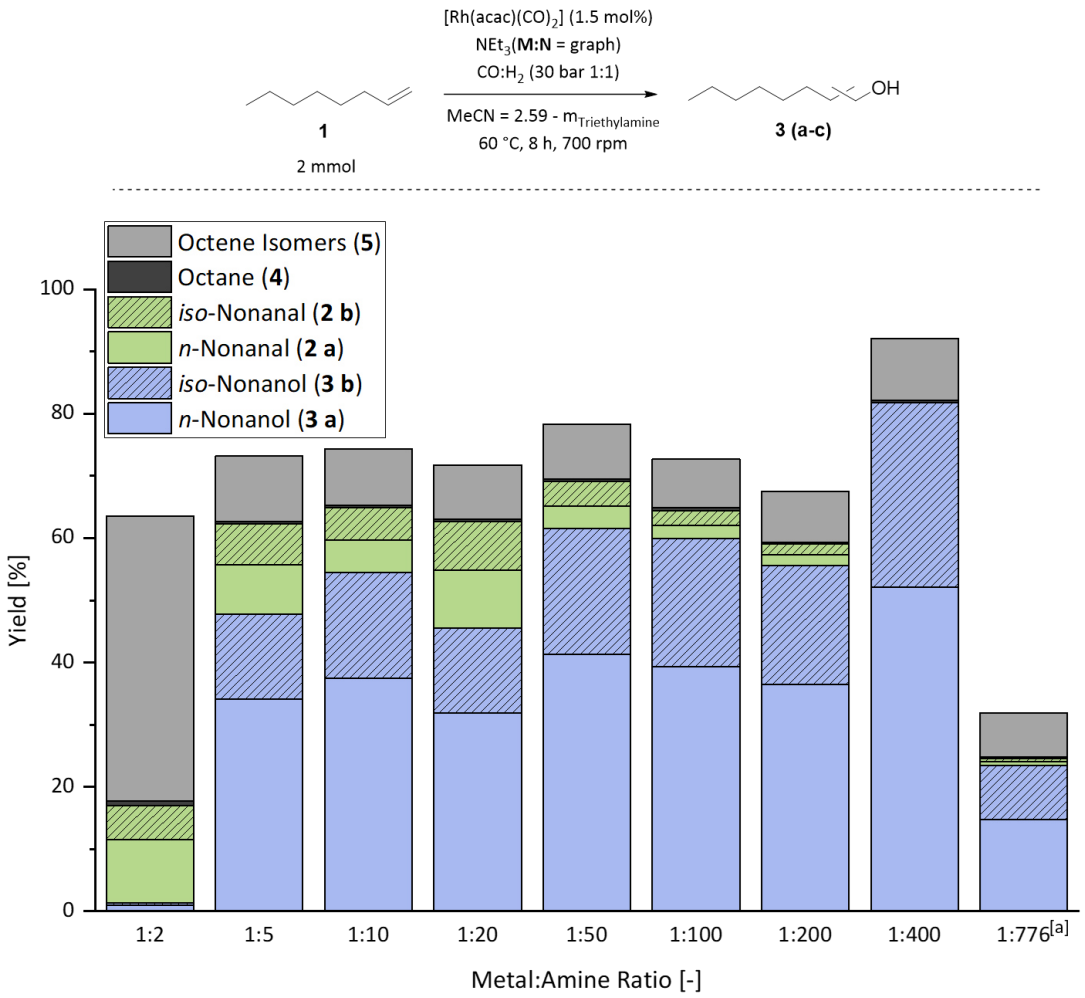

Figure 22: Investigation of the metal-to-amine ratio for the [Rh]/amine catalyzed reductive hydroformylation of 1-octene. [a]: no additional MeCN added, neat triethylamine. Quantitative/qualitative determination of product yields *via* GC-FID/GC-MS.

With metal-to-amine ratios of 1:5 to 1:20 the catalytic activity increases and alcohols are obtained as the main product (48% to 54%). Aldehyde intermediates are observed in yields between 18% and 11%. Overall, between 62% and 64% of the desired reaction products are formed. At even higher ratios above 1:50, a slight increase in hydrogenation activity can be observed. The highest selectivity towards alcohols is achieved at a metal-to-ligand ratio of 1:400. At this point 82% alcohols are generated and aldehyde intermediates can only be detected in traces, indicating a very high hydrogenation activity. At the same time less than 1% alkane side products (**4**) are observed, proving that the reaction is highly selective towards the hydrogenation of carbonyl double bonds. The only notable side products are alkene isomers (10%, **5**). At a ratio of 1:400 the concentration of triethylamine in solution is roughly about the same as the solvent acetonitrile. At this point, it must be considered if the metal-to-ligand ratio or the absolute concentration of the amine in solution is the determining factor, responsible for the increase of the hydrogenation activity. In fact, during prior experiments regarding the catalyst concentration when using a metal-to-ligand ratio of 1:5, it was not possible to lower the

catalyst concentration below 1.5 mol% without observing a heavy drop in catalytic activity (Appendix Table A 16). After adjusting the metal-to-amine ratio to 1:100, the drop in catalytic activity was not observed anymore and the catalyst concentration could be decreased below 1.5 mol% (Appendix Table A 16). This hints that the initial drop was merely an effect of the low absolute amine concentration as a result of lowering the total metal loading and that the total concentration of amine in solution is more important than the actual metal-to-ligand ratio. The yield-time-profile with such a high metal-to-ligand ratio of 1 to 400 show that already after two hours 66% alcohols (**3 a+b**) are generated (Figure 23).

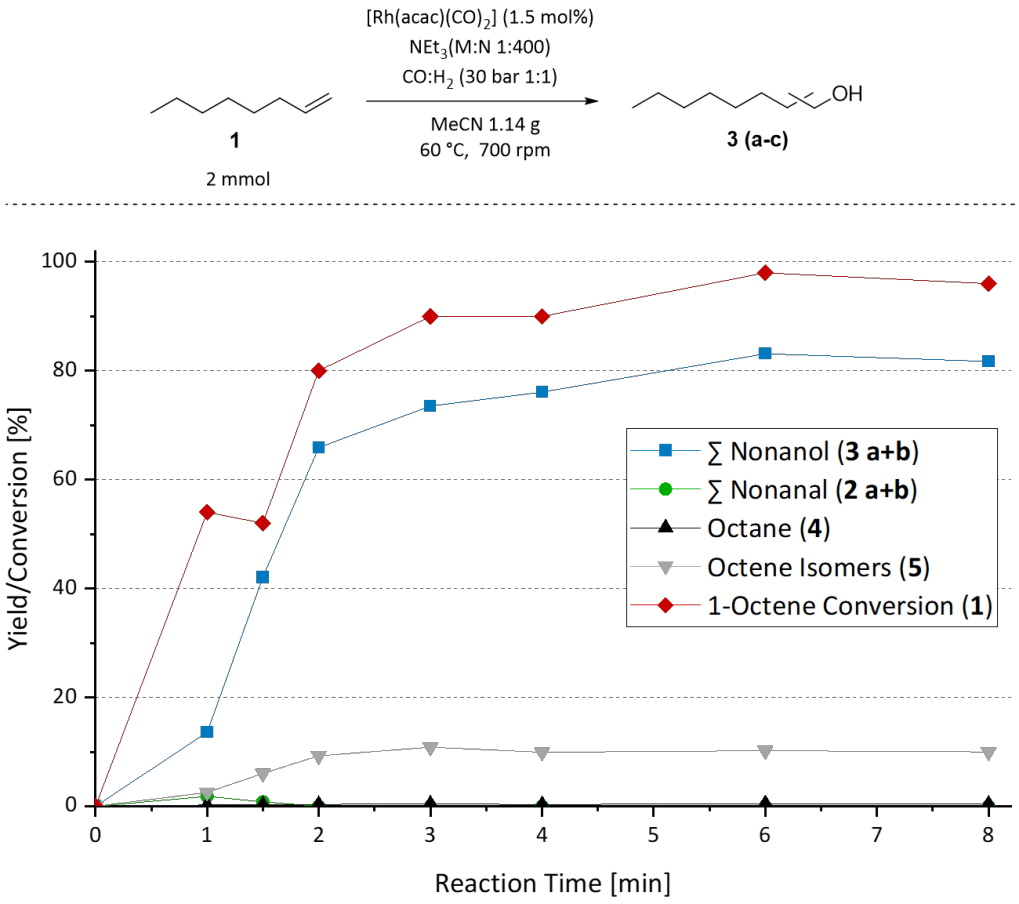

Figure 23: Yield-time plot for the reductive hydroformylation of 1-octene at high amine concentrations with a metal-to-ligand ratio of 1:400. Connections between dots are for visualization purposes and do not represent experimental data. Quantitative/qualitative determination of product yields *via* GC-FID/GC-MS.

This translates to a catalytic activity with a TOF of 22 h^{-1} and represents a four-fold increase to the initially observed catalytic activity. More importantly, aldehyde intermediates could not be observed in significant amounts at any point in time during the reaction, suggesting a very high hydrogenation activity when using such high amine concentrations. At this point, the hydroformylation seems to be the rate determining reaction.

4.1.3 Influence of the Carbon Monoxide Partial Pressure on the [Rh]/Amine Catalyzed Reductive Hydroformylation

When investigating the effect of the total synthesis gas pressure and the ratio of hydrogen and carbon monoxide on the activity of the reaction, a strong dependency of the hydrogenation activity and the hydroformylation activity on the carbon monoxide partial pressure was found. Several different ratios of synthesis gas pressure ranging from $CO:H_2$ 2:1 to 1:5 and total pressures ranging from 15 bar to 60 bar have been tested (Figure 24).

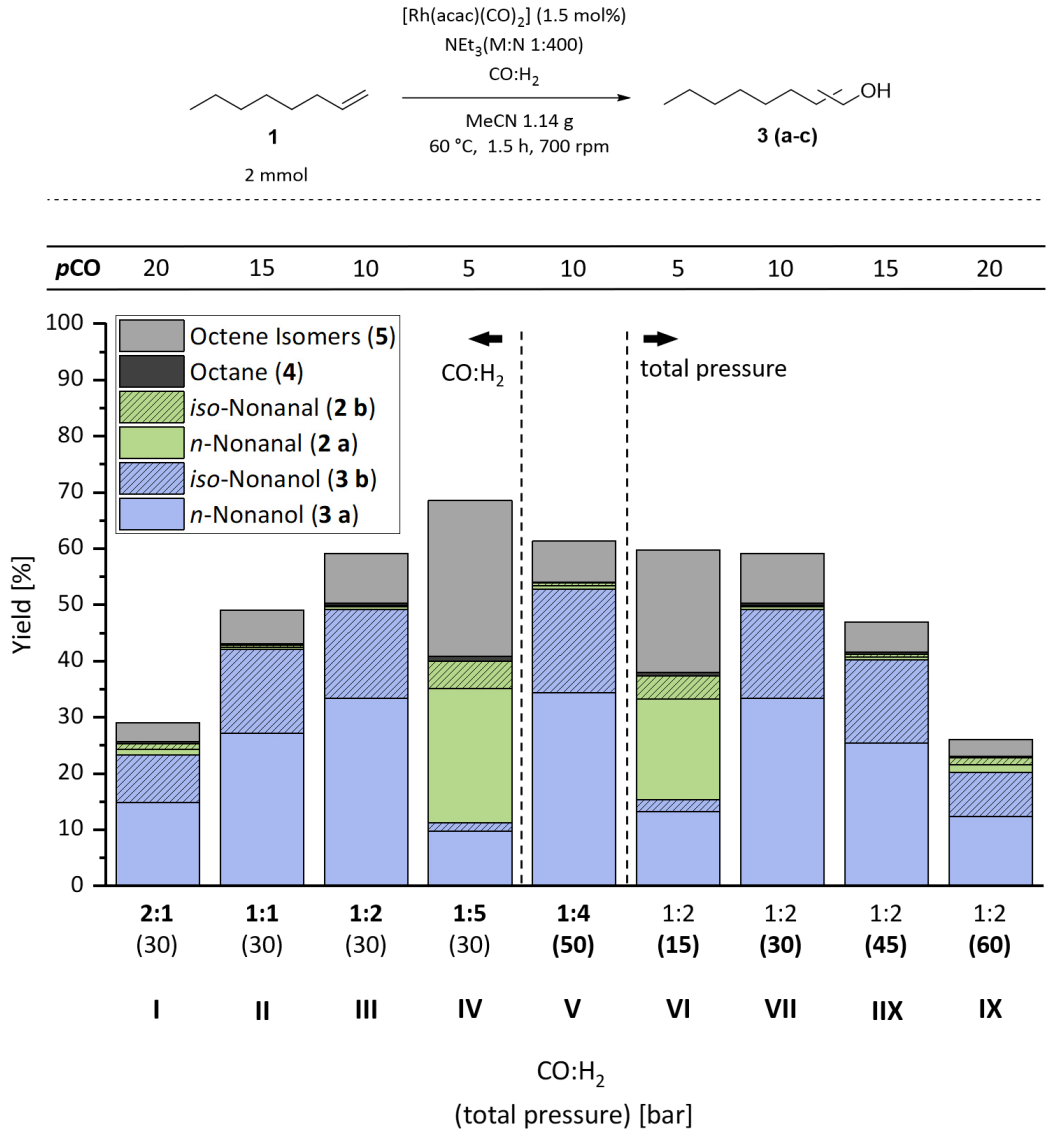

Figure 24: Influence of the variation of the carbon monoxide and hydrogen partial pressure ratio and the total pressure on the catalytic activity of the reductive hydroformylation of 1-octene using rhodium/tertiary amine catalysts. Quantitative/qualitative determination of product yields *via* GC-FID/GC-MS.

The highest catalytic activity, with an alcohol yield of 53%, was observed when using a carbon monoxide partial pressure of 10 bars (**III** and **VII**). The hydrogen partial pressure does not seem to influence the reaction significantly. Increasing the hydrogen partial pressure from 20 bar

(**III**, $Y_{alc.}$ = 47%) to 40 bar (**V**, $Y_{alc.}$ = 53%) increases the alcohol yield by 5%. In contrast, increasing the carbon monoxide partial pressure from 10 bar to 20 bar (**I** and **IX**) decreases the hydroformylation activity significantly and only about half the initial hydroformylation products (combined yield of aldehydes and alcohols) are formed. Furthermore, it does not matter if the synthesis gas ratio is increased (**I**; $Y_{alc.}$ = 22%) or if the total pressure is increased (**IX**, $Y_{alc.}$ = 17%). Both cases lead to the same activity and selectivity, hinting towards the importance of the carbon monoxide partial pressure.

When decreasing the carbon monoxide partial pressure (**IV** and **VI**), mostly the hydrogenation activity is abolished, leading to 10% and 13% alcohols, respectively. Main products are aldehyde intermediates. Also, in this case the decrease of the synthesis gas ratio (**IV**) or the decrease of the total pressure (**VI**) leads to roughly the same product distribution. Since carbon monoxide is not only a reactant but is also involved in the formation of active catalytic species (see chapter 2.3), it can be assumed that the carbon monoxide partial pressure dictates the formation of the active species for the hydroformylation as well as for the hydrogenation. Even though a dependency of the catalytic activity on the pressure and synthesis gas ratio is known for hydroformylation reactions, such a strong dependency on the carbon monoxide partial pressure is remarkable. Several spectroscopic techniques have been applied to investigate the nature of the catalyst and the role of the amine for its formation. They will be discussed later in this work (chapter 4.1.5).

After investigating the influence of the pressure on the reaction, a short screening for the influence of the reaction temperature was conducted. The results of these experiments can be found in the appendix but shall not be intensively discussed here (appendix Table A 17). Increasing the reaction temperature to 100 °C showed a beneficial effect on the overall activity and the reaction temperature for the following experiments was adjusted accordingly. Furthermore, the increase of the overall activity by an adjustment of the carbon monoxide partial pressure and the reaction temperature made a decrease of the catalyst concentration from 1.5 mol% to 1 mol% possible.

4.1.4 Influence of Electronic and Steric Effects of the Amine Additive on the Catalytic Activity and Selectivity

Even though experimental findings hint towards a binding of the amine during the catalytic cycle and in literature the binding of the amine is generally assumed,[112,114] the role of the amine as ligand is not proven. Tertiary amines are weak ligands and could just as well act as a base or be involved in outer sphere mechanisms such as supporting the hydrogen cleavage.

An important parameter for the reaction system, which at the same time could shine some light on the role of the amine is the nature of the amine itself. Commonly, a strong dependency on the selectivity and activity is observed for homogeneous transition metal catalyzed reactions depending on the electronic and steric properties of the ligands binding to the metal center.[98,145]

To systematically investigate the effect of changing the electronic and steric properties of the amine on the reaction, thirteen different tertiary amines have been tested as additive for the reductive hydroformylation of 1-octene using [Rh(acac)$(CO)_2$] as catalyst precursor (Figure 26).

For the selection of the amines a wide variety of different functional groups was chosen. To classify the electronic properties of phosphorus type ligands, the Tolman-Electronic-Parameter (TEP) is often used in literature.[146,147] For the TEP, the σ-bonding and π-backbonding capabilities are estimated by determining the frequency of CO vibrations of a [Ni$(CO)_3$L] complex with L being the ligand of interest.[148,149] In the case of tertiary amines, the basicity can be used as a good approximation for the electronic properties since basically no π-backbonding has to be considered and the basicity can be used as a descriptor for the σ-donor capacity. The pK_a values for most amines can be found in literature. For *N*,*N*,*N*',*N*'-tetramethyl-1,4-butandiamin the pK_a was determined *via* acid titration instead. It should be noted that the pK_a is usually given in water and can slightly differ in other solvents.

Concerning the steric properties, the cone angle determined from computational optimized structures *via* a Mathematica tool developed by ALLEN and his group specifically for such cases is used. An example for this is displayed Figure 25.[146]

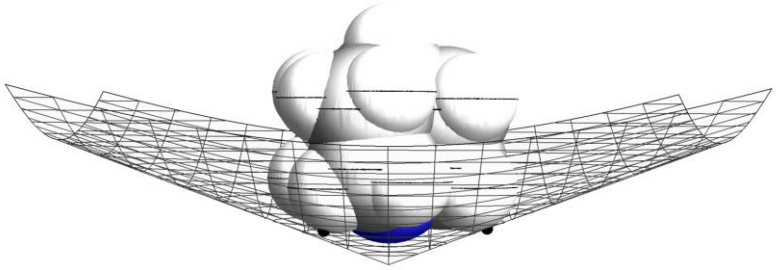

Figure 25: Cone angle determined from the computationally optimized structure of quinucloidine binding to a [Ni$(CO)_3$L] complex with L = quinuclidine. The central metal atom is located at the intersect of the plane. The plane is spanned between the central atom and the intersection points (small balck dots) with outer-most edges of the van der Waals spheres of the ligand.

The cone angle is defined as the angle between the central metal atom and the two outer-most edges of the van der Waals spheres of the ligand atoms. To better compare calculated angles with related Tolman-Angles for phosphorus-type ligands, the optimized structures of the amine binding to a $[Ni(CO)_3L]$ complex ($[Ni(CO)_2(L\cap L)]$ for bidentate ligands) is used. A comparison of the calculated cone angles is in accordance with the few examples known in literature for cone angles of tertiary amine ligands (Table 2).

Table 2: Comparison of cone angles for tertiary amines determined by the method described above and cone angles described in literature for tertiary amines binding to a bis(dimethylphosphino)ethan)methylpalladium(II)-cation.[150]

Entry	Amine	Cone-angle (this work) [°]	Cone-angle (literature) [°][150]
2.1	Trimethylamine	132	132
2.2	Dimethylethylamine	136	132
2.3	Methyldiethylamine	142	145
2.4	Triethylamine	149	150

Detailed informations about the DFT (Density-Functional-Theory) calculations used during the optimization and coordinate tables of the resulting complexes can be found in the Appendix 6.2.2. Cone angles for amines containing two amine functionalities have been calculated as bidentate ligands except when the optimization indicated monodentate binding (*N*,*N*,*N*',*N*'-Tetramethyl-1,3-phenylendiamine). It should be noted that later calculations of the energy density at exemplary rhodium/amine complexes suggest that bidentate binding of amines is unlikely (see chapter 4.1.5). In Figure 26 the calculated cone angles are plotted against the basicity of the tested amines. The color indicates the amount of alcohol products for the respective amine when it is used as additive in the reductive hydroformylation of 1-octene.

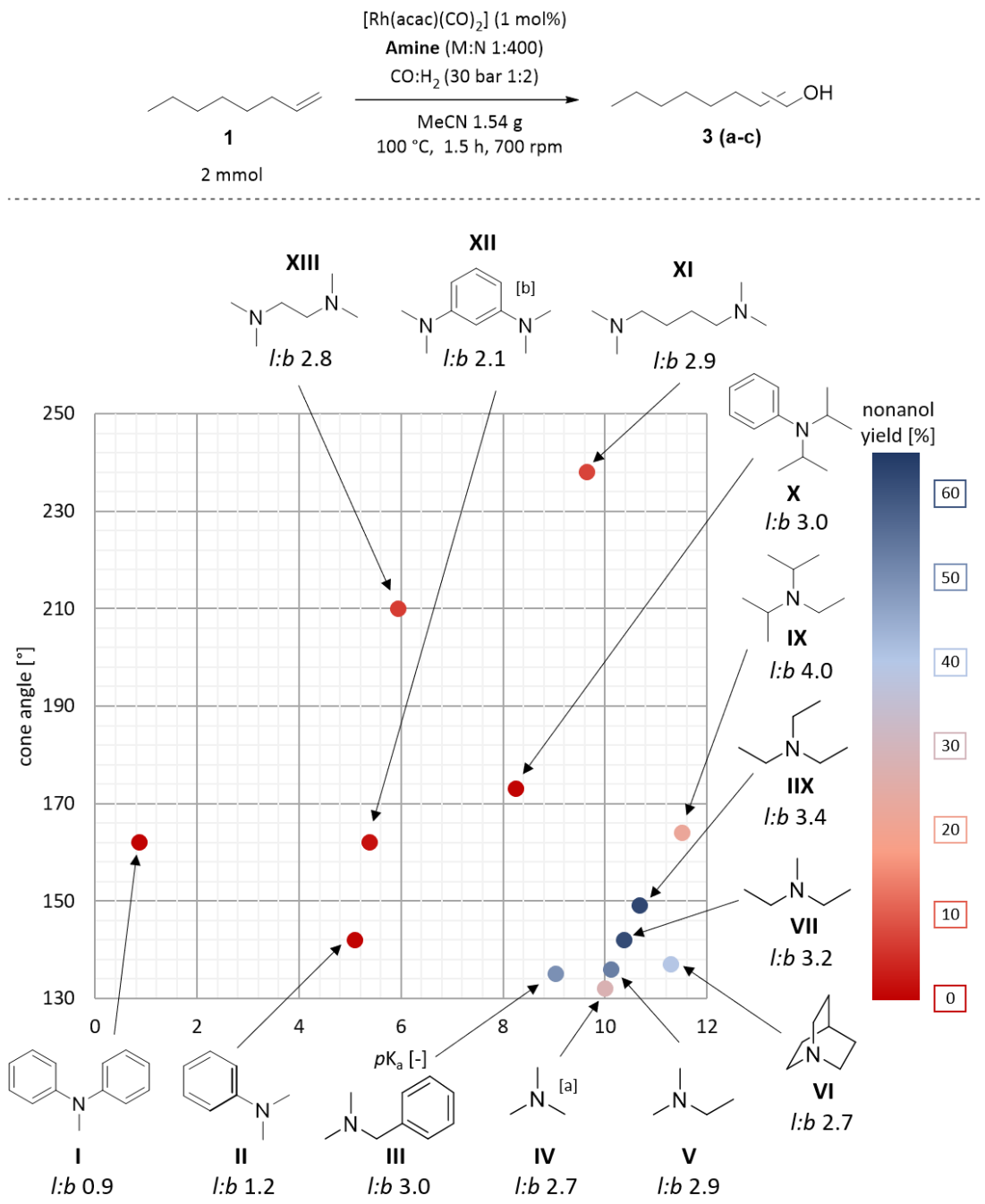

Figure 26: Catalytic activity of thirteen different amines in the reductive hydroformylation of 1-octene plotted against their electronic and steric properties, represented by their pK_a value and the calculated cone angle upon binding to a $[Ni(CO)_3L]$ complex. Adapted from RÖSLER.[151] [a] Metal-to-amine ratio of 1:250 was used [b] The amine is binding as a monodentate ligand. Quantitative/qualitative determination of product yields *via* GC-FID/GC-MS.

The smallest cone angle of 132° is achieved for trimethylamine (**IV**). A stepwise exchange of methyl groups with ethyl groups increases the cone angle from 132° to 149° for triethylamine (**IIX**) while the pK_a is not significantly influenced (10.0 for trimethylamine, 10.7 for triethylamine). When increasing the cone angle, the alcohol yield increases from 28% for trimethylamine (**IV**) to 62% for triethylamine (**IIX**) and diethylmethylamine (**VII**). Interstingly, a stepwise increase of the linear-to-branched ratio, correlating to the increase of the cone angle, can be observed going from trimethylamine (*l:b* 2.7) to triethylamine (*l:b* 3.4). This influence of

the steric properties of the amine on the linear-to-branched ratio is a strong indicator that the amine is involved during the olefin insertion step during the catalytic cycle. This trend can be continued at the example of diisopropylethylamine (**IX**). The sterically demanding isopropyl groups lead to a comparatively wide cone angle of 164°. While higher cone angles do not seem to favor the catalytic activity and only 22% alcohols are generated, the linear-to-branched ratio increases to 4.0. Plotting the cone angle against the linear-to-branched ratio of those five alkylamines shows a linear correlation between the cone angle and linear-to-branched ratio (Figure 27).

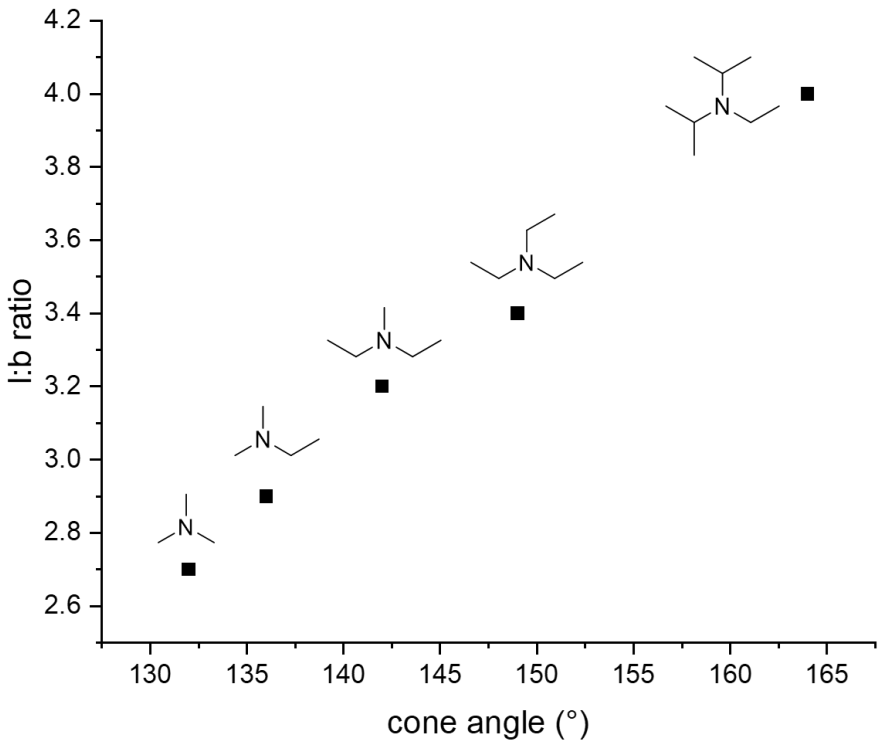

Figure 27: linear-to-branched ratio correlating with the cone angle for several alkylamines in the reductive hydroformylation of 1-octene.

The bidentate amines tetramethylbutanediamine (**XI**) and tetramethylethylenediamine (**XIII**) do not follow this trend and their linear-to-branched ratio is comparable to that of dimethylethylamine (**V**), further suggesting that those amines indeed bind as monodentate ligands and the calculated cone angles are overestimated.

Adding phenyl groups instead of alkyl groups significantly decreases the basicity of the amine. Compared to trimethylamine (**IV**) with a pK_a of 10.0, dimethylaniline (**II**) only has a pK_a of 5.1 and methyldiphenylamine (**I**) a pK_a of 0.86. At this point the amine can hardly be considered bases and it is likely that the low basicity, and therefore weak sigma-donor capacity, prevents binding of the amine. This is supported by the fact that no hydrogenation activity is observed in

conjunction with a low hydroformylation activity (19% and 31% aldehydes respectively). The low *l:b* ratio of around 1.2 suggests the hydroformylation by unmodified rhodium species.

Overall, the basicity and the cone angle seem to play a vital role for the activity of the catalyst in the reductive hydroformylation. Best results with an alcohol yield up to 62% have been achieved for alkylamines with a pK_a between 10 and 11 and a cone angle between 135° and 150°. The dependency of the linear-to-branched ratio on the cone angle is an indicator on the binding of the amine during the catalytic cycle.

In addition to testing the influence of different trialkylamine ligands on the catalytic activity of the reductive hydroformylation, the combination of trialkylamine ligands with several phosphorus ligands in deficit concentrations was tested. The idea was to form rhodium phosphorus species in low concentrations to boost the hydroformylation activity. It was found though that the addition of different phosphorus ligands in all tested ranges of concentration severely hinders the hydrogenation activity and does not significantly enhance the hydroformylation activity. The results shall not be further discussed here but can be reread in the Appendix Table A 20 and Table A 21.

4.1.5 Characterization of Catalytic Rhodium Species Formed in the Presence of Tertiary Amines

To further investigate the role of the amine during the catalytic cycle, a combination of spectroscopic methods supported by computational determination of energetic profiles for the formation of rhodium/amine complexes was used. ^{13}C-NMR, ^{103}Rh-NMR and *in situ* ^{1}H-Nuclear-Magnetic-Resonance-Spectroscopy (NMR) was used to characterize catalytic rhodium species in presence of tertiary amines while *in situ* Infra-Red-Spectroscopy (IR) helped to further investigate equilibria under reaction conditions.

A common method to characterize homogeneous catalytic species is to interpret the chemical shift of NMR active isotopes. Since in this case no phosphorus ligands are used and ^{1}H-NMR can only track comparatively unstable hydride species, the ^{13}C isotope of the carbon monoxide ligand was used to characterize catalytic rhodium species, which are formed in the presence of tertiary amines. Signals derived from carbon monoxide ligands show distinctive chemical shifts below 180 ppm which can be easily distinguished from organic carbon signals. To support the ^{13}C-NMR measurements, ^{103}Rh-NMR spectra have been recorded.

Prior to the measurement, the catalyst precursor [Rh(acac)(CO)$_2$] and triethylamine dissolved in acetonitrile have been heated under reaction conditions (100 °C, 30 bar CO:H$_2$ 1:1) for 90 minutes. After cooling, the catalyst solution is transferred into an NMR-tube under synthesis gas atmosphere (<3 bar). Because of the low natural abundance of the ^{13}C-isotope (1.1%), ^{13}C-enriched (40% ^{13}CO) synthesis gas was used during the reaction.

In Figure 28, the ^{13}C-NMR carbonyl region of the post reaction catalyst solution measured at 0 °C is displayed.

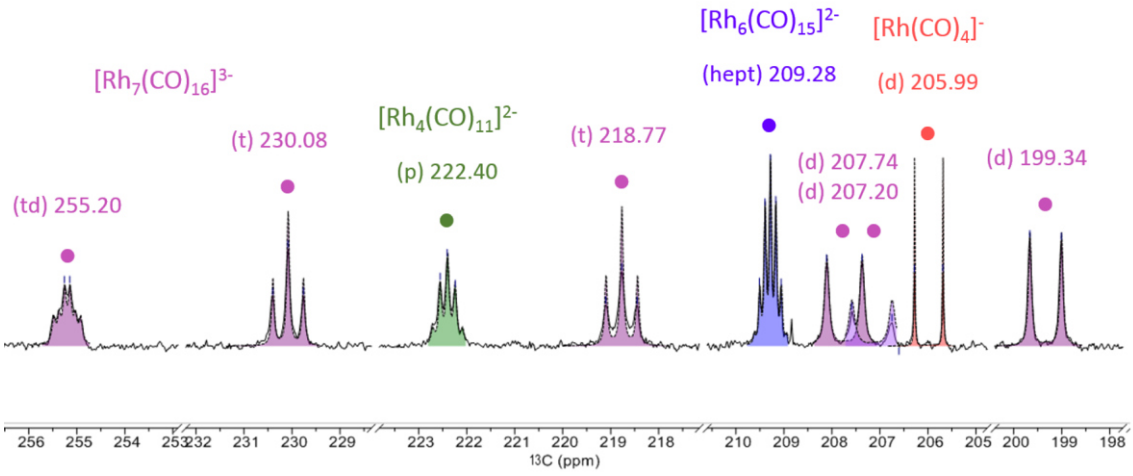

Figure 28: ^{13}C-NMR spectrum (126 MHz, d$_3$-acetonitrile, 0 °C) of a catalyst solution after heating under reaction conditions (40 mg [Rh(acac)(CO)$_2$] in 0.33 mL NEt$_3$ and 0.66 mL d$_3$-acetonitrile, 100 °C, 30 bar CO:H$_2$ 1:2, 1 h). Adapted from RÖSLER.[151] The signals of facial and bridging CO´s in [Rh$_4$(CO)$_{11}$]$^{2-}$ and [Rh$_6$(CO)$_{15}$]$^{2-}$ coincide to a multiplet because of rapid intramolecular CO exchange.[152] d = duplet, t = triplet, p = pentet, hept = heptet, td = triplet of a duplet.

In the range of 180 ppm to 260 ppm several multiplet signals can be observed. The existence of several multiplet signals with a multiplicity above 2 (e.g. a heptet at 209 ppm), indicates carbonyl ligands binding to several different rhodium centers in the form of bridging or on plane carbonyl ligands in multinuclear rhodium clusters. For further identification of the multinuclear rhodium species, 2-dimensional ^{13}C-^{103}Rh HMBC spectra have been measured (Figure 29; for further details on the NMR methods see chapter 6.3.4). To find all rhodium signals, spectra with different ^{103}Rh offsets have been measured. Furthermore, to undoubtably assign the multiplets to the different rhodium species, specific rhodium nuclei have been ^{13}C decoupled. Upon coinciding of different multiplet signals to singlets after decoupling of specific rhodium frequencies, and with the help of literature known data, four different anionic rhodium species have been identified in the catalyst solution.

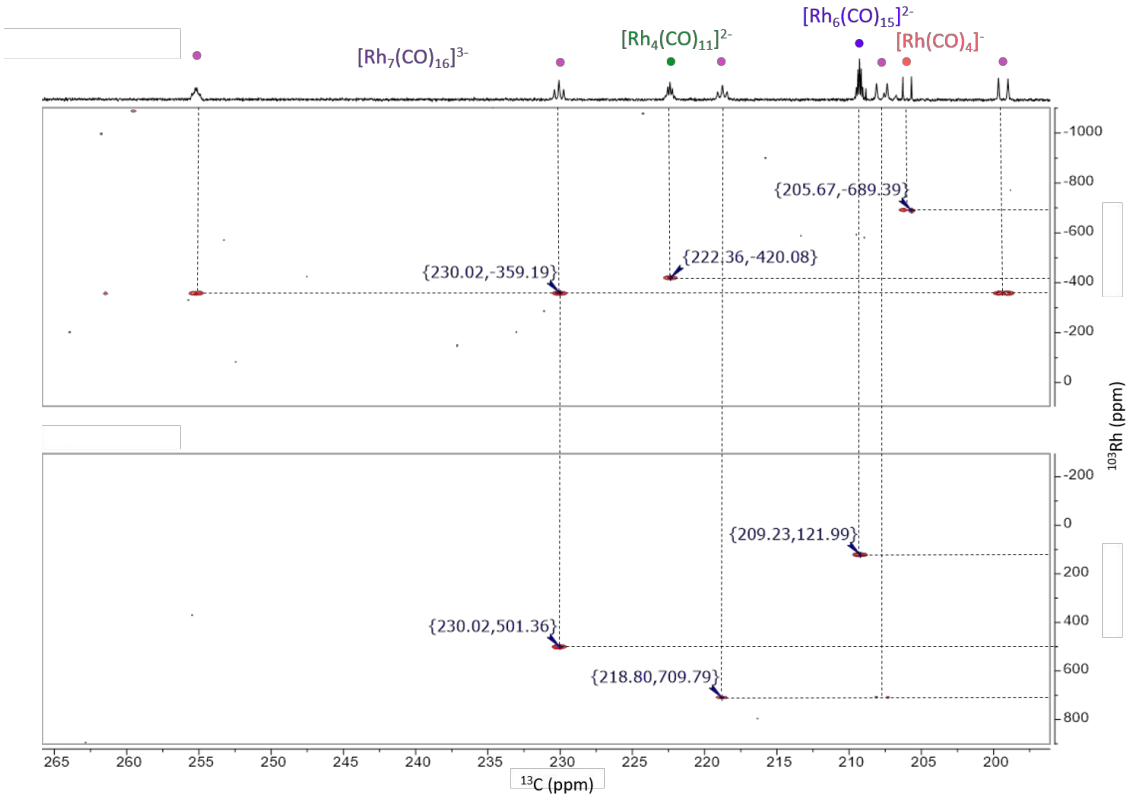

Figure 29: 2D^{13}C-^{103}Rh HMBC spectra (126 MHz (^{13}C), 16 MHz (^{103}Rh), d_3-acetonitrile, -30 °C) with two different offsets in the ^{103}Rh dimension (top: -1100 ppm to 100 ppm, bottom: -300 ppm to 900 ppm) of anionic $[Rh_7(CO)_{16}]^{3-}$, $[Rh_4(CO)_{11}]^{2-}$, $[Rh_6(CO)_{15}]^{2-}$ and $[Rh(CO)_4]^-$ species. Adapted from RÖSLER.[151] Catalyst solution (40 mg $[Rh(acac)(CO)_2]$ in 0.33 mL NEt_3 and 0.66 mL d_3-acetonitrile) after heating under reaction conditions (100 °C, 30 bar $CO:H_2$ 1:2) for one hour.

The highest concentration by far, under conditions used during the NMR measurement, was observed for the heptanuclear anionic complex $[Rh_7(CO)_{16}]^{3-}$, followed by the hexanuclear $[Rh_6(CO)_{15}]^{2-}$ complex. It should be mentioned that the hexanuclear $[Rh_6(CO)_{15}]^{2-}$ complex contains facial and bridging carbonyl ligands which coincide to a heptet signal because of rapid intramolecular CO exchange.[152] The lower nuclear complex $[Rh_4(CO)_{11}]^{2-}$ and the mono nuclear

anionic species $[Rh(CO)_4]^-$ are observed in much lower concentrations. The equilibrium favors the higher nuclear complexes under those conditions. In Table 3 the spectroscopic information about all anionic species are summarized. Since those anionic complexes are not formed in absence of the tertiary amine and since in literature tertiary amines are especially used for the formation of anionic rhodium species,[152,153] it can be concluded that ammonium cations serve as the counter ion for the stabilization of those anionic clusters in solution. Literature regarding rhodium cluster chemistry, suggests that anionic rhodium cluster species are in a delicate equilibrium with each other which can be easily shifted depending on the conditions.

Table 3: Nuclear-Magnetic-Resonance spectral information gathered about anionic rhodium species in presence of tertiary amines.[153,154] Catalyst solution (40 mg $[Rh(acac)(CO)_2]$ in 0.33 mL NEt_3 and 0.66 mL d_3-acetonitrile) after heating under reaction conditions (100 °C, 30 bar $CO:H_2$ 1:2) for one hour.

Rhodium Species	δ ^{13}C [ppm]	δ ^{103}Rh (-30°C) [ppm]	Reference
$[HNEt_3]^+[Rh(CO)_4]^-$	206.0 (d, 74.8 Hz)	-689	[153]
$[HNEt_3]_2^+[Rh_4(CO)_{11}]^{2-}$	222.40 (p, 19.6 Hz)	-420	[154]
$[HNEt_3]_2^+[Rh_6(CO)_{15}]^{2-}$	209.3 (hept, 14.2 Hz)	122	[154]
$[HNEt_3]_3^+[Rh_7(CO)_{16}]^{3-}$	255.2 (td, 28.5 Hz, 14.0 Hz) 230.1 (t, 40.0 Hz) 218.8 (t, 41.3 Hz) 207.7 (d, 92.5 Hz) 207.2 (d, 105.1 Hz) 199.3 (d, 82.5 Hz)	-359 501 710	[154]

The anchor point of this equilibrium is the mononuclear rhodium species $[Rh(CO)_4]^-$, which acts as building block for the exchange or formation of higher nuclear species.[152] A sensitive equilibrium between the different anionic species in the catalyst solution can be observed when changing the temperature during the measurement (Figure 30) or the rhodium concentration in the initial catalyst solution (Figure 31). Regarding the temperature dependency of the equilibrium, the heptanuclear complex $[Rh_7(CO)_{16}]^{3-}$ is present at all temperatures and acts as the main species at lower measurement temperatures of −30 °C and 0 °C. At −30 °C the concentration of the mononuclear rhodium species $[Rh(CO)_4]^-$ seems to be much higher than at 0 °C, while at room temperature the concentration of the mononuclear complex even seems to be so low that it is not observed anymore at all. In contrast, the formation of the hexanuclear rhodium complex $[Rh_6(CO)_{15}]^{2-}$, which is one of the most commonly observed anionic rhodium species in literature, seems to be favored at higher temperatures. At room temperature,

$[Rh_6(CO)_{15}]^{2-}$ is by far the highest concentrated among anionic species followed by $[Rh_7(CO)_{16}]^{3-}$ and $[Rh_4(CO)_{11}]^{2-}$. At temperatures above 21 °C it is not possible to track the formation of the different rhodium species using ^{13}C-NMR anymore, since rapid intra and extra molecular carbonyl exchange significantly broadens the specific ^{13}CO signals.

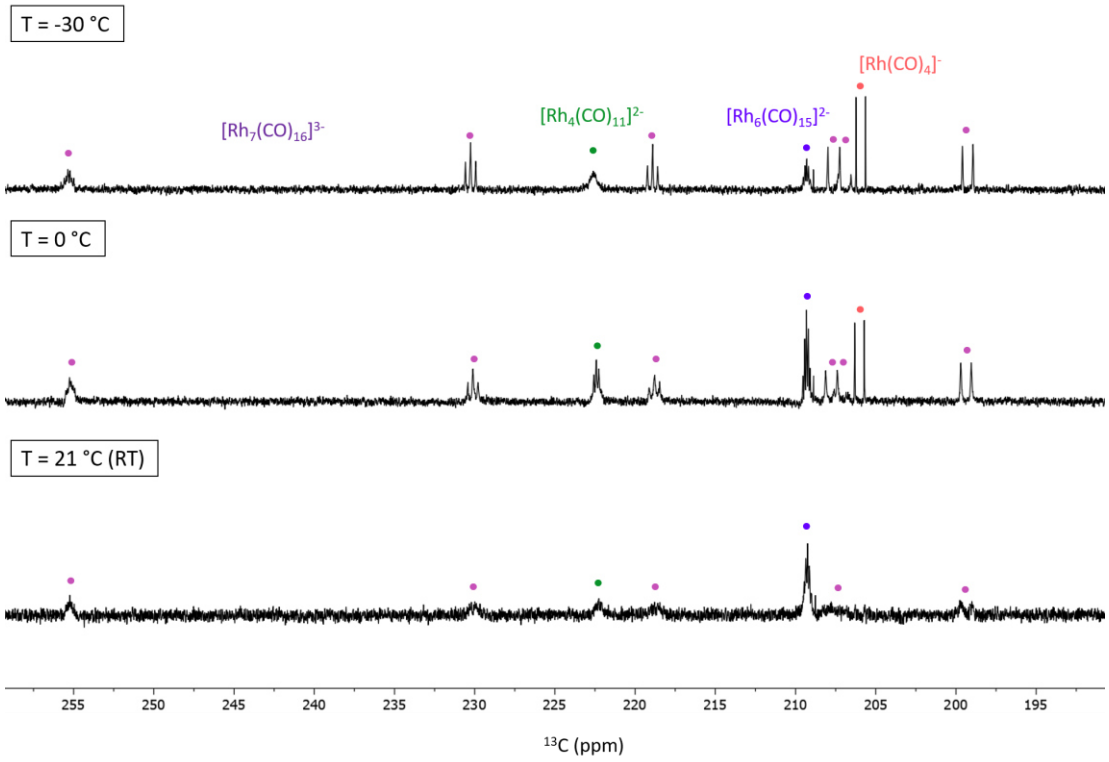

Figure 30: ^{13}C-NMR spectra (126 MHz, d_3-acetonitrile) for the equilibrium of anionic rhodium species depending on the temperature. Catalyst solution (40 mg $[Rh(acac)(CO)_2]$ in 0.33 mL NEt_3 and 0.66 mL d_3-acetonitrile) after heating under reaction conditions (100 °C, 30 bar $CO:H_2$ 1:2) for one hour.

A strong dependency can also be observed for the concentration of the rhodium precursor (Figure 31). The initial spectra were recorded using a highly concentrated catalyst solution, using 26 mg mL^{-1} $[Rh(acac)(CO)_2]$. At such high concentrations and at room temperature, $[Rh_6(CO)_{15}]^{2-}$ is the main species formed. More importantly, the mononuclear species $[Rh(CO)_4]^-$ cannot be observed at all. Using only one quarter of the rhodium concentration (6.5 mg mL^{-1}), resembling a concentration much closer to the actual composition during the reaction, significantly shifts the equilibrium especially towards the mononuclear $[Rh(CO)_4]^-$ species. While integration shows that $[Rh_6(CO)_{15}]^{2-}$ is still the main species in solution, followed by $[Rh_6(CO)_{15}]^{2-}$, the mononuclear $[Rh(CO)_4]^-$ species can be observed in high concentrations. The signal for the tetranuclear $[Rh_4(CO)_{11}]^{2-}$ species cannot be observed anymore. It is reasonable that a lower concentration of rhodium in solution favors the formation of $[Rh(CO)_4]^-$ compared to higher nuclear complexes.

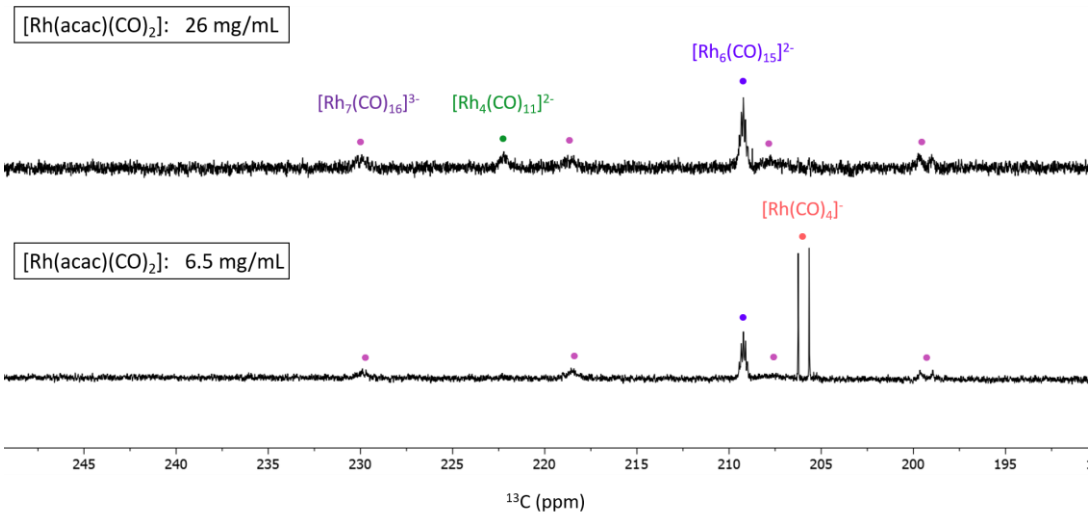

Figure 31: ^{13}C-NMR spectra (126 MHz, d_3-acetonitrile, 21 °C) for the equilibrium of anionic rhodium species depending on the rhodium concentration. Catalyst solution (40 mg/10mg $[Rh(acac)(CO)_2]$ in 0.33 mL NEt_3 and 0.66 mL d_3-acetonitrile) after heating under reaction conditions (100 °C, 30 bar $CO:H_2$ 1:2) for one hour.

Even though, further decrease of the concentration up to the actual concentration during the reaction (1.7 mg mL^{-1}) was not possible while still being able to reliably measure all ^{13}CO signals within a reasonable time.

While the ^{13}C- and ^{103}Rh-NMR spectra helped to clearly identify the formation of anionic rhodium species and proved a sensible equilibrium between the several anionic species, no spectral data concerning the equilibrium under reaction conditions, namely under high pressure synthesis gas, at high temperatures and with low catalyst concentrations can be obtained using this method.

4.1.6 Testing for the Formation of Rhodium Nanoparticles *via* Mercury Drop Test and 1,10-Phenanthroline Poisoning Experiments

After discovering the formation of high nuclear rhodium clusters in the presence of amines, the question if rhodium nanoparticles (NP's) could be responsible for the hydrogenation activity was raised. From literature it is known that amines are used as reducing agents for the formation of nanoparticles from metal salts, including rhodium.[155–157]

Since the presence of nanoparticles would severely change the interpretation of the catalytic activity of the reaction system, but would not be noticed using the analytical methods up until now (NMR spectroscopy and GC-FID/GC-MS analysis), two different sets of experiments, testing for nanoparticles, have been conducted. First, a mercury drop test was used. Mercury is known to amalgate or adsorb on the surface of nanoparticles while molecular catalysts are only affected in few cases. Although this test is not an ultimate proof for the absence of nanoparticles it is an easy quick way to give first hints. For the experiment, two droplets of liquid mercury (≈300 mg) have been added to the reaction solution prior to the reaction. No decrease in catalytic activity or selectivity was observed in comparison to the control experiment (Figure 32).

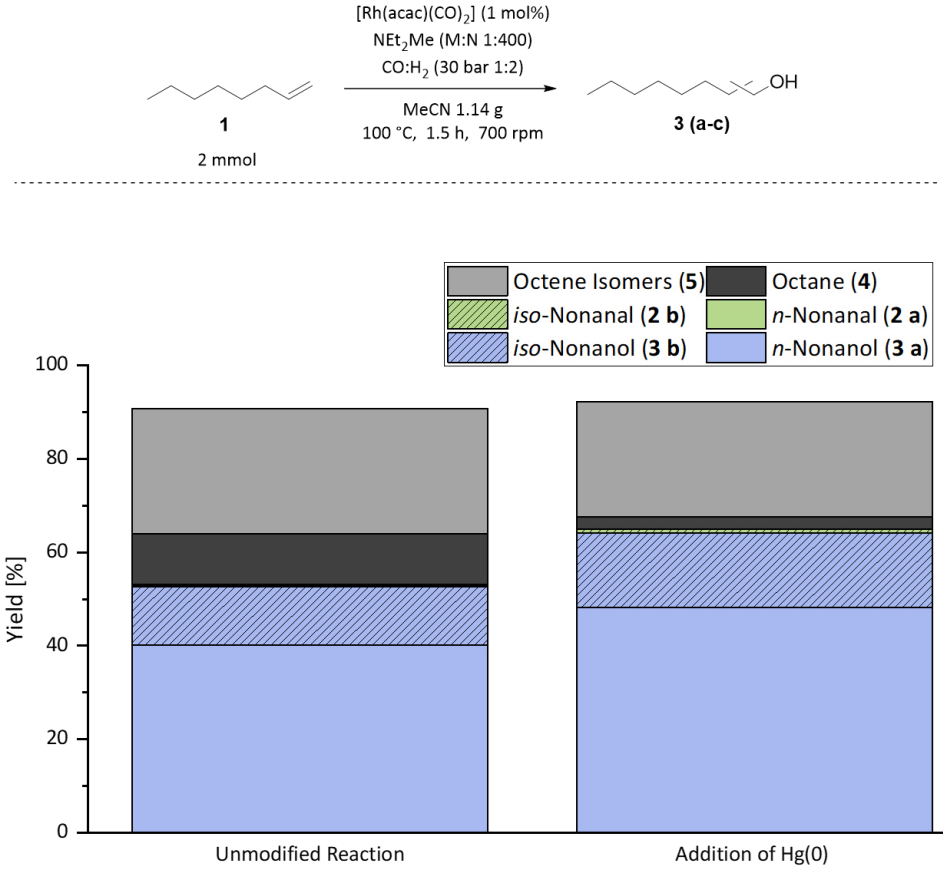

Figure 32: Influence of the addition of a few drops of Hg(0) on the catalytic activity and selectivity of the reductive hydroformylation using rhodium/tertiary amine catalysts. Quantitative/qualitative determination of product yields *via* GC-FID/GC-MS.

As a second and more qualitative test, a series of experiments were conducted in which 1,10-phenanthroline was added to the reaction. 1,10-Phenanthroline binds on the surface of nanoparticles and complexates molecular catalysts alike, poisoning them in the processes. Considering the assumption of strong binding (every 1,10-phenanthroline binds to a NP surface or a molecular rhodium species until no further binding is possible), 1,10-phenanthroline loadings should be much lower than the actual metal loading to completely poison nanoparticles (usually around 0.1-0.2 eq.) because most metal atoms are located in the core of metal nanoparticles and do not actively participate in the catalytic cycle. For molecular catalysts, the amount of poison necessary for a complete deactivation depends on the average nuclearity of the molecular metal complexes but is usually much higher than for nanoparticles. A linear dependency of the catalytic activity on the amount of poison is often not given when very low amounts of poison or very high amounts of poison are used, referred to the total amount necessary for a complete deactivation of the catalyst. Therefore, the necessary amount of catalyst poison to achieve a complete deactivation is derived by linearization of the declining catalytic activity when approximating the concentration necessary for the complete deactivation. The theoretical amount of 1,10 phenanthroline necessary for a complete deactivation can be derived from the intersection of the linearization with the x axsis. In Figure 33 the decrease of the overall catalytic activity in the reductive hydroformylation of 1-octene is displayed when adding 1,10-phenanthroline in concentrations ranging from 0.20 eq. up to 0.35 eq., referring to the amount of rhodium catalyst. In the range of 0.20 eq. to 0.35 eq. a linear decrease of the relative catalytic activity can be observed. At even lower 1,10-phenanthrolin concentrations no statistically significant effect is observed (see Appendix Table A 22). When adding 0.20 eq. of 1,10-phenanthrolin, still 88% of the initial relative activity is observed. The presence of alcohols in the post reaction solution proves that hydrogenation still occurs. A linear decrease can be observed for up to 0.35 eq. of 1,10-phenanthrolin. At this point only 18% of the initial catalytic activity is observed. A linearization of the decrease in catalytic activity depending on the 1,10-phenanthrolin concentration leads to the conclusion that at a theoretical concentration of 0.39 eq. is needed to achieve a complete deactivation of the catalyst. This is a higher concentration than would be necessary to completely poison nanoparticles and fits the previous observation of multinuclear molecular species.

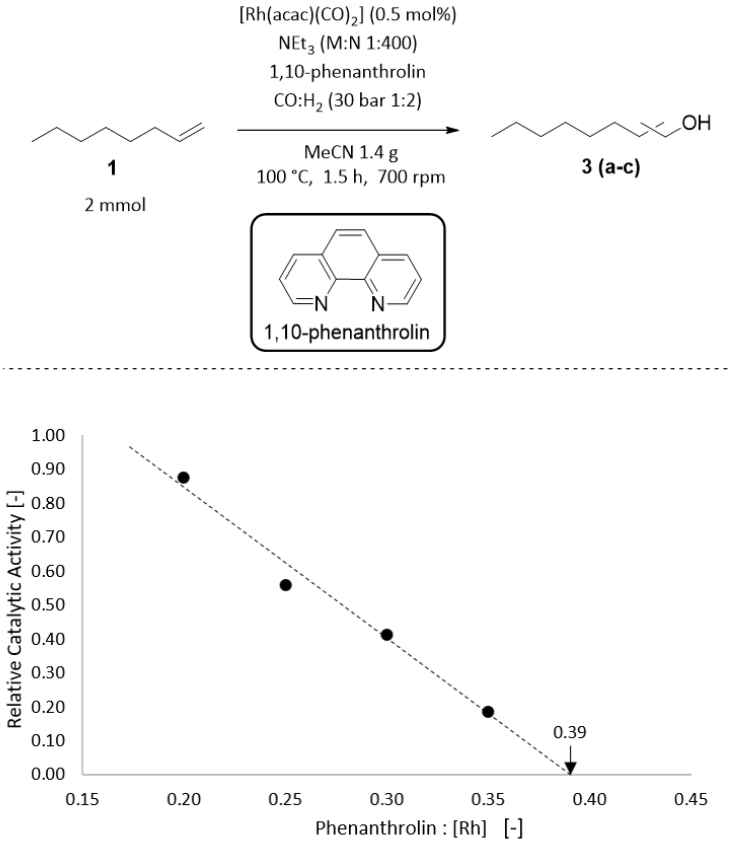

Figure 33: Phenanthrolin poisoning experiments to test for nanoparticles in the reductive hydroformylation of 1-octene. [a] The relative catalytic activity is based on the total amount of catalytic products (aldehydes + alcohols), whereas alcohols are factored times two because two catalytic steps are needed for their formation, referred to the total amount of catalytic products observed when no catalyst poison is added. Quantitative/qualitative determination of product yields *via* GC-FID/GC-MS.

It should be mentioned that just based on these experiments the involvment of nanoparticles can not be completely excluded. For example, if nanoparticles would be present in low concentrations, which do not react with Hg(0,) and furthermore 1,10-phenanthrolin favours the complexation of the molecular species, these tests would likely show the same results.

Even though, in unison with the success of recycling strategies described later in this thesis (chapter 4.2) and by S. PÜSCHEL,[158,159] which are based on the assumption of molecular catalytic species, the presence of rhodium nanoparticles can be ruled out as the explanation for the hydrogenation activity.

4.1.7 *In situ* ^{1}H-NMR Spectrometry of the Rhodium Hydride Species

Since it was not able to observe the equilibrium of the multinuclear anionic rhodium complexes observed previously under reaction conditions and and it is known that rhodium hydride complexes must be involved during the catalytic cycle, which have not been identified so far, ^{1}H-NMR spectra under reaction conditions have been measured. To achieve this, a high-pressure quartz NMR tube (see chapter 6.3.4) was used to observe rhodium hydride species in the reaction solutions. Although high catalyst concentrations are still necessary in order to observe hydride signals, hydride species at reaction temperature and under synthesis gas pressure can now be observed (Figure 34). Due to the fact that a less sensitive 300 MHz NMR-spectrometer was used for high pressure NMR experiments and ^{13}CO ligands rapidly exchange at temperatures above RT, an observation of the ^{13}C and ^{103}Rh nuclei have not been possible under those conditions. When triethylamine is used as the tertiary amine additive (Figure 34, left spectrum) a very distinctive singlet at -18.7 ppm (at 100 °C) is observed as the main species over the temperature range of 25 °C to 100 °C. Higher temperatures seem to favor the formation of this hydride species. The highest concentration is measured at 100 °C which represents the maximum operation temperature of the NMR-spectrometer.

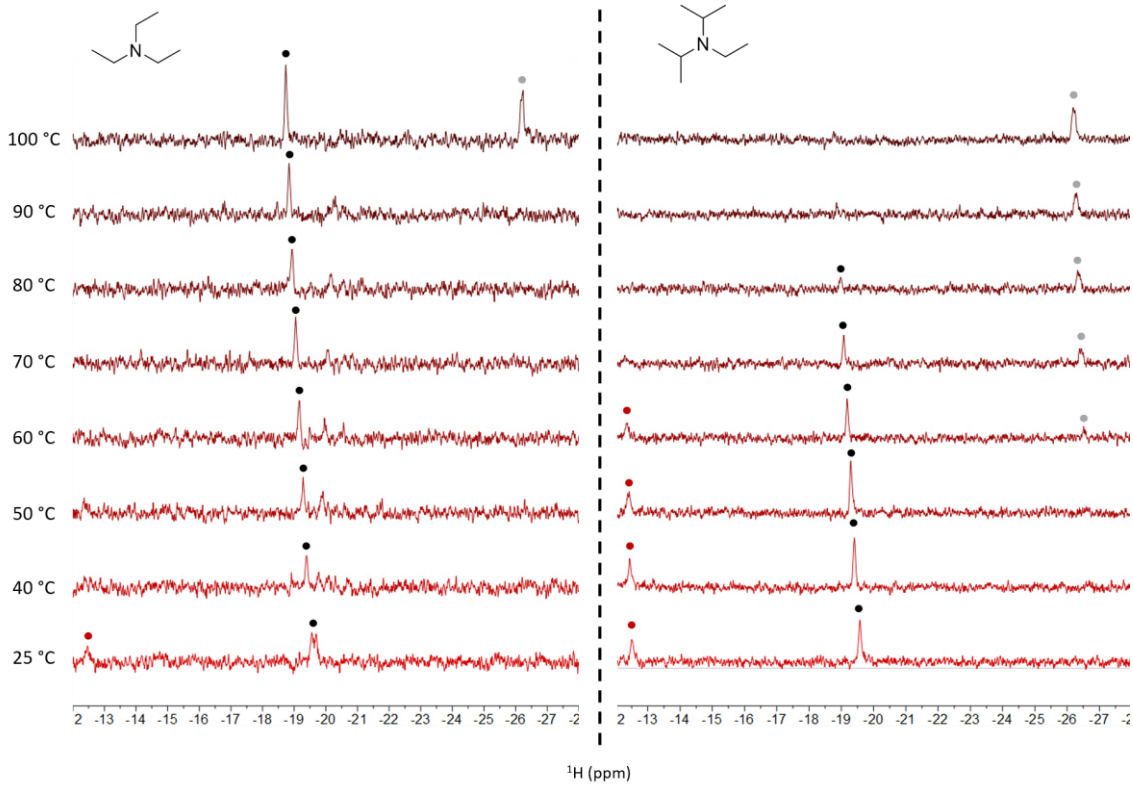

Figure 34: Temperature dependent ^{1}H-NMR spectrum (300 MHz, d_3-acetonitrile) of the hydride region taken from a reaction solution (2.4 mg $[Rh(acac)(CO)_2]$ and 18 mg 1-octene dissolved in 60 mg triethylamine/diisopropylethylamine and 120 mg d_3-acetonitrile) of the reductive hydroformylation of 1-octene under 30 bar $CO:H_2$ 1:2.

It should be mentioned that considering the sensitivity of ^{1}H-NMR and the high catalyst concentration necessary to observe hydride species, the actual concentration of those hydrides is rather low. Upon comparing the integrals of the hydride signals measured at 100 °C with the integral of the CH signal of the dissociated acetylacetonate (acac) ligand from the [Rh(acac)(CO)$_2$] precursor, the concentration of hydrides was determined to be 1.0% of the initial concentration of [Rh(acac)(CO)$_2$] when using NEt$_3$ as the amine additive and 0.7% when using NEt*i*Pr$_2$ as the amine additive. Two more hydride species can be identified in the ^{1}H-spectra. At room temperature a signal with low intensity at -12.4 ppm (at 25 °C) is observed. At temperatures above 25 °C the concentration of this species is below the detection limit. Furthermore, at 100 °C a hydride signal with strong shielding (and therefore high field shift) at -26.2 ppm is observed, which is not observed at temperatures below 100 °C. A strong shielding such as the signal at -26.2 ppm is reported for multihydride clusters.[160–162] Regarding the main species with a hydride shift at -18.7 ppm, the shielding is too low compared to multihydride clusters but still stronger than the shielding of mononuclear hydride complexes (-9 to -12 ppm).[163–165] A possible explanation is the binding of an electron donor such as the amine, even though the Rh–N bond has not been proven directly. Since this species is the only one observed in significant concentrations at all temperatures at which catalytic activity in the reductive hydroformylation reaction is reported (60 °C to 100 °C), it is likely that this is the catalytically active species.

Diisopropylethylamine is sterically more demanding than triethylamine and showed a lower hydrogenation activity during the investigation of different amines for the reaction (see chapter 4.1.4). When using diisopropylethylamine as the amine source during *in situ* ^{1}H-NMR experiments (Figure 34, right side) a clear difference to triethylamine concerning the concentration of different hydride species is observed. In contrary to the observations for triethylamine, the concentration of the presumable catalytically active species at -18.7 ppm is the highest at lower temperatures from 25 °C to 50 °C. When increasing the temperature above 50 °C, the concentration decreases. At temperatures above 80 °C, the concentration is below the detection limit. At all times the concentration is lower than the maximum concentration at 100 °C for triethylamine. At the same time the supposedly multihydride species at -26.2 ppm is formed already at 60 °C and its concentration increases up to 100°C.

A vast difference for the equilibrium of different hydride species depending on the nature of the amine is observed. The lower hydrogenation activity observed for diisopropylethylamine in accordance with the low concentration of the hydride species at -18.7 ppm at reaction temperature further supports the importance of this hydride species for the reaction.

4.1.8 *In Situ* Monitoring of Rhodium Carbonyl Species under Reaction Conditions Using Infrared-Spectroscopy

Since ^{1}H-NMR spectroscopy only allowed for the observation of hydride species under reaction conditions was possible, *in situ* Infrared Spectroscopy (IR-Spectroscopy) was used as a complementary method for the investigation of carbonyl species under reaction conditions. Previous ^{13}C and ^{103}Rh-NMR spectra proved that the anionic species are formed in a delicate equilibrium but it was not possible to measure those spectra under high pressure synthesis gas or using low rhodium concentrations. Furthermore, the conditions in an NMR tube vary from an autoclave reactor significantly, especially since only a slow and limited gas uptake is possible. For the interpretation of possible catalytically active species for the reductive hydroformylation it is important to know the equilibrium under reaction conditions. Using a 20 mL autoclave reactor, connected to a sample loop which leads through an FTIR-spectrometer (chapter 6.3.5), *in situ* monitoring of the catalytic carbonyl species under reaction conditions (26 bar CO:H_2 1:2, 100 °C) was possible. For the experiment [Rh(acac)$(CO)_2$] was dissolved in MeCN and synthesis gas, triethylamine and 1-octene were added stepwise. The liquid substrates were added using a HPLC (High-Pressure-Liquid-Chromatography) pump. The time resolved 3D spectrum of the IR-absorbance for the range in which carbonyl vibrations are observed is displayed in Figure 35. The absorbance of exemplary spectra for the initial [Rh(acac)$(CO)_2$] precursor dissolved in MeCN (**a**), the changes upon addition of synthesis gas to the precursor (**b**) and upon addition of synthesis gas and triethylamine (**c**) are displayed separately. The initial spectrum of [Rh(acac)$(CO)_2$] in MeCN (**a**) fits the IR-spectra reported in literature with two carbonyl vibrations attributed to the carbon monoxide ligands at 2015 cm^{-1}, 2085 cm^{-1} and carbonyl vibrations from the acetylacetonato ligand at 1530 cm^{-1} and 1570 cm^{-1}.[166,167] No dissociation of the acetylacetonato ligand is observed up until the addition of synthesis gas after 10 minutes. With the addition of synthesis gas, a slow dissociation of the acetylacetonato ligand accompanied by the formation of new unmodified rhodium carbonyl species, visible at emerging carbon monoxide vibrations at 2063 cm^{-1}, 2105 cm^{-1} and 2121 cm^{-1}, can be observed (**b**). After 24 minutes triethylamine is added to the mixture. Upon the addition of triethylamine, a fast transition of the rhodium carbonyl species is observed (**c**). Within five minutes all carbonyl vibrations above 2000 cm^{-1} disappear, and new species are formed, showing two broad signals of high intensity at 1904 cm^{-1}, 1944 cm^{-1} and another broad signal of lower intensity at 1817 cm^{-1}. These new signals cannot be explained by mono- or multinuclear uncharged carbonyl complexes which show carbonyl vibrations above 2000 cm^{-1}.[166,168] The shape and the position of the signals fit very well with the formation of anionic carbonyl species as described before.

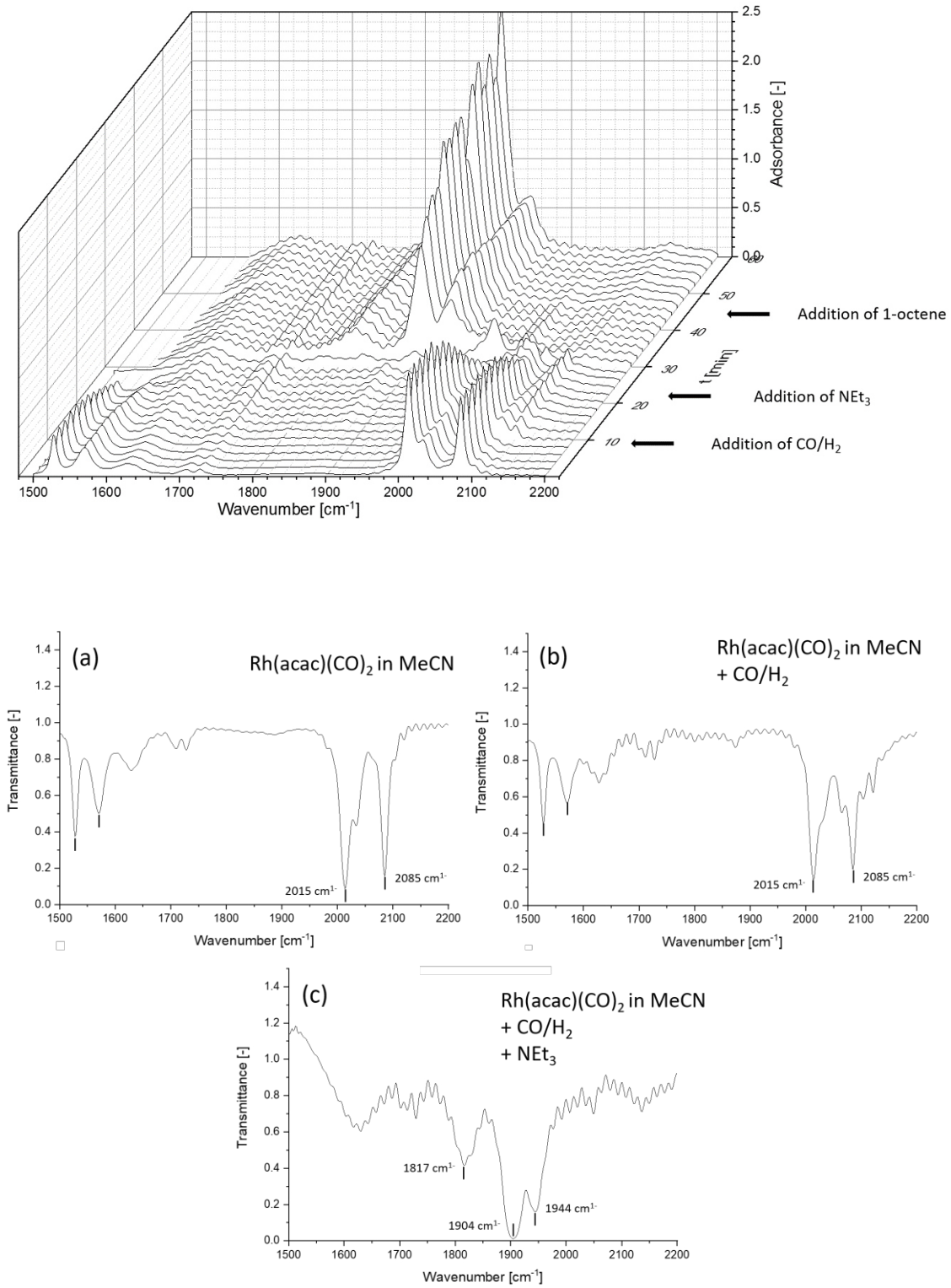

Figure 35: *In situ* infrared spectra of the reaction solution upon addition of synthesis gas, triethylamine and 1-octene. Time resolved IR-spectra (top) and representative individual spectra (bottom). The analytical procedure for the measurement of the *in situ* IR spectra can be found in the experimental section chapter 6.3.5.

Upon comparison with literature, the signal of the highest intensity at 1904 cm^{-1} can be assigned to the formation of the mononuclear anionic complex $[Rh(CO)_4]^-$, [169] while the small signal at 1817 cm^{-1} and the signal at 1944 cm^{-1} fit the spectra reported for the tetranuclear $[Rh_4(CO)_{11}]^{2-}$

species.[170] With increasing reaction times $[Rh(CO)_4]^-$ becomes more and more the predominant species in solution. Comparing the species identified under reaction conditions with *in situ* FTIR-spectroscopy to the ones identified *via* ^{13}C- and ^{103} Rh-NMR spectroscopy, the reaction conditions seem to favor the formation of the lower nuclear complexes while under NMR conditions, especially the higher nuclear complexes $[Rh_6(CO)_{15}]^{2-}$ and $[Rh_7(CO)_{16}]^{3-}$ are predominant. The equilibrium towards the lower nuclear complexes under reaction conditions can be explained with the increased carbon monoxide concentration in solution. Hence, the equilibrium shifts towards species that on average bind more carbon monoxide. Compared to the multinuclear species, $[Rh(CO)_4]^-$ is able to bind much more carbon monoxide per rhodium center (e.g. almost two times more than $[Rh_6(CO)_{15}]^{2-}$ and $[Rh_7(CO)_{16}]^{3-}$).

With the high concentration of $[Rh(CO)_4]^-$ under reaction conditions it is reasonable to assume that it is the main species involved in the reductive hydroformylation. Even though, it is unlikely that $[Rh(CO)_4]^-$ is directly involved in the catalytic cycle but rather represents a resting state since hydride species are necessary for both reaction steps. Furthermore, several experimental observations such as the strong dependency of the linear-to-branched ratio on the cone angle of the tertiary amine (see chapter 4.1.4) and the shielding of the hydride signal assigned to the catalytically active species during *in situ* ^1H-NMR spectroscopy (see chapter 4.1.7) indicate the role of the amine being more than just a counter ion to the anionic complexes.

To further validate the importance of the tertiary amine beyond the role of a counter ion, several other counter cations ($NEt_4^+Cl^-$, PNP^+Cl^-, $PPh_3Me^+Br^-$) such as the base KOH and a combination of KOH and $NEt_4^+Cl^-$, which have been described in literature for the formation of $[Rh(CO)_4]^-$,[171,172] have been tested for the reaction. No significant activity for the hydrogenation reaction and a significantly lower activity for the hydroformylation reaction was observed for all other additives (Appendix Table A 18).

4.1.9 Computational Investigation of Rhodium/Amine Complexes

To check this hypothesis, the structure of several mononuclear rhodium hydride species have been optimized and their absolute electronic energies (*E*) such as the relative Gibbs free energies (G_{rel}) compared to the [Rh(acac)(CO)$_2$] precursor have been calculated (for more information about the computational methods see chapter 6.2.3).

Using this method, four different mono-trialkylamine coordinated rhodium hydride species have been calculated (Table 4, A1 to A4), two rhodium species binding two triethylamine ligands (A5 and A6), the anionic $[Rh(CO)_4]^-[NEt_3H]^+$ complex (A7) such as the rhodium tetracarbonyl hydrido complex (C1), which is known to be the active species in unmodified rhodium catalyzed hydroformylation reactions.[171,173] As indicator for the energy needed for the formation of a specific complex from [Rh(acac)(CO)$_2$], the relative Gibbs free energy (G_{rel}) is used. Looking at the four mono amine coordinated complexes **A1** to **A4**, all complexes show a positive G_{rel} compared to [Rh(acac)(CO)$_2$]. That being said, the energy barrier for the formation of the penta-coordinated complex $[HRh(CO)_3(NEt_3)]$ (**A1**) is rather low with 2.9 kJ mol^{-1}. The formation of $[HRh(CO)_3(NEt_3)]$ would be possible, especially taking into account the high concentration of triethylamine in solution, which has not been considered for the calculation. Nevertheless, looking at the anionic $[Rh(CO)_4]^-[NEt_3H]^+$ complex (**A7**), a very high endergonic free Gibbs energy of -79.6 kJ mol^{-1} was calculated, which suggests that the formation in the presence of trialkylamines is very likely and further supports the experimental observations during *In situ* FTIR-spectroscopy experiments.

On a side note, the calculation of several rhodium amine species coordinated by two triethylamine ligands proves that the binding of more than one tertiary amine to a rhodium center is basically impossible because of the high electron density at the rhodium center. Several attempts to calculate such complexes immediately resulted in the repelling of the second amine. The only success was achieved when calculating the tetracoordinated complexes **A5** and **A6**, likely because repelling of the second amine would result in a tri coordinated rhodium complex. The energy barrier for their formation, of above 100 kJ mol^{-1}, proves that their formation is not possible.

Table 4: Absolute electronic energy (E), and Gibbs free energy (G) in Hartree for the computed [Rh] hydrido carbonyl (C1) and [Rh] amino hydrido carbonyl (A1 to A6) complexes and the precursor complex $Rh(acac)(CO)_2$ (P). The relative Gibbs Free Energies at 60 °C and 471 atm for the formation of the complexes from the precursor and - if applicable - the Rh-N distances are given. The geometries were optimized using the M06-LGrid6 fuctional with the def2-TZVP basis set (triple ζ level).

Abbreviation	Structure	E / E_H	G_{rel} [kJ mol^{-1}]	Rh–N [Å]
P	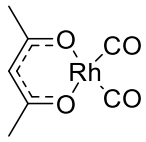	–682.7	0.0	–
A1	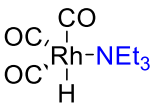	–743	2.9	2.54
A2	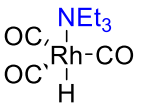	–743	3.0	2.39
A3	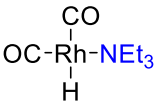	–630	29.0	2.27
A4	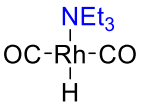	–630	36.3	2.31
A5	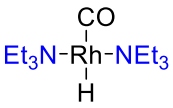	–809	151.7	2.21/ 2.21
A6	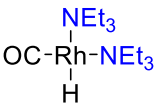	–809	108.8	2.35/ 2.46
A7	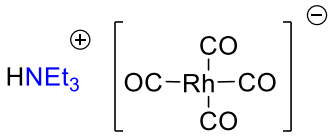	–857	–79.6	–
C1	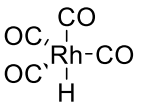	–565	–31.3	–

4.1.10 Proposing a Catalytically Active Rhodium Hydride Species Based on Spectroscopic and Experimental Observations

After several spectroscopic techniques have been applied to investigate the formation and equilibrium of rhodium species in the presence of amines, supported by experimental and computational results, the role of the amine during the reaction shall be proposed based on those results.

From ^{13}C-NMR spectra, it is known that a sensible equilibrium of anionic rhodium carbonyl species in solution exists with $HNEt_3^+$ as the counter ion, ranging from mononuclear $[Rh(CO)_4]^-$ to multinuclear complexes up to $[Rh_7(CO)_{16}]^{3-}$ (Figure 36, left side).

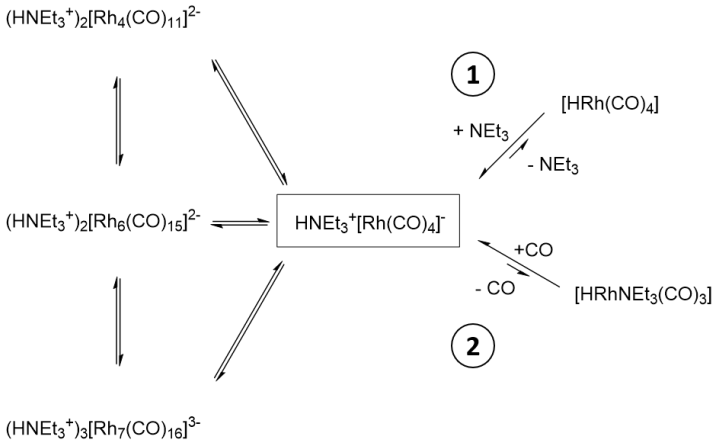

Figure 36: Proposed reaction network for the formation of rhodium hydride species during the reductive hydroformylation using rhodium/amine catalysts.

From rhodium cluster chemistry it is known that $[Rh(CO)_4]^-$ acts as "monomer" and anchor point in the equilibrium for the formation of higher nuclear rhodium complexes. By a variation of the concentration and reaction temperature in combination with *in situ* FTIR-spectroscopy it was observed that $[HNEt_3]^+[Rh(CO)_4]^-$ is the rhodium species with the highest concentration under reaction conditions (see chapter 4.1.5 and 4.1.8). Under the premise that the reaction was optimized towards the highest catalytic activity, it can be assumed that $[HNEt_3]^+[Rh(CO)_4]^-$ plays a vital role for the catalytic activity. Nevertheless, rhodium hydride species are necessary to catalyze the reaction, which excludes the direct involvement of the observed anionic complexes. Two reactions are reasonable for the formation of rhodium hydride species starting from $[HNEt_3]^+[Rh(CO)_4]^-$. The protonation of $[Rh(CO)_4]^-$ to $[HRh(CO)_4]$ (Path 1 in Figure 36) or the binding of $[HNEt_3]^+$ to form $[HRhNEt_3(CO)_3]$ with simultaneous dissociation of a carbonyl ligand (Path 2 in Figure 36).

There are several experimental observations opposing the catalysis by $[HRh(CO)_4]$. For once, $[HRh(CO)_4]$ is well known as catalyst in rhodium hydroformylation chemistry.[168,174,175] Although

the species is known to be very active for the hydroformylation reaction, there is no literature suggesting an activity of $[HRh(CO)_4]$ for the aldehyde hydrogenation reaction. Furthermore, the strong shielding of the hydride species, observed under reaction temperature and pressure suggests an electron rich rhodium center. Last but not least, the steric influence of the tertiary amine (chapter 4.1.4) could not be explained by $[HRh(CO)_4]$ as the catalytic hydride species.

A more likely explanation is that $[HRh(CO)_4]$ is formed from the $[Rh(acac)(CO)_2]$ precursor and acts as the starting point for the formation of $[HNEt_3]^+[Rh(CO)_4]^-$ in an acid/base reaction. The formation of $[HNEt_3]^+[Rh(CO)_4]^-$ is supported by the calculated free Gibbs energy for their formation starting from $[Rh(acac)(CO)_2]$ (chapter 4.1.9). After the initial formation, $[HNEt_3]^+[Rh(CO)_4]^-$ is in an equilibrium with $[HRhNEt_3(CO)_3]$, whereas the equilibrium strongly favours the ionic species as proven by the low concentrations of hydride species under reaction conditions (chapter 4.1.7). The same active species was suggested by WADE for the formation of ethylene glycol from synthesis gas using rhodium/trialkylamine catalysts. Even though in this case the only evidence was a high concentration of $[Rh(CO)_4]^-$ in solution as proven by IR-spectroscopy.[169]

The ultimate proof that this hydride species exists and is responsible for the hydrogenation activity is to be made though. Some questions remain, such as why $[HNEt_3]^+[Rh(CO)_4]^-$ would favour the equilibrium with $[HRhNEt_3(CO)_3]$ instead of $[HRh(CO)_4]$. An effective way of proving the existence of a Rh–N bond in the hydride species would be complementary ^{15}N-NMR spectroscopy using isotope labeled NEt_3 under reaction conditions.

4.2 Development of a Catalyst Recycling Strategy for Rhodium/Amine Catalysts in the Reductive Hydroformylation of Linear Alkenes

Previously the investigation and optimization of a reaction system for the reductive hydroformylation using a rhodium catalyst in combination with tertiary alkylamines was described (chapter 4.1). Throughout this process, a reaction system with remarkable selectivity and at the same time high activity towards alcohols was developed. Additionally, using several spectroscopic tools, the major rhodium species present during the reaction was identified.

Even though these are important insights, the ultimate goal of this work is to develop new synthetic routes for the production of alcohols as bio-synthetic fuels. One major point which has to be addressed in order to highlight any significance for application is a concept for the recycling of the rhodium catalyst.

The difficult recycling of homogeneous compared to heterogeneous catalysts is often pointed out as the major drawback for their large-scale application. Especially with the goal of producing alcohols as potential fuels, a concept for the highly efficient recycling of the rhodium catalyst must be presented in order to make a possible process economically and ecologically feasible. The development of a recycling strategy for rhodium/tertiary amine catalysts will be investigated in the following.

In this work the immobilization of the catalyst in a high molecular weight trialkylamine phase and the recycling of the rhodium/tertiary alkylamine catalysts by the extraction of product alcohols using supercritical *sc*CO_2 will be investigated.

Simultanously to the recycling approach described in this work, two other concepts for the recycling of rhodium/tertiary amine catalysts have been developed in close cooperation within our group. The results about those recycling approaches have been reported by S. PÜSCHEL just recently and shall be summarized shortly to allow a comparison with the recycling strategy presented in this work.

In the first concept described by PÜSCHEL for the recycling of the rhodium/tertiary amine catalyst a biphasic liquid/liquid reaction system is used, similar to the Ruhrchemie-Rhône-Poulenc process. The rhodium catalyst is held in a water phase by deploying water soluble alkanolamines while products and substrates separate in a second organic phase. Although the separation proved to be possible, careful adjustment and controlling of the phase composition is necessary in order to keep the reaction system biphasic. Additionally, it was not possible to completely circumvent leaching of the alkanolamines into the organic phase.[159]

The second approach described by PÜSCHEL utilized an inherent feature of alkanolamines for the catalyst separation: Their ability to bind CO_2 and the resulting formation of carbamates.[158] While the reaction proceeds under monophasic conditions, a pressurization with CO_2 after the reaction

induces the formation of ionic carbamates, causing the mixture to separate into a polar catalyst and a non-polar substrate and product phase. Although this represents a very unique and elegant approach, it was found that a certain CO_2 concentration is necessary for a complete separation while higher CO_2 concentrations seem to partially deactivate the catalyst. Concluding, a tradeoff between rhodium leaching and catalytic activity has to be made.

The use of *sc*CO_2 for the extraction of product alcohols as presented in this work has several beneficial effects. For once, CO_2 is a readily available and abundant ressource which is non-toxic and non-flammable, making the resulting process comparatively safe to operate. The critical point of CO_2 (31 °C, 74 bar) is within reasonable reach for an industrial process. Furthermore the polarity of *sc*CO_2 can be adjusted by the used temperature and pressure during the extraction to exhibit characteristics resembling solvent properties ranging from *n*-pentane to pyridine.[82,83] This makes *sc*CO_2 a highly flexible extraction agent. Last but not least, *sc*CO_2 can be separated from the reaction products after the extraction simply by relieving the pressure. The only downside regarding industrial processes is, that CO_2 has to be constantly recompressed before the extraction which can be energy demanding. Nevertheless, *sc*CO_2 as extraction agent is already used with great success on an industrial scale e.g. in the decaffeination of coffee beans.[62,63]

All experiments discussed in the following are conducted in 10 mL autoclave reactors. A detailed experimental procedure for high pressure experiments conducted in 10 mL to 20 mL autoclave reactors can be found in the experimental section in chapter 6.2.1. Reactions during the recycling experiments were conducted in a 50 mL autoclave reactor. The extraction was conducted using a setup specifically designed for the extraction with supercritical CO_2. The recycling procedure will be described in short in the following. Detailed experimental procedures can be found in the experimental section chapter 6.2.6. The quantitative analysis of the reaction mixture was conducted *via* GC-FID as discussed in chapter 6.3.1. For the qualitative assignment of products, a combination of GC-MS and ^{1}H-NMR is used (chapter 6.3.4.1). The composition of the extract obtained during the catalytic recycling experiments has been analyzed *via* quantitative ^{1}H-NMR as described in chapter 6.3.4.4 instead. Experiments displayed in graphical form can be found in the Appendix (chapter 10.2).

Parts of this chapter are published in:

T. Rösler; J. Betting; S. Püschel; A. J. Vorholt; W. Leitner, "Solvent Design for Catalyst Recycling of Rhodium/Amine Catalysts via $scCO_2$ Extraction in the Reductive Hydroformylation of Alpha Olefins", Green Chem. **2022**, 24 (17), 6578–6588. DOI: 10.1039/D2GC01252A.

Whereas authors contributed as follows (using CRediT standardized contribution descriptions):

T. Rösler:	Writing – original draft, investigation, methodology
J. Betting:	Investigation (masters thesis), methodology
S. Püschel:	Investigation (assistance for the recycling setup)
A. J. Vorholt:	Methodology, supervision, writing – review and editing
W. Leitner:	Conceptualization, supervision, writing – review and editing

4.2.1 Solvent Screening for the Recycling of Rhodium/Amine Catalysts

Every concept for the recycling of the homogeneous catalyst is closely linked to the solvent system which is used during the reaction. During previous investigations of the reaction system, a short screening of solvents with a range of different polarities was carried out in which it was found that polar solvents seem to be necessary to achieve a high catalytic activity (see Appendix Table A 19). With the insights gained during the spectroscopic investigation of the catalytic species (chapter 4.1.5), it can be assumed that polar solvents help to stabilize anionic complexes which are formed in the presence of tertiary amines.

Nevertheless, for the further investigation of a recycling concept, more sophisticated knowledge about the requirements of a solvent allowing high reactivity is necessary. More than twenty promising solvents have been identified and tested in the reductive hydroformylation of 1-pentene using [Rh(acac)$(CO)_2$] in combination with methyldiethylamine as the catalyst (Figure 37). For the choice of solvents several criteria have been considered. In regard to a technical process highly cancerogenic or toxic solvents have been avoided. Furthermore, the solvents must be reasonably priced and, if possible, be able to be derived from renewable resources. For simplicity, the total alcohol yield in the reductive hydroformylation when using the respective solvent is displayed as means to the catalytic activity of the reaction system. The full product spectrum for each solvent can be found in the Appendix (Table A 7). Triethylene glycol has already been identified as promising solvent during previous investigations (see Appendix Table A 19). Triethylene glycol is non-toxic, non-flammable and can be produced from renewables.[176] Combined with the wide variety of ethyleneglycole-based solvents available with different molecular weights or terminal functionalization, they pose the perfect building block for tailor made polar solvents (**1**-**9**). Triethylene glycol (**1**) such as tetraethylene glycol (**2**) both support a high catalytic activity with 60% respectively 65% alcohols obtained in the reaction. Furthermore, a derivatization of the terminal alcohol groups with ester (**9**) or methyl groups (**4**, **8**) is tolerated and no significant drop of catalytic activity is observed. Contrary, the addition of longer chain alkyl groups at the example of diethylene glycol monohexyl ether (**6**) significantly lowers the catalytic activity and only 39% alcohols are obtained. It should be noted though that that the hydrogenation activity is still comparatively high and only 6% of the aldehyde intermediates are observed. In this case the hydroformylation activity seems to be hindered. Main products are pentene isomers (46%). The same trend can be observed when using tripropylene gylcol monobutyl ether (**7**) as solvent. In this case 24% alcohols are gained while 57% hexene isomer by products are observed.

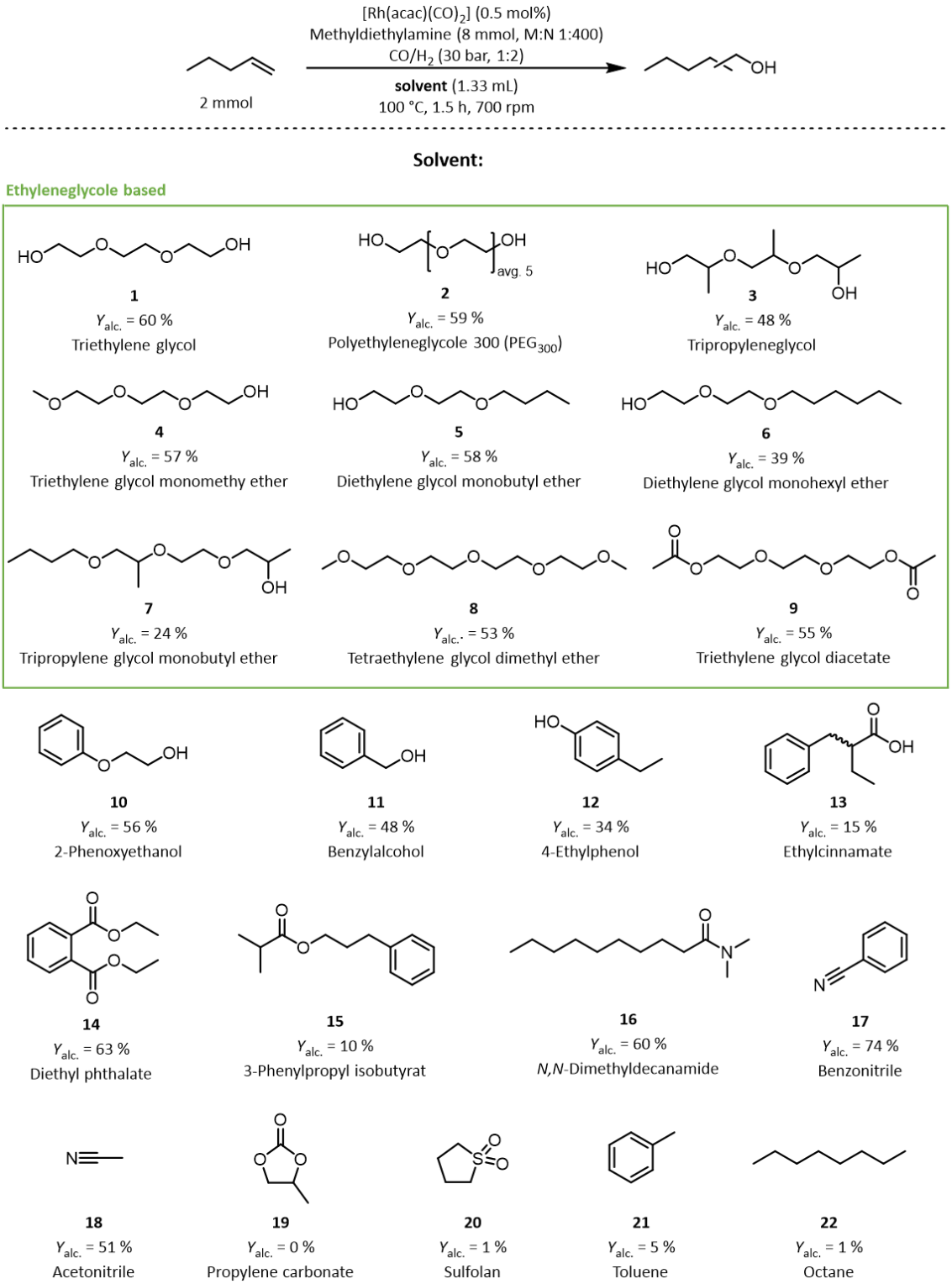

Figure 37: Results for the screening of 23 solvents in the reductive hydroformylation of 1-pentene using a rhodium/diethylmethylamine catalyst. Quantitative/qualitative determination of product yields *via* GC-FID/GC-MS

Besides ethylene glycol-based solvents, solvents with a variety of different functional groups such as alcohols (**10, 11, 12**), esters (**14, 15**), nitriles (**17, 18**), carboxylic acids (**13**) or amides (**16**) have been tested. High alcohol yields were achieved for 2-phenoxyethanol (**10**; 56%), diethylphtalate (**14**; 63%) and benzonitrile (**17**; 74%). Worth highlighting is the comparatively high yield of alcohols (60%) when using *N,N*-diethyldecanamide (**16**). Even though the overall

polarity of the molecule is supposed to be low. A possible explanation could be the surfactant like structure with a polar amide group and a long non-polar alkyl chain. Following the proposed stabilizing effect of polar groups for the ionic rhodium species described in chapter 4.1.5, *N,N*-diethyldecanamide polar groups to stabilize anionic species could be possible.

4.2.2 Hansen-Solubility-Parameters for the 22 Solvents

After the more qualitative consideration of solvents for the reductive hydroformylation, in Figure 37 a more quantitative evaluation for the requirements of the solvent was sought after. To achieve this, the Hansen-Solubility-Parameters for each solvent were determined and the catalytic performance of the candidates has been plotted against their Hansen-Solubility-Parameters (HSP) in a 3D-Hansen-space (Figure 38).

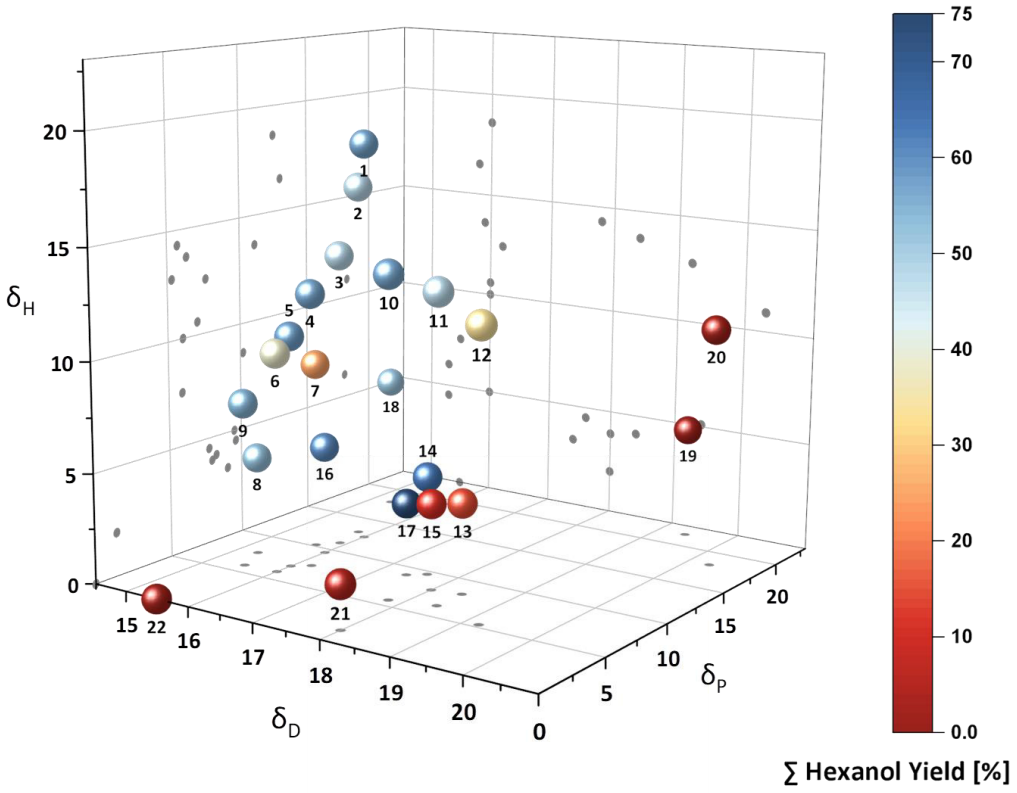

1	TEG	12	4-Ethylphenol		
2	TetraEG	13	Ethyl cinnamate		
3	TPG	14	Diethyl phtalate		
4	TEG monomethyl ether	15	3-Phenylpropyl isobutyrat		
5	DEG monobutyl ether	*16*	*N,N*-Dimethyldecanamide		
6	DEG monohexyl ether	17	Benzonitrile		
7	TPG monobutyl ether	18	Acetonitrile		
8	TetraEG dimethyl ether	19	Propylene carbonate	DEG:	Diethylene glycole
9	TEG diacetate	20	Sulfolane	TEG:	Triethylene glycole
10	2-Phenoxyethanol	21	Toluene	TPG:	Tripropylene glycole
11	Benzylalcohol	22	Octane	TetraEG:	Tetraethylene glycole

Figure 38: Categorization of 23 solvents tested in the reductive hydroformylation of 1-pentene in a three-dimensional Hansen-space based on their Hansen-Solubility-Parameters (HSP): dispersion forces (δ_D), dipole-dipole interactions (δ_P) and hydrogen-bonding-contribution (δ_H). Quantitative/qualitative determination of product yields *via* GC-FID/GC-MS.

The HSP concept is used as a model to characterize a solvent based on three characteristics. The dispersion forces (δ_D), the dipole-dipole interactions (δ_P) and the hydrogen-bonding-contribution (δ_H). Owing to the quantification of these three parameters, a more accurate description than polar and non-polar, allows a much more precise description of a solvent.

The parameters δ_D, δ_P and δ_H can be displayed as coordinates in a cartesian coordinate system. The resulting Hansen-space graphically illustrates the Hansen properties and allows for a graphical evaluation of necessary solvent properties. The cited literature allows for a more detailed overview about the Hansen-space and the determination of Hansen-Solubility-Parameters.[177,178]

Looking at the 3D-Hansen-space created by the chosen solvents, a wide range of combinations of different Hansen-Solubility-Parameters has been covered. Nevetheless, there are few blind spots such as solvents with high hydrogen-bonding-contribution (δ_H) and at the same time high dipole-dipole interactions (δ_P) and/or high dispersion forces (δ_D). Those blind spots must be accepted since solvents with these parameters are bound to form biphasic reaction systems with diethylmethylamine. Comparing the catalytic activity of the resulting reaction system (resembled by the alcohol yield obtained during the reaction) with the Hansen-Solubility-Parameters, vague trends can be observed regarding necessary solvent properties. At the same time the catalytic activity seems to rely much more on the presence of individual functional groups than on the overall physio-chemical properties. For example, solvents with lower dispersion-forces (δ_D) seem to generally support a higher catalytic activity.

A good example for this are the alcohol solvents **10** to **12**. They contain the same functional group and about the same hydrogen-bonding-contribution (δ_H) and dipole-dipole interactions (δ_P) but differ in the dispersion forces (δ_D). Plotting the dispersion forces against the combined alcohol yield reveals an almost linear dependency of the alcohol yield on the dispersion forces (δ_D) (Figure 39). In sharp contrast, comparing benzonitrile (**17**) and 3-phenylpropyl isobutyrate (**15**), the Hansen-Solubility-Parameters for both solvents are very similar, which is resembled in their close proximity in the Hansen-space. Nevertheless, the catalytic activity when using those as solvent in the reaction system is vastly different. While benzontrile (**17**) supports a high catalytic activity and 74% alcohols are generated, only 10% alcohols are generated when using 3-phenylpropyl isobutyrat (**15**) as solvent. Regarding hydrogen-bonding-contribution (δ_H) and dipole-dipole interactions (δ_P) no clear correlation with the catalytic activity can be observed within the delimitations of the studied solvents. This can be observed at the example of ethylene glycol-based solvents (**1-9**).

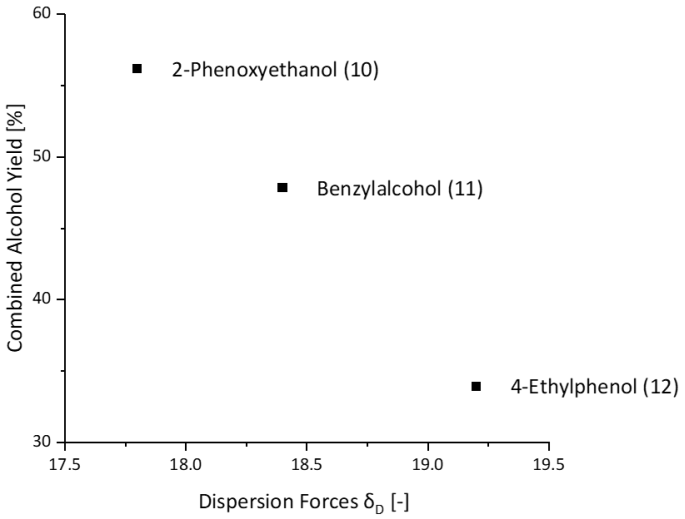

Figure 39: Influence of the dispersion forces (δ_D) of a solvent on the catalytic avtivity in the reductive hydroformylation of 1-pentene at the example of three alcoholic solvents with comparable hydrogen-bonding-contribution (δ_H) and dipole-dipole interactions (δ_P). 2-Phenoxyethanol (δ_H = 14.3, δ_P = 17.8), Benzylalcohol (δ_H = 13.7, δ_P = 18.4), 4-Ethylphenol (δ_H = 12.8, δ_P = 19.2).

Although a considerably widespread area regarding the hydrogen-bonding-contribution (δ_H) and dipole-dipole interaction (δ_P) forces is covered by ethylene glycol-based solvents, no correlation to the catalytic activity is observed. Again, the influence of individual functional groups seems to dominate over the physio-chemical properties.

4.2.3 Amine Functionalized Alohols and Ethers as Solvents and Ligands during the Rhodium Catalyzed Reductive Hydroformylation

Despite the fact that the highest yield of alcohol during the solvent screening has been achieved when using Benzonitrile (**17**, $Y_{alc.}$ = 74%), ethylene glycol solvents proved to allow a high catalytic activity and represent a highly flexible platform regarding molecular weight or functionalization of the terminal groups. In addition the fact that ethylene glycol could potentially derived from renewables[176], it is non-toxic and non-flammable in its basic or polymerized form makes it especially attractive for a potential sustainable process.

With those ethylene glycol solvents in mind, several tertiary amine functionalized alcohol amines or ethers have been tested as solvent and at the same time amine (ligand) for the reaction (Figure 40). To estimate the influence of polar alcohol and ether groups, hexadecyl dimethylamine was also tested for the reaction. In preliminary experiments it was found that, when using aminated solvents a much higher activity is achieved at a total pressure of 60 bar instead of 30 bar for the reaction as claimed in chapter 4.1.3. It was found that this is due to the variable gas solubility in aminated solvents.

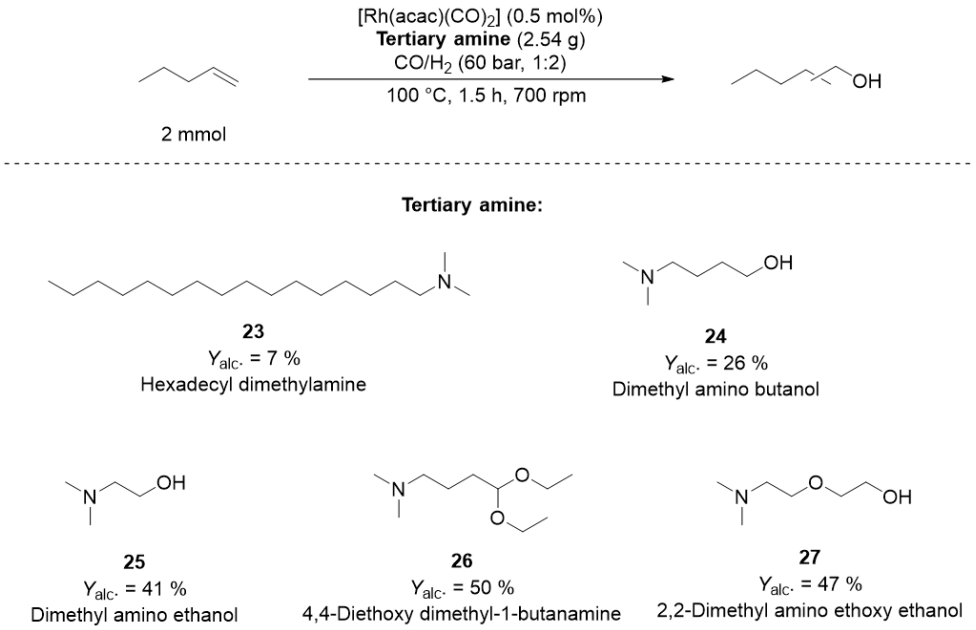

Figure 40: Combined alcohol yield (*n*-/*iso*-alcohol) when using five different aminates solvents in the reductive hydroformylation of 1-pentene. Quantitative/qualitative determination of product yields *via* GC-FID/GC-MS.

The combination of solvent and amine (ligand) was surprisingly successful when combining alcohol and/or ether groups with dimethylamine groups in one molecule. The highest activity was achieved when ether groups are incorporated at the example of 4,4-diethoxy diethyl-1-butanamine (**26**, $Y_{alc.}$ = 50%) and 2,2-dimethyl amino ethoxy ethanol (**27**, $Y_{alc.}$ = 47%). The high activity when ether functionalities are incorporated might also explain the high tolerance for terminal functionalization when ethylene glycol-based solvents are used (see

Figure 38). As expected, hexadecyl dimethylamine (**23**) as solvent/amine did not support a high catalytic activity which highlights the importance of the presence of polar groups again. Since 2,2-dimethyl amino ethoxy ethanol (**27**) resembles a mono aminated version of diethylene glycol (DEG) and can be regarded as amine functionalized ethylene glycol derivate, it is well suitable as model solvent for further investigations regarding aminated ethylene glycol-based solvents.

By successfullly incorporating the amine group into the solvent, the reaction system now only consists of three components (not counting gaseous reactants): The alkene, the rhodium precursor and the solvent/amine. This severely simplifies the reaction system and therefore the recycling of the homogeneous catalyst. Moreover, due to the incorporation of the amine into the solvent, allowing for very high concentrations of tertiary amine functionalities, a significant increase of the substrate concentration was possible without a notable decrease in activity or change in selectivity (Figure 41).

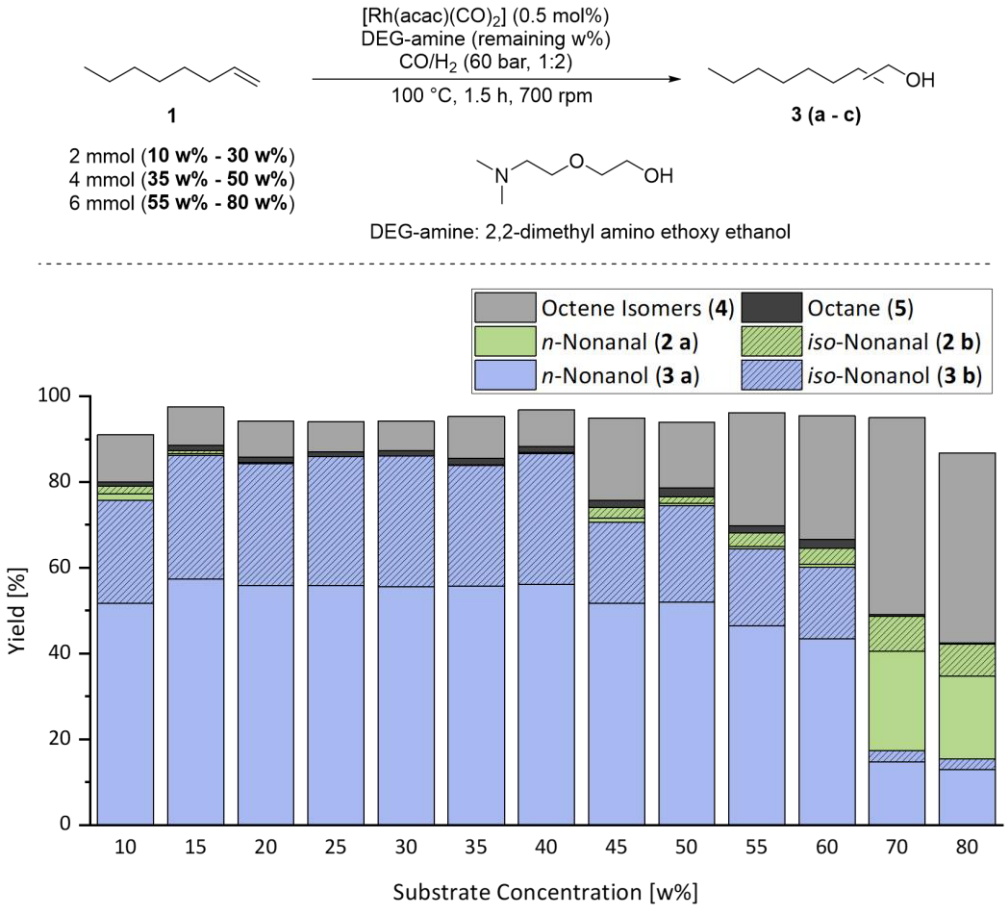

Figure 41: Increasing the substrate concentration when using DEG-amine as the solvent and ligand in the reductive hydroformylation of 1-octene with a rhodium catalyst. Quantitative/qualitative determination of product yields *via* GC-FID/GC-MS.

Using 2,2-dimethyl amino ethoxy ethanol, hereafter referred to as DEG-amine, as the aminated solvent allows the increase of the substrate concentration from 10 w% to 40 w% (Figure 41). Increasing the substrate concentration from 10 w% to 15 w% even allows a slight increase in catalytic activity. Using a substrate concentration of 40 w%, an alcohol yield of 87% is achieved after 1.5 hours of reaction time with 9% of unconverted pentene isomers and only 1% pentane side products. At higher substrate concentrations above 40 w% a stepwise decrease in hydroformylation activity, accompanied by a slight decrease in hydrogenation activity can be observed. Finally, for very high substrate concentrations above 60 w% a significant decrease in hydrogenation activity is observed. Nevertheless, even with a substrate concentration of 80 w% still 15% alcohol and 27% aldehyde products are observed (resulting in a total of 42% hydroformylation products). The decrease in activity at substrate concentrations above 40 w% can be explained with the decreasing concentration of amine groups in solution, which has been determined earlier as one of the important parameters to maintain a high catalytic activity (see chapter 4.1.2). The increase of the substrate concentration does not only increase the space-time-yield but is important for most recycling concepts since a lot of product separation techniques are significantly more efficient at higher product concentrations.

The high alcohol yield and high selectivity towards alcohols when using DEG-amine as the solvent/amine for the reaction suggests a significant increase in catalytic activity compared to the previous approach when using a tertiary amine in combination with a separate second solvent. To get a better understanding for the changed reactivity a yield-time profile for the reductive hydroformylation of 1-octene when using DEG-amine as the solvent was investigated by analyzing batch reactions after different reaction times (Figure 42).

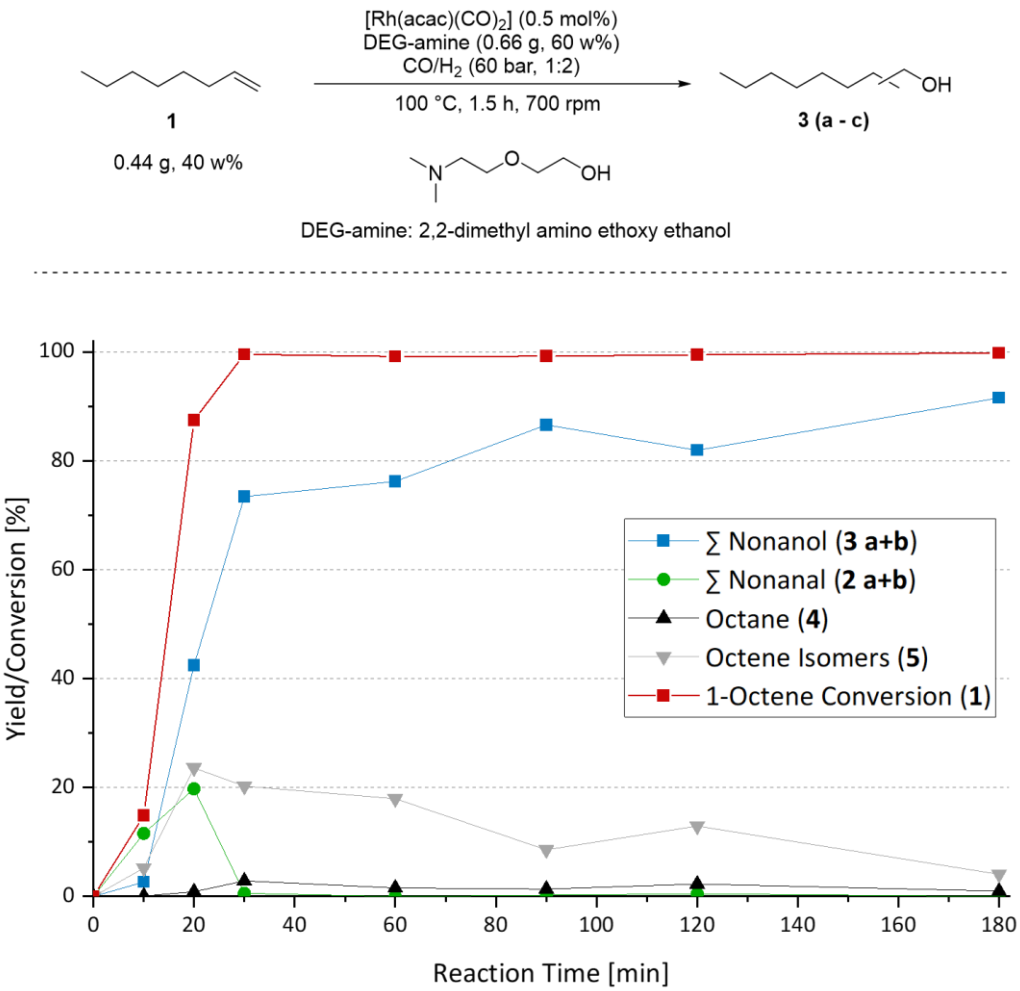

Figure 42: Yield-time plot for the reductive hydroformylation of 1-octene using 2,2-dimethyl amino ethoxy ethanol (DEG-amine) as the solvent/amine (ligand). Reactions have been conducted in 20 mL autoclaves. Datapoints have been derived from batch reactions. Connections between data points are for visualization purposes. Quantitative/qualitative determination of product yields *via* GC-FID/GC-MS.

According to the resulting yield-time plot, already after 30 minutes 73% alcohols were generated which corresponds to a catalytic activity with a Turn-Over-Frequency of 280 h^{-1}. Aldehyde intermediates can only be observed within the first 20 minutes of reaction time with a maximum yield of 20% after 20 minutes which suggests a high hydrogenation activity and the hydroformylation reaction being the rate limiting reaction. After 30 minutes all initial 1-alkenes have been converted and only internal 1-alkene isomers (20%), derived from *ß* -hydride transfer, are left. As internal double bonds undergo hydroformylation at a much slower rate, alkene isomers are converted over the next two and a half hours. After three hours 92% of alkenes have been converted to alcohols and only 4% of internal double bond isomers are left. The only side products formed during the reaction are about 1% of alkanes, derived from the hydrogenation of alkene double bonds. This highlights the extraordinary selectivity of the hydrogenation catalyst towards C=O double bonds, which makes alcohol selectivities above 90% possible.

4.2.4 Recycling of Rhodium/Amine Catalysts by Immobilization in an Amine Functionalized PEG Phase and Product Extraction using Supercritical CO_2

The overall high catalytic activity of amine functionalized ethylene glycol-based solvents, as shown at the example of DEG-amine (Figure 42), in unison with the high tolerance of terminal functionalization makes amine functionalized ethylene glycol derivates promising candidates for the immobilization of the rhodium catalyst in catalyst recycling approaches. While this could be potentially taken advantage of in a variety of recycling concepts, a very promising approach is the extraction of product alcohols and aldehydes using supercritical CO_2 ($sc CO_2$) as the extracting medium.

The extraction of aldehydes from poly ethylene glycol phases has previously been described.[76-78,80,81] This concept makes use of the insolubility of high molecular weight and polar molecules (like polyethylene glycol) in dense CO_2 phases as means to immobilize the catalyst in those phases while smaller and less polar products are extracted from the reaction solution. For more information, I refer to extensive literature described in the introduction of this work (chapter 2.2.2). The general concept of this recycling approach is displayed in Figure 43.

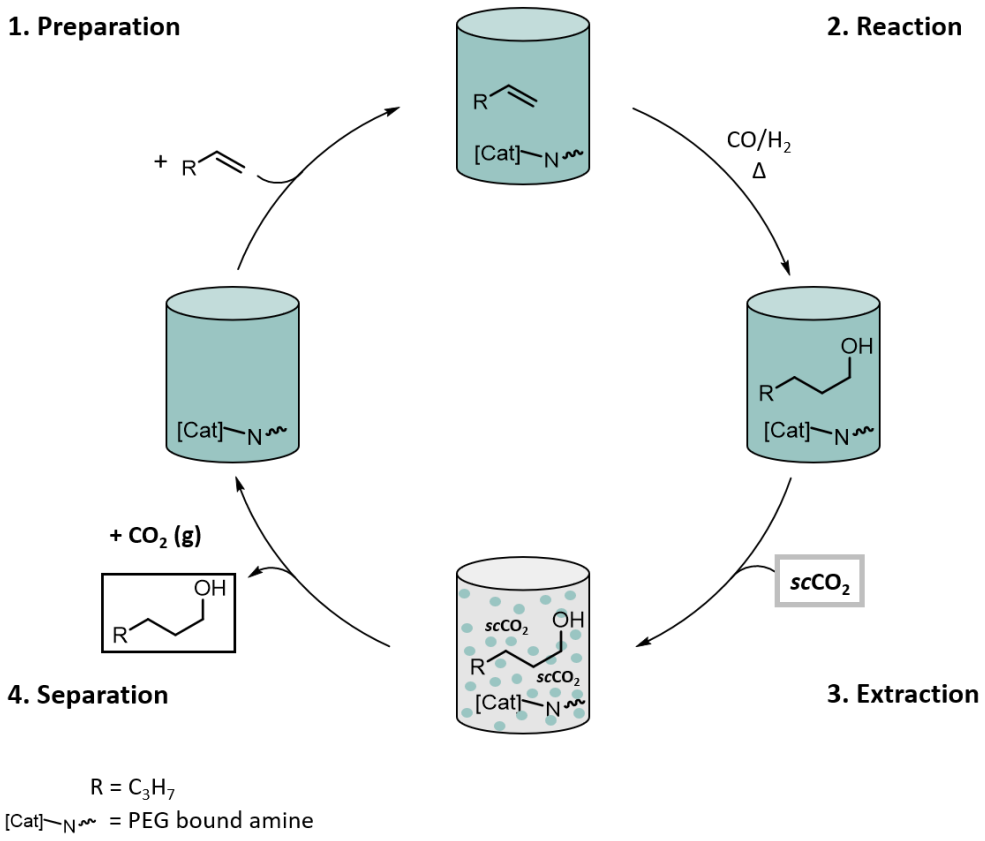

Figure 43: Schematic cycle for the recycling experiments using $sc CO_2$ as the extraction agent for product alcohols. 1: Preparation of the reaction mixture; 2: Reductive hydroformylation under synthesis gas pressure; 3: Extraction of product alcohols/aldehydes and leftover substrates using $sc CO_2$; 4. Separation of product alcohols/aldehydes from CO_2 by depressurization of $sc CO_2$.

To start the first reaction, substrate is added to the rhodium precursor and the aminated ethylene glycol-based solvent (**1. Preparation**). The reaction is conducted by adding synthesis gas under reaction conditions (**2. Reaction**). After the reaction, remaining synthesis gas is released and CO_2 is added to the reaction solution under supercritical conditions (T >31 °C, p >74 bar). To enhance the extraction efficiency, the stationary catalyst phase and the *sc*CO_2 phase are intensely mixed. Alcohols, aldehydes such as alkanes and alkenes are enriched and extracted in the *sc*CO_2 phase. The rhodium catalyst is immobilized in the *sc*CO_2 insoluble aminated ethylene glycol phase (**3. Extraction**). After the extraction, the *sc*CO_2 phase can be released and products/substrates separate from *sc*CO_2 simply by degassing (**4. Separation**). Starting with the next cycle, fresh substrate is added (**1. Preparation**). This process can be operated batchwise or continuously by physically separating the reaction and extraction process.

To investigate the recycling strategy presented in Figure 43 a setup for the batch wise reaction/extraction was developed, which will be used for all recycling experiments presented in the following. The optimized setup for the extraction after some iterations is displayed in Figure 44 and will be shortly explained hereafter.

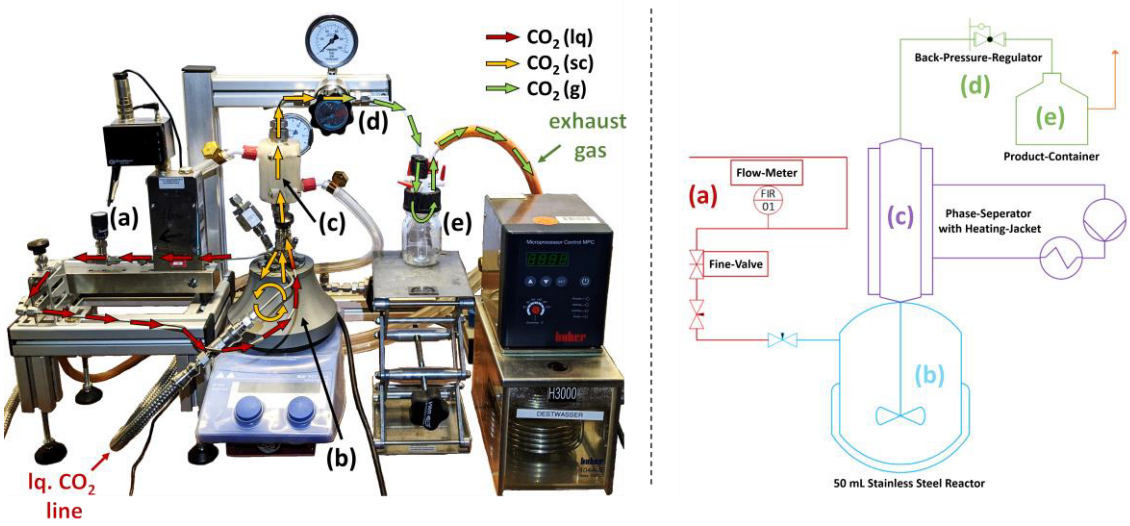

Figure 44: Setup for the extraction of alcohols from ethylene glycol-based stationary phases as described in chapter 4.2.4. Adapted from RÖSLER.[179] Left: Picture of the setup with marked CO_2 streams, right: Simplified flowsheet of the setup. (a) Reactor on stirring plate with heating cone, (b) CO_2 supply line with flow meter and fine valve, (c) phase separator with heating jacket, (d) back-pressure-regulator (BPR), (e) product container.

During the extraction a 50 mL reactor (**b**) is connected to a CO_2 supply line (**a**) and a phase settler (**c**). The phase settler is connected *via* a back-pressure regulator (**d**) to the product container (**e**). CO_2 can be supplied continuously during the extraction in liquid form *via* the supply line (**a**) with a maximum pressure of 110 bar. A flow meter is used to measure the amount of used CO_2 during the extraction and The CO_2 flowrate can be adjusted using a fine valve inserted into the supply line. The liquid CO_2 supplied to the reactor (**b**) is heated to 50 °C in the reactor and mixed with

the stationary phase using a magnetic stirring bar and a stirring speed of 1000 rpm. The backpressure-regulator (BPR) (**d**) at the backend is set above 75 bar to assure supercritical state in the reactor. When the pressure in the reactor reaches the designated pressure, the BPR partially opens, and the pressure is released. When the CO_2 pressure in the supply line is higher than the pressure set for the BPR and the flowrate into the reactor is adjusted carefully, a steady and continuous stream of CO_2 passing to the reactor is ensured. Flowrates must be set to assure a phase transition of *lq*CO_2 to *sc*CO_2 in the reactor.

Preliminary experiments in a 200 mL window reactor allowed to observe the phase behavior of CO_2 and a PEG_{200} mixture under those conditions and was used to observe formation of the supercritical state and phase separation (Figure 45).

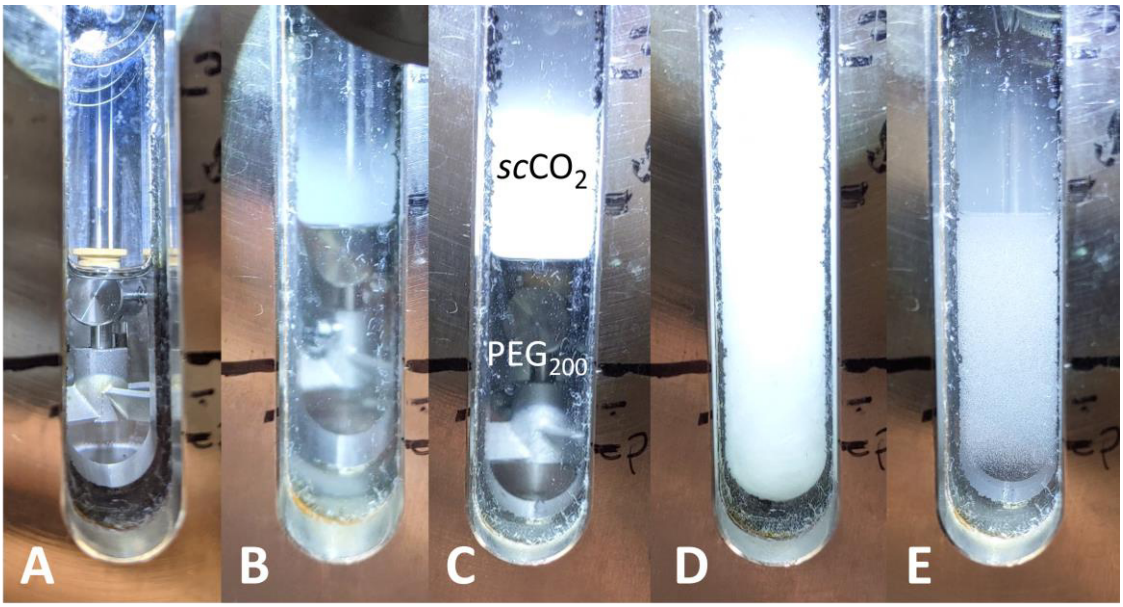

Figure 45: Phase behavior for a biphasic mixture consisting of *sc*CO_2 at 50 °C and up to 95 bar and a PEG_{200} mixture in a 200 mL window reactor. A: PEG_{200} before addition of *sc*CO_2, B: Beginning of the formation of a *sc*CO_2 phase, C: *sc*CO_2 phase and PEG_{200} unmixed, D: Mixing both phases at 1000 rpm, E: Segregation of the two phases five seconds after stopping of mixing.

During those experiments it was already observed that, when mixing of the two phases (Figure 45, **D**), a considerable volume increase is observed. Additionally, the phase separation takes at least a few seconds (Figure 45, **E**). This was confirmed using the setup described in Figure 44 without the phase settler (**c**). Using the setup in Figure 44 during the model extraction of 1-hexanol from PEG_{200} it was observed that the stationary phase is dragged out of the reactor in considerable amounts because complete phase separation cannot be achieved. To solve this, a phase settler was added (**c**) after the reactor. As phase settler a 12 cm long 1/2 inch piping surrounded by a 3D-printed (PE) heating jacket connected to a heated water pump (set to 55 °C), to ensure supercritical state, was used. The phase settler is connected using a 6 cm long 1/8-inch piping to the back-pressure regulator (**d**). Within the back-pressure-regulator the phase

transition from *sc*CO_2 to *g*CO_2 occurs and dissolved products/substrates condensate. *Via* the continuous *g*CO_2 stream condensed products and substrates are transported into the product container (e).

The reaction can be carried out simply by disconnecting the reactor from the CO_2 supply line, exchanging the phase settler with a manometer and pressurizing the reactor with CO/H_2. To evaluate this setup for the general extraction process and to test the separation of product alcohols from ethylene glycol phases, the extraction of hexanol from model mixtures has been investigated first (Table 5).

Table 5: Extractions of alcohols from model mixtures using the extraction setup displayed in Figure 44.

Initial Solution	Extraction Conditions	Extracted Compounds
PEG_{200} + 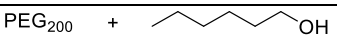 60:40 w% (PEG_{200}:1-hexanol), total mass 9.5 g	50 °C, 80 bar, 335 g *sc*CO_2 (2.7 g min^{-1})	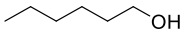 >98 %
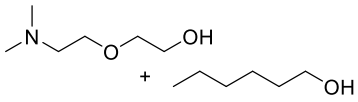 60:40 w% (DEG-amine:1-hexanol), total mass 14.5 g	50 °C, 80 bar, 280 g *sc*CO_2 (2.7 g min^{-1})	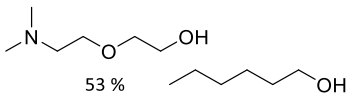 53 % 47 %

In a first experiment hexanol was extracted from a PEG_{200} mixture. Analysis of the extracted compounds in the product container was conducted *via* quantitative NMR (*q*NMR). More information of the analytical procedure can be found in the experimental part 6.3.4. Although a significant amount of *sc*CO_2 was needed for an almost complete extraction under those conditions, it was possible to extract hexanol from the PEG_{200} mixture in very high purity (>98%). This proves the insolubility of higher molecular weight ethylene glycols in *sc*CO_2 and the suitability of the setup for the extraction.

Unsurprisingly, when using the previously investigated DEG-amine as the stationary phase instead of PEG_{200}, leaching of the stationary phase increases significantly. Hexanol and the DEG-amine are extracted almost in similar efficiency with a slight preference for hexanol. The solubility in *sc*CO_2 is mainly influenced by the molecular weight and the polarity of the target molecule. As a rule of thumb, the higher the molecular weight and the polarity of a molecule, the lower is the solubility in *sc*CO_2. It should be mentioned that the density of the *sc*CO_2 phase and therefore the polarity can change significantly depending on the pressure and temperature.[82,83] The DEG-amine has a comparatively low molecular weight of 133 g mol^{-1}. Additionally, the exchange of the alcohol group with a tertiary amine compared to its ethylene glycol analogue significantly decreases the polarity. Tertiary amine functionalized PEG derivatives are not commercially available. Therefore, synthetic strategies for the functionalization of ethylene glycol oligomers or polymers have been investigated.

4.2.5 Synthesis of an Amine Functionalized PEG_{300} Mixture and Its Application as Stationary Catalyst Phase

In a first attempt the ruthenium catalyzed alcohol amination has been investigated (Figure 46). In literature several protocols for the amination of functionalized alcohols using hydrogen borrowing methodologies are described. The group of WILLIAMS described the alcohol amination of alkyl-, benzyl-, phenyl- and amino substituted alcohols with tertiary amines using a ruthenium catalyst in combination with DPEphos as ligand.[180]

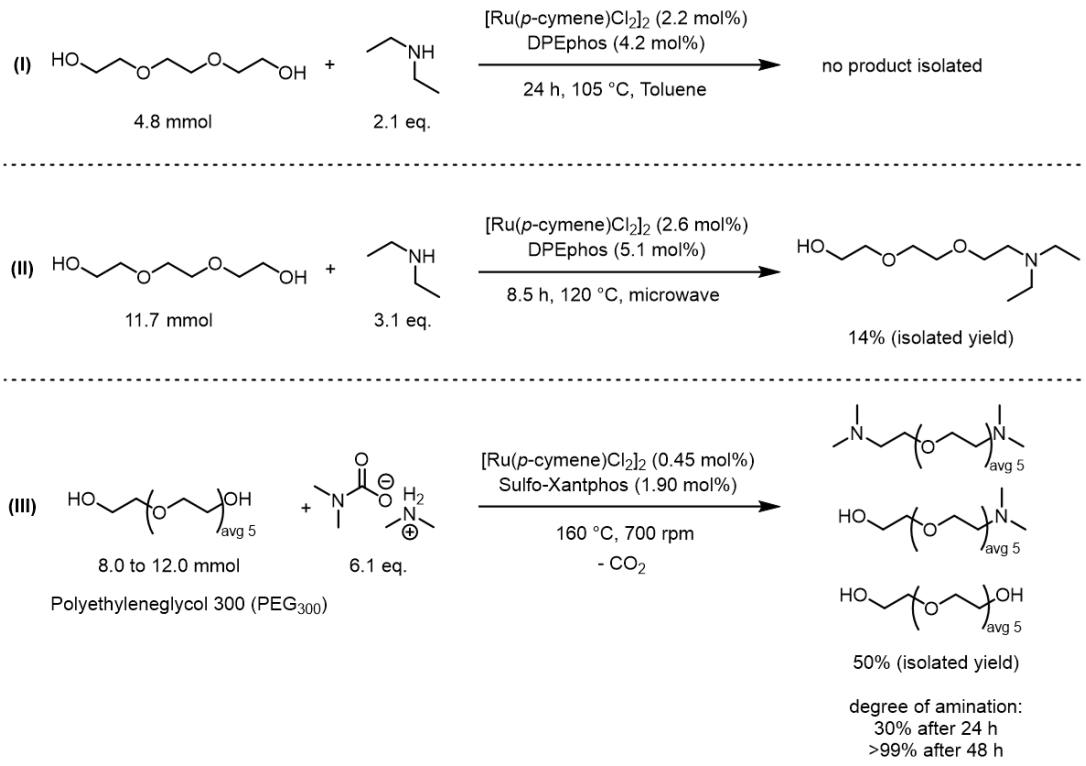

Figure 46: Alcohol amination protocols applied to the amination of ethylene glycol oligomers.Alcohol amination in glass ware following the procedure reported by the group of WILLIAMS[180], (**II**) Microwave assisted alcohol amination as described by the group of WILLIAMS[181], (**III**) Alcohol amination using dimethylammonium dimethylcarbamate (DimCarb) as dimethylamine source as described by the group of SEIDENSTICKER[59].

Unfortunately applying the procedure described by WILLIAMS ET AL to triethylene glycol (TEG) as model substrate and diethylamine as amination agent failed and it was not possible to isolate alcohol amination products in significant amounts after the reaction.

A similar approach using microwave heating was reported by the group of WILLIAMS two years later.[181] Although the reaction products were observed and it was able to isolate 14% of mono-aminated products in this case, the reactivity when using triethylene glycol is still low. Additionally, a GC analysis of the product mixture suggests that partial cleavage of ether bonds and fragmentation occurs. A different approach is reported by the group of SEIDENSTICKER.[59] In

their method, dimethylammonium dimethylcarbamate (DimCarb) is used as the amination agent. The *in situ* decomposition to dimethylamine and CO_2 occurs, which makes the amination with dimethylamine groups possible without using gaseous reactants. DimCarb is used as the reactant and solvent at the same time. As a catalyst ruthenium in combination with sulfoxantphos was used. Due to the decomposition of DimCarb under reaction conditions this reaction was conducted in autoclave reactors instead of glass apparatuses.

The reaction protocol reported by SEIDENSTICKER was successfully applied to TEG, TetraEG and PEG_{300} as substrate. The degree of amination can be effectively controlled by adjusting the reaction time. APCI-spectra of the reaction solution when using PEG_{300} as substrate (Appendix Figure A 4) revealed that after 24 hours about 30% of alcohol groups are aminated and a mixture of non-, mono-, and di-aminated PEG_{300} is obtained. Conducting the reaction for 48 hours results in an almost complete amination with amination degrees of alcohol groups above 98%. After the purification about 50% of the isolated product was obtained. The complete experimental procedure can be found in chapter 6.2.4.

To assure that a similar catalytic activity to the previously used DEG-amine is achieved when using the amine functionalized PEG_{300} derivatives, they have been applied in the reductive hydroformylation of 1-octene (Figure 47).

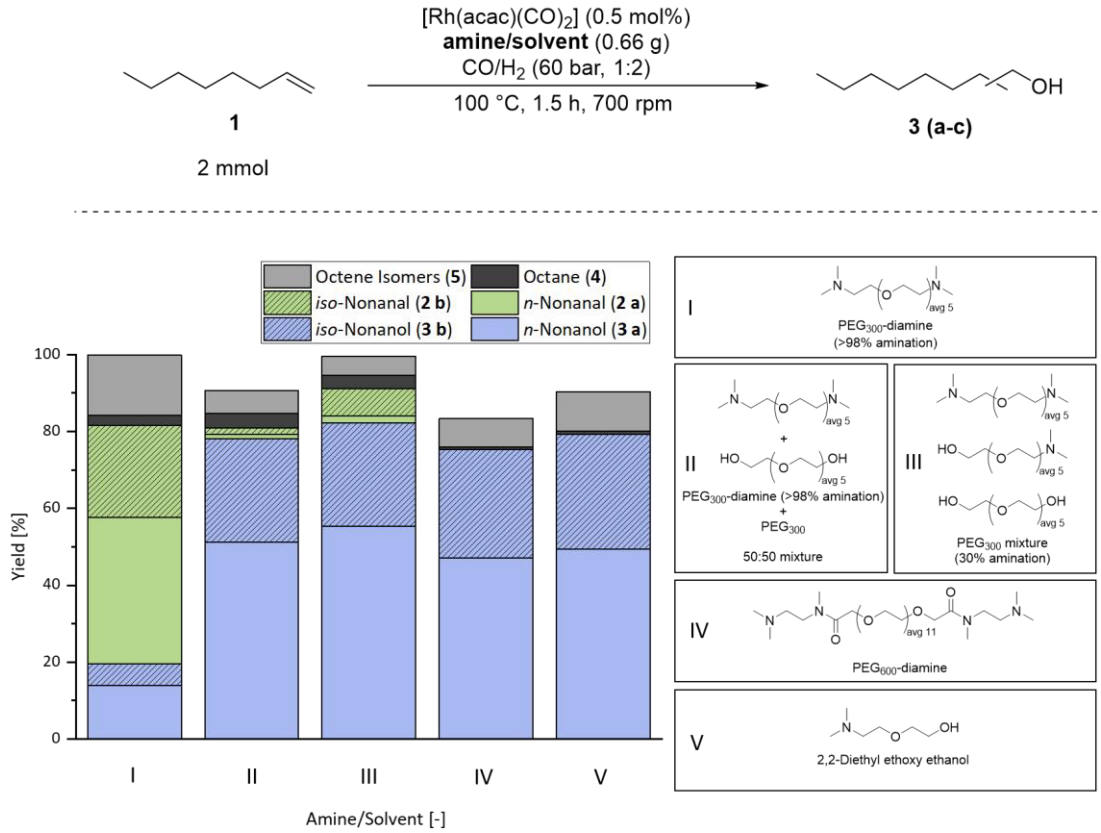

Figure 47: Application of several aminated high molecular weight solvents for the reductive hydroformylation of 1-octene and comparison with the DEG-amine reference. Quantitative/qualitative determination of product yields *via* GC-FID/GC-MS.

To test the influence of the degree of amination on the catalytic activity, PEG_{300} with a degree of amination of >98% (I) and 30% (III) was used as solvent for the reaction. As a reference, the same experiment with DEG-amine as a solvent (V) is displayed.

Surprisingly, when using the PEG_{300} with almost full amination (I) the hydrogenation activity seems to be severely hindered. Compared to the DEG-amine as solvent, the alcohol yield drops from 79% to 20%. The main products are aldehyde intermediates (62%). The overall high selectivity towards hydroformylation products (81%) shows that the hydroformylation activity is not affected. It seems that the presence of hydroxy groups is important to maintain the hydrogenation activity in this case. This was confirmed when the PEG_{300}-amine with a degree of amination of only 30% (III) or a mixture of the fully aminated PEG_{300} and non aminated PEG_{300} (II) was used as solvent. In both cases hydrogenation activity was restored and 82%, respectively 78%, alcohols are generated. This highlights the importance of the presence of certain polar functional groups. Likely, the polar hydroxy groups help to stabilize catalytic species involved during the hydrogenation step. By synthesizing a dimethylamine functionalized PEG_{300}-amine mixture with a degree of amination of 30% an amine functionalized high molecular weight analogue to DEG-amine which shows comparable catalytic activity was found (Figure 47, III).

Subsequently this PEG_{300}-amine mixture was used as solvent during the reductive hydroformylation of 1-pentene and as the stationary phase during the extraction of alcohols from the reaction solution as described for the recycling setup in chapter 4.2.4. Using this methodology, a total of nine consecutive recycling experiments have been conducted in which only fresh 1-pentene has been added after each run. For the extraction, a temperature of 50 °C for the reactor and 55 °C for the heating pump of the phase settler were used. The back-pressure-regulator was set to 95 bar and the extraction was performed until 200 g CO_2 passed the reactor. As sample taking after the reaction would inevitably alter all consecutive recycling runs, only the extract in the product container obtained after each extraction was analyzed *via* quantitative NMR (see chapter 6.3.4). It should be noted though that the extracted compounds can be used to evaluate the stability of the catalyst and the success of the catalyst recycling but should not be regarded as yields. Yields can only be obtained under the assumption of complete and perfect extraction. To evaluate the leaching of the rhodium catalyst, Inductively-Coupled-Plasma-Mass-Spectrometry (ICP-MS) analysis of the extract was conducted. Figure 48 shows the extracted mass of the individual compounds as determined by *q*NMR and the rhodium leaching in ppm for each recycling run.

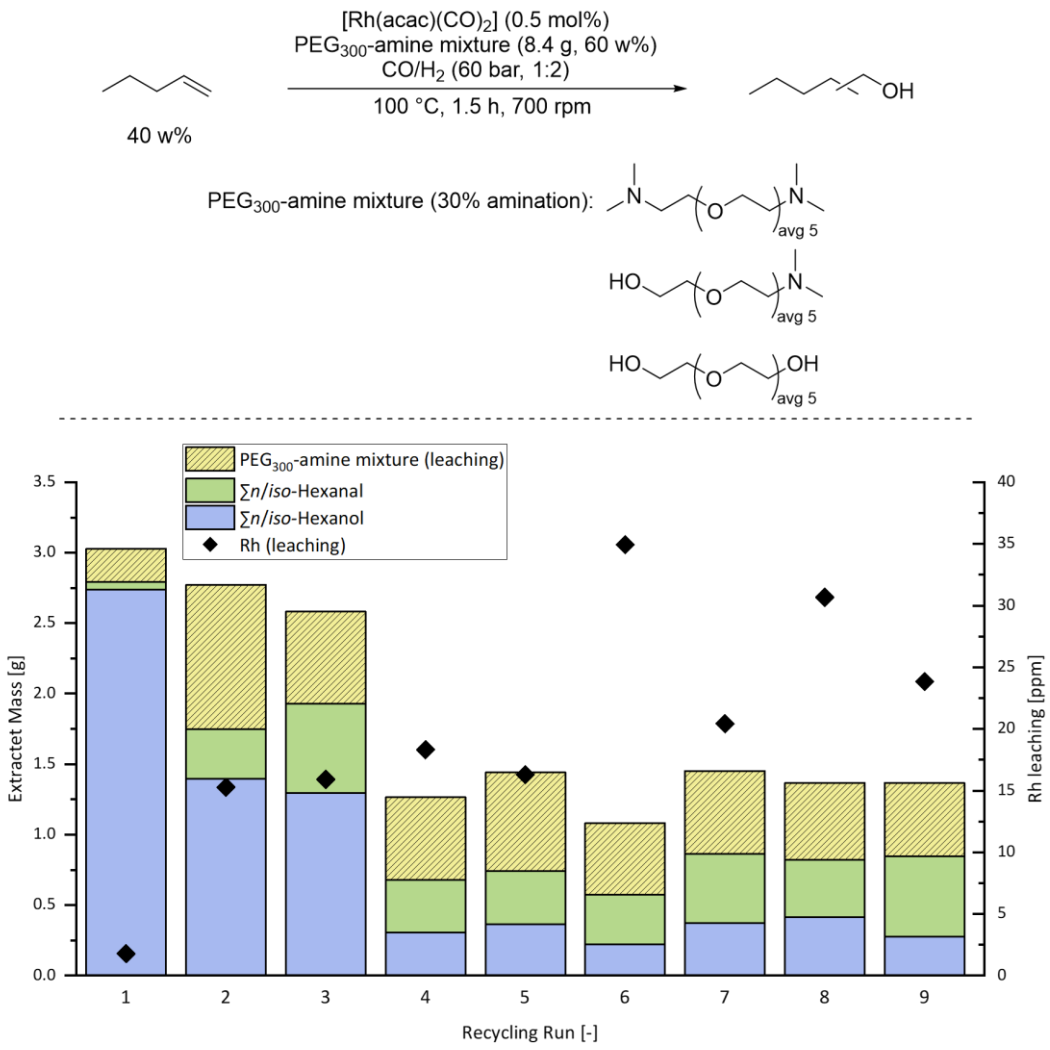

Figure 48: Catalyst recycling of a rhodium catalyst in PEG_{300} amine mixture by extraction of product alcohols with *sc*CO_2. Displayed are the composition of the collected extract fractions after the recycling and rhodium leaching as determined *via* ICP-MS. Quantitative determination of product yields *via* quantitative NMR spectroscopy (*q*NMR). Determination of rhodium leaching by ICP-MS.

In the initial run 3.03 g extract was obtained during the extraction. 91 w% of this proved to be alcohol products which correlates to a theoretical alcohol yield of 36% under the assumption of complete extraction. The neglectable amount of aldehyde intermediates (<1 w%) proves a high hydrogenation activity. Nevertheless 8 w% of the extracted compounds were found to consist of the PEG_{300}-amine mixture. This comparatively high leaching of the stationary phase suggests that the amine functionalization of hydroxy groups severely increases the solubility in *sc*CO_2. Especially considering that during previous experiments using the same setup with the lower molecular weight PEG_{200} as stationary phase almost no leaching was observed (see Table 5). Surprisingly, APCI-spectra of the extract (see Appendix Figure A 4 and Figure A 5) show no preference for lower molecular weight fractions or di-aminated PEG_{300} during the extraction. The PEG_{300}-amine mixture in the extract is almost identical to its initial composition. An explanation would be that the overall polarity of the stationary phase determines the leaching

and because of strong intermolecular interactions shares of the stationary phase rather than individual molecules are dragged into the *sc*CO_2 phase. Even though, a considerable leaching of the stationary phase is observed, rhodium leaching in the extract was determined to be rather low with only 1.8 ppm (corresponding to approximately 0.01 % of the initial amount of rhodium), which suggests that leaching of the stationary phase does not automatically induce a leaching of the rhodium catalyst.

After the second reaction, the amount of extract decreases slightly to 2.78 g. More importantly, the mass of extracted products significantly decreases. Only 50 w% of the extract can be attributed to alcohols with another 13 w% of aldehyde products. In unison, leaching of the stationary phase significantly increases and contributes with 37 w% to the extract. The decrease in extracted products and the increased mass of extracted aldehydes suggest a drop in hydroformylation and hydrogenation activity. This can be partially attributed to the leaching of the stationary phase and a decrease in the ratio of the stationary phase to the substrate (see Figure 41). Even though, until the second run only 0.3 g out of 8.4 g of the PEG_{300} mixture was leached out of the reactor which suggests that the decrease in catalytic activity is likely due to partial deactivation of the catalyst after the first run. Rhodium leaching increases to 15 ppm in the second run (0.1% of initial rhodium).

In run four another significant drop in catalytic activity is observed. Overall, only 1.3 g of extract are gained from which 0.7 g can be attributed to alcohol and aldehyde products and 0.6 g to a leaching of the PEG_{300}-amine phase. From run five to run eight the catalytic activity remains low but comparatively constant. Leaching of the stationary catalyst phase remains high between 0.5 g and 0.7 g each run. The leaching of rhodium catalyst increases to over 30 ppm (0.2% of initial rhodium) in run six and eight. During the last run, a further drop in hydrogenation activity is observed and only 0.25 g of alcohols are extracted (corresponding to a theoretical alcohol yield of about 3%). At this point it is obvious that the continuous leaching of amine will abolish the reaction. After the last extraction only 3.6 g of the initial 8.4 g PEG_{300}-amine mixture was left in the reactor. Even though about 60% of the initial stationary phase was leached out of the reactor during all nine recycling runs combined, the combined rhodium leaching amounts to less than 1% of the initial amount of rhodium, proving that the immobilization of rhodium in the stationary phase was successful and that the rhodium leaching is mostly independent from the leaching of the stationary phase. Assuming the formation of anionic rhodium species with ammonium ions as counter ions as described in chapter 4.1.5, those species would be much less soluble in *sc*CO_2 than PEG_{300}-amines not involved in the formation of ionic species and are much more unlikely to be extracted.

Overall, the first recycling attempt using an amine functionalized PEG_{300}-mixture as the stationary phase proved that the general recycling concept is feasible but the increased solubility

in *sc*CO_2 by exchanging hydroxy with tertiary amine groups makes further adjustments of the aminated solvent necessary to reduce the leaching of the stationary phase and maintain a high catalytic activity.

As discussed previously, an easy way to decrease the solubility in *sc*CO_2 is to increase the molecular weight. Nevertheless, since it was found that the exchange of hydroxy with tertiary amine groups significantly increased the solubility in *sc*CO_2, but at the same time a high concentration of tertiary amine groups benefits the catalytic activity, an incorporation of polar functional groups in the backbone of the target molecule would certainly significantly decrease the solubility in *sc*CO_2.

4.2.6 Synthesis of Diamine Functionalized PEG_{600} Containing Polar Amide Functional Groups and its Application as Stationary Catalyst Phase

A very promising approach to combine both concepts (increase of MW and incorporation of polar functional groups) is the amide condensation of PEG_{600}-diacid with trimethyldiaminoethane as displayed in Figure 49.

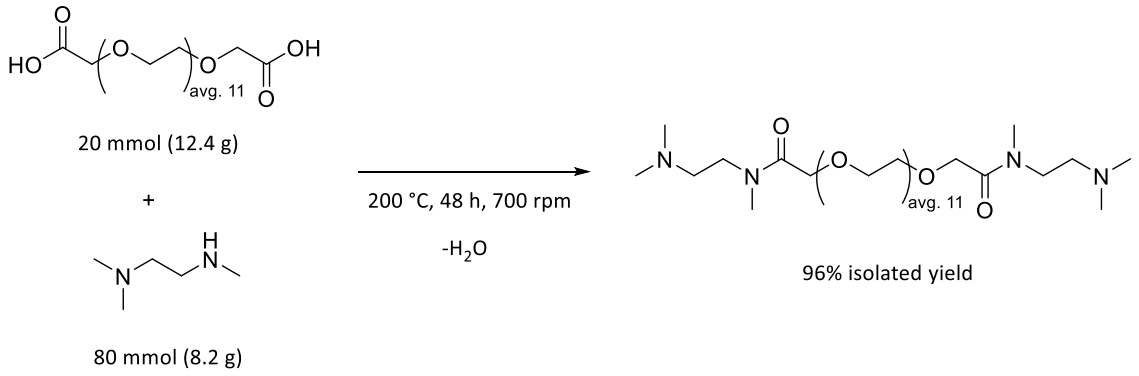

Figure 49: Reaction protocol for the amide condensation reaction of PEG600-diacid and trimethyldiaminoethane to a diamine functionalized PEG_{600} derivative containing polar amide groups (PEG_{600}-diamine).

The reaction proceeds without any catalyst and the only byproduct is water. Full amination is achieved after 48 hours of reaction time. As product a bis-dimethylamine functionalized ethylene glycol oligomer is obtained with an average MW of 787 g mol^{-1}, containing amide groups in its backbone. Hereafter referred to as PEG_{600}-diamine. Solvents containing amide groups have been proven to support a high catalytic activity for the reaction during the previous screening of solvents (see Figure 37). Because no catalyst is needed, the product can be purified simply by removing the reaction water and excess trimethyldiaminoethane under reduced pressure after the reaction (the full experimental procedure can be found in chapter 6.2.5). The product is obtained with an isolated yield of 96%.

Testing of the PEG_{600}-diamine as solvent for the reductive hydroformylation of 1-octene under optimized conditions (Figure 47, IV) shows that a comparable catalytic activity to DEG-amine (Figure 47, V) is achieved. Overall, 75% alcohol products are obtained while no aldehyde intermediates are observed, supporting a high hydrogenation activity. Comparing the catalytic activity of the PEG_{600}-diamine (Figure 47, IV) with the results of the diamine functionalized PEG_{300} as solvent (Figure 47, I) highlights the influence and importance of the amide group on the hydrogenation activity. Both solvents are structurally similar, except for the amide groups incorporated in the PEG_{600}-diamine backbone. Still, the hydrogenation activity is vastly different. Using the diamine functionalized PEG_{300} as solvent, little more than ¼ of the alcohol yield than using the amide containing PEG_{600}-diamine as solvent are gained.

After those promising results, the novel PEG_{600}-diamine was used as catalyst phase in a consecutive of nine recycling runs, in a similar procedure to the previous attempt, hoping to

achieve a better immobilization of the stationary phase during the extraction than in the previous attempt (Figure 50).

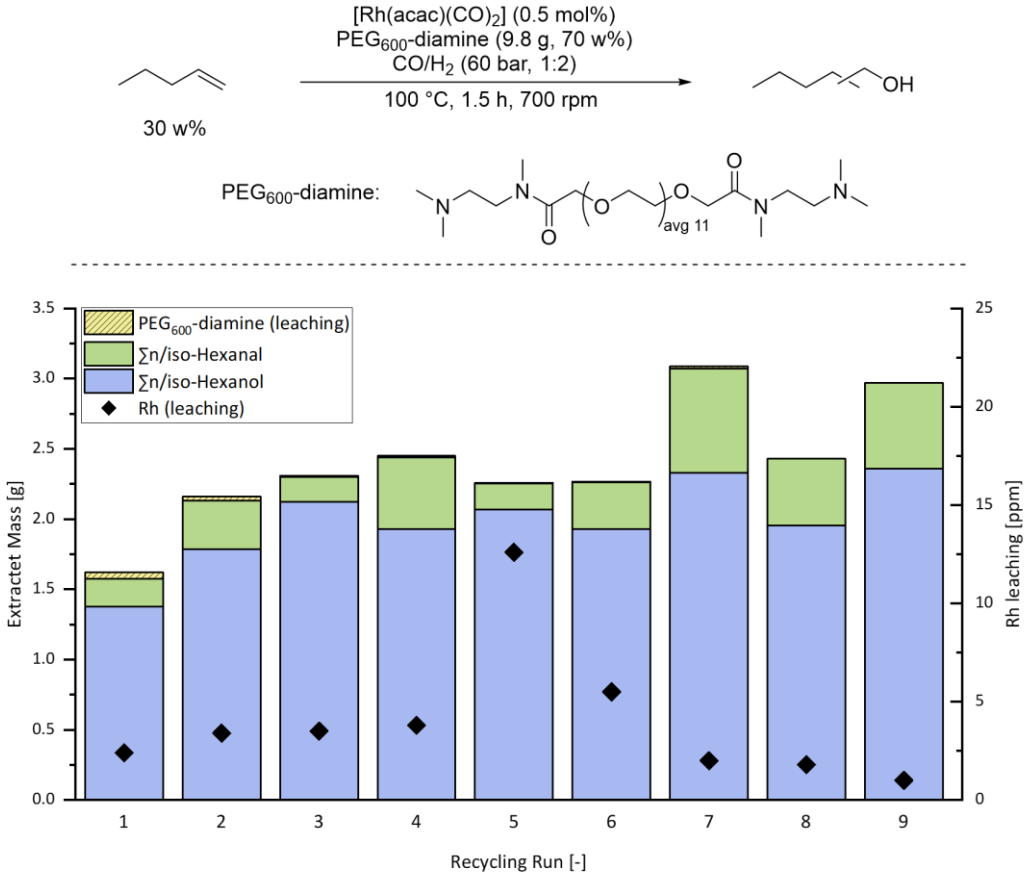

Figure 50: Catalyst recycling of a rhodium catalyst in diaminated PEG_{600} by extraction of product alcohols with *sc*CO_2 as adapted from [179]. Displayed are the composition of the collected extract fractions after the recycling and rhodium leachings as determined *via* ICP-MS. Quantitative determination of product yields *via* quantitative NMR spectroscopy (*q*NMR). Determination of rhodium leaching by ICP-MS.

As only adjustment to the previous recycling experiment, the substrate concentration was reduced from 40 w% to 30 w%. Additionally, the amount of CO_2 during each extraction was reduced from 200 g to 150 g. Weighing of the product container and comparing the extracted amount of product with the amount of consumed CO_2 during the first extraction run revealed that the extraction efficiency (mass of extract gained per gramm of *sc*CO_2 used) after 150 g of *sc*CO_2 is used already dropped to 1/5 th compared to the initial efficiency, making any further extraction not productive (Figure 51). During the first recycling run 1.6 g of extract was gained (Figure 50). Although, overall a lower amount was extracted compared to the first recycling run using the PEG_{300}-amine mixture as stationary phase (see Figure 48), 85 w% of the extracted mass consisted of alcohols (corresponding to a theoretical alcohol yield of 25% under the assumption of complete extraction) and 12 w% of aldehydes. Leaching of stationary PEG_{600}-diamine phase contributed with less than 3 w% to the extract.

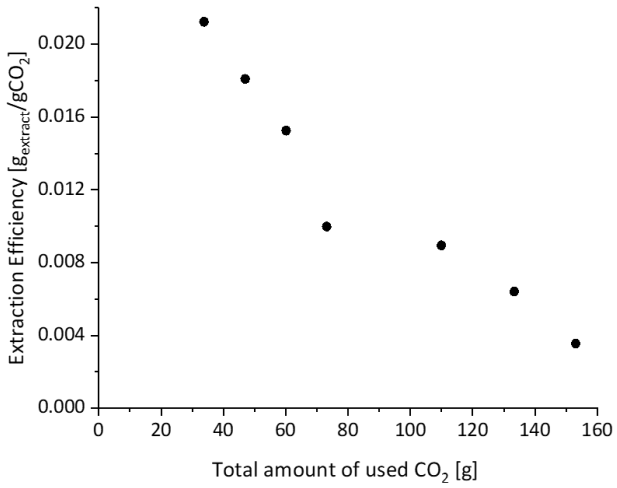

Figure 51: Declining extraction efficiency with the amount of consumed CO_2 during the extraction of product alcohols for the first recycling experiment using PEG_{600}-diamine as the stationary catalyst phase.

In unison, ICP-MS of the extract confirmed minimal rhodium leaching with a concentration of 2.4 ppm (<0.005% of the initial amount of rhodium). During the second and the third recycling run the extracted mass increases up to 2.3 g. The selectivity towards alcohols remains high with alcohols making up 83 w% and 92 w% respectively (corresponding to alcohol yields of 33% and 39%) of the extract. Leaching of the stationary phase decreases to 0.5 w% of the extract in the third run and rhodium leaching levels at around 3 ppm per run. During the following runs the extracted mass levels around 2.2 g to 2.4 g except for run seven and nine in which around 3 g of extract are gained. During all runs a high selectivity of the extracted fractions towards alcohols is maintained with alcohols making up between 75 w% and 92 w% of the extract. Leaching of the PEG_{600}-diamine phase decreases further. During the eighth and ninth run the amount of PEG_{600}-diamine leaching proved to be below the quantification limit of the *q*NMR (<0.1 w%). Rhodium leaching was determined to be between 1 ppm and 4 ppm during all runs except for run five and six. In all nine runs combined about 0.1% of the initial rhodium was transferred out of the reactor. Again, a correlation between leaching of the stationary phase and rhodium leaching is not observed. During the experiments a Total-Turn-Over-Number (TTON) of 700 is achieved.

The consistent selectivity towards alcohols in unison with the amount of extract gained during all runs shows that no deactivation of the catalyst within the frame of this experiment occurs. The unchanged catalytic activity and selectivity even during the last run suggests that more recycling runs are easily possible.

4.2.7 Comparison of Recycling Techniques for Rhodium/Amine Catalysts Reported Over the Last Two Years

Including the herein presented approach, three different techniques for the recycling of rhodium amine catalysts have been reported by our group within the last two years (short description of the ones reported by PÜSCHEL in the introduction of chapter 4.2). Upon comparison of the recycling approach presented in this work, it can be concluded that so far, the extraction with $scCO_2$ shows the lowest leaching of rhodium catalyst. Furthermore, there were no concerns regarding the catalyst stability over the course of the recycling experiments (Table 6).

Table 6: Comparison of recycling strategies for rhodium/amine catalysts reported in the molecular catalysis group of the Max Planck Institute for chemical energy conversion.

Concept for the recycling of the catalyst:	**Biphasic liquid/liquid catalyst recycling with dimethylaminoethanol as polar phase**[159]	**CO_2 induced switch to a biphasic reaction system after the reaction**[158]	**Extraction of alcohols with $scCO_2$ from PEG-amine phases (*this work*)**[179]
Rhodium leaching	>1% per run	37% over ten runs	0.1% over nine runs
Stability	Dimethylaminoethanol make up stream necessary	Catalyst deactivation at high CO_2 concentrations	Stable over nine runs; no sign of deactivation
Products	C_6-C_{11} Alcohols	Nonanol	Hexanol
TTON	1263	2810	700

It should be noted though that the herein presented approach has only been conducted in batch experiments and not in a continuous process. The Total-Turn-Over-Numbers (TTON) is lower compared to the other approaches. Furthermore, the extraction efficiency of higher molecular weight alcohols has not been tested and will strongly depend on their solubility in *sc*CO_2.

The next step would be to investigate and optimize the recycling process in a more sophisticated continuously operated setup which allows to investigate the catalyst stability over longer periods of time and to optimize the extraction process, e.g. by *in situ* monitoring of the temperature, optimized mixing, or higher *sc*CO_2 pressures.

4.2.8 Short Recollecting of the Results Achieved during the Investigation of Rhodium/Tertiary Amine Catalysts for the Reductive Hydroformylation of Alpha Olefins

The goal during the first half of this work was to investigate the auto tandem catalyzed reductive hydroformylation using rhodium/amine catalysts. Within the greater picture of contributing to the development of new synthetic routes towards alcohols as synthetic fuel additives, it was of special interest to not only understand the catalytic system on a molecular level but to develop a robust and highly active catalytic system, including a process for the recycling rhodium catalyst. Figure 52 gives a short overview of the most important results achieved concerning the initial goals (see Figure 19).

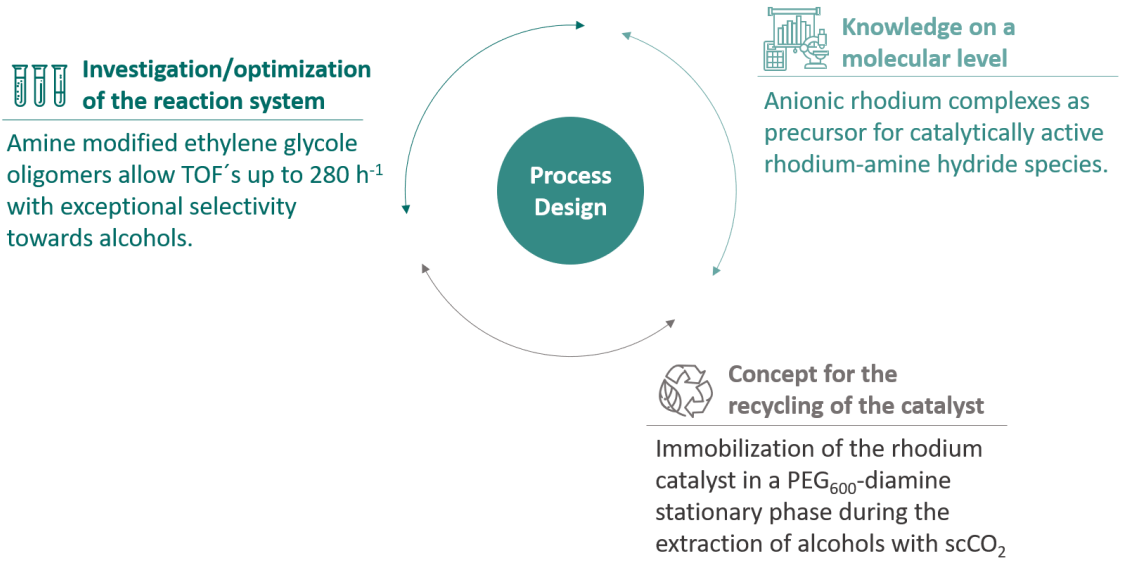

Figure 52: Main results achieved for the the reductive hydroformylation of linear alkenes with rhodium/tertiary amine catalysts.

Over the course of chapter 4.1 a highly active and selective catalytic system based on rhodium catalysts in combination with tertiary alkylamine ligands was developed. Especially the CO partial pressure and the electronic and steric characteristics of the used tertiary amine proved as essential to achieve a high hydrogenation activity. In combination with spectroscopic investigations, which revealed a sensibile equilibrium of several anionic rhodium complexes with ammonium cations as the counter ion, a mechanism for the formation of catalytically active rhodium/amine hydride species was postulated.

Understanding of the system on a molecular level helped to further optimize the system and allow catalytic activities with a TOF of up to 280 h^{-1}. To the best of my knowledge this is one of the highest reported catalytic activites for the rhodium catalyzed reductive hydroformylation so far and is only exceeded by similar catalytic systems based on the use of rhodium in combination

with water soluble alkanolamines reported by S.PÜSCHEL.[159] By combining amine (ligand) and solvent properties in the form of amine functionalized PEG derivatives, the recycling of the rhodium catalyst *via* the extraction of product alcohols with *sc*CO_2 was possible in high efficiency. Over nine consecutive runs, no change in activity or selectivity was observed and leaching of the rhodium catalyst was determined to be 0.1% of the initial amount of rhodium for all nine runs combined. The product was obtained by simply degassing *sc*CO_2 after the extraction. The results described in this work clearly mark the potential of these, in my opinion, underrated kind of catalytic systems for the reductive hydroformylation of middle to long chain alcohols. I hope these impulses encourage the scientific community to their further investigation.

4.3 One-Pot Conversion of Synthesis Gas to Alcohols by Combining Fischer-Tropsch-Synthesis and Reductive Hydroformylation Reaction in a Novel "Multi-Tandem-Approach"

In the previous chapter the conversion of olefins to middle to long chain alcohols was discussed. The rising importance of those alcohols is linked to the prospect of application as fuel additives in Biomass-to-Liquid (BtL) or Power-to-Liquid concepts (PtL) (see chapter 2.1 and 2.4). A key center piece in the majority of those concepts is the Fischer-Tropsch synthesis to convert synthesis gas (CO/H_2) into hydrocarbons of various chain lengths.[16,119,182] Thereby, alkanes are produced as the major products of Fischer-Tropsch processes, with alcohols and alkenes being minor fractions. Significant scientific effort has been made to tune the selectivity of Fischer-Tropsch catalysts to derive either a high olefin selectivity (e.g. in the concept of the REDIFUEL project), or to directly steer the selectivity to high alcohol shares. While in the REDIFUEL project (chapter 2.1) a Fischer-Tropsch catalyst with an extraordinary high selectivity towards olefins, developed by PRIETO ET AL (with a hydrocarbon olefin selectivity of 30%), is described, Fischer-Tropsch catalysts selectively producing high shares of alcohols are still lacking severe disadvantages (see chapter 2.4.2). Contrary to the existing Fischer-Tropsch to alcohol approaches, a highly innovative concept for the direct conversion of synthesis gas to alcohols was envisioned in this work. The combination of Fischer-Tropsch (FT) synthesis and reductive hydroformylation reaction (Hyfo) in a tandem catalytic system (Figure 53) would allow to convert synthesis gas to alcohols, while circumventing some of the major drawbacks associated with other appraoches.

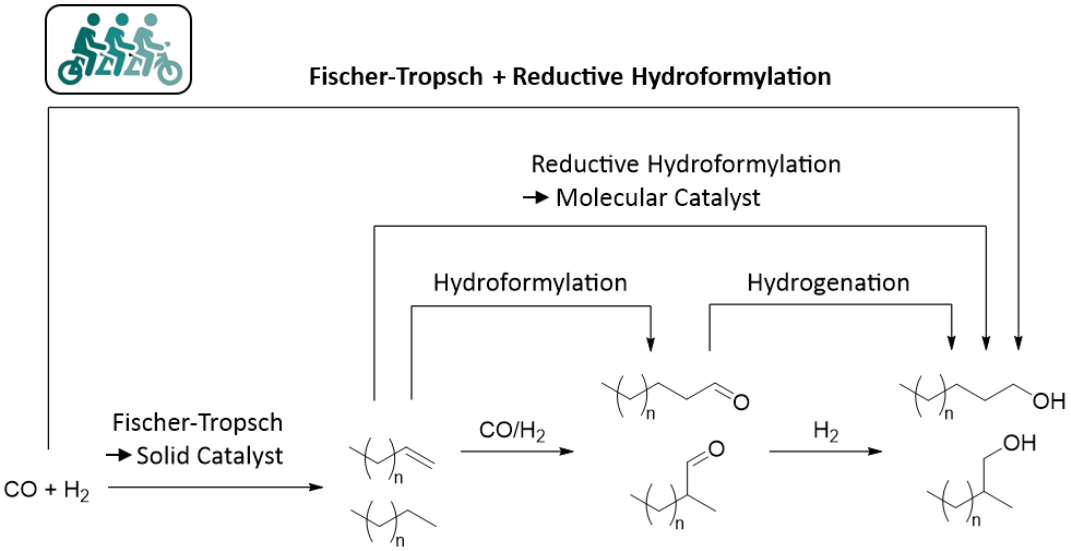

Figure 53: Principle for the combination of the heterogeneously catalyzed Fischer-Tropsch reaction and homogeneously catalyzed reductive hydroformylation reaction in a novel "multi-tandem" approach for the direct conversion of synthesis gas to alcohols.

In this concept the Fischer-Tropsch catalyst produces alkanes and alkenes whereas the reductive hydroformylation catalyst directly converts the *in situ* generated alkenes to alcohols. Traditionally the Fischer-Tropsch reaction is conducted at temperatures considered too high for hydroformylation catalysts (>200 °C), which would inevitably lead to the decomposition of the homogeneous hydroformylation catalyst.[98] The Fischer-Tropsch catalyst developed by PRIETO does not only produce high shares of olefins, beneficial to the hydroformylation step, but is operated at comparatively low temperatures of 195 °C. While those temperatures are still too high for rhodium-based catalysts, as they are state of the art in industry, cobalt-based hydroformylation catalysts are known to reliably produce alcohols at temperatures up to 200 °C.[102]

In the following chapters, the combination of a cobalt-based Fischer-Tropsch catalyst developed by the group of PRIETO and a reductive hydroformylation catalyst based on cobalt in combination with alkylphosphine ligands will be investigated. Both catalysts will be applied in a slurry phase One-Pot reaction (chapter 4.3.3). Nevertheless, before both catalysts can be combined, important parameters for the reductive hydroformylation of 1-octene, catalyzed by a cobalt/trialkylphosphine catalysts, and the characterization of cobalt species on solution will be discussed (chapter 4.3.1). These experiments are important to observe the influence of critical reaction parameters and will serve as reference and starting point for the experiments during the combined approach.

The Fischer-Tropsch catalyst, used during this project, was developed and characterized by JESKE and PRIETO. Even though this has not been conducted by the author of this thesis, some important characteristics of this novel type of Fischer-Tropsch catalyst and its performance in gas-phase Fischer-Tropsch reaction are essential for the later discussion and will be briefly summarized (chapter 4.3.2).

During the preliminary investigations of the cobalt catalyzed reductive hydroformylation, such as in the combined approach, 10 mL autoclave reactors have been used. A detailed experimental procedure can be found in chapter 6.2.7 and chapter 6.2.10. For the preliminary investigation of the Fischer-Tropsch catalyst during gas-phase reactions, a fixed bed continuous flow reactor has been used. The detailed experimental procedure can be found in chapter 6.2.9. Quantitative analysis of the reaction mictures during the investigation of the cobalt catalyzed reductive hydroformylation of 1-octene was conducted *via* GC-FID as discussed in chapter 6.3.1. For qualitative assignment of products, a combination of GC-MS and ^{1}H-NMR was used (chapter 6.3.4.1). Experiments during the combined approach were analyzed *via* a combination of GC-FID, GC-TCD and TGA analysis as described in chapter 6.3.2 and 6.3.3. Experiments displayed in graphical form in chapter 4.3.1 can be found tabulated in the Appendix (chapter 10.2).

The results presented in the following have been accomplished in close collaboration with Dr. K. Jeske and Dr. G. Prieto. Hereby, the investigation and optimization of the reductive hydroformylation catalyst (chapter 4.3.1) were conducted in this group and the characterization of the Fischer-Tropsch catalyst (chapter 4.3.2) was conducted in the group of Dr. Prieto. During the investigation of the combined approach (chapter 4.3.3), the project partners contributed equally.

Parts of this chapter are published in:

K. Jeske; T. Rösler; M. Belleflamme; T. Rodenas; N. Fischer; M. Claeys; W. Leitner; A. J. Vorholt; G. Prieto, "Direct Conversion of Syngas to Higher Alcohols via Tandem Integration of Fischer-Tropsch Synthesis and Reductive Hydroformylation", Angew. Chem. Int. Ed., **2022**, 61, e20220100, DOI: 10.1002/anie.202201004.

Whereas authors contributed as follows (using CRediT standardized contribution descriptions):

K. Jeske*:	Writing – original draft, investigation, methodology
T. Rösler*:	Writing – original draft, investigation, methodology
T. Belleflamme:	Investigation (masters thesis), methodology
T. Rodenas:	Investigation (assistance for ICP analysis)
N. Fischer:	Investigation (3-Dimensional GC analysis)
M. Claeys:	Investigation (3-Dimensional GC analysis)
A. J. Vorholt:	Methodology, supervision, writing – review and editing
G. Prieto:	Methodology, supervision, writing – review and editing
W. Leitner:	Conceptualization, supervision, writing – review and editing

*: Authors contributed equally

4.3.1 Investigation of Important Parameters for the the Cobalt/Trialkylphosphine Catalyzed Reductive Hydroformylation

In the first chapter the reductive hydroformylation of alpha olefins using cobalt alkylphosphine catalysts will be investigated. While the reductive hydroformylation using cobalt catalysts is well known (see chapter 2.3), the goal in this work is to investigate the cobalt catalyzed reductive hydroformylation with regards to the application in combination with the NaPr-CoRu@AOmM Fischer-Tropsch catalyst developed by JESKE and PRIETO ET AL. Therefore, the focus of the following experiments is to develop a robust catalytic system for the reductive hydroformylation of alpha olefins which operates at reaction conditions applicable in combination with the Fischer-Tropsch catalyst. Furthermore, understanding the influence of chosen parameters and identification of important catalytic species, will be used to interpret the results during the combination of the Fischer-Tropsch and the reductive hydroformylation catalysts.

For the investigation of the reductive hydroformylation step 1-octene was used as model substrate. 1-Octene represents the average chain length expected for the Fischer-Tropsch olefin product spectrum and therefore enables a good estimation of the reactivity during the later combined experiments. In Figure 54 the reaction network for the reductive hydroformylation of 1-octene using cobalt/trialkylphosphine catalysts is displayed.

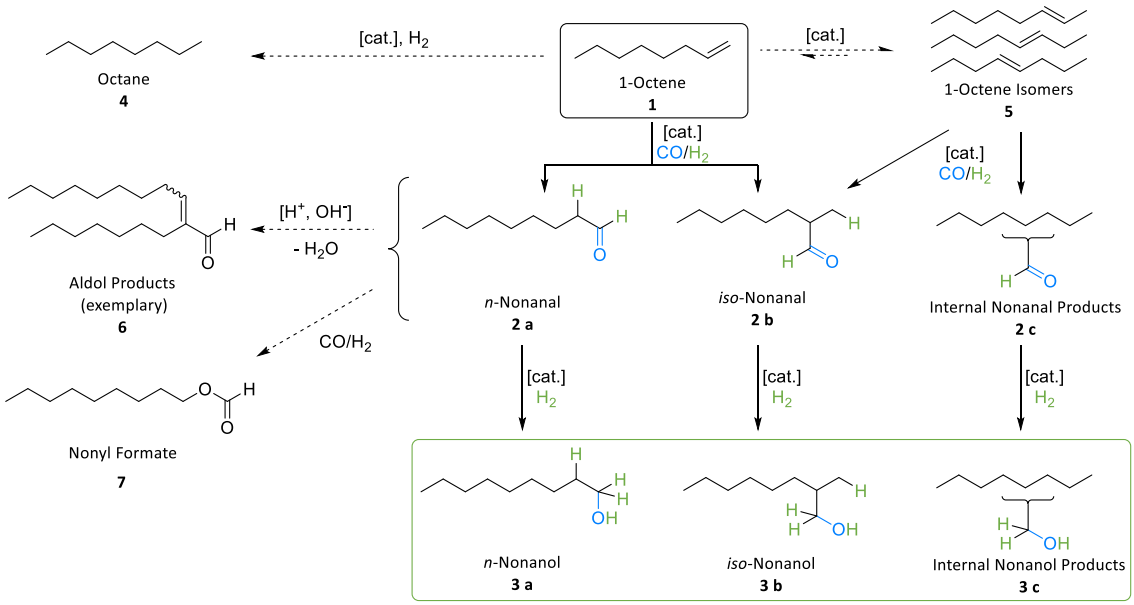

Figure 54: Reaction network for the cobalt/trialkylphosphine catalyzed reductive hydroformylation of 1-octene.

The general reaction sequence is similar to the one described in chapter 4.1.: *Via* hydroformylation of 1-octene (**1**) linear and branched aldehydes (**2 a+b**) are formed which are subsequently hydrogenated to linear and branched alcohols (**3 a+b**). Besides hydroformylation of the starting olefin, commonly the hydrogenation of the double bond to the corresponding alkane (**5**) and isomerization to internal double bonds (**4**) is observed. Whereas hydrogenated

starting material is lost for the reaction, isomers of the starting olefin (**4**) can also undergo hydroformylation/hydrogenation reactions, leading to branched aldehyde and alcohol products (**2 b+c**; **3 b+c**). The Aldol condensation of intermediate aldehydes to higher molecular branched aldehydes (**6**) has not been observed. In contrast to the previously described reaction network for the reductive hydroformylation, as described in chapter 4.1, the formation of formate products (**7**) by carbonylation and hydrogenation of aldehyde intermediates has been observed in low amounts (<2%) and under certain reaction conditions.

The reaction conditions used during the first experiments are based on investigations of SLAUGH and MULLINEAUX on the cobalt tributylphosphine catalyzed reductive hydroformylation.[102] The investigations of SLAUGH and MULLINEAUX have been used as the foundation for the Shell hydroformylation process to higher alcohols.[101] In the reaction conditions reported by SLAUGH and MULLINEAUX A reaction temperature of 195 °C is used, which fits very well with the reaction conditions of the Fischer-Tropsch step (see chapter 4.3.2). As catalyst, the combination of $Co_2(CO)_8$ and tricyclohexylphosphine (PCy_3) was used in a ratio of $Co:PCy_3$ = 1:1. During the original report by SLAUGH and MULLINEAUX, tributylphosphine was used as the igand.[102] Tricyclohexylphosphine has a similar basicity compared to tri-*n*-butylphosphine but is more oxygen resistant and has therefore been chosen as substitute to tri-*n*-butylphosphine. Unless stated otherwise, the conversion for each experiment displayed in the following is >95%.

4.3.1.1 Influence of Synthesis Gas Pressure and Syn-Gas Ratio on the Reductive Hydroformylation using Cobalt/Tricyclophexylphosphine Catalysts

As the first parameter the total pressure at a carbon monoxide, hydrogen ratio of 1:1 was investigated (Figure 55) as critical parameter for the later combined approach. Cobalt hydroformylation catalysts are known to require comparable high carbon monoxide partial pressures (>90 bar) to stabilize catalytically active mononuclear cobalt carbonyl complexes.[183] Although it has been recently shown that the reaction also proceeds at lower pressures if the catalytic species can be stabilized.[88,184] Contrary, gas-phase Fischer-Tropsch reactions are operated at much lower pressures,[117,122] although higher pressures are usually accepted but not beneficial. The optimized synthesis gas pressure for the gas phase Fischer-Tropsch catalyst (NaPr-CoRu@AOmM) is 30 bar. In the original work of SLAUGH and MULLINEAUX a synthesis gas pressure of 120 bar is used for the reductive hydroformylation.

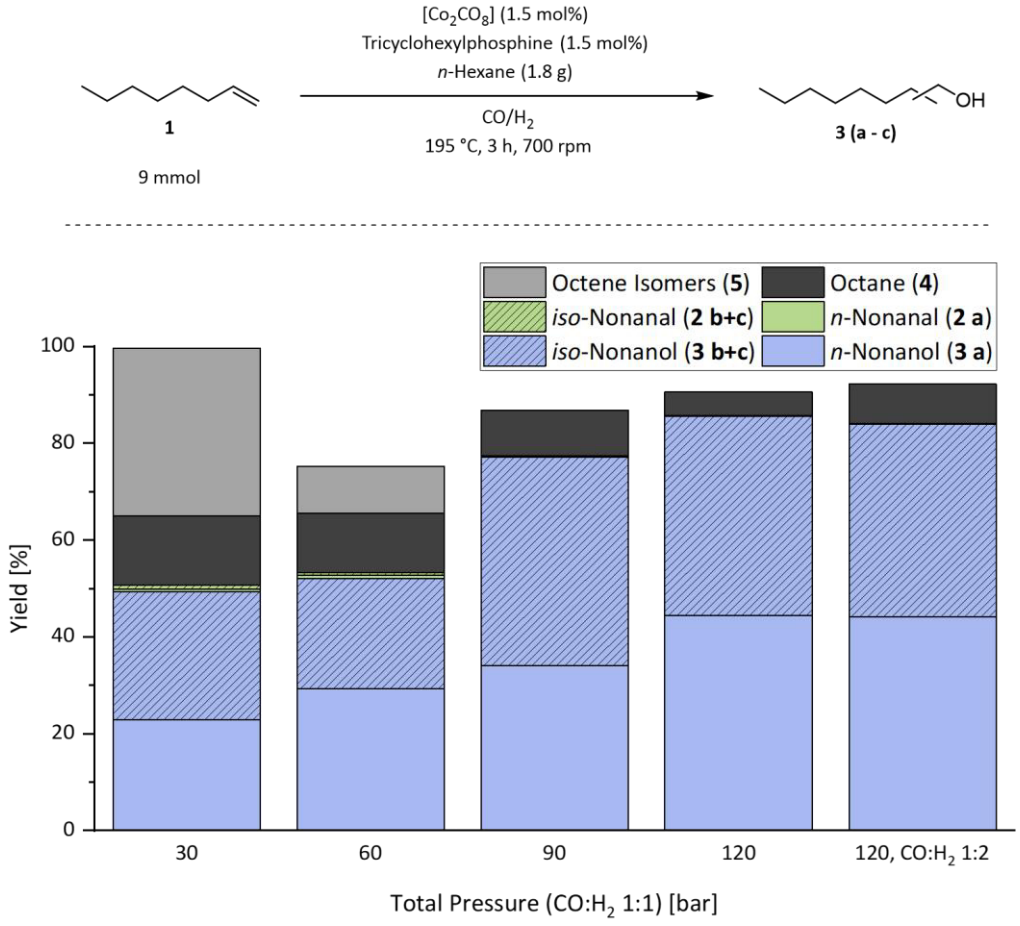

Figure 55: Product yield in the reductive hydroformylation of 1-octene using a $[Co_2(CO)_8]/PCy_3$ catalyst at various combinations of pressure and $CO:H_2$ ratios.Quantitative/qualitative determination of product yields *via* GC-FID/GC-MS.

Surprisingly, even at comparatively low synthesis gas pressures of 30 bar, 49% alcohols are obtained within three hours of reaction time during the reductive hydroformylation of 1-octene

(Figure 55, left bar). Nevertheless, a significant amount of starting olefin gets hydrogenated (14%) and a comparatively high amount of olefin isomers (35%) are formed, which suggests the hydroformylation activity is low compared to the isomerization reaction. The linear-to-branched ratio (*l:b* 0.9:1.0) is exceptionally low, compared to similar reaction systems reported by SLAUGH and MULLINEAUX.[102] To a big part, this can be attributed to the hydroformylation of 1-octene isomers, which are converted to branched products (see Figure 54). The ratio of skeletal alcohol isomers is 4.7 : 3.2 : 1.2 : 1 (*n*-nonanol : 2-methyl-octanol : 2-ethyl-heptanol : 2-propyl-hexanol). When increasing the total pressure to 60 bar the isomerization reaction gets inhibited. In this case 52% alcohols are derived but only 10% octene isomers are observed. The *l:b* ratio increases to 1.3. Using 90 bar of synthesis gas pressure, a significant leap in hydroformylation activity was observed and 78% alcohols were generated. At this point no olefin isomers were observed. Even though, the low *l:b* ratio of 0.8, suggests a fast isomerization. Furthermore, a decrease of the hydrogenation activity to alkanes was observed (9%) which can be linked to the increased hydroformylation activity.

Increasing the total pressure to 120 bar increases the hydroformylation activity further. Only 5% of alkane side products are observed. At this point the maximum operating pressure of the autoclave reactor was reached. Since for the Fischer-Tropsch reaction a carbon monoxide to hydrogen ratio of 1:2 is beneficial due to the ratio of consumed synthesis gas during the reaction, an experiment with an increased hydrogen partial pressure was conducted. Except for a slight increase in hydrogenation of starting olefin (8%) no significant difference to a synthesis gas ratio of 1:2 is observed.

From preliminary experiments, regarding gas-phase Fischer-Tropsch reaction, it was known that the total gas pressure has only minor effect on the Fischer-Tropsch catalyst. Contrary, the hydroformylation activity is closely linked to the total pressure. Therefore, for future experiments during the reductive hydroformylation of 1-octene and as starting conditions for the later combined approach (chapter 4.3.3) a total synthesis gas pressure of 120 bar was chosen. Regarding the synthesis gas ratio, a ratio of 1:2 was chosen for future experiments because it represents the optimized synthesis gas ratio for the Fischer-Tropsch catalyst but no negative effect of an increased synthesis gas ratio on the reductive hydroformylation was observed. Furthermore, the comparatively high hydroformylation activity even at lower synthesis gas pressures up to 30 bar is an important finding for the combination of the Fischer-Tropsch and hydroformylation catalyst later experiments. The high consumption of synthesis gas by the Fischer-Tropsch reaction for the chain propagation reaction will inevitably lead to decreasing synthesis gas pressures over the course of the experiments in the combined approach.

4.3.1.2 Influence of the Metal-to-Ligand Ratio on the Catalytic Activity and Linear-to-Branched Selectivity

The exceptional low linear-to-branched ratio observed during previous experiments could indicate that non-modified cobalt species exist, which inhibit a lower *l:b* ratio.[98] Since one of the main risks when using a heterogeneous Fischer-Tropsch catalyst and a homogeneous hydroformylation catalyst in the same reactor is unwanted cross interactions between both catalysts, non-modified cobalt species could be prone to deposition on the Fischer-Tropsch surface. In addition, unmodified cobalt hydride species are especially sensitive to the concentration of CO and tend to metal plating.[185] On the other hand, excess of phosphorus could induce leaching of cobalt from the Fischer-Tropsch surface. In any case, the influence of the metal to phosphorus ratio for the homogeneous reductive hydroformylation catalyst will be an important parameter during the later combined experiments. Therefore, knowledge about the influence of the metal-to-ligand ratio on the reductive hydroformylation step is essential.

In Figure 56 different M:L ratios ranging from 1:1 to 1:10 for the $[Co_2(CO)_8]/PCy_3$ catalyzed reductive hydroformylation of 1-octene are investigated.

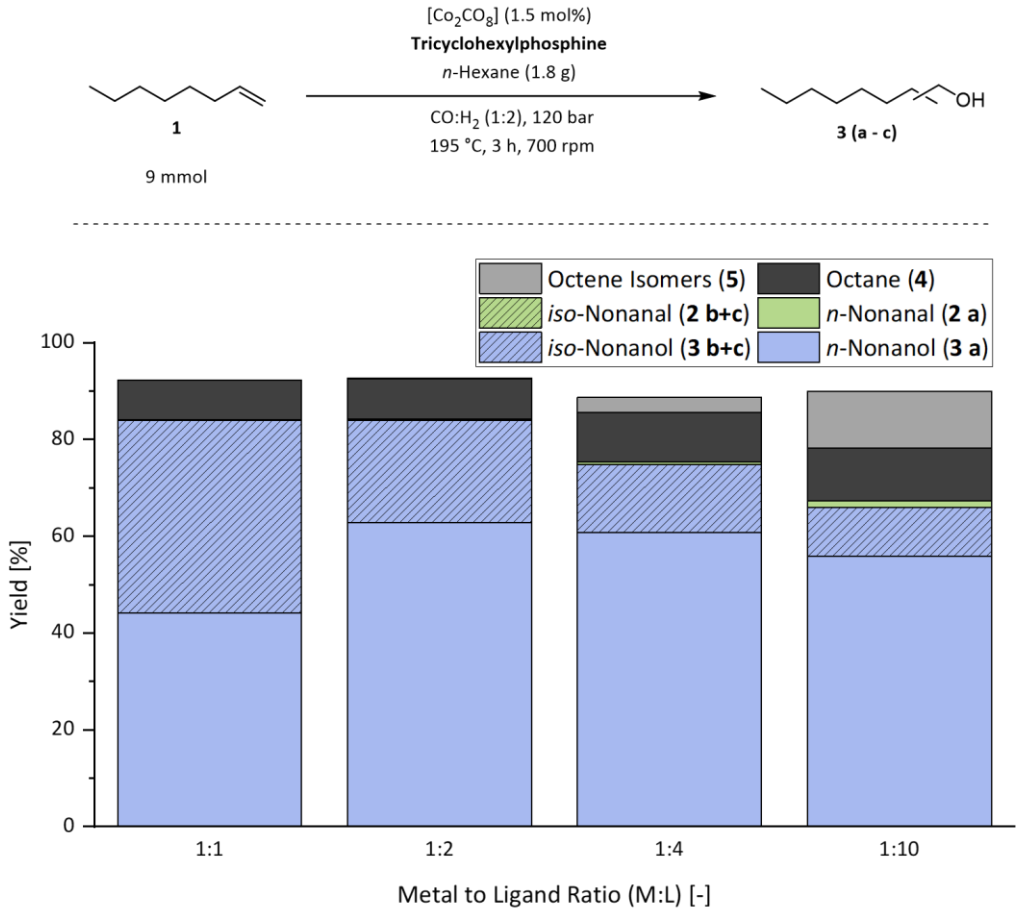

Figure 56: Product yield in the reductive hydroformylation of 1-octene using a $[Co_2(CO)_8]/PCy_3$ catalyst at various metal-to-ligand (M:L) concentrations. Quantitative/qualitative determination of product yields *via* GC-FID/GC-MS.

When increasing the M:L ratio to 1:2 no change in the overall alcohol selectivity is observed although the ratio of linear-to-branched alcohol products increases significantly from 1.1 to 3.0, indicating that there is indeed a shift in the equilibrium between phosphorus modified species. This effect continues when increasing the M:L ratio to 1:4 and 1:10. Using a M:L ratio of 1:10, a *l:b* ratio of 5.5 is observed. Hand in hand, a decrease in hydroformylation activity is observed though. At higher metal to ligand ratios 12% unconverted isomers and 11% alkane side products are obtained. For the application as bio-synthetic fuels the linear-to-branched ratio is not of particular interest for the final product mixture and a higher hydroformylation activity would be preferred over a high *l:b* ratio. Therefore, a low *l:b* ratio of 1:1 was chosen for future experiments in unison with observations made later during the investigation of cobalt species in the post reaction solution when using a *l:b* ratio of 1:1 (chapter 4.3.1.4).

4.3.1.3 Decrease of the Catalyst Concentration

As last experimental parameter before application in the combined approach, the catalytic activity of the reductive hydroformylation system was investigated in more depth. To get a better understanding for the catalytic activity, the catalyst concentration was stepwise lowered from 1.5 mol% to 0.1 mol% (Figure 57).

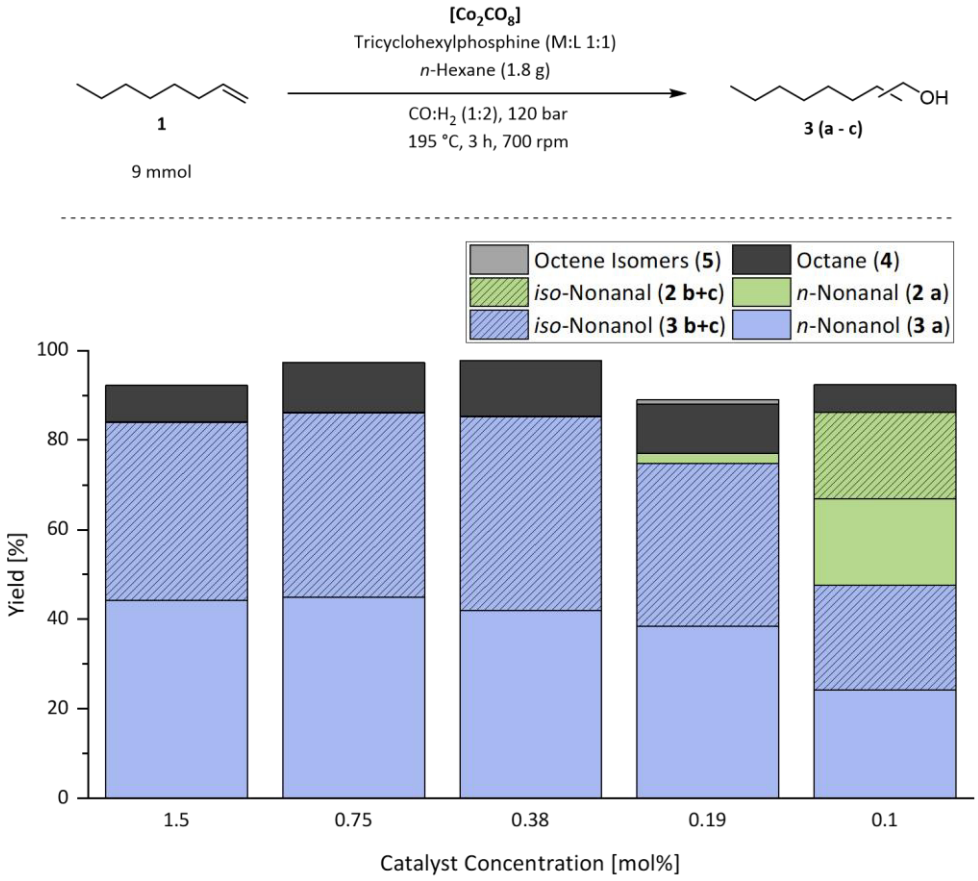

Figure 57: Product yield in the reductive hydroformylation of 1-octene using a $[Co_2(CO)_8]/PCy_3$ catalyst at various catalyst concentrations. Quantitative/qualitative determination of product yields *via* GC-FID/GC-MS.

When using 1.5 mol% of catalyst, complete conversion was achieved, which makes it difficult to estimate the catalytic activity. The theoretical Turn-Over-Frequency (TOF) using 1.5 mol% of cobalt was determined to be 11 h^{-1}. Likely this is not an accurate representation of the catalytic activity. This was confirmed when the catalyst concentration is lowered to 0.75 mol% and 0.38 mol%. Even at lower catalyst concentrations full conversion and an unchanged selectivity is observed. When decreasing the catalyst concentration to 0.19 mol%, intermediate aldehyde and alkene isomer products are observed in low concentrations (<3%). Finally, at a catalyst concentration of 0.1 mol% a significant decrease of hydrogenation products is observed (48%) and aldehyde intermediates are gained in significant amounts (40%). This hints towards an incomplete hydrogenation after three hours of reaction time. The-Turn-Over-Frequency when using 0.1 mol% of cobalt was determined to be 159 h^{-1}.

4.3.1.4 Spectroscopic Investigation of Catalytic Molecular Cobalt Species

To investigate the presence of catalytic species at low M:L ratios and for comparison with later spectroscopic results in the combined approach, ^{1}H- and ^{31}P-NMR spectra of the post reaction solution when using a M:L ratio of 1:1 been recorded. The ^{31}P-NMR spectrum of a post reaction solution at room temperature is displayed in Figure 58.

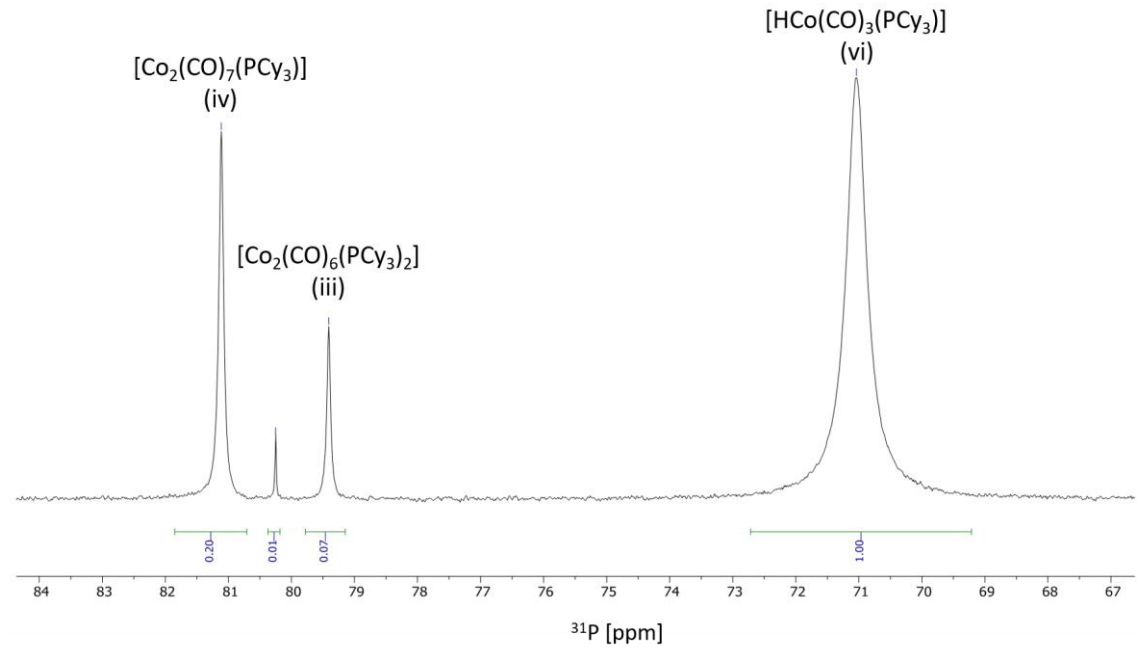

Figure 58: ^{31}P-NMR (202 MHz, $CDCl_3$, room temperature) of cobalt phosphorus species in the post reaction solution after the reductive hydroformylation of 1-octene using a homogeneous $[Co_2(CO)_8]/PCy_3$ catalyst. **Reaction conditions**: 1-Octene (9 mmol), $[Co_2CO_8]$, PCy_3 (1,5 mol%, M:L = 1:1), *n*-hexane (1.8 g), CO/H_2 (120 bar, 1:2), 195 °C, 3 h, 700 rpm. Informations about the exact analytical procedure regarding ^{31}P- and ^{1}H-NMR spectroscopy can be found in the experimental section chapter 6.3. Full spectrum in the Appendix (Figure A 6).

The ^{31}P-spectrum showed three major species with (normalized) chemical shifts of δ_{31P} = 71.0 ppm, δ_{31P} =79.4 ppm and δ_{31P} =81.1 ppm. Furthermore, complementary ^{1}H-NMR spectrometry revealed the presence of a hydride complex in comparatively high concentrations with a hydride shift of δ_{1H} = -10.9 ppm (Figure 59). The formation of catalytic species in the cobalt/trialkylphosphine catalyzed reductive hydroformylation has been intensively studied in

literature.[185–189]

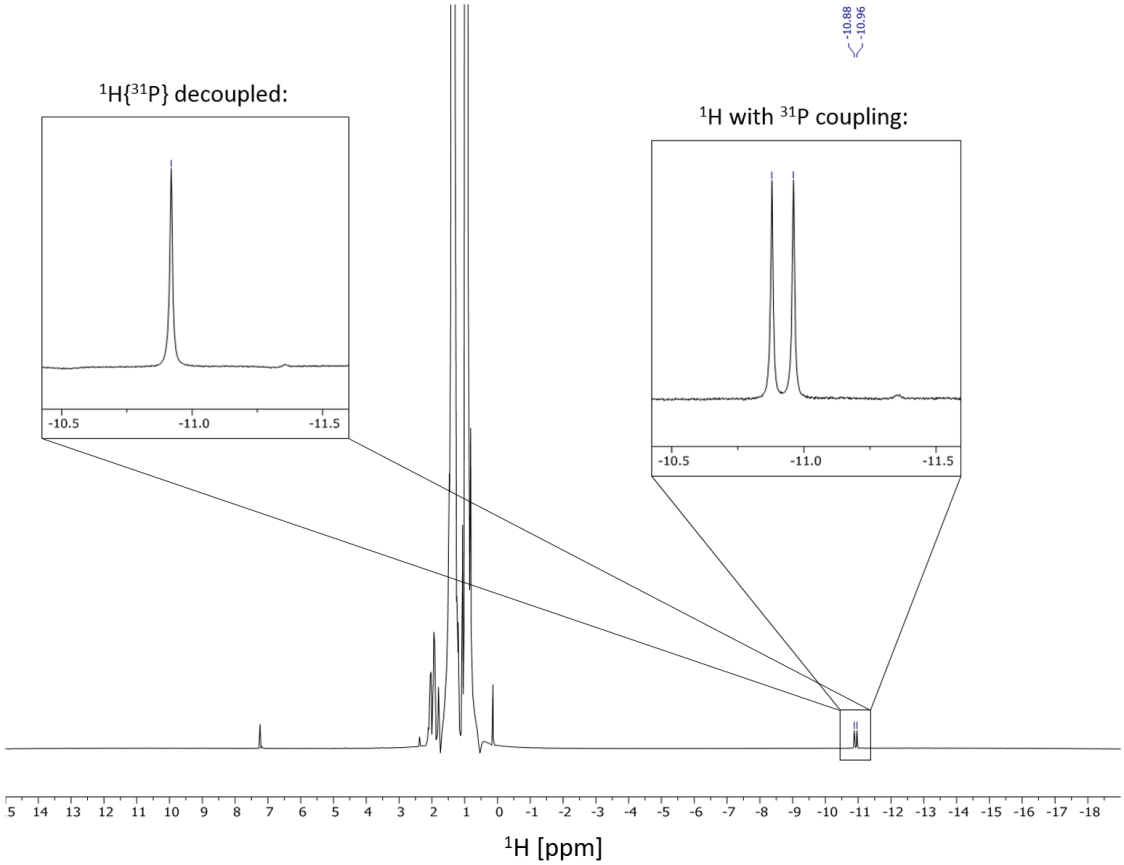

Figure 59: ^{1}H-NMR (500 MHz, $CDCl_3$, room temperature) hydride region for cobalt hydride species in the post reaction solution after the reductive hydroformylation of 1-octene using a homogeneous $[Co_2(CO)_8]/PCy_3$ catalyst. **Reaction conditions**: 1-Octene (9 mmol), $[Co_2CO_8]$, PCy_3 (1,5 mol%, M:L = 1:1), *n*-hexane (1.8 g), CO/H_2 (120 bar, 1:2), 195 °C, 3 h, 700 rpm. Information about the exact analytical procedure regarding ^{31}P- and ^{1}H-NMR spectroscopy can be found in the experimental section 6.3.

An overview for the *in situ* equilibrium between the major catalytic species with $Co_2(CO)_8$ as precursor and trialkylphospines as ligands has been reported by DWYER (Figure 60).[185] The formation of catalytically active cobalt/phosphorus hydride species (**vi**) usually proceeds *via* the highlighted equilibria (**i** → **ii** → **iii** → **vi**). At low ratios of cobalt metal to phosphorus ligand, the phosphorus starved dimeric intermediate species (**iv**) is formed in higher concentrations. Unmodified cobalt hydrides (**v**) are formed at even lower cobalt to phosphorus ratios or when no phosphorus ligand is used. Comparing the observed ^{31}P-NMR and ^{1}H-NMR spectra with the equilibrium postulated by DWYER ET AL and NMR-Data available in literature[186] allowed the identification of the dimeric complex $[Co_2(CO)_6(PCy_3)_2]$ (**iii**), the phosphorus starved dimeric complex $[Co_2(CO)_7(PCy_3)]$ (**iv**) and the phosphorus coordinated hydride complex $[HCo(CO)_3(PCy_3)]$ (**vi**) as the major species when using a metal to ligand ratio of 1:1. Surprisingly, even though a low linear-to-branched ratio was observed during the reaction, no unmodified cobalt carbonyl hydride was identified in the ^{1}H-NMR. Either $[HCo(CO)_4]$ (**v**) is not formed in the post reaction equilibrium or in very low concentrations.

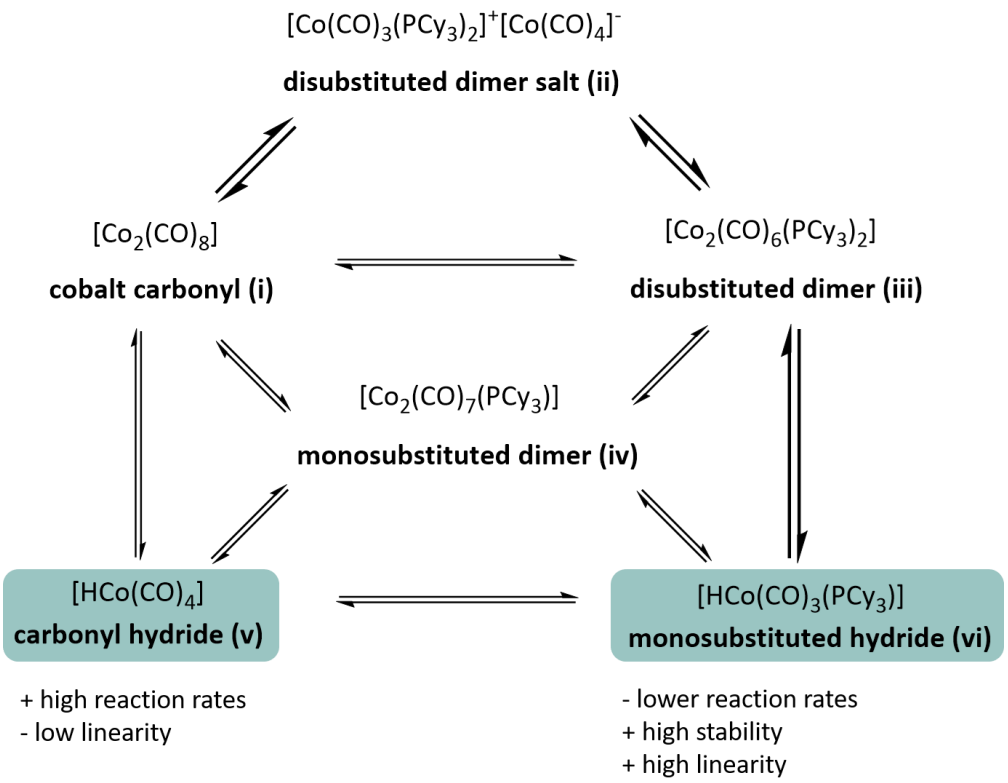

Figure 60: Formation and equilibrium between different cobalt species in the reductive hydroformylation reaction when using $Co_2(CO)_8$ in combination with trialkylphosphines as described by DWYER ET AL.[185] Formation of the catalytically active mono phosphine hydride species (**vi**) proceeds *via* (**i**) → (**ii**) → (**iii**) → (**vi**).

Furthemore, no signal of the free PCy_3 ligand in relevant concentrations was found in the ^{31}P-NMR, suggesting that the phosphorus starved monosubstituted dimer (**iv**) acts as a buffer between unsubstituted cobalt carbonyl (**i** + **v**) species and free phosphorus ligand. Since unmodified cobalt carbonyl species and free phosphorus ligand bear a high risk to negatively affect the heterogeneous Fischer-Tropsch catalyst by either precipitation or leaching of cobalt from the Fischer-Tropsch surface, it was chosen that a M:L ratio of 1:1 offers a good starting point for the combined approach.

4.3.2 Characterization and Performance during Gas-Phase Fischer-Tropsch-Synthesis of novel NaPr-CoRu@AOmM Catalysts

The second part of the preparation for the combined approach of Fischer-Tropsch-Synthesis and reductive hydroformylation reaction involves characterization and optimization of the Fischer-Tropsch catalyst.

As this part of the project was performed by Dr. Kai Jeske and Dr. Prieto Gonzalo, who are specialized in the fields of heterogeneous catalysis with a focus on Fischer-Tropsch synthesis, I will not describe this in detail as part of this work.

Nevertheless, some results concerning the spectroscopic characterization and gas-phase performance of the Fischer-Tropsch catalyst are essential for the later discussion about the combination of Fischer-Tropsch synthesis and reductive hydroformylation reaction. Therefore, they will be shortly presented in the following. It should be noted, that those experiments are part of the cooperation with Dr. Kai Jeske and Dr. Prieto Gonzalo but have been conducted by said project partners. For more information regarding the synthesis, characterization and performance of the herein used Fischer-Tropsch catalyst I refer to the published article presented at the beginning of this chapter (4.3)[144] and to literature published by JESKE and PRIETO concerning meso/macro-porous Fischer-Tropsch catalysts.[118,134,138]

Furthermore, from herein on the evaluation of the reaction system will be based on standard procedures applied for the description of Fischer-Tropsch reactions, most importantly the analysis of hydrocarbon distributions rather than analysis of individual compounds. A detailed description of the Fischer-Tropsch reaction and the determination of parameters can be found in the theoretical background (see chapter 2.4.1). The analytical procedure describing the analysis of Fischer-Tropsch product mixtures can be found in chapter 6.3.

4.3.2.1 Characterization and Comparison of Meso/Macroporous NaPr-CoRu@AOmM Catalysts with a Commerciall CoRu@AOm Catalyst

For the incorporation of the Fischer-Tropsch catalyst into a tandem catalytic system with a cobalt-based hydroformylation catalyst, several criteria must be met. For once, the catalyst must be able to operate at temperatures which are suited for the reductive hydroformylation catalyst and no decomposition occurs. Furthermore, it can be assumed that a high selectivity of the Fischer-Tropsch catalyst towards olefins (e.g. a low activity for the secondary hydrogenation of olefins) is beneficial to support a high alcohol selectivity in the combined approach since olefins serve as substrates to the reductive hydroformylation step (see Figure 53).

The group of PRIETO et al recently described a Fisher-Tropsch catalyst capable of producing highly olefin selective Fischer-Tropsch cuts at comparatively low temperatures around 195 °C.[33,118]

Based on this, an improved Fischer-Tropsch catalyst was developed by PRIETO ET AL for the purpose of the herein described tandem catalytic system. The exact procedure for the synthesis of this novel catalytic material and its exact characterization can be reread in the literature mentioned earlier.[134,144]

In short, the core of this novel Fischer-Tropsch catalyst consists of cobalt nanoparticles dispersed on an alumina oxide support. As a second metal, to increase the the selectivity towards olefins, ruthenium is used for the formation of Co/Ru nanoparticles. Finally, the catalyst is doped with sodium (NaO_x) and praesodymium (PrO_x). Hereinafter the catalyst will be referred to as NaPr-CoRu@AOmM. The detailed experimental procedure for the impregnation and activation of the catalyst can be found in the experimental section (chapter 6.2.8). For further information explaining the effect of metal doping with Na/Pr in more detail, the published literature about it by PRIETO is recommended.[118] Besides careful adjustment of the metal loadings and doping of the catalyst, a key feature to achieve the high olefin selectivity is the combination of meso- and macro-pores in the structure of the alumina support. Initially, most Fischer-Tropsch hydrocarbons leave the surface of the catalyst as olefins *via ß*-H-elimination (Figure 61, **II**).

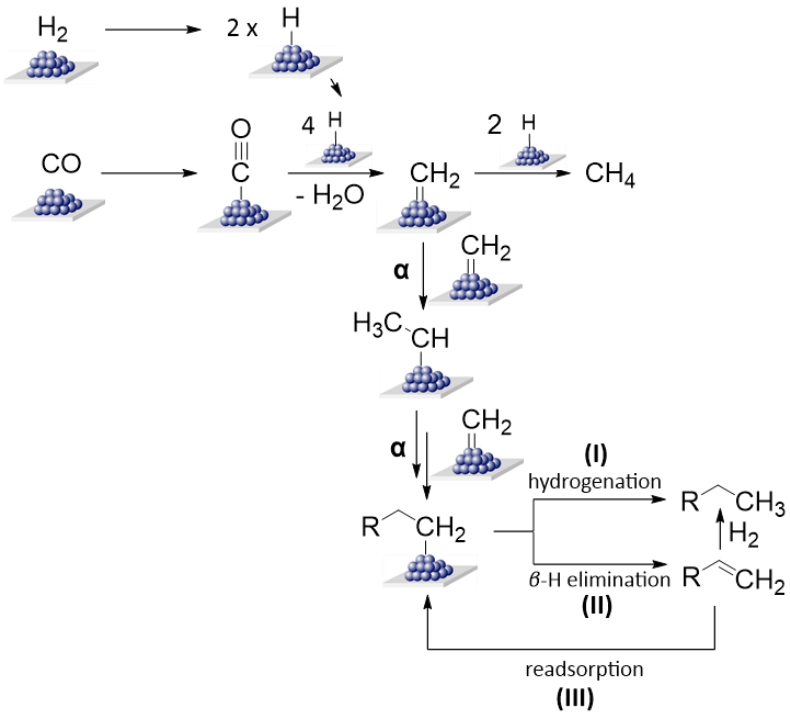

Figure 61: Simplified Fischer-Tropsch chain propagation and surface elimination mechanisms.

After cleavage from the Fischer-Tropsch surface, they can be readsorbed and hydrogenated (**III**). Hence, most of the products ultimately leave the Fischer-Tropsch pores are alkanes. By combining macropores and mesopores in the support structure of the catalyst, initial olefins can be transported out of the pores at a much faster pace, minimizing the chance of readsorption

(**III**) and secondary hydrogenation (**I**). At the same time mesopores are responsible to maintain a high catalytic surface area and ultimately a high reactivity.

Figure 62 shows representative Scanning-Electron-Microscope (SEM) images of the catalyst surface and the average pore diameters, determined by Hg-intrusion experiments, for the herein used NaPr-CoRu@AOmM catalyst (**a** + **b**) in comparison with a commercially available cobalt-based Fischer-Tropsch catalyst (**c** + **d**), referred to as CoRu@AOm.

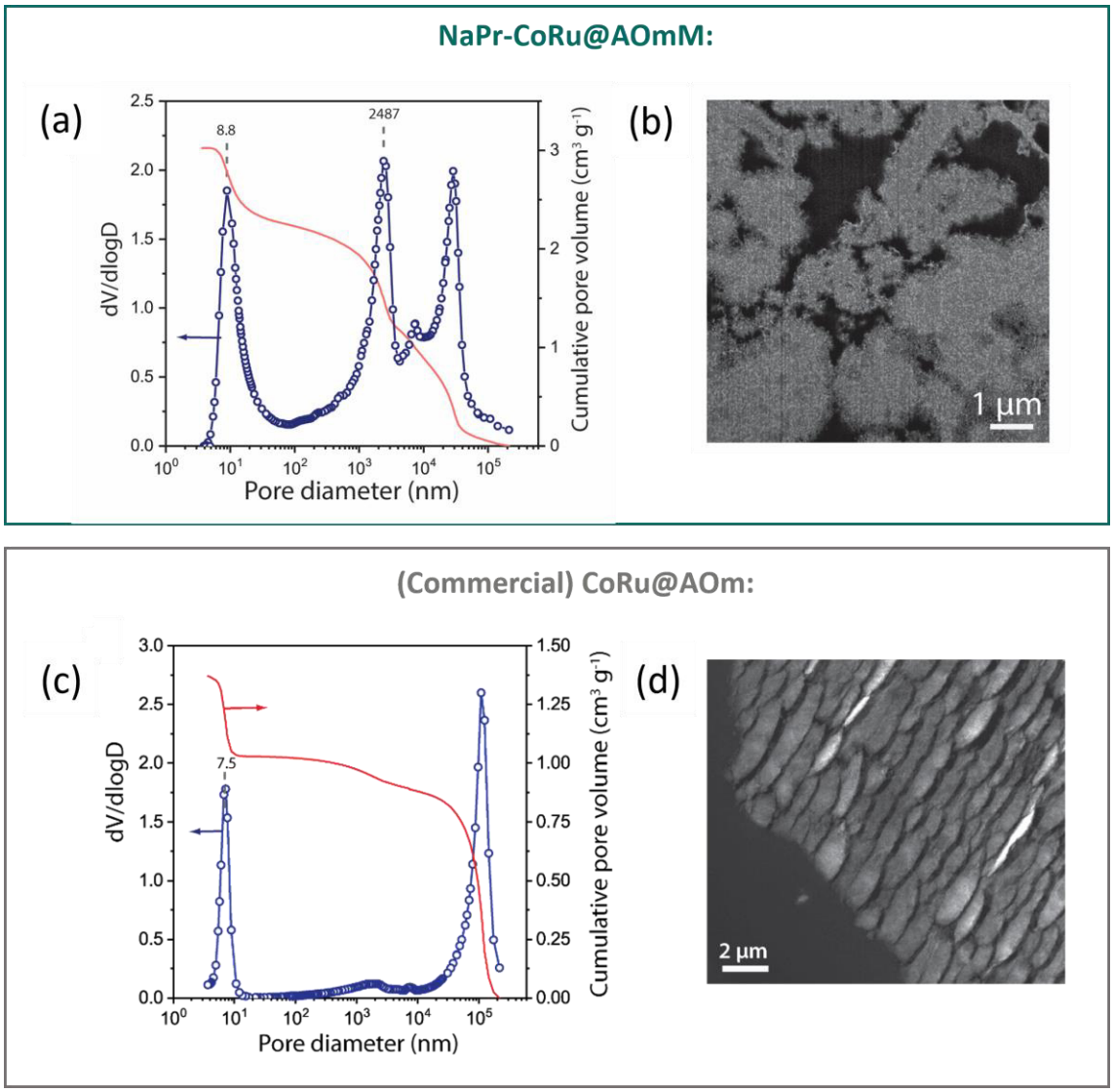

Figure 62: SEM mapping at 1 μm/2 μm magnification **(b)**; **(d)** of the Fischer-Tropsch surface and pore-diameter determined by Hg intrusion experiments **(a)**; **(c)** of the Na/Pr promoted meso/macroporous NaPr-CoRu@AOmM catalyst (top) and a commercial CoRu@AOm catalyst (bottom). Adapted from JESKE and RÖSLER.[144] More information about the individual analytical methods can be found in the experimental section chapter 6.3.

The SEM images of both catalysts provide a good impression regarding the difference in their structural hierarchy. In the SEM image of the meso/macroporous NaPr-CoRu@AOmM catalyst with a magnificantion of 1 µm (**b**) a fine structured porous material with intersectional macropore openings is visible. Hg-intrusion experiments (**a**) confirmed the presence of macropores with a wide size distribution but with its maximum at pore diameters between

1000 nm and 4000 nm. In addition, quantitative FIB-SEM (Focused-Ion-Beam Scanning-Electron-Microscopy) tomography found the average 3D-transport length from a mesoporous domain to the nearest macroporous domain to be 0.57 µm.[144] This is around two orders of magnitude lower than the average particle size[144] and highlights the effect of the macropores to reduce the average transport distance of primary Fischer-Tropsch products out of the mesoporous domains.

In comparison, the commercial CoRu@AOm catalyst with a magnification of 2 µm (**d**), shows an almost finished surface with an undulating structure. The average pore diameter as determined *via* Hg-intrusion experiments (**c**) certified the presence of mesopores with pore diameter between 5 nm to 10 nm. Besides those mesopores, no macropores in the range of 10^2-10^4 nm were observed in relevant quantitiy. EDS analysis mapping for both catalysts proved cobalt nanoparticles with an average size of 13 nm for the NaPr-CoRu@AOmM catalyst and 11 nm for the commercial CoRu@AOm catalyst.[144]

4.3.2.2 Performance of Novel NaPr-CoRu@AOmM Catalysts during Gas-Phase Fischer-Tropsch Synthesis

Finally, before using the Fischer-Tropsch catalyst and the reductive hydroformylation catalyst in a combined approach, the NaPr-CoRu@AOmM Fischer-Tropsch catalyst has been tested during gas-phase Fischer-Tropsch synthesis. This experiment is especially important for the later combined approach. The performance of the NaPr-CoRu@AOmM during this experiment will be used as a reference to derive the influence of liquid reaction media on the Fischer-Tropsch catalyst and to benchmark the performance of the gas-phase Fischer-Tropsch reaction in comparison with the tandem catalytic approach. Figure 63 shows the selectivity and the carbon chain-length distribution of the NaPr-CoRu@AOmM catalyst during a gas phase reaction in comparison with the commercial CoRu@AOm catalyst.

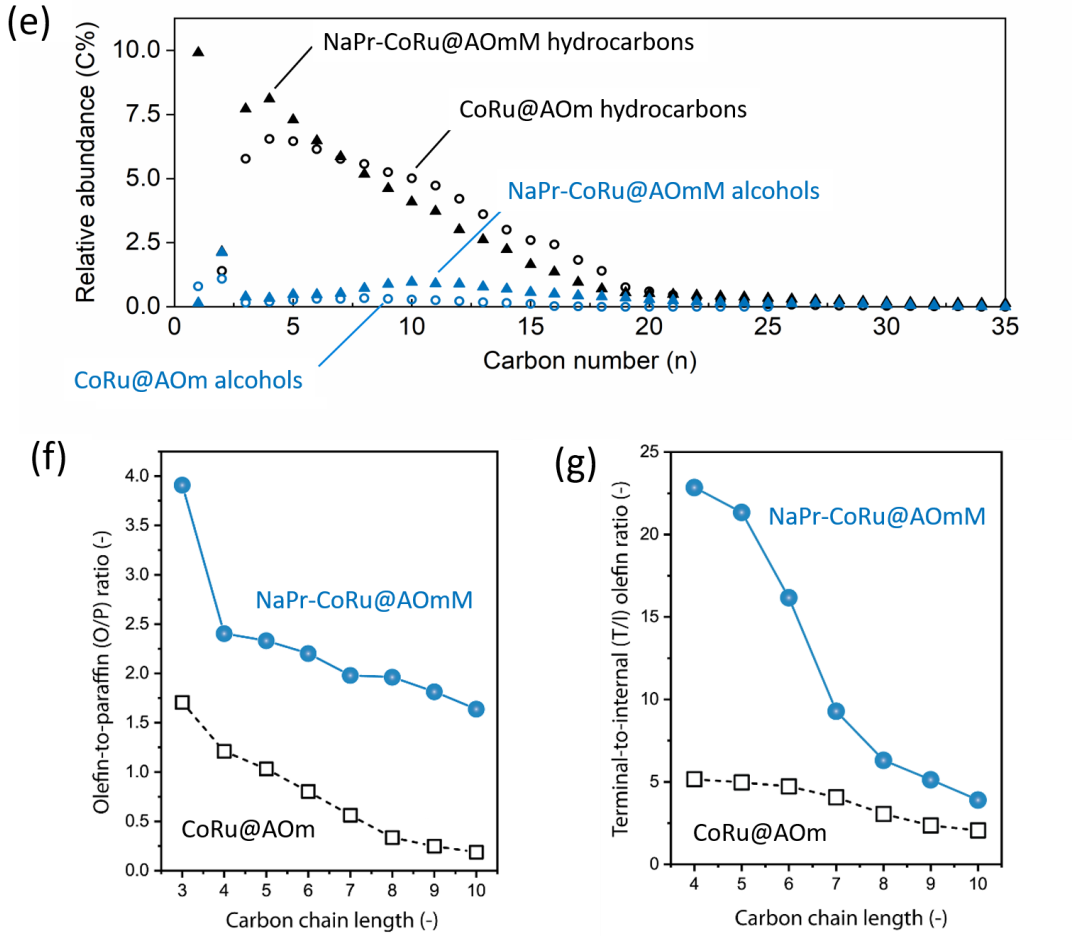

Catalyst	$S(olefin_{C3-C10})$	$S(CO_2)$ [C%]	$S(CH_4)$ [C%]	S_{C5+} [C%]	S_{ROH} [C%]	α_{alkan} [-]	α_{ROH} [-]	*CTY* [$mmol_{CO}gCo^{-1}h^{-1}$]
CoRu@AOm	16.3	0.4	14.2	70.3	5.0	0.79	0.70	149.9
NaPr-CoRu@AOmM	31.8	0.9	9.9	68.6	14.4	0.77	0.74	46.9

Figure 63: Fischer Tropsch gas-phase reaction using the CoRu@AOm and NaPr-CoRu@AOmM catalyst. S_x: Carbon Selectivity towards target product(s), α: chain growth probability, *CTY*: Cobalt-Time-Yield (Fischer-Tropsch cobalt specific catalytic activity), C_{5+}: Hydrocarbon products with a chain length >5, ROH: alcohol products. **Reaction conditions:** Fixed bed reactor loaded with NaPr-CoRu@AOmM, 200 °C, 20 bar H_2:CO 2:1, X_{CO} = 20 ∓ 3%.

The experiment was conducted in a fixed bed reactor at CO-conversion rates of 20 ∓ 3%. A more detailed description of the reactor setup and the experimental procedure can be found in chapter 6.2.9. Comparing the performance of both catalysts in gas-phase Fischer-Tropsch reaction, vast differences can be observed. While both catalysts showed about the same hydrocarbon chain growth probability for alkanes (α = 0.77 to 0.79*)*, a clear difference in the selectivity of the Fischer-Tropsch reaction was observed. The unpromoted CoRu@AOm catalyst mainly produced saturated hydrocarbons with minor fractions of alcohols (5 C%) and olefins (16 C%). Contrary, the combination of meso/macropores and the Na/Pr promotion in the NaPr-CoRu@AOmM catalyst led to a two-fold increase of olefins products, resulting in an olefin selectivity of 32 C% (**f**). Furthermore, when using the NaPr-CoRu@AOmM catalyst, the selectivity towards terminal olefins was increased significantly (**g**). Additionally, the selectivity towards alcohols increased from 5 C% to 14 C%. As a compromise for the increased selectivity towards functionalized products, the cobalt specific activity decreases from 149 $mmol_{CO}g_{Co}^{-1}h^{-1}$ to 47 $mmol_{CO}g_{Co}^{-1}h^{-1}$ when using the NaPr-CoRu@AOmM catalyst. This is a direct consequence of the promotion with NaO_x and PrO_x which decreases the hydrogenation activity of the cobalt NP´s. Hence, increasing the olefin selectivity but at the same time partially poisoning the catalyst.

Even though, for the combination of the Fischer-Tropsch reaction and the reductive hydroformylation reaction, a high olefin selectivity of the NaPr-CoRu@AOmM catalyst is valued higher than the cobalt specific catalytic activity.

4.3.3 Combining Fischer-Tropsch-Synthesis and Reductive Hydroformylation Reaction in a Slurry Phase "Multi-Tandem" Approach

During the previous chapters the individual reaction steps and catalytic systems for the Fischer-Tropsch synthesis and reductive hydroformylation reaction have been investigated and characterized. Consequently, with the knowledge gained during those preliminary experiments, both catalytic systems were combined in a One-Pot approach.

For the combination of both catalytic systems some adjustments to the reaction system were made. Most commonly the Fischer-Tropsch synthesis is conducted as gas-phase reaction. Since the homogeneous catalyst needs a solvating medium, the experiments were conducted in slurry phase batch experiments. For this, 10 mL autoclave reactors as shown in Figure 64 were used. Hence, both catalysts (NaPr-CoRu@AOmM and $[Co_2(CO)_8]/PCy_3$) were added as fine powders and dissolved in *iso*-hexane. *Iso*-hexane is structurally similar to the previously used *n*-hexane, during the investigation of the reductive hydroformylation step, but is no integral part of the Fischer-Tropsch product spectrum. Since the Fischer-Tropsch reaction is a polymerization reaction, a spectrum of hydrocarbons of various chain lengths is obtained. Reaction products separate into the gas (C_1-C_5), liquid (C_5-C_{25}) and solid (C_{25+}) phase. For the analysis of low boiling point hydrocarbons and to determine the conversion of carbon monoxide in the gas phase a combination of GC-FID (hydrocarbons) and GC-TCD (CO_2, CO, Ar and H_2) was used.

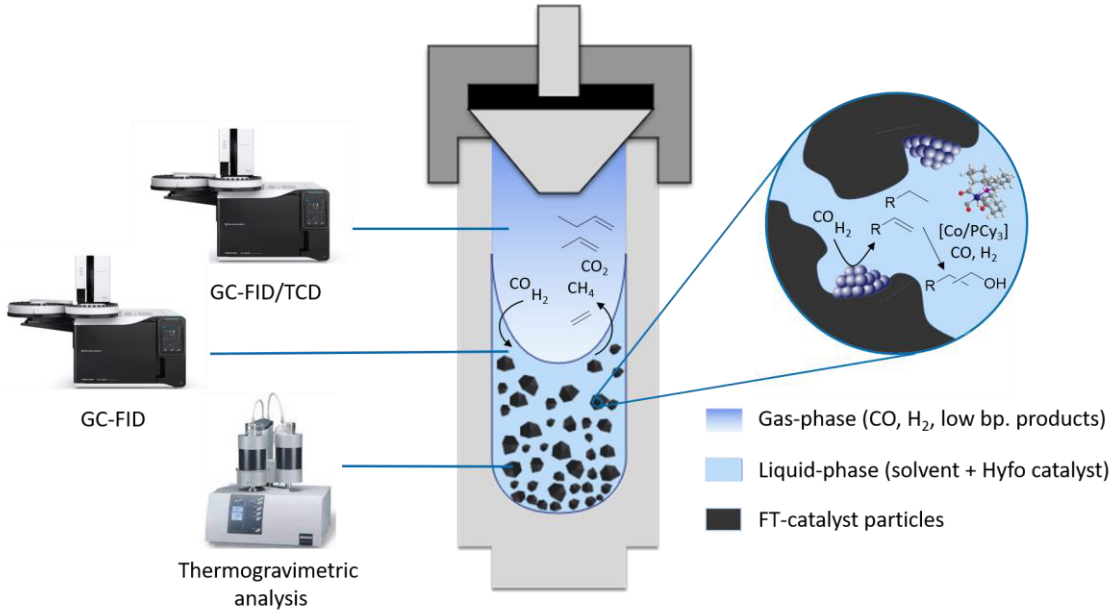

Figure 64: Concept for autoclave slurry phase experiments in the combined Fischer-Tropsch /hydroformylation approach.

To determine the CO-conversion a low concentration of argon (10 bar) was added together with the synthesis gas. After the reaction, argon was used as internal standard for gaseous products.

Most of the hydrocarbon products separate into the liquid phase and can be analyzed *via* GC-FID. This includes hydrocarbons with a carbon chain-lengths up to approximately C_{25}. It should be noted though, that in practical use the determination of hydrocarbons longer than C_{15} is not reliably possible due to very low product concentrations. Hence, for alkanes $>C_{14}$ and alcohols $>C_{12}$ the Anderson-Schulz-Florey (ASF) distribution (see chapter 2.4.1), derived from the hydrocarbon distribution in the C_2-$C_{14/12}$ region, was used to modulate their concentration.

Hydrocarbons distributing into the solid phase (waxes) were determined only for selected experiments *via* thermogravimetric analysis. In all cases the share of solid Fischer-Tropsch products was determined to be >2 C%. Hence the ASF-distribution was used as a more accurate description of solid products. A detailed description of the individual analytical methods can be found in experimental section (chapter 6.3).

As previously mentioned, experiments in the following will be described in the form of product distributions, hydrocarbon selectivities, and chain growth probabilities. Regarding the cobalt-time-yield (*CTY*) as means to describe the catalytic activity of the Fischer-Tropsch catalyst, it cannot be distinguished between synthesis gas consumed by the Fischer-Tropsch catalyst or the hydroformylation catalyst. Since the amount of synthesis gas consumed during the chain propagation reaction is significantly higher than the ampount consumed for the hydroformylation reaction, the *CTY* is still considered accurate to express the catalytic activity of the Fischer-Tropsch catalyst.

4.3.3.1 Tandem Combination of Fischer-Tropsch and Reductive Hydroformylation Reaction during Slurry Phase Experiments with Varying Catalyst Ratios

During the first experiments a Fischer-Tropsch catalyst (NaPr-CoRu@AOmM) loading of 40 mg (referring to a cobalt loading of 170 μmol), dissolved in 1 mL of *iso*-hexane and a reaction time of 24 hours, based on loose calculations comparing the moles of synthesis gas with the average Cobalt-Time-Yield (*CTY*) during gas phase experiments, was used. Opposing to most homogeneously catalyzed reactions, the substrate for the hydroformylation catalyst is generated *in situ*. Therefore, the amount of hydroformylation catalyst is based on the ratio of $n\mathrm{Co_{FT}}$:$n\mathrm{Co_{Hyfo}}$ instead of relating it to the substrate concentration. In the first experiment a $n\mathrm{Co_{FT}}$:$n\mathrm{Co_{Hyfo}}$ ratio of 170:18 was used, assuming a much higher activity of the hydroformylation catalyst compared to the Fischer-Tropsch catalyst (Figure 65, top left).

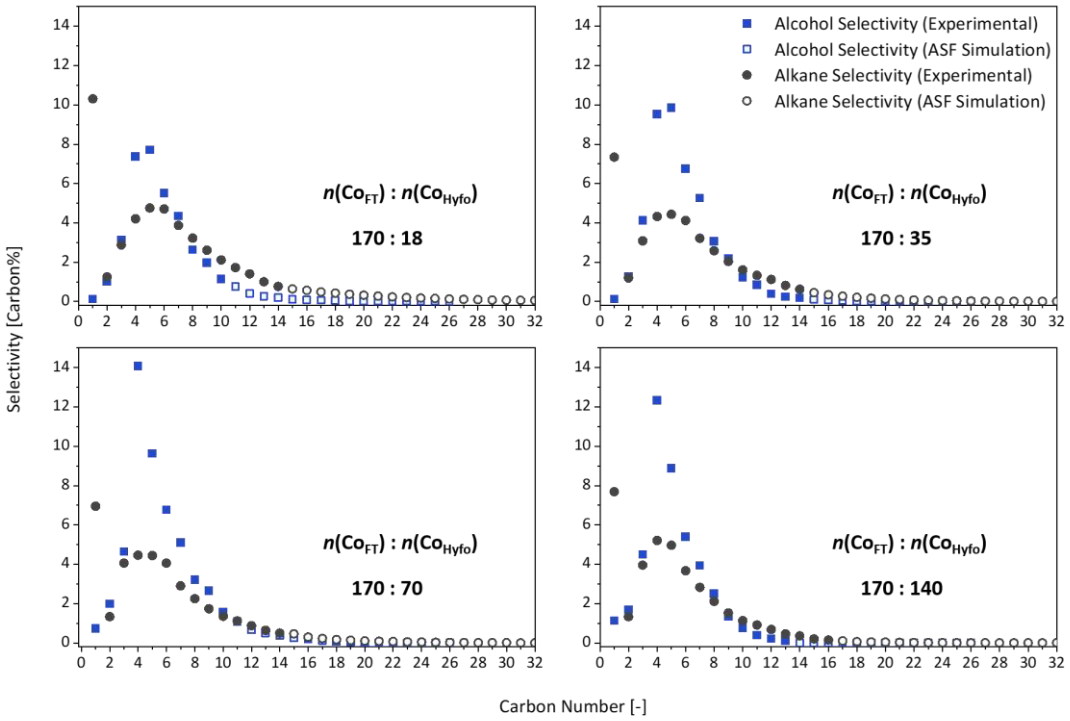

$n(\mathrm{Co_{FT}}) : n(\mathrm{Co_{Hyfo}})$ [μmol]	X_{CO} [%]	$S(CO_2)$ [C%]	$S(CH_4)$ [C%]	S_{C5+} [C%]	S_{ROH} [C%]	ROH *n*:*iso*	α_{alkan} [-]	α_{ROH} [-]	*CTY* [$mmol_{CO}gCo^{-1}h^{-1}$]
170 : 18	35.1	1.8	10.3	66.9	37.0	4.2	0.71	0.58	26.1
170 : 35	34.0	2.0	7.3	66.2	45.3	3.8	0.74	0.62	25.3
170 : 70	34.0	2.2	6.9	59.1	53.7	5.8	0.71	0.61	25.3
170 : 140	24.1	0.9	7.7	57.5	43.3	3.3	0.67	0.55	17.9

Figure 65: Combination of a NaPr-CoRu@AOmM Fischer-Tropsch catalyst and a Co/PCy_3 Hyfo catalyst in a slurry phase tandem reaction to convert synthesis gas to alcohols at different FT/Hyfo catalyst ratios. X_{CO}: Carbon monoxide conversion, S_x: Carbon Selectivity towards target product(s), α: chain growth probability, *CTY*: Cobalt-Time-Yield (Fischer-Tropsch cobalt specific catalytic activity), C_{5+}: Hydrocarbon products with a chain length >5, ROH: alcohol products. **Reaction conditions:** NaPr-CoRu@AOmM 40 mg, $Co_2(CO)_8$ (concentration see $n\mathrm{Co_{Hyfo}}$), PCy_3 ($n\mathrm{Co_{Hyfo}}$: $n\mathrm{PCy_3}$ 1:1), *iso*-hexane 0.9 g, 195 °C, 120 bar (at RT) $CO:H_2$ 1:2, 24 h, 700 rpm.

Furthermore, for the slurry phase reaction, the optimized reaction conditions (195 °C, 120 bar $CO:H_2$ 1:2, 700 rpm) elaborated earlier (chapter 4.3.1; 4.3.2) have been applied. Surprisingly already during these early experiments a significant increase of the selectivity towards alcohols compared to the gas-phase reaction of the sole Fischer-Tropsch catalyst (see chapter 4.3.2) is achieved. The carbon selectivity towards alcohols, increases from 14 C% to 37 C% in presence of the homogeneous hydroformylation catalyst. At the same time, a comparatively high CO-conversion of 35% is obtained. During GC-FID analysis of the reaction liquor no traces of olefinic products have been found, proving that olefins are converted to alcohols in high efficiency (if not mentioned otherwise, in all following experiments olefin concentrations are <0.1 C%).

Furthermore, a low CO_2 (1.8 C%) and CH_4 (10.3 C%) selectivity is maintained, indicating that the Fischer-Tropsch catalyst is not oxygenated or otherwise decomposed over the course of the experiment. The chain growth probability for alcohols (α_{ROH} = 0.58) is lower than the chain growth probability of alkanes (α_{alkane} = 0.71) with its maximum at pentanol (C_5). More than 95% of alcohol products have a chain length between C_2 and C_{12}. The presence of C_1 and C_2 alcohols proves that alcohols produced on the Fischer-Tropsch surface contribute, at least partially, to the total alcohol selectivity. The *CTY* of the Fischer-Tropsch catalyst in slurry phase reaction, was determined to be 26.1 $mmolCOgCo^{-1}h^{-1}$ compared to the 46.9 $mmol_{CO}gCo^{-1}h^{-1}$ achieved during the gas-phase reaction. The decrease in catalytic activity can be explained with decreased pore diffusion coefficients in liquid-phase compared to gas-phase reactions. Interestingly the *n*:*iso* ratio (*l*:*b* 4.2:1) for the hydroformylation reaction is significantly higher compared to previous experiments regarding the reductive hydroformylation of 1-octene (chapter 4.3.1; *l*:*b* around 1.0). The reason for this will be examined later (chapter 4.3.3.4).

Because in this novel approach two inherently different catalysts are used, the ratio of Fischer-Tropsch to hydroformylation catalyst was assumed to be one of the crucial parameters. Consequently, following the first experiment, the influence of the ratio of Fischer-Tropsch catalyst to the hydroformylation catalyst was investigated. To increase the FT:Hyfo catalyst ratio, the concentration of the hydroformylation catalyst was stepwise increased from 170:18 to 170:140. The Fischer-Tropsch catalyst concentration was kept at a constant (Figure 65, top right and bootom). When increasing the hydroformylation catalyst concentration to 170:35 and 170:70 an almost linear increase of the alcohol selectivity to 45 C% (170:35) and 54 C% (170:70) was observed (Figure 66). The CO-conversion of 34% did not change significantly, indicating an unaffected activity of the Fischer-Tropsch catalyst. Again, no leftover olefins were detected in the post reaction solution. The increase of the alcohol selectivity upon increase of the hydroformylation catalyst concentration is a clear indicator that the hydroformylation catalyst contributes to the high alcohol selectivity.

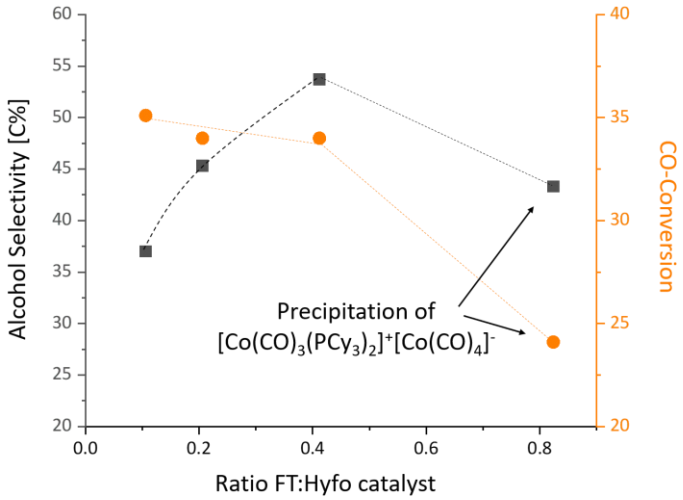

Figure 66: Dependency of alcohol selectivity and CO-conversion on the ratio of Fischer-Tropsch and hydroformylation catalyst.

Furthermore, the fact that the Fischer-Tropsch activity (evident at the unchanged carbon monoxide conversion and *CTY*) was not influenced by the hydroformylation catalyst concentration is a first hint that no limiting cross interactions between the two catalysts occur. Increasing the concentration of the hydroformylation catalyst further up to a $n\text{Co}_{\text{FT}}$:$n\text{Co}_{\text{Hyfo}}$ ratio of 170:140 lead to a sudden decrease of the carbon monoxide conversion and the alcohol selectivity. Closer investigation of catalyst residues revealed precipitation of a red/orange powder on the walls of the reactor and on the solid Fischer-Tropsch catalyst. During earlier investigations this powder was identified as the dimeric $[Co(CO)_3(PCy_3)_2]^+[Co(CO)_4]^-$ salt, which is formed at high catalyst concentrations and shows limited solubility in organic solvents. The drop in Fischer-Tropsch activity is likely due to pore blocking of the Fischer-Tropsch catalyst caused by precipitation of $[Co(CO)_3(PCy_3)_2]^+[Co(CO)_4]^-$.

Already during those early experiments, the selectivity towards alcohols of 54 C%, achieved with a FT:Hyfo cobalt ratio of 170:70, is among the highest selectivities towards oxygenates for Fischer-Tropsch-based synthesis gas to alcohol approaches reported in literature so far.[139] More importantly, this high alcohol selectivity is achieved at a comparatively high carbon monoxide conversion and with minimal CH_4 side production or WSGR activity to CO_2. Upon comparing these results with the selectivity reported for the NaPr-CoRu@AOmM catalyst during the gas phase reaction (Figure 63), it is evident that the alcohol selectivity, when using the Fischer-Tropsch catalyst and the hydroformylation catalyst in the combined approach, is considerably higher than the combined olefin and alcohol selectivity for the sole Fischer-Tropsch catalyst during gas-phase reaction. A possible explanation would be that the hydroformylation catalyst is able to increase the alcohol selectivity above the theoretical olefin selectivity of the

Fischer-Tropsch catalyst by intercepting *in situ* generated olefins in the Fischer-Tropsch pores before readsorption and secondary hydrogenation occurs as depicted in Figure 67.

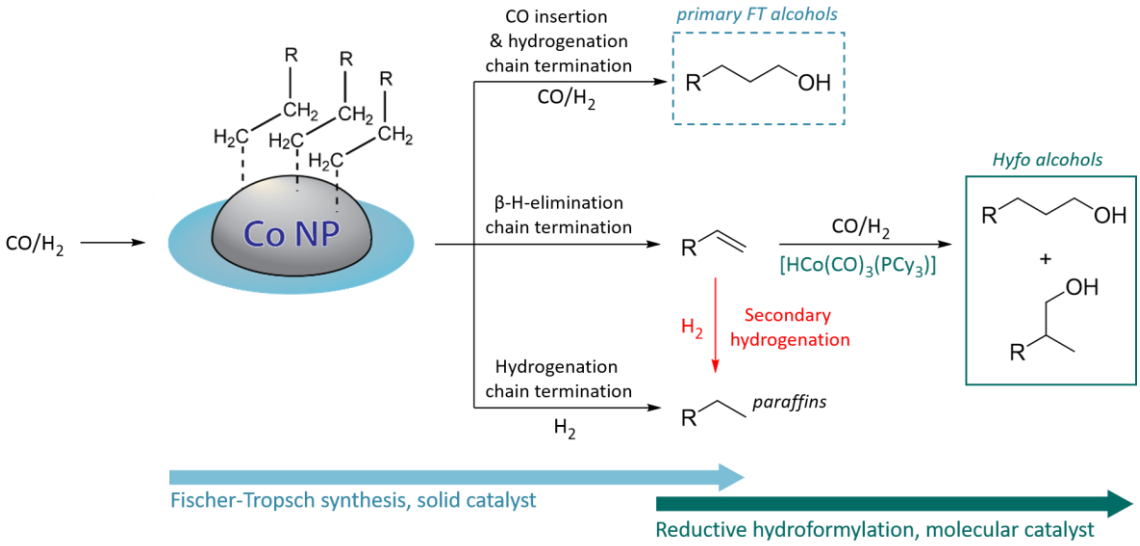

Figure 67: Reaction scheme for the Fischer-Tropsch /hydroformylation tandem reaction and interception of olefins before secondary hydrogenation occurs. Adapted from JESKE and RÖSLER.[144]

This is an inherent benefit of the herein developed tandem catalytic system compared to other Fischer-Tropsch to alcohol approaches, as the alcohol selectivity directly correlates to the hydroformylation activity without any adjustments of the Fischer-Tropsch catalyst. This is supported by the fact that, while no leftover olefins were observed during any experiment so far, the alcohol selectivity still increases when increasing the hydroformylation catalyst concentration (see Figure 66).

4.3.3.2 Performance of the Sole Fischer-Tropsch Catalyst and the Fischer-Tropsch Catalyst in Combination with Phosphorus ligand but Without Molecular Cobalt Source in Slurry Phase Experiments

As means to check this hypothesis and to investigate possible cross interactions between the two catalysts, reference experiments, in which the sole Fischer-Tropsch catalyst and the Fischer-Tropsch catalyst with the PCy_3 ligand but without any homogeneous cobalt source is used during slurry phase reactions, have been conducted (Figure 68).

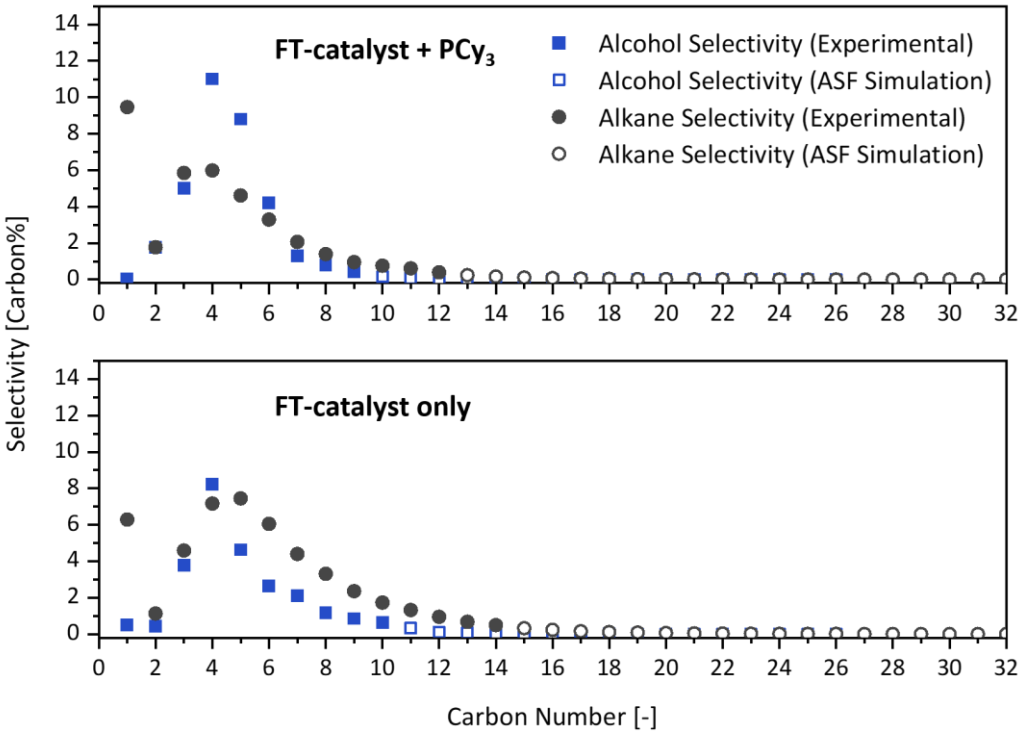

Catalyst	X_{CO} [%]	$S(CO_2)$ [C%]	$S(CH_4)$ [C%]	S_{C5+} [C%]	S_{ROH} [C%]	ROH *n*:*iso*	α_{alkan} [-]	α_{ROH} [-]	*CTY* [$mmol_{CO}gCo^{-1}h^{-1}$]
FT + Hyfo (reference)	34.0	2.2	6.9	59.1	53.7	5.8	0.71	0.61	25.3
FT + PCy_3	21.8	1.1	9.5	55.4	33.6	6.4	0.63	0.44	16.2
FT only	36.1	1.5	6.3	64.9	25.5	2.2	0.66	0.54	26.9

Figure 68: Reference experiments for the sole FT-catalyst and FT-catalyst + PCy_3 in slurry phase Fischer-Tropsch reaction. X_{CO}: Carbon monoxide conversion, S_x: Carbon Selectivity towards target product(s), α: chain growth probability, *CTY*: Cobalt-Time-Yield (Fischer-Tropsch cobalt specific catalytic activity), C_{5+}: Hydrocarbon products with a chain length >5, ROH: alcohol products. **Reaction conditions:** NaPr-CoRu@AOmM 40 mg, $Co_2(CO)_8$ 12 mg (0.035 mmol), PCy_3 20 mg (0.07 mmol), *iso*-hexane 0.9 g, 195 °C, 120 bar (at RT) $CO:H_2$ 1:2, 24 h, 700 rpm.

Using the sole Fischer-Tropsch catalyst in a slurry phase experiment (Figure 68, bottom) further supports the critical involvement of the hydroformylation catalyst for the alcohol selectivity. When no hydroformylation catalyst is added, the selectivity towards alcohols drops from 54 C% to 26 C%. For the first time unconverted olefin products are found in traces (>2 C%). Overall, the selectivity towards alcohols and olefins is 28 C%: This is far below the alcohol selectivity which

was observed in presence of the hydroformylation catalyst (54 C%). Nevertheless, the alcohol selectivity is significantly higher than during gas-phase Fischer-Tropsch experiments (Figure 63). ICP-MS analysis of the post reaction solution after filtration of the Fischer-Tropsch catalyst found traces of dissolved cobalt (7 μg/ml) in the reaction solution (Table 7).

Table 7: Cobalt concentrations in the post reaction solution as determined *via* ICP-MS.

Catalyst	**[Co] in the post reaction solution [μg/ml]**
NaPr-CoRu@AOmM + $[Co_2(CO)_8]$/PCy_3	685
NaPr-CoRu@AOmM + PCy_3	51
NaPr-CoRu@AOmM	7

In accordance with the presence of branched alcohol products and a low *n*:*iso* ratio of 2.2 it is likely that alcohols are produced mainly by unmodified cobalt carbonyl species such as $[HCo(CO)_4]$, which are highly active for the reductive hydroformylation reaction but exhibit a low *l:b* ratio. The fact, that even such low cobalt carbonyl concentrations, which is two magnitudes lower than the molecular cobalt concentration during the combined experiments (685 μg/ml), is enough to convert almost all olefins produced during the Fischer-Tropsch reaction highlights their catalytic activity. Even though, the presence of olefins in the reaction liquid hints that the ability to intercept olefins before secondary hydrogenation occurs is significantly reduced at such low molecular cobalt concentrations.

When adding tricyclohexylphosphine (PCy_3) together with the Fischer-Tropsch catalyst (Figure 68, top), the alcohol selectivity increases to 34 C%. Olefins can not be detected after the reaction. ICP-MS analysis of the post reaction solution proved an increased leaching of cobalt with a concentration of 51 µg/ml (Table 7). This is an almost eight-time increase compared to the sole Fischer-Tropsch catalyst and indicates that free phosphorus ligand is able to actively detach cobalt from the Fischer-Tropsch surface. This is supported by the decreased activity of the Fischer-Tropsch catalyst in presence of the free PCy_3 ligand, represented by a decreased CO-conversion from 36 % to 24 % and a likewise decreased *CTY*. ^{1}H- and ^{31}P-NMR spectra of the post reaction solution proved the presence of the catalytically active $[HCo(CO)_3(PCy_3)]$ hydride species (Appendix Figure A 7). This highlights the importance of the homogeneous cobalt source in order to circumvent deactivation of the Fischer-Tropsch catalyst.

4.3.3.3 Influence of Different Phosphorus Ligands on the Activity and Selectivity for the Tandem Combination of Fischer-Tropsch Reaction and Reductive Hydroformylation Reaction

In order to investigate the influence of the homogeneous catalyst ligand on the selectivity of the tandem catalytic reaction, several other phosphorus ligands, in unison with an experiment in which no ligand at all was used, have been tested. As ligands, tri-*n*-butylphosphine (P*n*Bu_3), triphenylphosphine (PPh_3) and a polymer-bound-triphenylphosphine ligand (P-PPh_3) have been tested. Tri-*n*-butylphosphine is commonly used in literature for cobalt-based reductive hydroformylation reactions. Contrary to alkylphosphine ligands, triphenylphosphine is known to produce aldehydes besides alcohols when used with cobalt as catalyst metal in the reductive hydroformylation reaction under very similar reaction conditions.[102] Finally, polymer-bound-triphenylphosphine (P-PPh_3) will be used to investigate the importance of the homogeneous catalyst distributing into the pores of the Fischer-Tropsch catalyst. Polymer-bound PPh_3 cannot enter Fischer-Tropsch mesoporous regimes and will therefore only be able to convert olefins which already diffused out of the mesopores. This should give further insights on how much the interception of *in situ* generated olfeins contributes to the overall alcohol selectivity. The results obtained when using these different types of phosphorus ligands, in comparison to an experiment in which no ligand is added, are displayed in Figure 69.

When no phosphorus ligand was used with the homogeneous cobalt precursor ($Co_2(CO)_8$) (Figure 69, top left), the alcohol selectivity droped from 54 C% to 20 C%. This was unexpected since unmodified cobalt catalysts are known for their high hydroformylation activity. Hand in hand, a slight increase in CO-conversion was observed, indicating an increase in the Fischer-Tropsch activity. A possible explanation would be that when no stabilizing ligand is present, homogeneous cobalt precipitates on the surface of the Fischer-Tropsch cobalt NP´s. Hence, effectively increasing the Fischer-Tropsch surface. This was not ultimately proven though. Using P*n*Bu_3 instead of PCy_3 does not significantly influence the selectivity of the reaction although the *CTY* decreases from 25 $mmol_{CO}gCo^{-1}h^{-1}$ to 20 $mmol_{CO}gCo^{-1}h^{-1}$ (Figure 69, top right). When PPh_3 is used as the ligand a slight decrease in the selectivity towards alcohols from 48 C% to 45 C% and a decrease of the *CTY* from 25 $mmol_{CO}gCo^{-1}h^{-1}$ to 21 $mmol_{CO}gCo^{-1}h^{-1}$ is observed (Figure 69, bottom left). More significantly, no aldehyde intermediates are observed. Either aldehydes get hydrogenated to alcohols on the Fischer-Tropsch surface, or the long reaction times increase the selectivity towards alcohols of the homogeneous hydroformylation catalyst. As a sharp contrast to the other tested phosphorus ligands, when PPh_3 is covalently bound to a polystyrene polymer (Figure 69, bottom right), the alcohol selectivity drops from 48 C% to 17 C%.

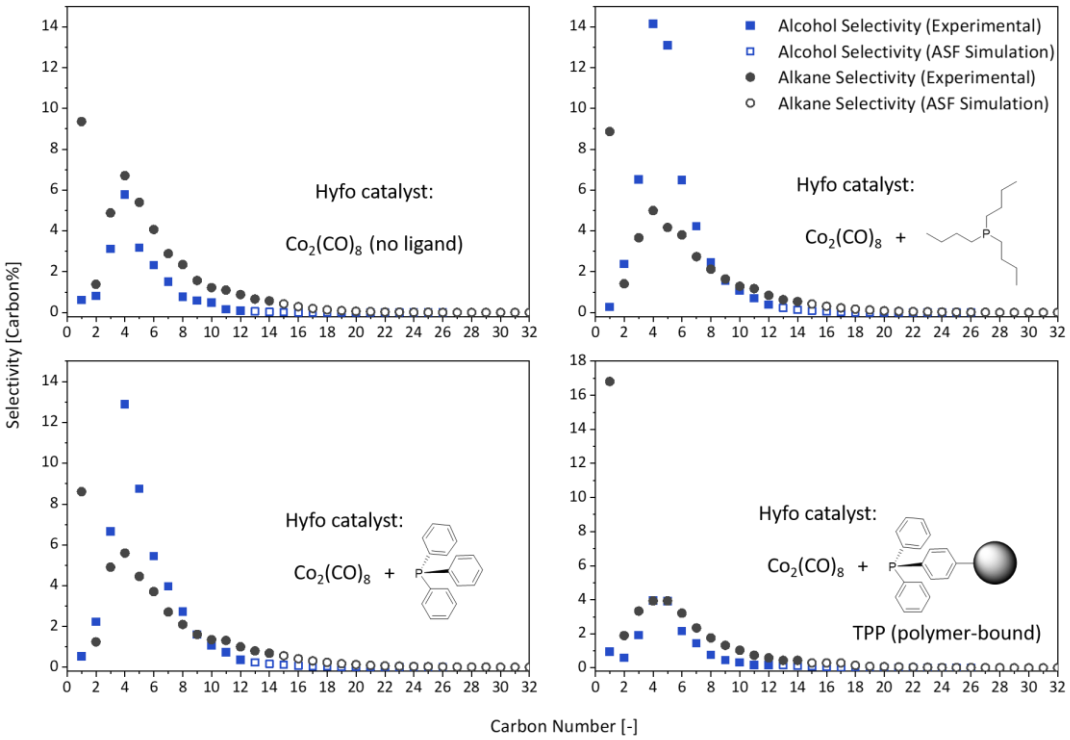

Hyfo Cat. Ligand	X_{CO} [%]	$S(CO_2)$ [C%]	$S(CH_4)$ [C%]	S_{C5+} [C%]	S_{ROH} [C%]	ROH *n*:*iso*	α_{alkan} [-]	α_{ROH} [-]	*CTY* [$mmol_{CO}gCo^{-1}h^{-1}$]
PCy_3 (reference)	34.0	2.2	6.9	59.1	53.7	5.8	0.71	0.61	25.3
No ligand	41.8	1.6	9.4	50.6	19.5	2.1	0.64	0.54	31.1
P*n*Bu_3	26.8	4.9	8.9	55.7	53.8	4.6	0.69	0.53	20.0
PPh_3	28.8	2.3	8.6	55.3	47.7	3.1	0.70	0.57	21.4
PPh_3 (polymer-bound)	31.9	1.1	16.8	63.4	17.3	3.5	0.75	0.62	23.7

Figure 69: Different phosphorus ligands for the combination of a NaPr-CoRu@AOmM Fischer-Tropsch catalyst and a homogeneous cobalt catalyst. X_{CO}: Carbon monoxide conversion, S_x: Carbon selectivity towards target product(s), α: chain growth probability, *CTY*: Cobalt-Time-Yield (Fischer-Tropsch cobalt specific catalytic activity), C_{5+}: Hydrocarbon products with a chain length >5, ROH: alcohol products. **Reaction conditions:** NaPr-CoRu@AOmM 40 mg, $Co_2(CO)_8$ 12 mg (0.035 mmol), phosphorus ligand 0.07 mmol, *iso*-hexane 0.9 g, 195 °C, 120 bar (at RT) CO:H_2 1:2, 24 h, 700 rpm.

Immobilization of the PPh_3 ligand to the styrene polymer, makes it impossible for the reductive hydroformylation catalyst to enter the Fischer-Tropsch mesopores. This shows that the presence of the homogeneous catalyst in close spacial proximity to the Fischer-Tropsch surface, and therefore the ability to intercept olefins before they get hydrogenated, is essential to achieve alcohol selectivities >20 C%. Furthermore, this experiment can be regarded as an indicator on how much the conversion of olefins before hydrogenation occurs contributes to the overall alcohol selectivity. To validate that the reduction in alcohol selectivity can be attributed to the exclusion of the hydroformylation catalyst from the Fischer-Tropsch pores and it is not the consequence of a change in the hydroformylation activity, reference experiments have been conducted. When P-PPh_3 is used as a ligand during the reductive hydroformylation of 1-octene, a similar hydroformylation activity compared to PCy_3 was obtained (Appendix

Table A 24).

4.3.3.4 Time Resolved Experiments for the Tandem Combination of Fischer-Tropsch Synthesis and Reductive Hydroformylation Reaction

To get a deeper insight for the sequence of reactions and to observe the influence on the catalytic activity at high carbon monoxide conversions, but also to investigate cross interactions between the two catalysts, several batch experiments with reaction times ranging from 1 hour to 72 hours were conducted. The yield-time plot, depicting the alcohol selectivity, the CO-conversion and the linear to branched ratio of product alcohols over 72 hours, is displayed in Figure 70.

Over the course of the experiments, a linear increase in CO-conversion was observed up to 70% after 72 h. Furthermore, a consistently low selectivity towards CO_2 (around 2 C%) and CH_4 (around 9 C%) was maintained. The constant Fischer-Tropsch catalyst activity over the course of the experiments shows that no continuous deactivation or decomposition of the Fischer-Tropsch catalyst occured. Regarding the alcohol selectivity, an increase was observed, leveling around 50 C% after 20 hours. It is highly unlikely that 20 hours are needed for the formation of the molecular active hydroformylation species. Taking a closer look revealed that there was a similar increase in the linear-to-branched (*l*:*b*) ratio of the obtained alcohols, which showed an exponential growth within the first few hours of the reaction.

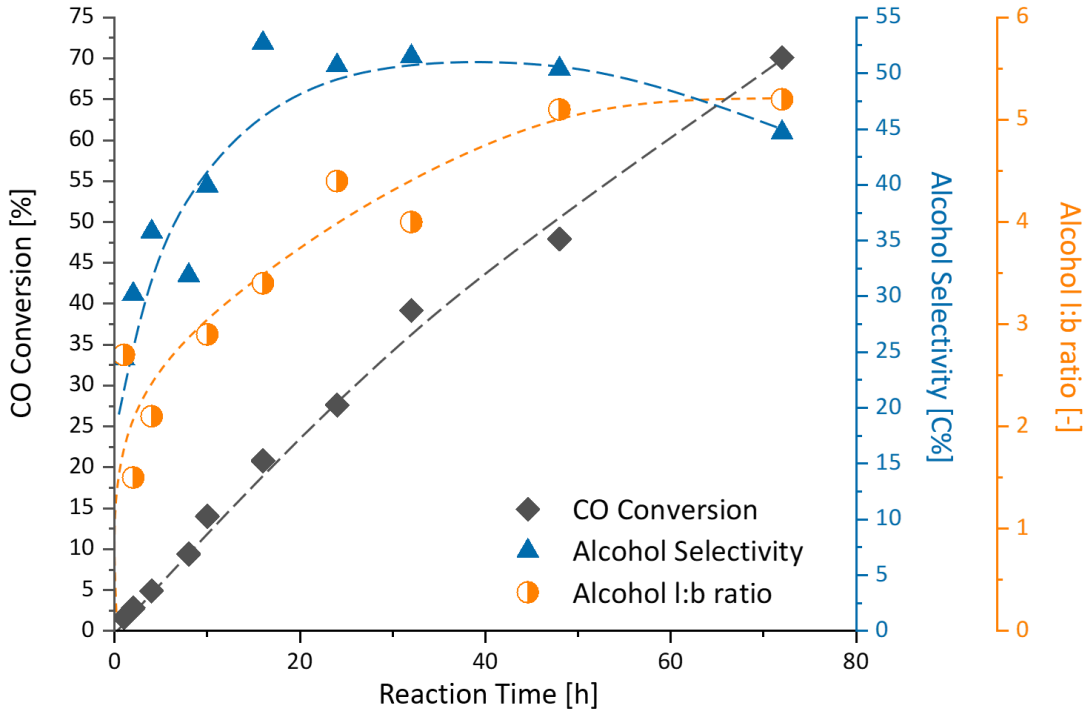

Figure 70: CO-conversion, alcohol selectivity and linear-to-branched ratio over time for the combination of Fischer-Tropsch synthesis and hydroformylation in the direct conversion of synthesis gas to alcohols. Dashed lines are for visualization purposes and do not represent actual data. **Reaction conditions:** NaPr-CoRu@AOmM 40 mg, $Co_2(CO)_8$ 12 mg (0.035 mmol), PCy_3 20 mg (0.07 mmol), *iso*-hexane 0.9 g, 195 °C, 120 bar (at RT) $CO:H_2$ 1:2, 700 rpm.

The linear to branched ratio increased from 1.5 after two hours to 3.4 after 16 hours. As stated earlier (chapter 4.3.1), the linear-to-branched ratio is closely linked to the metal-to-ligand ratio of the hydroformylation catalyst. Indeed, ^1H- and ^{31}P-NMR of the post reaction solution after 24 hours revealed the presence of the catalytically active $[HCo(CO)_3(PCy_3)]$ and the dimeric $[Co_2(CO)_6(PCy_3)_2]$ species, but contrary to the previously measured NMR´s during the reductive hydroformylation of 1-octene (Figure 58), no phosphine starved $[Co_2(CO)_7(PCy_3)]$ species is observed. Additionally, free PCy_3 ligand was found in the post reaction solution (Figure 71).

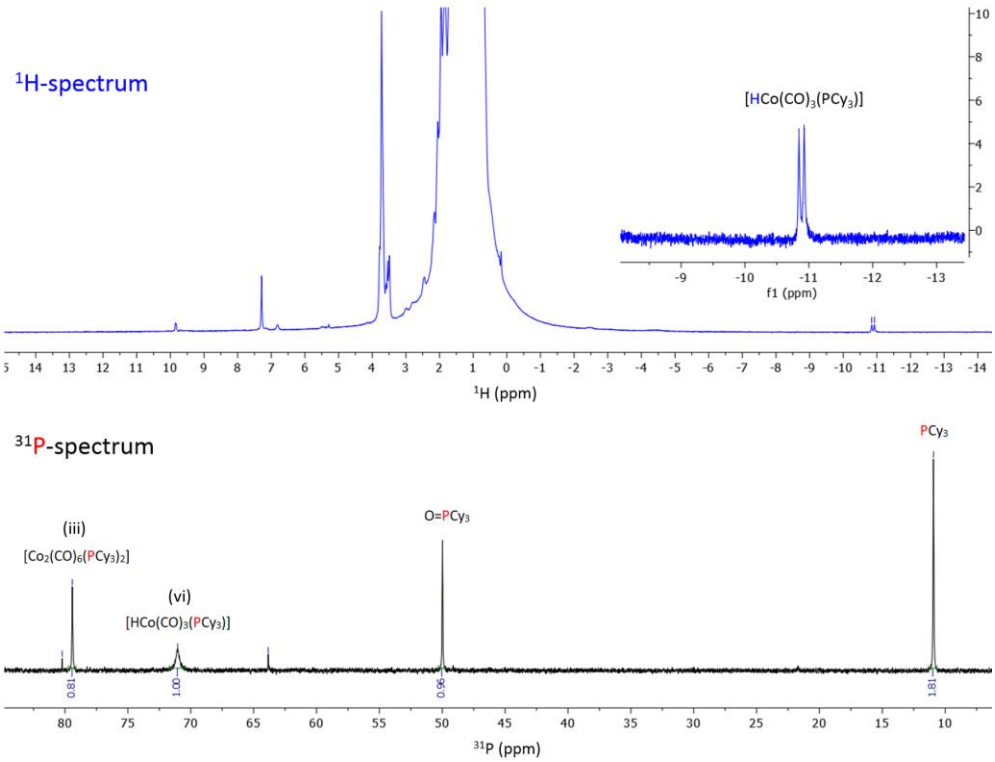

Figure 71: ^{1}H-NMR (500 MHz, $CDCl_3$, room temperature) spectra (top) and ^{31}P-NMR (202 MHz, $CDCl_3$, room temperature) spectra (bottom) of cobalt species in the post reaction solution for the combined Fischer-Tropsch/hydroformylation approach.

Since a Co:PCy_3 ratio of 1:1 is applied for the reaction, free phosphorus ligand suggests that the molecular cobalt catalyst partially precipitates during the first few hours of the reaction. Hence, increasing the metal-to-ligand ratio and ultimately the linear-to-branched ratio of alcohols. This phenomenon seems to occur only during the first few hours of the reaction until an equilibrium is reached. The performance of the Fischer-Tropsch catalyst was not affected nor did it lead to a continuous deactivation of the hydroformylation catalyst, which was supported by the stabilization of the linear-to-branched ratio and the alcohol selectivity after 20 hours. The slight decrease in alcohol selectivity to 45 C% after 72 hours is linked to the decreasing total synthesis gas pressure for the batch experiments. As described earlier, a total pressure >60 bar is necessary to maintain a high hydroformylation activity (chapter 4.3.1). After 72 hours only about 35 bar of synthesis gas was left in the reactor.

Overall there was no evidence for deactivation of the homogeneous hydroformylation or the heterogeneous Fischer-Tropsch catalyst within the time frame of 72 h. The fact that alcohol selectivities >40 C% can be achieved at CO-conversion rates of 70%, with minor CO_2 and CH_4 side production, clearly separates this approach from the existing literature about alcohol selective Fischer-Tropsch synthesis.[139]

4.3.3.5 Effect of Supercritical Reaction Media on the Tandem Combination of Fischer-Tropsch Synthesis and Reductive Hydroformylation Reaction for the Direct Conversion of Synthesis Gas to Alcohols

Whereas the alcohol selectivity was increased significantly by combining the Fischer-Tropsch and the hydroformylation catalyst in a slurry phase reaction, the Cobalt-Time-Yield (*CTY*) decreased compared to the gas-phase reaction (see Figure 63). This can be attributed to a decreased mass transfer in liquid phase compared to gas-phase, which reduces availability of CO and H_2 on the Fischer-Tropsch surface. In an attempt to increase the Fischer-Tropsch activity, the reaction in a supercritical solvent was investigated. Supercritical media has a lower viscosity than liquid media and often exhibits advantageous mass transfer properties. As supercritical solvent *iso*-pentane was used. *Iso*-pentane has similar properties than *iso*-hexane. Furthemore, supercritical state of *iso*-pentane is simply achieved when the reaction temperature is increased from 195 °C to 200 °C. In Figure 72 the results when using supercritical *iso*-pentane are displayed.

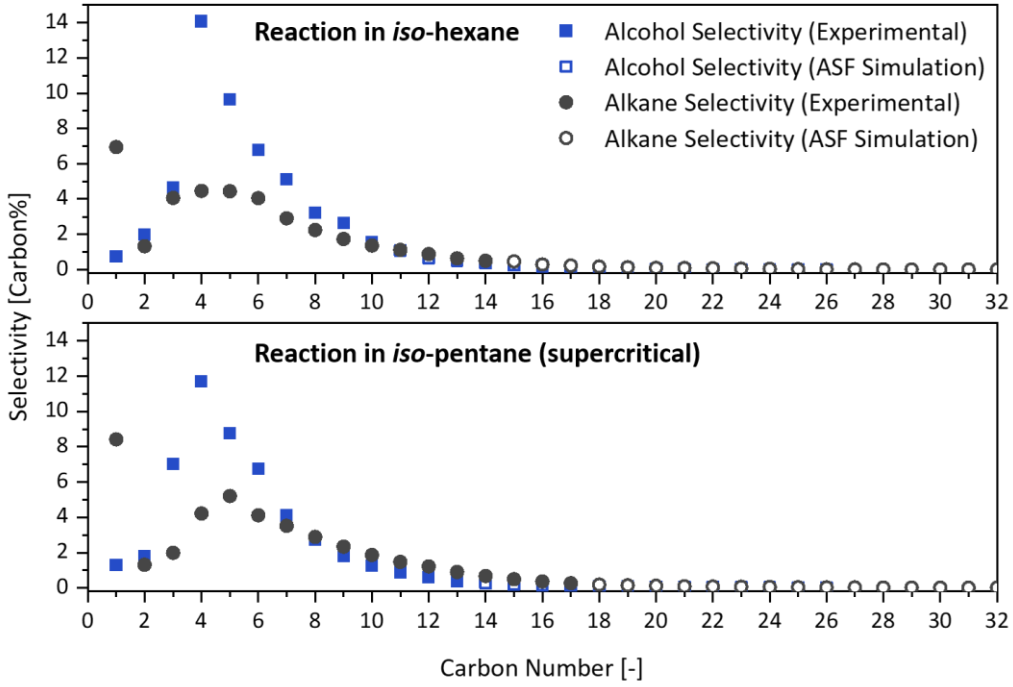

Solvent	X_{CO} [%]	$S(CO_2)$ [C%]	$S(CH_4)$ [C%]	S_{C5+} [C%]	S_{ROH} [C%]	ROH *n*:*iso*	α_{alkan} [-]	α_{ROH} [-]	*CTY* [$mmol_{CO}gCo^{-1}h^{-1}$]
iso-hexane (reference)	34.0	2.2	6.9	59.1	53.7	5.8	0.71	0.61	25.3
iso-pentane (sc)	36.1	1.5	6.3	64.9	25.5	2.2	0.66	0.54	26.9

Figure 72: Combination of Fischer-Tropsch and hydroformylation for the direct conversion of synthesis gas to alcohols in supercritical reaction media. X_{CO}: Carbon monoxide conversion, S_x: Carbon selectivity towards target product(s), α: chain growth probability, *CTY*: Cobalt-Time-Yield (Fischer-Tropsch cobalt specific catalytic activity), C_{5+}: Hydrocarbon products with a chain length >5, ROH: alcohol products. **Reaction conditions:** NaPr-CoRu@AOmM 40 mg, $Co_2(CO)_8$ 12 mg (0.035 mmol), PCy_3 20 mg (0.07 mmol), *iso*-hexane/*iso*-pentane 0.9 g, 195 °C (*iso*-hexane), 200 °C (*iso*-pentane), 120 bar (at RT) $CO:H_2$ 1:2, 700 rpm.

In comparison to *iso*-hexane, the change to a supercritical reaction medium did lead to a slight increase of the Fischer-Tropsch activity, evident at an increase of the *CTY* from 25 $mmol_{CO}gCo^{-1}h^{-1}$ to 27 $mmol_{CO}gCo^{-1}h^{-1}$. However, at the same time a drastic decrease in the alcohol selectivity from 54 C% to 26 C% was observed. The reason for this was identified when the reactor was opened after the reaction: During the reaction, the hydroformylation catalyst precipitated on the reactor walls and within the reactor piping. It can be assumed that the precipitation already occurred under supercritical conditions. Hence, it seems that the solubility of the hydroformylation catalyst in supercritical *iso*-pentane is severely altered. Precipitation of the molecular catalyst leads to a decrease of the hydroformylation catalyst concentration in the supercritical medium. Besides precipitation of the catalyst, it can not be excluded that the catalytic activity of the hydroformylation catalyst in supercritical medium is also reduced. Neverthless, the low alcohol selectivity in exchange for a slight increase in the Fischer-Tropsch activity shows that supercritical *iso*-pentane is not suited as solvent for the reaction.

4.3.3.6 Pushing the Alcohol Selectivity and the CO-Conversion by Varying the Synthesis Gas Composition, the Reaction Time and the Catalyst Concentration

Finally, the influence of the synthesis gas composition and an increased catalyst concentration was investigated (Figure 73 and Figure 74). In literature, a synthesis gas composition of CO:H_2 1:1 is often described as the optimal ratio for the cobalt catalyzed reductive hydroformylation.[183] As the natural gas consumption during the Fischer-Tropsch synthesis relates to a CO:H_2 ratio of 1:2 it was chosen as the starting conditions during previous experiments. In order to observe the effect of a reduced synthesis gas composition on the hydroformylation activity, experiments with a CO:H_2 ratio of 1:1 after 24 hours of reaction time and at prolonged reaction times of 72 hours were conducted (Figure 73).

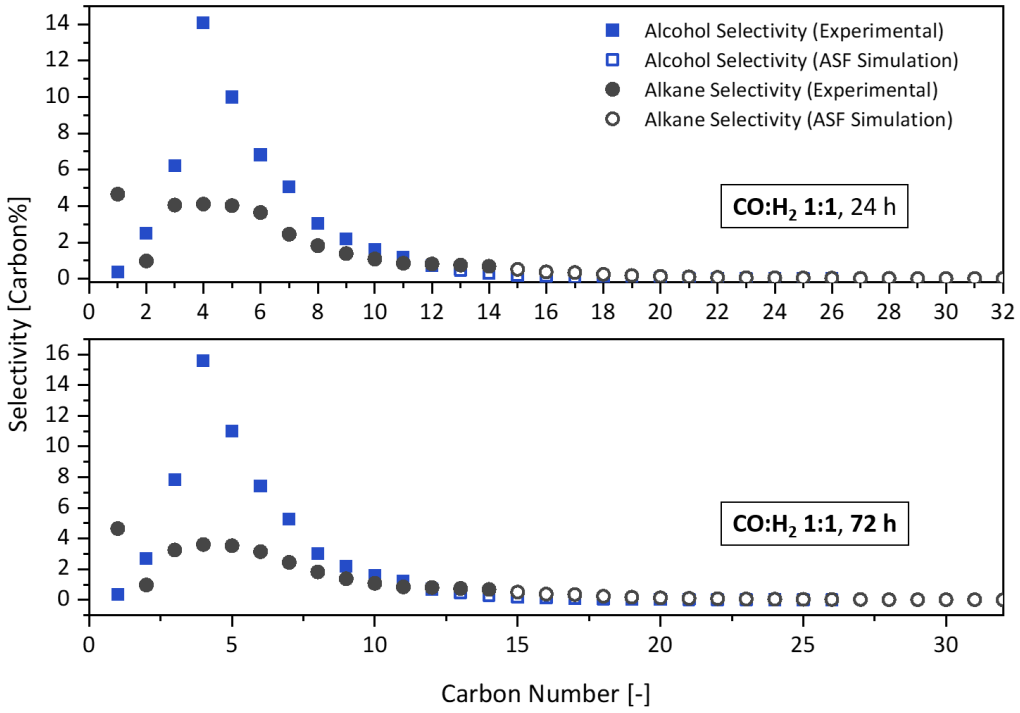

CO:H_2	$n(Co_{FT})$: $n(Co_{Hyfo})$ [μmol]	t [h]	X_{CO} [%]	$S(CO_2)$ [C%]	$S(CH_4)$ [C%]	S_{C5+} [C%]	S_{ROH} [C%]	ROH *n:iso*	α_{alkan} [-]	α_{ROH} [-]	*CTY* [$mmol_{CO}gCo^{-1}h^{-1}$]
1:2 reference	170:70	24	34.0	2.2	6.9	59.1	53.7	5.8	0.71	0.61	25.3
1:1	170:70	24	21.7	5.9	4.6	52.6	55.0	4.0	0.74	0.65	24.2
1:1	170:70	**72**	52.3	8.5	7.0	56.9	60.1	3.9	0.72	0.60	19.5

Figure 73: Combination of Fischer-Tropsch and hydroformylation for the direct conversion of synthesis gas to alcohols at CO:H_2 ratios of 1:1. $n(Co_{FT})$:$n(Co_{Hyfo})$: ratio of cobalt in the FT catalyst to cobalt in the Hyfo precursor ($Co_2(CO)_8$), X_{CO}: Carbon monoxide conversion, S_x: Carbon selectivity towards target product(s), α: chain growth probability, *CTY*: Cobalt-Time-Yield (Fischer-Tropsch cobalt specific catalytic activity), C_{5+}: Hydrocarbon products with a chain length >5, ROH: alcohol products. **Reaction conditions:** NaPr-CoRu@AOmM 40 mg, $Co_2(CO)_8$ 12 mg, PCy_3 20 mg, *iso*-hexane 0.9 g, 195 °C, 120 bar (at RT) CO:H_2 1:1, 700 rpm.

Reduction of the synthesis gas composition to 1:1 has only very minor effect on the catalytic activity of the Fischer-Tropsch or the hydroformylation catalyst. While the CO-conversion

decreased from 34% to 22%, due to of the the increased CO partial pressure, only a neglectable decrease of the *CTY* from 25 $mmol_{CO}gCo^{-1}h^{-1}$ to 24 $mmol_{CO}gCo^{-1}h^{-1}$ was observed. The alcohol selectivity increased slightly from 54 C% to 55 C%. When increasing the reaction time to 72 hours while using a reduced synthesis gas ratio of 1:1 (Figure 73, top right) a CO conversion of 52% is achieved. Considering the increased CO concentration, this relates to a *CTY* of 20 $mmol_{CO}gCo^{-1}h^{-1}$. This catalytic activity is comparable to the activity of the Fischer-Tropsch catalyst after 72 hours when a synthesis gas ratio of 1:2 is used and shows again that a lower synthesis gas ratio does not significantly affect the Fischer-Tropsch activity. In contrast, the alcohol selectivity reached an all-time high of 60 C% after 72 hours when using a synthesis gas ratio of 1:1, compared to the alcohol selectivity achieved with a synthesis gas ratio of 1:2 after 72 hours (45 C%). This is an increase of 15 C% and shows the importance to maintain a high CO partial pressure for the activity of the hydroformylation catalyst.

During the two last experiments the influence of the total catalyst concentration was tested while using prolonged reaction times (Figure 74). The aim of these experiments was to push the CO-conversion even further than during previous experiments to investigate how this effects the alcohol selectivity and to test the limits of this reaction system. Since previously the CO-conversion already reached 70% after 72 hours (Figure 70), the reaction time was adjusted to 48 hours when increasing the catalyst concentration to the 1.5-fold compared to the initial concentration (Figure 73, bottom left) and to 36 hours when increasing the catalyst concentration to the two-fold concentration compared to the initial one (Figure 73, bottom left). After increasing the catalyst concentration to 1.5-fold of the initial concentration a CO-conversion of 80% is observed after 48 hours. The *CTY* for the Fischer-Tropsch catalyst (20 $mmol_{CO}gCo^{-1}h^{-1}$) proved that the activity of the Fischer-Tropsch catalyst can be held even at higher catalyst loadings. Remarkably, even at this high CO-conversion, an alcohol selectivity of 43 C% is observed. Increasing the catalyst loading further to the two-fold of the initial concentration and adjusting the reaction time to 36 hours, lead to a slight increase of the *CTY* to 22 $mmol_{CO}gCo^{-1}h^{-1}$ and an increase in the CO-conversion to 87%. An alcohol selectivity of 38 C% is achieved, which is still remarkable considering the very high CO-conversion.

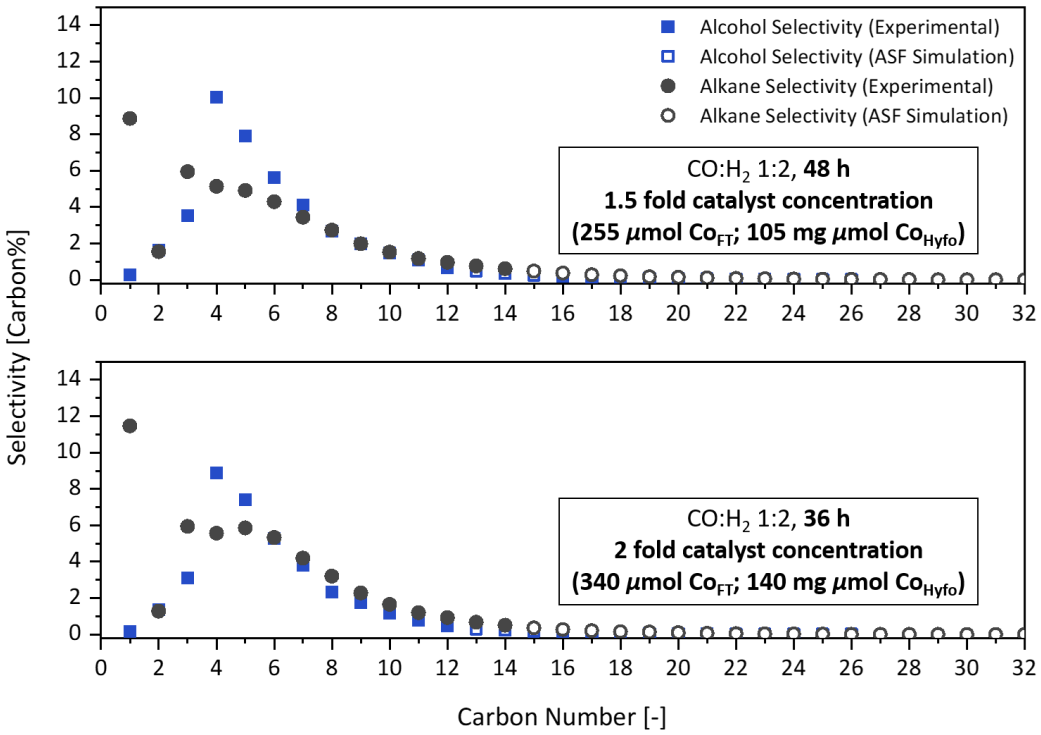

CO:H_2	$n(Co_{FT})$: $n(Co_{Hyfo})$ [µmol]	*t* [h]	X_{CO} [%]	$S(CO_2)$ [C%]	$S(CH_4)$ [C%]	S_{C5+} [C%]	S_{ROH} [C%]	ROH *n:iso*	α_{alkan} [-]	α_{ROH} [-]	*CTY* [$mmol_{CO}gCo^{-1}h^{-1}$]
1:2 reference	170:70	24	34.0	2.2	6.9	59.1	53.7	5.8	0.71	0.61	25.3
1:2	**255:105 (1.5-fold)**	**48**	80.3	4.8	8.9	54.3	42.7	6.1	0.71	0.70	19.9
1:2	**340:140 (2-fold)**	**36**	87.4	5.0	11.5	55.1	37.5	6.2	0.68	0.70	21.7

Figure 74: Combination of Fischer-Tropsch and hydroformylation for the direct conversion of synthesis gas to alcohols using high catalyst concentrations. $n(Co_{FT}):n(Co_{Hyfo})$: ratio of cobalt in the FT catalyst to cobalt in the Hyfo precursor ($Co_2(CO)_8$), X_{CO}: Carbon monoxide conversion, S_x: Carbon selectivity towards target product(s), α: chain growth probability, *CTY*: Cobalt-Time-Yield (Fischer-Tropsch cobalt specific catalytic activity), C_{5+}: Hydrocarbon products with a chain length >5, ROH: alcohol products. **Reaction conditions:** NaPr-CoRu@AOmM 40 mg (for the optimized cat. conc.), $Co_2(CO)_8$ 12 mg (for the optimized cat. conc.), PCy_3 20 mg (for the optimized cat. conc.), *iso*-hexane 0.9 g, 195 °C, 120 bar (at RT) CO:H_2 1:2, 700 rpm.

At this point, only about 16 bar of synthesis gas was left in the reactor after the reaction. When operated at those low pressures the activity of the hydroformylation catalyst is significantly reduced (see chapter 4.3.1). It can be assumed that the majority of the alcohols in the reaction mixture after 48 hours is generated at higher synthesis gas pressures. Nevertheless, those last experiments showed that the tandem catalytic system is highly flexible and able to maintain a high catalytic Fischer-Tropsch activity and alcohol selectivity at very high CO-conversions.

4.3.4 Placement of the Presented Tandem Catalytic Approach in the Context of Current Synthesis Gas to Alcohol Literature

The high alcohol selectivity up to 60 C% achieved with at the same time high CO-conversions >50%, as shown during the last experiments (Figure 73) and the time resolved reaction profile (Figure 70), represents a significant improvement compared to other Fischer-Tropsch based synthesis gas to alcohol approaches. The group of PÉREZ-RAMÍREZ summarized the results of other approaches in a CO-conversion/oxygenate selectivity plot covering literature published on this field until 2017 (Figure 75).[139]

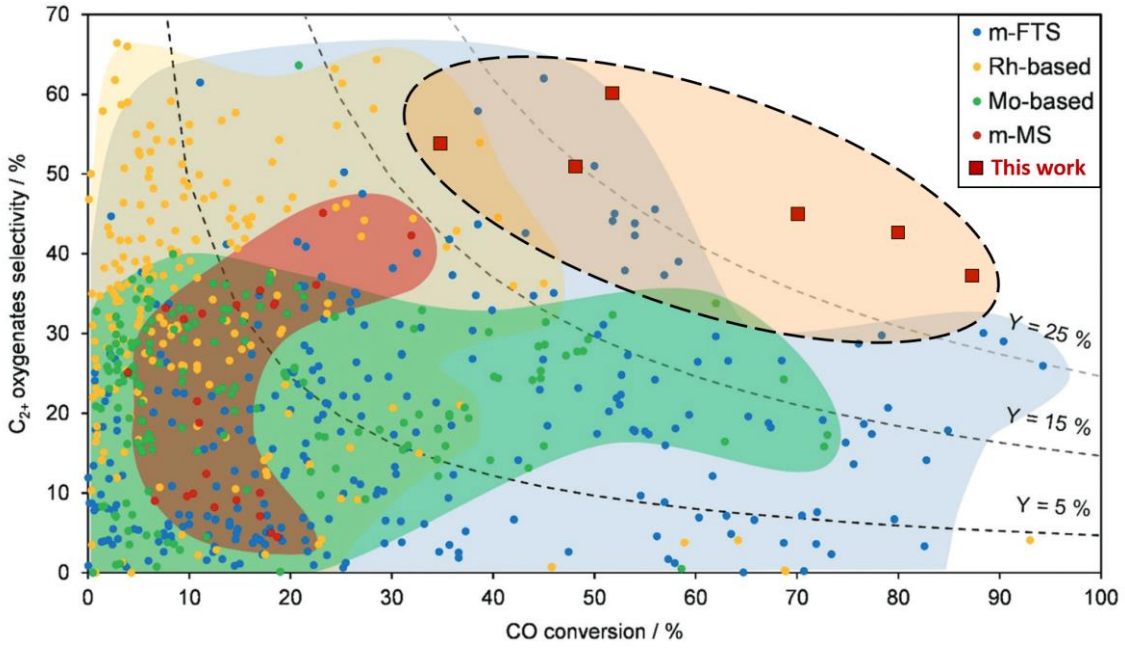

Figure 75: Comparison of synthesis gas to alcohol approaches known in literature as adapted from PÉREZ-RAMÍREZ [139] with the tandem catalytic approach presented in this work. m-FTS = modified Fischer-Tropsch catalysts, Rh-based = rhodium-based heterogeneous catalysts, Mo-based = molybdenum-based heterogeneous catalysts, m-MS = modified methanol synthesis catalysts.

As can be seen from this comprehensive overview, it is difficult to access regimes in which a high alcohol selectivity, with at the same time high CO-conversion, is achieved. Few reported catalytic systems achieve oxygenate selectivities higher than 40 C% while CO-conversions above 50% are held. The herein reported catalytic system allows for alcohol selectivities of up to 60 C% at CO-conversions above 50% and alcohol selectivities higher than 40 C% at CO-conversion levels above 70%, with at the same time low CO_2 and CH_4 side production. This represents a novelty in synthesis gas to alcohol conversion and can be linked to the inherent benefit of the herein presented tandem catalytic approach of olefin selective Fischer-Tropsch synthesis and highly active reductive hydroformylation reaction. The separation of the catalytically active centers for the Fischer-Tropsch reaction and the alcohol evolution reaction, circumvents the inherent challenges connected with other alcohol selective Fischer-Tropsch approaches (see chapter 2.4.3).

5 Summary and Outlook

Synthetic fuels will be needed in our future energy economy. Middle to long chain alcohols have been identified as valuable additives for synthetic fuels. The current processes however, are designed for the production of alcohols as intermediates in our current chemicals value chain and not as fuel additives. Energy and resource efficient transformation protocols are highly sought after. In this work, two novel tandem catalytic protocols for the synthesis of middle to long chain alcohols and Fischer-Tropsch-based paraffin/alcohol mixtures are presented.

In the first approach, the tandem catalytic reductive hydroformylation of linear alkenes to alcohols has been investigated. While this reaction is known since the 1960s, novel rhodium/phosphorus catalysts struggle to catalyze the hydrogenation step in high activity. In this work, the use of rhodium catalysts in combination with tertiary amine additives has been investigated. By combining experimental results and spectroscopic investigations, anionic rhodium complexes and clusters have been analyzed as the catalytic resting states. These are postulated to be precursors for a catalytically active monodentate rhodium hydride species $[RhH(NR_3)(CO)_3]$. Important parameters and constraints have been identified for the tertiary amine ligand which helped to attain catalytic systems with a high catalytic activity and excellent selectivity for the conversion of linear alkenes to alcohols. The highest activity with a TOF of 280 h^{-1} was achieved when the polar 2,2-dimethyl amino ethoxy ethanol was used as solvent and ligand at the same time. The combination of amine ligand and solvent inspired a recycling strategy in which trialkyl amine functionalized PEG derivatives were used as the stationary catalyst phase and product alcohols are extracted using supercritical CO_2. After designing a setup for the recycling under supercritical conditions, a diamine functionalized PEG_{600}-derivative, synthesized *via* an amide condensation, was found to be highly effective as solvent for the reaction and as stationary phase during the recycling with *sc*CO_2. Over nine consecutive recycling runs no decrease in catalytic activity or selectivity was observed when using this PEG_{600}-derivative as the stationary catalyst phase. Furthermore, during all nine runs a total of only 0.1% of the initial amount of rhodium metal has been transferred out of the reactor.

Overall, an integrated process for the reductive hydroformylation using rhodium in combination with tertiary amines is presented starting from the understanding on a molecular level and leading to a highly efficient catalytic system with a successful catalyst recycling. This highlights the potential of these catalytic systems and hopefully encourages further investigations. For example, a deeper understanding about the role of the amine in the hydrogenation step would aid the design of new and improved amine ligands. Furthermore, higher molecular weight PEG-amines, the incorporation of different polar functional groups or tertiary amine

functionalized polymers could help to further improve the catalytic activity and the retention of the rhodium catalyst during the herein presented recycling strategy.

In the second approach, a highly innovative concept for the direct conversion of synthesis gas to alcohols was presented. By combining a cobalt-based and olefin selective Fischer-Tropsch catalyst, and a cobalt-based, highly active, molecular reductive hydroformylation catalyst, a tandem catalytic reaction system, in which olefins are generated by the Fischer-Tropsch catalyst and converted *in situ* to alcohols by the reductive hydroformylation catalyst, was developed. Alcohol selectivities reaching 60 C% were achieved, with at the same time high conversions of CO of over 50%. Additionally, the production of CO_2 (around 2 C%) and CH_4 (around 9 C%) side products was low at all times during the investigations. This sets new records in the chemistry related to the conversion of synthesis gas to higher alcohols, while avoiding inherent drawbacks accompanied by other approaches like a high CH_4 side production or a low carbon chain growth. It was shown that by applying the two catalysts in spatial proximity the alcohol selectivity can be increased far above the theoretical olefin selectivity of the Fischer-Tropsch catalyst, intercepting the *in situ* generated olefins before they get reabsorbed on the Fischer-Tropsch surface and are hydrogenated to paraffins. Time-resolved experiments proved that both catalysts are stable for at least 72 hours, even though an initialization phase is needed. Even at very high CO-conversions of 70% alcohol selectivities above 40% were achieved. The slight decrease in alcohol selectivity at very high CO conversions is likely due to a decrease in hydroformylation activity at reduced pressures.
As products, paraffin/alcohol mixtures are obtained which would be promising precursors for synthetic diesel fuels. Since this tandem approach is highly innovative, the next step would be to investigate the catalyst stability in a continuous process and to develop a strategy for the recycling of the homogeneous cobalt catalyst.

In retrospect, although the key element of this work is based in the field of molecular catalysis, the success of both projects has only been possible by combining expertise in a variety of different scientific fields. As an example, during the investigation of the reductive hydroformylation using rhodium/amine catalysts, fundamental understanding of the catalyst has been accomplished by combining spectroscopic, computational and experimental results. This played a key role in the improvement of the catalytic system. It furthermore served as a guideline for the development of the catalyst recycling strategy. Subsequently, for the successful recycling of the catalyst, fundamental knowledge in the fields of reaction engineering was necessary. Last but not least, the exchange with project partners in the REDIFUEL project was invaluable to get an understanding for the greater picture and requirements connected to alcohols as fuel additives.

Concerning the second project dealing with the direct production of alcohols from synthesis gas, a combination of skills in the fields of heterogeneous Fischer-Tropsch synthesis and homogeneous reductive hydroformylation was mandatory for the success of the project. The presented strategy of combining homogeneous and heterogeneous transition metal catalysis, is not only a novelty in the field of synthesis gas to alcohol research, but is one of the rare examples for the tandem combination of homogeneous and heterogeneous transition metal catalysts in general. This showcases that those kind of cooperations are by no means common practice in chemical research.

Confronted with the need for fundamental changes in our value chains, future research will more so than before, rely on the combination of specialized knowledge in a variety of fields. As individual researchers we can contribute to this by accepting the equal importance of different scientific fields and actively foster cooperations and the exchange of knowledge.

6 Experimental and Analytical Procedures

In the following, the experimental and analytical procedures applied in this work will be described. First experimental standard procedures and synthetic protocols will be given in the order in which they appear in the results section (chapter 4). Afterwards analytical methods will be described (chapter 6.3). All chemicals used in the experimental and analytical procedures will be listed in chapter 6.4. The experimental and analytical procedures can also be found in the supporting information of the corresponding publications.

6.1 General Considerations

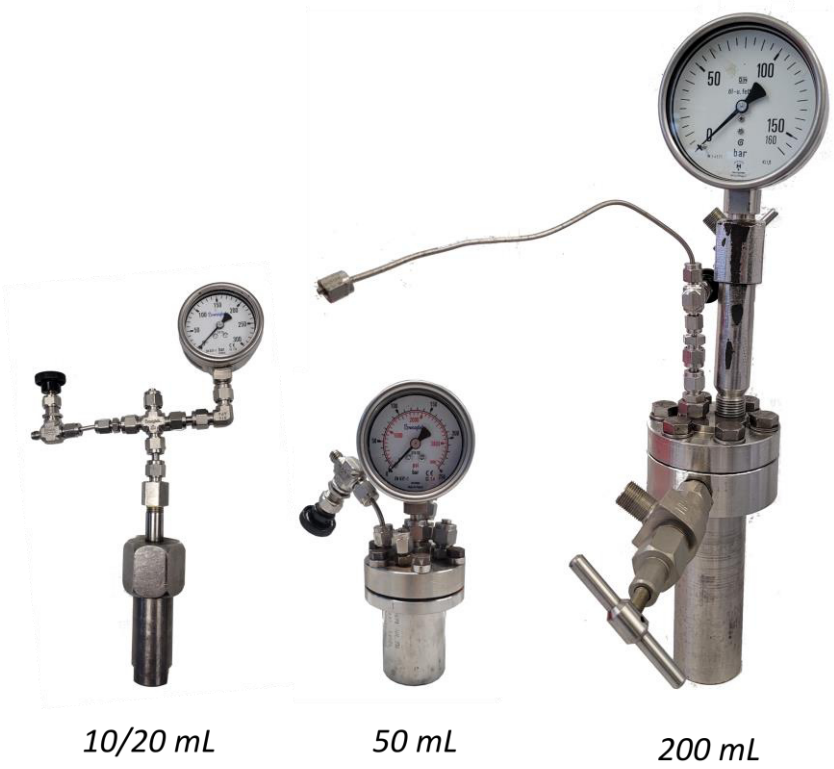

Figure 76: Autoclave reactors used during this work ranging from 10 mL to 200 mL. All autoclave reactors used during this work are equiped with a manometer and stirred with magnetic stirring.

For all catalytic experiments high pressure autoclave reactors, ranging from 10 mL to 200 mL were used. Examples are depicted in Figure 76. In general, to pressurize autoclave reactors, a high-pressure filling station by MAXIMATOR® was used, which can operate at pressures ranging from 5 to 200 bar. During the combined Fischer-Tropsch/hydroformylation experiments in chapter 4.3, the reactors have been pressurized manually, using a bottle containing a mixture of 60 vol% H_2, 30 vol% CO and 10 vol% Ar, instead. Before adjusting the final gas composition, the piping of the pressure station/gas bottle and suqsequently the reactors were flushed with 20 bar hydrogen for at least three times. All used reaction gases had a purity of >99.99%.

Air sensitive experiments (e.g. Fischer-Tropsch/hydroformylation experiments) were weighed in a glovebox under argon atmosphere. Liquid reactants and solvents were degassed, transferred to the glovebox and stored over activated molecular sieves. Air sensitive NMR-samples were prepared under argon atmosphere using standard Schlenk technique.

6.2 Experimental Procedures

6.2.1 Autoclave Experiments for the Reductive Hydroformylation of Alpha Olefins using Rhodium/Amine Catalysts

The following procedure applies for experiments conducted during the investigation of the reductive hydroformylation with rhodium/amine catalysts in chapter 4.1 to chapter 4.2.

For reductive hydroformylation experiments 20 mL high-pressure autoclave reactors (Figure 76) equipped with a manometer, a borosilicate glass inlet (10 mL) and a magnetic stirring bar were used. The catalyst precursor ([$Rh(CO)_2(acac)$] if not stated otherwise), the respective olefin (1-octene or 1-pentene), the solvent and, if used, the amine ligand were weighed into the glas inlet in this order. The glass inlet was inserted into the autoclave reactor and the autoclave reactor was sealed and flushed with 10 bar of hydrogen for at least two times. Afterwards the reactor was pressurized with the corresponding hydrogen partial pressure and carbon monoxide was added up to the total pressure used during the corresponding experiment.
The reactor was placed into a pre-heated alumina cone on a magneting stirring hot plate set to the desired reaction temperature. The magnetic stirrer was set to a stirring speed of 700 rpm and the reaction was proceeded for the stated reaction time. After the reaction, the reactor was cooled to ambient temperature in a water bath for at least 15 minutes and expanded to ambient pressure. Samples for GC and/or NMR analysis were taken from the post reaction mixture and analyzed following the procedure described in chapter 6.3.1.

6.2.2 DFT Calculation of Tertiary Amine Cone Angles Binding to $Ni(CO)_3L$

The cone angles of tertiary amines have been calculated with the help of Kathrin Koehnke. To determine the cone angles, the structures of the corresponding $Ni(CO)_3L$ complexes (for monodentate ligands L) and $Ni(CO)_2(L\cap L)$ complexes (for bidentate ligands $L\cap L$) were first optimized using DFT calculations. All DFT calculations were performed with the program ORCA, version 4.0.1. A geometry optimization of the structures in the gas phase using the M06 L functional of TRUHLAR[190] with the def2 SVP basic set[191,192] (double ζ level) was performed. The Grid6 integration grid (larger) was used. For the geometry-optimized structures, a frequency

calculation was then conducted to check whether the stationary point is the desired minimum (no imaginary oscillation) or a transition state imaginary oscillation.

The $Ni(CO)_4$ complex was used as a starting point, to better compare the results to known Tolman angles of phosphine ligands. From the optimized structures the coordinates of the central atom as well as the tertiary amine ligand were used to determine the cone angles with the Mathematica package "FindConeAngle" by ALLEN ET AL.[146] In short, the package is used to describe the atoms of the ligands by a sphere with the respective Van der Waals radius. Then a ligand cone is calculated, the tip of which is located in the metal center and which includes all ligand atoms. The angle of this cone is determined and specified by the program. The exact procedure for determining and calculating the cone angle can be found in literature.[146] The resulting cone angles and 3D-coordinates for all 14 tertiary amines can be found in the Appendix.

6.2.3 DFT Calculation of Free Gibbs Energies of Rhodium-Hydrido-Carbonyl and Rhodium-Amino-Hydrido-Carbonyl Complexes

The absolute electronic energies and free Gibby energies of several Rh-hydrido-carbonyl and Rh-amino-hydrido-carbonyl complexes were computed with the help of Kathrin Köhnke. For the DFT calculations the program ORCA was used (version 4.2.1).

The geometries were optimized using the M06-LGrid6 fuctional of Truhlar[190] with the def2-TZVP basis set[191,192] (triple ζ level). taking the effective core potential (ECP) of Rh[193] into account. Implicit solvation in acetonitrile was applied using the *Conductor-like Polarizable Continuum Model* (CPCM)[194] with the polarization charges on the cavity surface modelled as spherical Gaussians described as a scaled Van-der-Waals surface.[195,196] The DFT integration grid was increased by applying ORCA keywords “Grid6” and “Finalgrid6”.

Gibbs free energies were obtained based on ideal gas statistical mechanics using the quasi-rigid-rotor-harmonic-oscillator approach of Grimme[197] to compute the entropic contributions to the free energies. Thermal corrections were calculated for a temperature of 60 °C and an elevated pressure of 471 atm (derived from the density of acetonitrile) to account for solvation entropy effects.[198,199] Relative Gibbs free energies were calculated for the formation of the respective complexes from the $Rh(acac)(CO)_2$ precursor and the free ligands according to the following equation with x =-1; 0; 1; 2 and y = 1; 2

$$[Rh(acac)(CO)_2] + H_2 + x\,CO + y\,NEt_3 \longrightarrow [Rh(H)(CO)_{2+x}(NEt_3)_y] + Hacac$$

All attempts to optimize complexes of the structure $Rh(H)(CO)_2(NEt_3)_2$ resulted in the repellence of one amine.

6.2.4 Protocol for the Ruthenium Catalyzed Alcohol Amination of Poly Ethylene Glycols of Various Chain Lengths using Diethylamine (chapter 4.2)

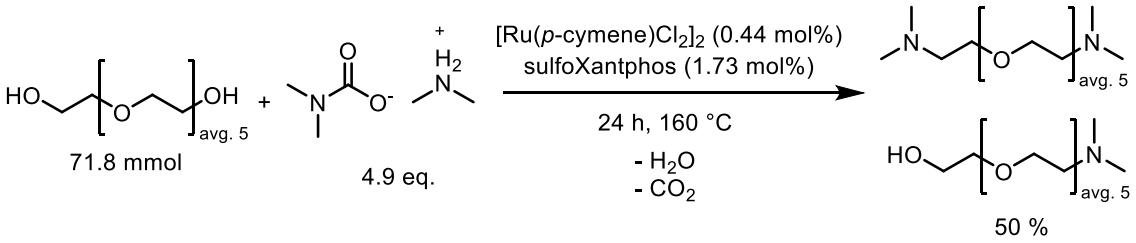

The diol (71.8 mmol, 1.0 eq.), dimethylcarbamate (45 mL, 351 mmol, 4.9 eq.), [Ru(*p*-cymene)Cl_2]$_2$ (195.2 mg, 0.32 mmol, 0.44 mol%) and sulfoXanphos (984.3 mg, 1.73 mmol, 1.73 mol%) were added to a 200 mL stainless steel reactor (Figure 76) with magnetic stirring bar. The reactor is sealed and heated to 160 °C for 24 h at a stirring speed of 700 rpm. After the reaction, the reactor is cooled to ambient temperature and the ruthenium catalyst is separated from the mixture by column chromatography over a combined silca/Al_2O_3 column (⌀ = 8 cm, silica ≈ 4 cm, Al_2O_3 ≈ 4 cm). The column is washed with 200 mL dichloromethane and the obtained solution is transferred to a round bottom flask. Afterwards, dichloromethane is removed under reduced pressure and the excess dimethylcarbamate is separated *via* a distillation under argon flow (90 °C, atm). The remaining orange liquid was purified a second time by column chromatography over a combined silca/Al_2O_3 column (⌀ = 8 cm, silica ≈ 6 cm, Al_2O_3 ≈ 6 cm). Dichloromethane is removed under reduced pressure. A mixture of di-, mono- and non-aminated poly ethylene glycole derivate was obtained as light-yellow viscous oil (11.8 g, 50% isolated product). The full ^{1}H-NMR spectrum of the isolated product can be found in the appendix.

^{1}H-NMR of a mixture of non- mono- di-aminated product with PEG_{300} as substrate: (400 MHz, $CDCl_3$, 21 °C) δ = 3.75 – 3.53 (m, 69H, **A**), 2.50 (t, J = 5.7 Hz, 2H, **B**), 2.25 (s, 6H, **C**) ppm.

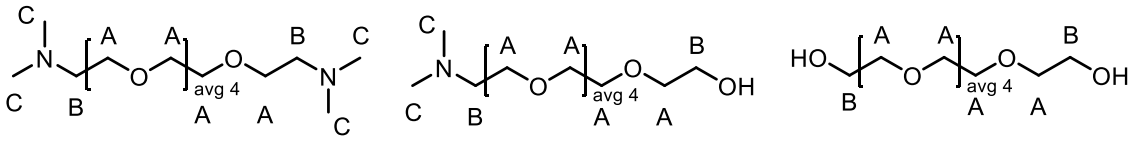

6.2.5 Protocol for the Amide Condensation of PEG_{600}-Diacid with Trimethyldiaminoethane (chapter 4.2)

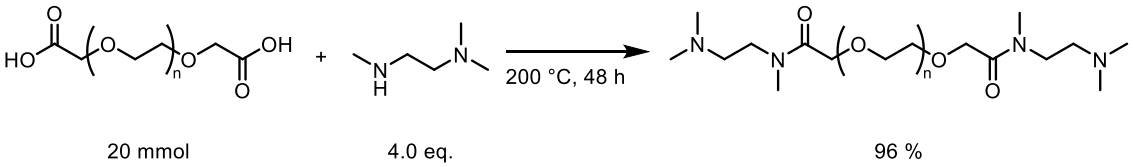

PEG_{600} carboxylic acid (12.00 g, 10.14 ml, 20.0 mmol, 1.00 eq.) and trimethyldiaminoethane (8.172 g, 10,16 mL, 80.00 mmol, 4.0 eq.) were added to a 200 mL stainless steel autoclave with magnetic stirring bar. The solution was heated to 200 °C for 48 h at 700 rpm. Afterwards, the reactor was cooled to ambient temperature. Excess trimethyldiaminoethane and reaction water was removed under reduced pressure (100 mbar at 55 °C to 24 mbar at 60 °C). The product is obtained as yellow viscous oil (14.74 g, 96% isolated yield). The full ^{1}H-NMR spectrum of the isolated product can be found in the appendix.

^{1}H-NMR: (400 MHz, $CDCl_3$, 21 °C) δ = 4.21 (s, 2H, **B**), 4.18 (s, 2H, **B**), 3.76 – 3.54 (m, 43H, **A**), 3.46 (dd, *J* = 15.3, 8.4 Hz, 2H, **E**), 3.36 (t, *J* = 7.1 Hz, 2H, **E**), 3.02 – 2.87 (m, 6H, **D**), 2.42 (t, *J* = 7.0 Hz, 4H, **F**), 2.23 (s, 12H, **C**) ppm.

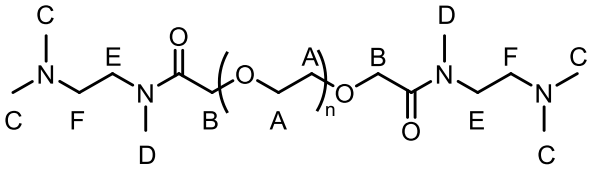

6.2.6 Catalyst Recycling and *sc*CO_2 Extraction Experiments during the Rh/Tertiary Amine Catalyzed Reductive Hydroformylation (chapter 4.2)

For all catalyst recycling experiments a 50 mL autoclave reactor (Figure 76) equipped with a manometer and a magnetic stirring bar was used. Unless stated otherwise the reaction was conducted as described in chapter 6.2.1. After the reaction, CO/H_2 was released, the manometer of the reactor was detached and the reactor was installed into the extraction set-up for *sc*CO_2 as depicted in Figure 77.

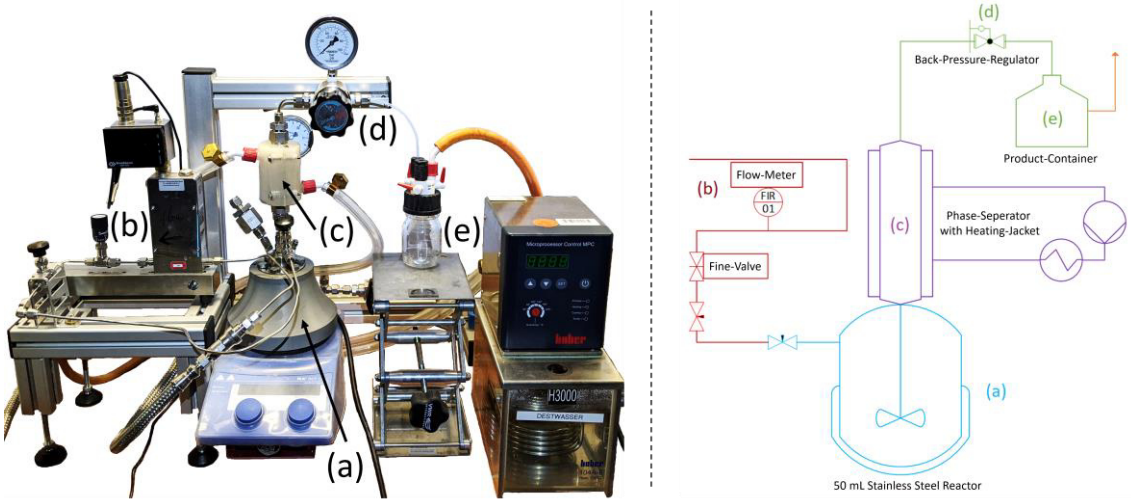

Figure 77: Extraction setup for for catalyst recycling experiments. (a) 50 mL stainless steel autoclave reactor, (b) Flow-meter (Bronkhorst, MFCs), (c) 3D-printed phase settler with heating circuit, (d) back-pressure-regulator (BPR), (e) 100 mL product container.

The valve of the reactor was connected to the CO_2 line and the thread of the former manometer was connected to the phase settler. Afterwards, the pressure of the CO_2 line was set to 100 bar before opening the fine valve regulating the CO_2 flow into the reactor. The reactor was filled with CO_2 at a flow rate of about 4 g min^{-1}. During this, the back-pressure regulator (BPR; *GCE BP301-01-S-100-V-P-02N-BL*) was set to 100 bars (maximum operating pressure), the temperature of the heating plate regulating the reactor temperature to 50 °C, and the water pump regulating the phase settler temperature to 55 °C. Shortly after reaching the critical pressure of CO_2 (74 bar) the valve of the reactor was closed to allow for an expansion to the supercritical state without backflow into the CO_2 line. After five minutes the valve was opened again and the reactor was filled up to 100 bar with *sc*CO_2. The BRP is now set to 95 bar to allow a constant *sc*CO_2 flow through the reactor caused by the pressure difference between the CO_2 line and the BPR. The flow can be adjusted using the fine valve of the CO_2 line. This marks the starting point of the extraction. During the extraction the product container was cooled with an ice bath and the fine valve was adjusted to allow a constant flow of *sc*CO_2 with 2.6 g min^{-1}. Every 20 minutes the BPR was heated with a heating gun to circumvent the formation of solid CO_2 at the point of phase transition from *sc*CO_2 to *g*CO_2 in the BPR. After the designated amount of CO_2

has passed the reactor, the CO_2 line was closed. This marks the end of the extraction. The product container was weighed and the extract was transferred into a sample container. Afterwards the product container was installed again. The heating of the reactor and the phase settler was turned off and the pressure at the BPR was reduced cautiously in steps of about 2 bar every 30 seconds until ambient pressure is reached. To start the next reaction, the reactor is detached from the CO_2 line and the phase settler and fresh substrate is added under inert gas flow. Finally, the manometer was attached again and the reactor is pressurized following the procedure described in chapter 6.2.1.

6.2.7 Autoclave Experiments for the Reductive Hydroformylation of 1-Octene using Cobalt/Trialkylphosphine Catalysts (chapter 4.3.1)

The performance of cobalt-based hydroformylation catalysts was evaluated using *1*-octene as model compound for mid-chain Fischer-Tropsch olefinic products. All experiments have been conducted using a 10 mL autoclave reactor (Figure 76) equipped with manometer, a borosilicate glass inlet (5 mL) and magnetic stirring bar. Under inert atmosphere the dicobalt octacarbonyl catalyst precursor $Co_2(CO)_8$, and the corresponding phosphine ligand, i.e. tricyclohexylphosphine (PCy_3), tri-*n*-butylphosphine (P*n*-Bu_3), triphenylphosphine (PPh_3), or polymer-bound triphenylphosphine (phenylphosphinated copolymer of styrene and divinylbenzene), were weighed into a borosilicate glass inlet of a 10 mL steel autoclave, equipped with a magnetic stirring bar under inert conditions (mBraun UNIlab ECO Glovebox with argon atmosphere, <0.1 ppm H_2O, <4 ppm O_2) . Afterwards, 1-octene, 0.1 g tetradecane, as internal standard for gas chromatography, and 2.75 mL of the designated solvent, i.e. typically 2-methyl pentane, have been added. The glass inlet was inserted into the reactor and the reactor was sealed and flushed with argon. After flushing with hydrogen, the reactor was pressurized to the designated partial pressure of hydrogen in the desired synthesis gas composition. Afterwards, carbon monoxide was added until the designated partial pressure of CO in the desired syngas composition was reached. After pressurizing, the autoclave was heated to the desired reaction temperature (typically 468 K) in a preheated aluminum block fitted on a magnetic stirring heating plate. The reaction was carried out while stirring (700 rpm) for the designated reaction time. After the reaction, the autoclave was cooled to ambient temperature and the pressure was released. Samples for GC and/or NMR analysis were taken from the reaction solution and analyzed following the procedure described in chapter 6.3.1 and 6.3.4.

6.2.8 Preparation of Co-based Fischer-Tropsch Catalysts and Promotion with Na/Pr

The supported cobalt-based Fischer-Tropsch catalyst which was used in chapter 4.3 was prepared by project partners (Kai Jeske and Dr. Prieto Gonzalo) using the following procedure: Fischer-Tropsch cobalt-based catalysts were prepared by incipient wetness impregnation of porous γ-Al_2O_3 support materials. Mesoporous γ-Al_2O_3 (denoted AOm) and meso-macroporous γ-Al_2O_3 (denoted AOmM) were obtained *via* thermal dehydration of Catapal® (Sasol Materials) and Versal® (Honeywell UOP) microparticulate pseudo-boehmite precursors at 550 °C (2 °C min^{-1} heating rate) for 5 hours in a muffle oven under stagnant air atmosphere. The resulting γ-Al_2O_3 supports were first dried under dynamic vacuum (150 °C) for 2 hours prior to impregnation under static vacuum with a stock aqueous solution containing $Co(NO_3)_2{\cdot}6H_2O$ and ruthenium (III) nitrosyl nitrate. To prepare this stock precursor solution, metal nitrates were dissolved in those amounts required to achieve an atomic ratio of Ru/Co=0.007, and the solution was further acidified with 0.25 vol% HNO_3. Following impregnation, the solid was dried in a tubular reactor at 70°C under argon flow for 10 hours and the nitrate precursors further decomposed at 350 °C for 4 hours under argon flow (heating rate of 1 °C min^{-1} from RT). To adjust the total metal loading in the catalysts, five impregnation/calcination cycles were performed in the case of AOm, while two cycles sufficed in the case of AOmM.

To prepare Na/Pr promoted catalysts (NaPr-CoRu@AomM), the following steps have been adjusted: The required amount of the unpromoted CoRu/γ-Al_2O_3 catalyst (in its as-calcined oxidic form) was dried under vacuum at 150 °C for 2 hours, and then impregnated with an aqueous solution of the nitrate precursors in 0.5 molar HNO_3. The concentration of the nitrate precursor in the impregnating solution was adjusted to achieve a preset surface-specific content of 0.2 $Na_{at}\,nm^{-2}$ and 0.8 $Pr_{at}\,nm^{-2}$. After mixing the solid in the impregnation solution, the solvent water was removed in a rotary evaporator at 50 °C. The dried solid was subsequently transferred to a tubular reactor and calcined at 350 °C for 4 hours under synthetic air flow at a heating rate of 1 °C min^{-1} from ambient temperature.

6.2.9 Gas-phase Reaction of CoRu-AOm and NaPr-CoRu@AOmM Fischer-Tropsch Catalysts (chapter 4.3.2)

The catalytic performance of supported cobalt-based catalysts was assessed by gas-phase Fischer-Tropsch experiments, conductet by project partners (Kai Jeske and Dr. Prieto Gonzalo) using the following procedure: Gas-phase catalytic tests of the Fischer-Tropsch were performed at 20 bar and 200 °C in a fixed-bed reactor setup. The setup is equipped with mass-flow controllers (Bronkhorst, MFCs) to feed H_2 and pre-mixed synthesis gas (30 vol% CO, 60 vol% H_2, 10 vol% Ar) to the reactor. Two-finned copper elements with embedded 180 W heating cartridges are used to heat the stainless steel fixed-bed micro-reactor (inner diameter = 12 mm). Two thermocouples are placed at the start and at the end of the catalyst bed to control the temperature inside the reactor. During the reaction an online gas chromatograph (modified Agilent 7890B) is used for product analysis. Prior to injection to the reactor, the syngas stream was first passed over an activated carbon bed (Norit®) at 30 bar and room temperature to remove metal-carbonyl impurities, and then through a grade stainless steel (length = 300 mm, inner diameter = 3 mm) capillary, heated to 200 °C to pre-heat the synthesis gas. The free volume in the reactor was reduced by inserting two stainless-steel spacers, one (l = 62 mm) upstream of the catalyst bed, and another (l = 50 mm) downstream of the catalyst bed. The spacers have been separated from the catalyst bed using two quartz wool plugs (l = 5 mm). Below the first quartz wool plug, a 3.4 cm^3 layer of SiC granules was placed to a pre-heat the synthesis gas and help establish a plug-flow before entering the catalyst bed. The catalyst bed consisted of an amount of catalyst equivalent to 100 mg of Co. This amount of supported catalyst was diluted with 6.2 cm^3 of SiC granules to improve heat transfer in the catalyst bed.

Before the Fischer-Tropsch reaction, metal species in the catalyst have been reduced in H_2 flow (200 cm^3 STP min^{-1}) at 400 °C for five hours at atmospheric pressure. Following catalyst reduction activation, the reactor was cooled to 350 °C in H_2 flow, followed by switching the flow to the synthetic syngas mixture (150 cm^3 min^{-1}). The system was then pressurized to 20 bar using a membrane dome regulator (GO regulator), and the reactor temperature was increased to 200 °C (0.15 °C min^{-1}). The start of the temperature ramp from 150 °C to 200 °C was marked as the start time onstream. After at least 24 h time-on-stream, the syngas flow was adjusted to determine catalyst performance at a conversion level of 20±3% CO.

Downstream of the reactor, two consecutive cold traps have been set at temperatures of 150 °C and 100 °C to collect heavy hydrocarbon products and water. All other downstream tubing was heated to 170 °C to prevent the condensation of reaction products. All gaseous components of

the gas stream leaving the traps were depressurized after passing the dome pressure regulator and analyzed *via* online gas chromatography (see chapter 6.3.1).

Liquid and solid hydrocarbons collected from the trap kept at 100 °C were separated by decanting and the individual liquid phases were further purified by centrifugation (9000 rpm, 15 min) to collect waxes and obtain liquid phases which were weighed separately. Solid waxy hydrocarbons collected from the trap kept at 150 °C and were blended together with those wax fractions collected by centrifugation of the liquid products, weighed, and dissolved in CS_2. Gas chromatography of aqueous phase products was performed following the description in chapter 6.3.1.

6.2.10 Slurry Phase Autoclave Experiments for the Fischer-Tropsch/Reductive Hydroformylation Tandem Catalyzed Conversion of Synthesis Gas to Alcohols (chapter 4.3.3)

Tandem Fischer-Tropsch synthesis/reductive hydroformylation catalytic experiments were performed in 10 mL stainless steel autoclave reactors (Figure 76) equipped with a manometer, a borosilicate glass inlet (5 mL) and a magnetic stirring bar. The solid Fischer-Tropsch catalyst (previously activated by reduction in H_2 flow at 400 °C for 5 hours and stored in a glove box under exclusion of air) was weighed into the glass inlet. To this, the corresponding amounts of dicobalt octacarbonyl ($Co_2(CO)_8$), organo-phosphine ligand and solvent were added. 2-methyl heptane (50 mg) was added as internal standard for gas chromatography quantification of liquid products. All substances were weighed and added under protective inert atmosphere (mBraun UNIlab ECO Glovebox with argon atmosphere, <0.1 ppm H_2O, <4 ppm O_2). Afterwards the autoclave was sealed and pressurized to the initial total pressure of 120 bar at ambient temperature, with a synthetic gas mixture containing 10 vol% Ar, 30 vol% CO, and 60 vol% H_2. Argon was added as an internal standard for gas chromatography quantification of headspace gases.

Afterwards, the autoclave was heated to the desired reaction temperature (typically 195 °C) in a preheated heating cone fitted on a heating plate with magnetic stirrer. The reaction was let to proceed under magnetic stirring with 700 rpm. After the reaction, the autoclave was cooled to ambient temperature in a water bath. Before releasing the pressure, the reactor was connected to a head-space GC equipped with a FID and TCD detector for analysis of the gas phase. For the exact GC-FID/TCD analytical procedure see chapter 6.3.1.

Afterwards, the pressure was released, the reaction mixture centrifuged in an ultra-centrifuge at 13.000 rpm and samples from the liquid phase are taken for GC-analysis as described in chapter 6.3.1. Furthermore, the solid Fischer-Tropsch catalyst residue was analyzed *via*

thermogravimetric analysis in the case of chosen samples (see chapter 6.3.3). For selected samples the sample was further analyzed by two-dimensional gas chromatography (see chapter 6.3.1)

The CO conversion (X_{CO}) and the metal-specific reaction rate (cobalt-time-yield (*CTY*)) were used to express catalytic activity. Selectivity to C_{5+} hydrocarbon products was determined by deducing the selectivity to C_{4-} carbon-containing products, including CO_2, from a closed carbon balance.

6.3 Analytical Procedures

6.3.1 Gas-Chromatography with Integrated Flame-Ionization-Detector (GC-FID), Thermal-Conductivity-Detector (GC-TCD) and Mass-Spectrometry Detector (GC-MS)

Different Gas-Chromatography (GC) methods have been used during the work presented in the results section. They will be listed and explained in the order they appear in the text.

6.3.1.1 Gas-Chromatography with Integrated Flame ionization Detector (FID) and Mass-Spectrometry Detector (MS) for Qualitative and Quantitative Identification of Products and Substrates in the Rhodium/Amine Catalyzed Reductive Hydroformylation

Gas-chromatography (GC) analysis of post reaction mixtures for the reductive hydroformylation of 1-octene and 1-pentene was performed to quantitatively determine conversion and product yields. For this a Nexis GC-2030 gas chromatograph equipped with a Flame-Ionization-Detector (FID), an AOC-20sPlus autosampler and an AOC-20iPlus injector by Shimadzu equipped with a Rtx-*1* column was used. For sample preparation, 25 mg tetradecane as internal standard, 200 mg of the post reaction solution and 800 mg *iso*-propanol in the case of 1-octene as substrate such as 1-butanol in the case of 1-pentene as substrate, have been weighed into a GC vial. The vial is inserted to a GC auto sampler by Shimadzu. The specifications of the GC program and column parameters are listed in Table 8. For quantification, calibration curves of the pure compounds have been measured. For simplicity reasons, the same calibration factor was used for the corresponding alkene and alkene isomers. Furthermore, the calibration factors of *n*- and *iso*-alcohols and *n*- and *iso*-aldehydes were assumed to be equal. The standard deviation of relevant analytes (alcohols and aldehydes) has been determined to be ≤5%.

Table 8: Gas-Chromatography with integrated Flame-Ionization-Detector (GC-FID) parameters used during analysis of reductive hydroformylation using rhodium/trialkylamine catalysts experiments.

Parameter	Value
Column	Restek Rtx-1 (length 30 m, diameter 0.25 mm, film thickness 0.50 µm)
Carrier gas	He
Split-ratio	01:35
Carrier gas flow	1.47 mL/min
Detector	FID/MS
Temperature program	35 °C hold 12 min, 8 °C/min to 180 °C, 20 °C/min to 245 °C, 245 °C hold 5 min
Injection volume	0.2 μL

For qualitative analysis of the individual compounds, gas chromatography with subsequent Mass-Spectrometry (GC-MS) was used. For this, a GCMS-QP2020 mass spectrometer with GC-2010-Plus gas chromatograph, AOC-20sPlus auto sampler and AOC-20iPlus injector (Shimadzu) have been used. For sample preparation the same procedure as for GC-FID has been applied or the same samples prepared for GC-FID was used directly for GC-MS analysis. GC-MS has been measured on the same column and following the same temperature program as listed in Table 8 with the exception that a MS detector instead of a FID detector was used and the injection volume was lowered to 0.1 μL due to the increased sensitivity of the GC-MS detector. MS-fragmentation patterns including all relevant peaks (peaks with a relative intensity >10% but at least the eight peaks with the highest relative intensity) of individual compounds are listed below:

1-Octene MS (EI^+): ***m/z*** (rel. Int.) **39** (39%), **40** (12%), **41** (91%), **42** (60%), **43** (80%), **45** (41%), **47** (10%), **55** (100%), **56** (63%), **57** (13%), **69** (34%), **70** (90%), **71** (11%), **79** (28%), **81** (43%), **83** (30%), **84** (17%).

Octane MS (EI^+): ***m/z*** (rel. Int.) **39** (10%), **41** (43%), **43** (100%), **55** (13%), **56** (21%), **57** (37%), **70** (15%), **71** (25%), **84** (10%), **85** (44%).

n*-Nonanal MS** (EI^+): ***m/z (rel. Int.) **54** (12%), **55** (45%), **56** (63%), **57** (100%), **67** (19%), **68** (26%), **69** (29%), **70** (38%), **71** (14%), **81** (26%), **82** (34%), **83** (12%), **95** (22%), **96** (21%), **98** (33%).

iso*-Nonanal MS** (EI^+): ***m/z (rel. Int.) **55** (9%), **56** (4%), **57** (29%), **58** (100%), **59** (4%), **71** (15%), **84** (4%), **100** (4%).

n*-Nonanol MS** (EI^+): ***m/z (rel. Int.) **39** (13%), **41** (74%), **42** (38%), **43** (72%), **55** (84%), **56** (100%), **57** (34%), **58** (26%), **68** (22%), **69** (35%), **70** (77%), **82** (12%), **83** (36%), **84** (25%).

iso*-Nonanol MS** (EI^+): ***m/z (rel. Int.) **39** (12%), **41** (65%), **42** (23%), **43** (91%), **55** (41%), **56** (54%), **57** (100%), **58** (45%), **69** (37%), **70** (39%), **71** (71%), **83** (23%), **84** (29%).

1-Pentene MS (EI^+): ***m/z*** (rel. Int.) **27** (34%), **29** (37%), **40** (11%), **41** (75%), **42** (100%), **55** (90%), **57** (11%), **70** (55%).

Pentane MS (EI^+): ***m/z*** (rel. Int.) **27** (19%), **29** (17%), **39** (20%), **41** (57%), **42** (61%), **43** (100%), **57** (20%), **72** (15%).

iso*-Hexanal MS** (EI^+): ***m/z (rel. Int.) **39** (14%), **41** (30%), **43** (100%), **55** (11%), **57** (17%), **58** (77%), **71** (18%), **72** (11%).

n*-Hexanal MS** (EI^+): ***m/z (rel. Int.) **39** (24%), **41** (77%), **42** (15%), **43** (58%), **44** (100%), **45** (23%), **55** (19%), **56** (96%), **57** (64%), **58** (16%), **67** (13%), **71** (10%), **72** (24%), **82** (18%).

iso*-Hexanol MS** (EI^+): ***m/z (rel. Int.) **39** (10%), **41** (31%), **42** (18%), **43** (100%), **55** (27%), **56** (25%), **69** (30%), **70** (32%), **71** (34%), **84** (10%).

n*-Hexanol MS** (EI^+): ***m/z (rel. Int.) **39** (9%), **41** (37%), **42** (37%), **43** (53%), **55** (48%), **56** (100%), **57** (8%), **69** (35%).

6.3.2 Combination of Gas-Chromatography with Integrated Flame-Ionization-Detector (FID) and Thermal-Conductivity-Detector (TCD) for Liquid and Gas Phase Analysis in Slurry Phase Fischer-Tropsch/Hydroformylation Experiments

Experiments investigating the reductive hydroformylation of 1-octene using cobalt/alkylphosphine catalysts (chapter 4.3.1) have been qualitatively and quantitively analyzed *via* a combination of GC-FID and GC-MS analysis following the same procedure as described during the previous chapter.

For quantification of the combined Fischer-Tropsch/hydroformylation experiments in slurry phase (chapter 4.3.3) the gas, liquid and solid phase was analyzed. For analysis of the gas phase a combination of headspace GC-FID and GC-TCD was used. After the reaction the reactor was cooled to ambient temperature and connected to a Swagelok piping leading to the GC-FID/GC-TCD instrument. A portion of the gas phase in the reactor was cautiously released to flush and fill two sampling loops of an Agilent 7890B gas chromatograph (GC) connected in series. One of those sample loops is then injected into a capillary column (Restek Rtx-1, 60 m) that elutes into a Flame-Ionization detector (FID), while the other sampling loop is injected into two consecutive packed-bed columns (HS-Q 80/120, 1x m + 1x 3 m), that elute into a Thermal-Conductivity detector (TCD) for H_2, CO_2, and C_2-C_3 hydrocarbon quantification. Further down that channel, a molecular sieve column separates Ar, CH_4, and CO permanent gases, by means of a second TCD. After sample injection, the GC oven temperature was kept at 35 °C for 10 min, after which the oven was heated to 210 °C (heating ramp 10 °C min^{-1}). Then, the temperature was kept at 210 °C for 45 min. CO, CH_4, and CO_2 were quantified using TCD response factors relative to argon. C_{2+} hydrocarbons and alcohols were quantified in the FID relative to the CH_4 peak which appears in both GC-FID and GC-TCD and has been quantified in the GC-TCD already. A representative chromatogram for the gas-phase analysis is displayed in Figure 78. For analysis of the liquid phase, condensed phases in the reactor after the reaction were collected and centrifuged 13.000 rpm, after which liquid and solif phases are separated. The liquid phase was decanted from the solid phase and injected after filling the collected

sample to 1 mL with tetradecane into an Agilent 7890B GC equipped with a capillary column (Restek Rtx-1, 60 m) and an FID detector.

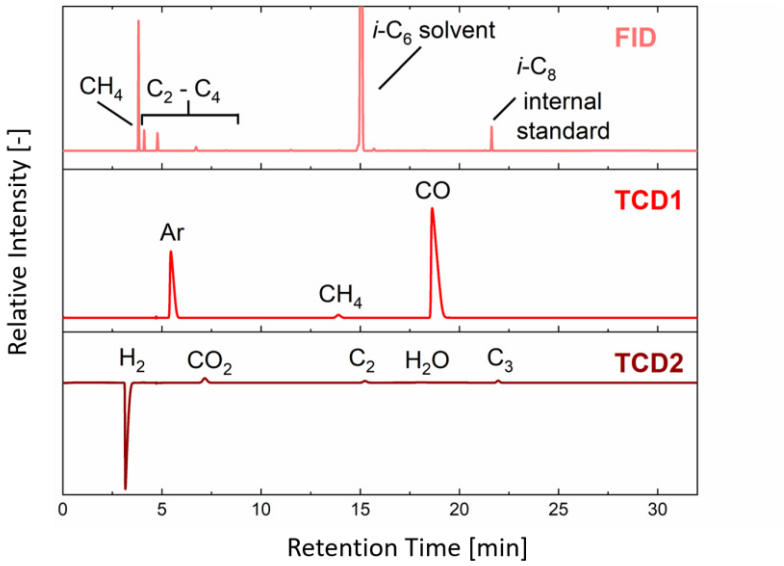

Figure 78: Representative gas phase GC-FID and GC-TCD chromatograms for slurry phase Fischer-Tropsch/hydroformylation experiments.

As temperature program, the GC oven temperature was heated from ambient to 220 °C (heating rate 5 °C min^{-1}), after which the temperature was kept at 220 °C for 50 min. Hydrocarbons and alcohols were quantified based on their FID signal relative to a known *iso*-octane standard which is added prior to the reaction. A representative chromatogram for the liquid phase analysis is displayed in Figure 79.

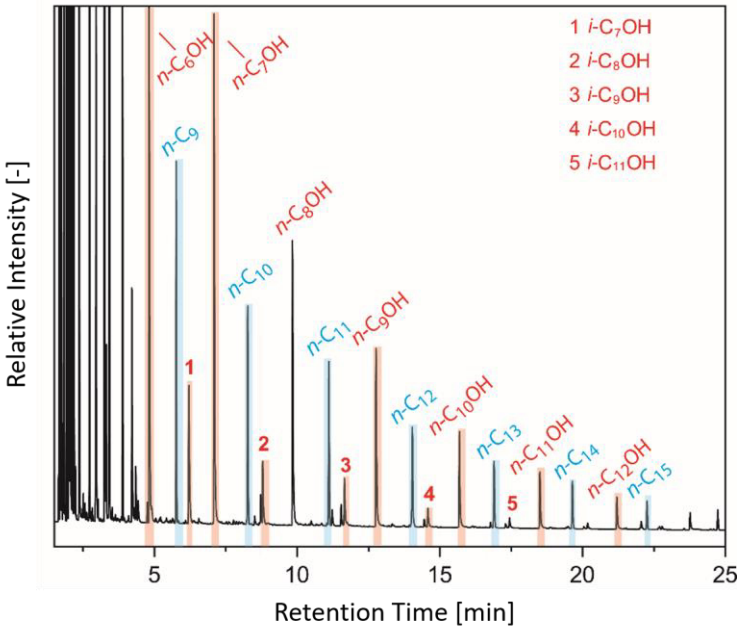

Figure 79: Representative liquid phase GC-FID chromatogram for slurry phase Fischer-Tropsch /hydroformylation experiments.

For selected tests, the liquid product fraction was additionally analyzed by two-dimensional gas chromatography by project partners of the Catalysis Institute and DSI-NRF Centre of Excellence in Catalysis at the University of Cape Town, south Africa. For this, a 2D GCxGC LECO Pegasus 4D chromatograph equipped with a flame ionization detector (FID) and a time-of-flight-mass spectrometer (TOF-MS) using an analysis protocol previously optimized for complex mixtures of hydrocarbons and higher oxygenates was used. The system was operated in reverse phase configuration, where the first dimension is a polar column (Stabilwax) and the second dimension is a non-polar column (Rtx-5). More detailed information about column specifications and temperature program are displayed in Table 9. Data analysis was performed using the TOF Chrom software package. Waxy hydrocarbons in the solid phase have been analyzed *via* thermogravimetric analysis as explained in the following chapter.

Table 9: 2D-GCxGC detailed analysis conditions and column specifications.

2D GCxGC	
Columns:	
1st dimension	Stabilwax (length 30 m, diameter 250 µm, film thickness 0.1 µm)
2nd dimension	Rtx-5, (length 1.39m, diameter 180 µm, film thickness 0.2 µm)
Carrier Gas	He
Injector temperature	250 ˚C
Split ratio	1:100
Temperature program	60 ˚C hold 1 min, 60 ˚C to 240 ˚C at 5 ˚C/min, hold 5 min
2D GC-FID	
Total flow rate	2.1 ml/min
Detector temperature	280 ˚C
2D GC-MS	
Total flow rate	1.1 ml/min
Ionization source temperature	225 ˚C

6.3.3 Thermogravimetric Analysis of Waxy Hydrocarbons in the Solid Phase of Slurry Phase Fischer-Tropsch/Hydroformylation Experiments

For selected experiments, the mass of waxy hydrocarbons in the solid pellet recovered after centrifugation was quantified by thermogravimetric analysis (TGA) in air using corundum crucibles in a Netzsch Jupiter STA 449 C thermo balance and exposing the sample to a heating ramp of 10 K min^{-1} from 298 K to 1023 K. The fraction of the total amount of combusted matter associated to waxy hydrocarbon products was estimated by subtracting contributions from (i) the release of CO ligands from $Co_2(CO)_8$ on the basis of the cobalt carbonyl stoichiometry, the Co/Al stoichiometry in the Fischer-Tropsch catalyst and the total cobalt content in the inorganic residue left behind in the crucible after the TGA experiment as determined by energy-dispersive X-ray analysis (EDS) in a Hitachi S-3500N scanning electron microscope equipped with an EDS detector (Oxford Instruments); and (ii) the combustion of organic ligands from the hydroformylation catalyst as determined based on the total phosphorous content in the ligand and the ligand-to-cobalt stoichiometry in the molecular hydroformylation catalyst. Wax contents determined this way were <2 C% in all cases which is why the ASL-distribution derived from liquid phase hydrocarbons was taken as a more accurate representation of waxy hydrocarbons in most cases.

6.3.4 Nuclear-Magnetic-Resonance Spectroscopy (NMR-spectroscopy)

Several different Nuclear-Magnetic-Resonance spectroscopy methods and spectrometers have been used during this work. They will be listed and explained in the order they appear in the text. In general, chemical shifts (*δ)* are given in ppm relative to tetramethylsilane (TMS) and the literature known chemical shifts of deuterated solvent peaks are used to reference the individual spectra on the TMS scale. Coupling constants are given in Hertz (Hz). $^{13}C\{1H\}$- and ^{13}C-NMR spectra were recorded with 256 scans each (relaxation delay times D_1 = 2 s, pulse sequence = zgpg 30), $^{31}P\{^1H\}$-NMR spectra with 128 scans each (D_1 = 2 s, pulse sequence = zgpg 30) and $^1H\{^{31}P\}$- and ^1H-NMR spectra with eight to sixteen scans each (D_1 = 1 s, pulse sequence = zg30), if not mentioned otherwise. Before integration, all recorded spectra have been processed by a 5th order polynomal baseline correction and the automated phase correction using the program MestReNova®.

6.3.4.1 ^{1}H-NMR Spectroscopy of Isolated Products During the Reductive Hydrofrmylation of 1-Octene

^{1}H-NMR spectroscopy was used to identify isolated substances in unison with GC-MS during the reductive hydroformylation of 1-octene. Spectra were recorded using a AV-400 spectrometer by Bruker. For sample preparation two drops of the sample are dissolved in 0.5 mL deuterated chloroform and transferred into a 1 mL quarts glas NMR tube. Chemical shifts δ in parts per million (ppm) are referenced to the signal (δ = 7.21 ppm) of deuterated Chloroform ($CDCl_3$). Signals received for the different products and substrates are listed in the following (s = singlet, d = duplet, t = triplet, m = multiplet):

1-Octene: ^{1}H-NMR (400 MHz, $CDCl_3$, 298 K): δ = 0.82 (t, 3 H, CH_3), 1.25 (m, 8 H, CH_2), 1.97 (m, 2 H, CH_2), 4.86 (m, 1 H, CH), 4.92 (m, 1 H, CH), 5.75 (m, 1 H, CH) ppm.

4-Octene: ^{1}H-NMR (400 MHz, $CDCl_3$, 298 K): δ = 0.82 (t,6 H, CH_3), 1.29 (q, 4 H, CH_2), 1.88 (q, 4 H, CH_2), 5.32 (t, 2 H, CH), ppm.

2-Octene: ^{1}H-NMR (400 MHz, $CDCl_3$, 298 K): δ = 0.82 (*t*,3 H, CH_3), 1.38 (m, 2 H, CH_2), 1.61 (d, 3 H, CH_3), 1.92 (m, 2 H, CH), 5.38 (m, 2 H, =CH) ppm.

Mixture of *n/iso*-nonanal: ^{1}H-NMR (400 MHz, $CDCl_3$, 298 K): δ = 0.80 (m, 6 H, CH_3), 0.98 (d, 3 H, CH_3), 1.21 (m, 18 H, CH_2), 1.49 (m, 2 H, CH_2), 1.61 (m, 2 H, CH_2), 2.22 (m, 1H, CH), 2.31 (m, 2 H, CH_2), 9.51 (d, 1 H, CH), 9.65 (t, 1 H, CH) ppm.

Mixture of *n/iso*-nonanol: ^{1}H-NMR (400 MHz, $CDCl_3$, 298 K): δ = 0.81 (*t*, 6 H, CH_3), 0.85 (*d*, 3 H, CH_3), 1.25 (*m*, 23 H, CH_2/CH), 1.49 (*m*, 2 H, CH_2), 1.52 (*m*, 2 H, CH_2), 3.39 (*m*, 2H, CH_2), 3.57 (*t*, 2 H, CH_2) ppm

6.3.4.2 ^{13}C- and ^{103}Rh-NMR Spectroscopy of ^{13}C Enriched Catalyst/Reaction Solutions for the Identification of Catalytic Species in the Reductive Hydroformylation using Rh/Trialkyl Amine Catalysts

During the investigation of catalytic species in the reductive hydroformylation of 1-octene using rhodium in combination with trialkylamines, several anionic rhodium species have been identified by a combination of ^{13}C- and ^{103}Rh-NMR spectroscopy. ^{13}C-NMR spectra of a 40 mol% ^{13}CO enriched catalyst solution (40 mg [Rh(acac)$(CO)_2$] in 0.33 mL NE_{t3} and 0.66 mL d_3-acetonitrile) were recorded using a 500 MHz cryo spectrometer by Bruker. Prior to the measurements, the catalyst solution was heated to 100 °C under a synthesis gas atmosphere of 30 bar CO:H_2 1:2 (40 mol% ^{13}CO) for one hour following the standard procedure described in chapter 6.2.1. After cooling down to RT, 0.5 mL of the reaction solution was taken from the reaction liquour under argon stream and transferred into a young tube under inert gas atmosphere. ^{13}C-NMR spectra of the sample have been measured at different temperatures. The ^{13}C-NMR spectrum at 0 °C is shown in Figure 80. ^{13}C-NMR spectra of the carbonyl region measured at different temperature ranging from –40 °C up to 25 °C can be found in the appendix Figure A 1.

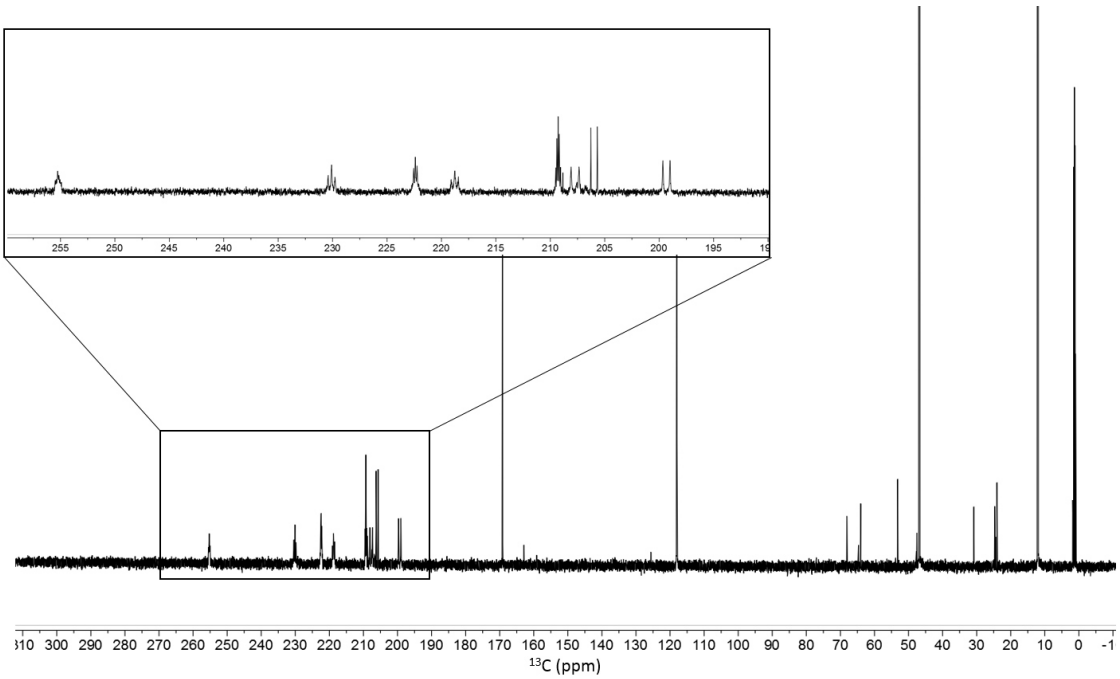

Figure 80: Full ^{13}C-NMR (126 MHz, d_3-acetonitrile, 21 °C) spectrum of the ^{13}CO enriched catalyst solution (40 mg [Rh(acac)$(CO)_2$] in 0.33 mL NE_{t3} and 0.66 mL d_3-acetonitrile) measured at 0 °C.

For further characterization the anionic rhodium species identified in the concentrated catalyst solution, ^{13}C-^{103}Rh-HMBC-NMR spectra (pulse sequence: hmbcgpnfqf) were acquired at –30 °C using a Bruker 500 MHz cryo spectrometer equipped with a TBI probe (^{1}H, ^{13}C, X(^{31}P-^{109}Ag) with Z-gradient. It was able to tune the X-channel below its specification to measrue the ^{103}Rh

nucleus. The ^{103}Rh chemical shifts have been referenced to the relative ^{1}H frequency with *(^{103}Rh) = 3.16* MHz. The ^{103}Rh π/2 pulse lengh was 90 µs. The magnetization transfer from ^{13}C to ^{103}Rh was optimized for an average coupling constant J_{CRh} of 60 Hz. Due to the long ^{103}Rh pulse length and the high chemical shift range, HMBC spectra with different offsets were acquired in order to find all ^{103}Rh signals (see Figure 29).

6.3.4.3 ^{1}H-NMR of Rhodium Hydride Species under Reaction Conditions in the Rhodium/Trialkyl Amine Catalyzed Reductive Hydroformylation of 1-Octene

It has not been possible to characterize and identify rhodium hydride species at room temperature and/or elevated pressures or synthesis gas atmosphere (3 bar). To record ^{1}H-NMR spectra under reaction conditions, a sealed sapphire glass-tube, able to withstand pressures up to 200 bars, was used for the characterization of rhodium hydride species under reaction conditions. The high pressure tube used during these experiments has been described in detail by ROE.[200] Spectra have been recorded using a Bruker Ascend 300 MHz wide-bore spectrometer. For the identification of hydride species, a catalyst solution consisting of 10 mg [Rh(acac)(CO)$_2$] dissolved in 0.06-0.07 g of the applied amine and 0.13 g d_3-acetonitrile is weighed directly into the sapphire NMR-tube. To support the mixing of all components the catalyst solution was cautiously mixed using a syringe. Afterwards the tube is sealed, purged with H_2 at least three times and pressurized to 30 bars CO:H_2 at a ratio of 1:2. Before the start of collecting data, the catalyst solution is heated in the NMR to 80 °C for at least 20 minutes in order to allow dissolvation of gaseous components. The dissolvation can be followed by the H_2 peak in the ^{1}H-NMR spectrum. After 20 minutes, the sample is heated to 100 °C. After another 15 minutes the first spectra is taken. Consecutively, the temperature was lowered stepwise and samples are taken every 10 °C. Before every new measurement a 15 minute time frame for equilibration of resting states was held.

6.3.4.4 Quantitative ^{1}H-NMR Spectroscopy (*q*NMR) for the Determination of Liquid Phase Compositions of the Extract during Catalyst Recycling Experiments (chapter 4.2)

Quantitative ^{1}H-NMR was used to analyze the composition of the extract during the recycling experiments in chapter 4.2. Determination of PEG-amine leaching was necessary which is not possible using the GC procedures applied during previous experiments.

For quantitative NMR (*q*NMR) analysis, a defined amount of sample together with a defined amount of mesitylene as internal standard are dissolved in deuterated chloroform ($CDCl_3$) and measured on a 400 MHz *Acend 400* spectrometer by Bruker. To allow complete relaxation of all spins before each pulse, relaxation time delays of 20 s (D1 = 20 s) have been used. Based on the number of protons of an isolated functional group (no overlap with other ^{1}H-NMR signals) which can be assigned to a specific analyte and comparison with the signal of the internal standard (mesitylene), the amount of analyte is calculated. In Table 10 the functional group and its chemical shift in the ^{1}H-NMR used for quantification is given for each analyte.

Table 10: List of signals used to quantify analytes in *q*NMR measurements during catalyst recycling experiments in the reductive hydroformylation of 1-pentene using rhodium/trialkylamine catalysts. [a] n-Hexanol CH_2 overlaps with ether CH_2 groups of the PEG-phase. If the Integral of the signal used to quantify the respective PEG phase is less than 1% compared to the signal at δ = 3.55 this can be ignored. Otherwise, ether CH_2 contribution of the PEG phase has to be determined and substracted from the integral at δ = 3.55. [b] Pentane was not found in the extract during any recycling run because of its evaporation during the extraction process. If leftover Pentane is present it can be identified by its CH_3 Signal at δ = 0.78, even though integration is not reliably possible because of its overlap with alcohol and aldehyde CH_3 signals at δ = 0.84.

Analyte	*q*NMR Functional Group	Chemical Shift δ [ppm]
n-Hexanal	C<u>H</u>O (1H, triplet)	9.70
iso-Hexanal	C<u>H</u>O (1H, duplet)	9.55
n-Hexanol	C<u>H</u>$_2$ (2H, triplet)[a]	3.55
iso-Hexanol	C<u>H</u>$_2$ (2H, duplet of multiplet)	3.37
PEG_{600}-diamine	2 x C<u>H</u>$_2$ (4H, duplet)	2.89, 2.93
PEG_{300}-amine mixture	2 x C<u>H</u>$_2$ (4H, triplet)	2.42
Pentene/Pentene-isomers	C<u>H</u> (1H, multiplet)	5.40-5.47
Pentane	C<u>H</u>$_3$ (3H, triplet distortet)[b]	0.78

The standard deviation of the *q*-NMR measurements was determined to be ≤1.5% within the concentration range of reaction product analytes. For all *q*NMR spectra the difference between the calculated total mass based on the *q*NMR analysis and the amount of extract received during the recycling process was determined to be above 10 w%. Therefore, calculated group contributions as determined by *q*NMR has been adjusted to fit the experimentally determined mass of the extract. All measurements were performed at room temperature. An example with assignment of all occurring species for the *q*NMR taken from the extract during a recycling experiment using the PEG_{300}-amine mixture as stationary phase is shown in Figure 81.

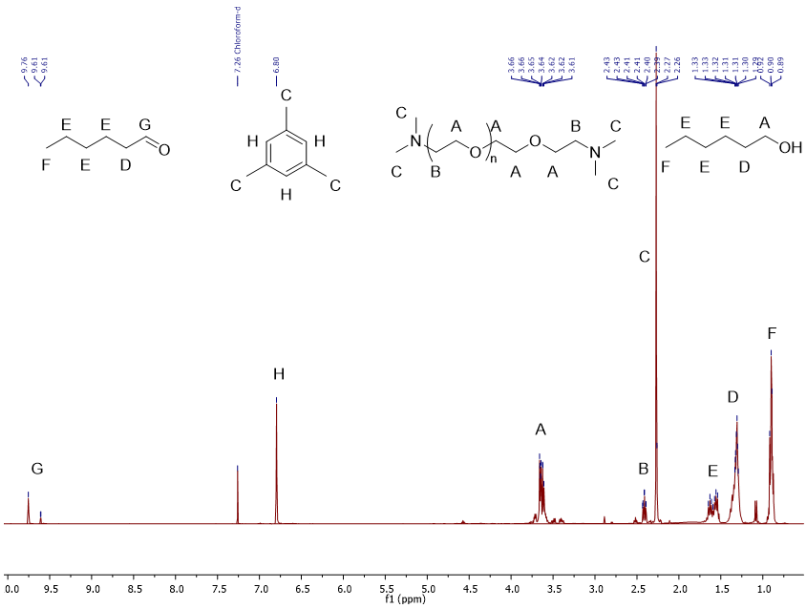

Figure 81: Example of an ^{1}H-*q*NMR (400 MHz, $CDCl_3$, 21 °C) spectrum of the second recycling run in the recycling experiments using a PEG_{300}-amine mixture as stationary phase. For simplification reasons it is not distinguished between *n*- and *iso*-products.

6.3.4.5 ^{1}H- and ^{31}P-NMR Spectroscopy for the Identification of Catalytic Cobalt Species in the Fischer-Tropsch/Hydroformylation Tandem Approach

The structure of the molecular cobalt reductive hydroformylation catalyst during the reductive hydroformylation of 1-octene and in the tandem Fischer-Tropsch/hydroformylation approach was assessed by combining ^{1}H{^{31}P} and ^{31}P{^{1}H}-NMR spectroscopy. For this, between 50 mg and 300 mg of the post reaction solution has been transferred under inert gas atmosphere to a NMR young-tube and diluted with 200 mg to 500 mg of deuterated chloroform ($CDCl_3$). Spectra have been measured using a 500 MHz *Avance III* NMR spectrometer by Bruker at 21 °C. ^{1}H{^{31}P}-NMR spectra have been collected with at least 128 scans each, to identify hydride signals of catalytic species in low concentrations.

6.3.5 *In Situ* FTIR-Spectroscopy

FTIR-measurements were performed using a Bruker Vertex 70v device with a 250 μm diamond cuvette. During the reaction, the 10 mL autoclave reactor was connected to an IR-device with a sample loop as depictet in Figure 82. Via the sample loop, the reaction solution is continuously pumped through the sample loop the FTIR-cuvette with a constant flow of 2 ml min^{-1}.

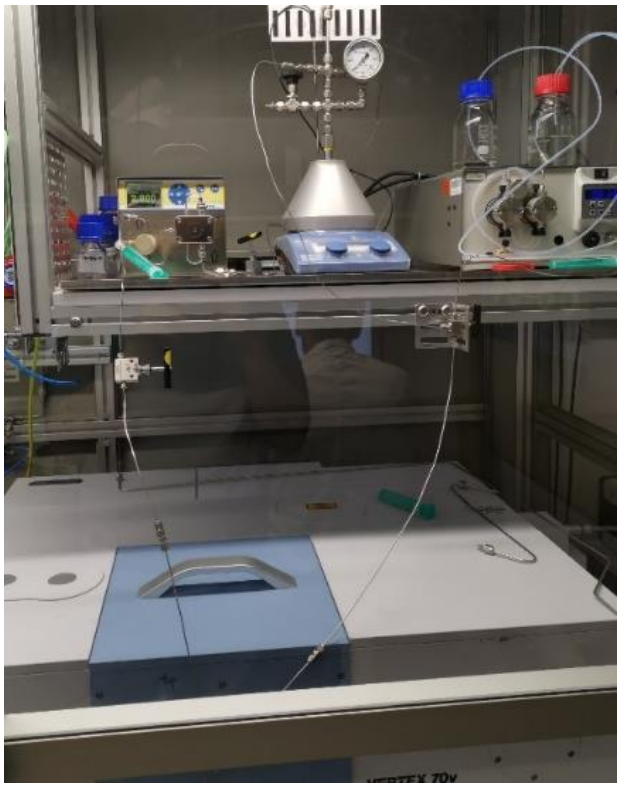

Figure 82: FTIR-setup (Bruker Vertex 70v) for *in situ* monitoring of catalyst solutions unde reaction conditions.

Before conducting the reaction for the FTIR measurement of rhodium species, the reactor was filled with 3.2 g of acetonitrile and heated to the reaction temperature of 60 °C. Upon reaching the reaction temperature, the pump for the sample loop was started and a background spectrum of acetonitrile was measured. The reactor was cooled for few minutes before 0.04 g of $[Rh(acac)(CO)_2]$ was added. Afterwards the Reactor was flushed with argon and heated to the reaction temperature of 60 °C again. At reaching the reaction temperature of 60 °C the pump for the sample loop was started and FTIR-spectra were measured every two minutes, taking 20 scans for each spectrum. Ten minutes after starting recording of the spectra, 15 bar H_2 and 9 bar CO were added. Another 14 minutes into the recording 1.4 g trimethylamine was added *via* a syringe pump connected to the reactor. Finally, 0.4 mL of 1-octene have been added *via* the syringe pump 46 minutes into the recording. Te resulting spectra are depicted in Figure 35.

6.3.6 Inductively-Coupled-Plasma Mass-Spectrometry (ICP-MS)

Metal contents in selected reaction liquors and in the extract solutions for catalyst recycling experiments (chapter 4.2.4) were determined by inductively-coupled-plasma mass spectrometry (ICP-MS). In general, samples have been prepared according to the following procedure: Organic material in the sample was digested by solving 10 mg of sample in 8 mL concentrated HNO_3 and heating in a microwave oven (CEM, Mars 6) up to 200 °C (1500 W, temperature ramp of 30 minutes from RT). At 200 °C the temperature was held for 15 minutes. After cooling, the sample was filled up to 100 mL with H_2O.

Following digestion of organic compounds, samples are ready for injection into the ICP-MS. The sample was injected to the ICP (ICPMS-2030, Shimadzu) and measured at least two times. Before each measurement, commercially available calibration standards (Carl Roth) for the target metal analyte (cobalt or rhodium), in the expected concentration range, where injected according to the same procedure in order to derive calibration curves. After measuring, metal concentrations in the organic reaction liquor have been determined by comparing the average of all measurements with the pre-measured calibration curve.

Metal contents for the recycling experiments using the PEG_{600}-diamine (chapter 4.2.4) instead have been measured at the Kolbe Microanalytical Laboratory in 46047 Oberhausen, Germany.

6.3.7 Hg Intrusion Porosimetry

Mercury intrusion porosimetry experiments have been conducted by project partners Kai Jeske and Gonzalo Prieto. Mercury intrusion porosimetry experiments were performed in a Micromeritics AutoPore IV 951 apparatus. 80-150 mg of the solid sample (0.08-0.10 mm sieve fraction) were dried at 110 °C for 72 hours before the measurement. The intrusion-extrusion isotherms were recorded at room temperature in the pressure range of $6.9 \cdot 10^4$-$4.1 \cdot 10^4$ Pa with an equilibration rate of 0.1 µL g^{-1} s^{-1}. For the determination of pore diameter and volume, a geometrical pore model was considered, with a Hg density of 13.55 g cm^{-3} and a contact angle of 141 degree.

6.3.8 Energy-Dispersive-X-ray Spectroscopy (EDS)

Energy-Dispersive-X-ray spectroscopy (EDS) experiments have been conducted by project partners Kai Jeske and Gonzalo Prieto. In order to quantify bulk promoter contents in promoted Fischer-Tropsch catalyst samples, energy-dispersive X-ray spectroscopy (EDS) was performed on a Hitachi S-3500N scanning electron microscope. The powder sample was ground and then applied onto a pin-stub SEM mount coated with double-adhesive-face conductive carbon-tab. EDS spectra of areas of 1 mm^2 were scanned using an Oxford Pentafet 10 mm^2 detector to make sure a statistically relevant number of catalyst particles was jointly analyzed.

6.3.9 Tomographic Focused-Ion-Beam Scanning-Electron-Microscopy (FIB-SEM)

Focused-Ion-Beam Scanning-Electron-Microscopy (FIB-SEM) experiments have been conducted by project partners Kai Jeske and Gonzalo Prieto. For this, catalyst microparticles (80-100 µm) were embedded in a low-viscosity epoxy resin and the resin cured at 70 °C for 12 hours. The resin-embedded sample block was then trimmed and polished in an ultramicrotome (Reichert Ultracut) using first a glass knife followed by a fine trimming with a diamond knife (Diatome). The trimmed specimen was mounted on a SEM stub with conductive colloidal graphite adhesive. The stub-mounted sample was sputter-coated with a ca. 20 nm carbon overlay using a LEICA EM MED020 spatter coater. Focused Ion Beam-Scanning Electron Microscopy (FIB-SEM) experiments were performed in a Zeiss Auriga Compact dual-beam microscope. First, a protective platinum layer was deposited on the region of interest (ROI) using the gas injection system. Then, the Ga^+ ion gun, operated at an intensity of 10 nA, was used to mill a front and two lateral trenches, delimiting the volume to be imaged, as well as a cross fiducial marker on the top surface of the ROI to be used for automated image recognition and drift correction during the slice-and-image procedure. Serial sectioning combined with SEM imaging was carried out with specimen drift and beam shift corrections. Slices with nominal thickness of 60 nm were milled off using the Ga^+ FIB gun operated at an intensity of 3 nA. The corresponding SEM micrographs of the consecutively exposed cross-sections were recorded with a secondary electron detector while the electron gun was operated at a voltage of 2 kV.

The stack of raw micrographs was corrected for the foreshortening caused by the tilt angle between the specimen cross-section and the SEM detector (54° in the dual beam microscope employed in this study). Next, a stack de-flicking filter was applied to correct inter-micrograph gray-value gradients within the stack of images. After stack alignment using an iterative cross-correlation algorithm, the reconstructed tomograms were segmented using a watershed algorithm followed by fine adjustment of the automatically recognized volumes *via* controlled erosion-dilation functions. After tomogram binarization, a 3D local Euclidean distance transform

was propagated along the three-dimensional skeleton of the solid alumina phase to quantify the shortest distances from any point within the mesoporous alumina domains to the nearest boundary to the macropore network in Avizo (Thermo Fischer Scientific). There, so-derived euclidean mesopore transport distances were corrected for a pore tortuosity (τ) factor estimated using the formula below:

$$\tau = \frac{\varepsilon}{1 - (1 - \varepsilon)^{2/3}}$$

Whereas ε is the void fraction of the material's mesoporosity derived from the mesopore volume using the formula below:

$$\varepsilon = \frac{1}{1 + \frac{1}{\rho \cdot PV_{meso}}}$$

In this formula, ρ is the materials skeletal density and PV_{meso} the mesopore volume as determined by Hg intrusion porosimetry.

6.4 List of Chemicals

Name/Formula	CAS No.	Supplier	Purity
Acetone HPLC grade	67-64-1	Sigma Aldrich	>99.9%
Acetonitrile	75-05-8	Carl Roth	>99.5%
Acetylacetonato dicarbonyl rhodium (I)	14874-82-9	abcr GmbH	99%
Benzene ruthenium (II) dichloride dimer	37366-09-9	abcr GmbH	97%
Bicyclo[2.2.2]hepta-2,5-dien-rhodium(I)-chlorid dimer	12257-42-0	Sigma Aldrich	96%
Bis(1,5-cyclooctadiene)rhodium(I) hexafluoroantimonate	130296-28-5	Sigma Aldrich	97%
Bis(triphenylphosphoranylidene)ammonium chloride (PNP^+Cl^-)	21050-13-5	abcr GmbH	97%
1-Butanol	71-36-3	abcr GmbH	99.9%
Carbon dioxide (liquid)	124-38-9	Westfalen Gas	>99.99%
Carbon disulfide	75-15-0	Sigma Aldrich	>99.9%
Carbon monoxide (gas)	630-08-0	Air Liquide	>99.99%
Chlorobis(ethylene)rhodium (I) dimer	12081-16-2	TCI Germany	>95%
Chloroform (deuterated)	865-49-6	Sigma Aldrich	99.8%
^{13}C-Labeled carbon monoxide	1641-69-6	Sigma Aldrich	>99%
Cobalt(II)nitrat-hexahydrat	10026-22-9	Sigma Aldrich	>98%
Cyclooctadiene rhodium chloride dimer	12092-47-6	Sigma Aldrich	98%
Di(µ-chloro)dichlorobis(p-cymene)diruthenium	52462-29-0	Sigma Aldrich	97%
Dichloromethane	75-09-02	Carl Roth	>99.5%
Di-μ-chloro-tetracarbonyldirhodium(I)	14523-22-9	Acros Organics	97%
Dicobalt octacarbonyl	10210-68-1	Acros Organics	95%
4,4-Diethoxy-N,N-dimethyl-1-butanamine	1116-77-4	TCI Germany	>98%
Diethylmethylamine	616-39-7	TCI Germany	98%
Diethylene glycol dibutyl ether	112-73-2	TCI Germany	>98%
Diethylene glycol hexyl ether	112-59-4	TCI Germany	>98%
Diethylene glycol monobutyl ether	112-34-5	TCI Germany	>99%
Diethylene glycol monobutyl ether acetate	124-17-4	TCI Germany	>98%
Diethylamine	109-89-7	Sigma Aldrich	>99.5%
Dihydrogen (gas)	1333-74-0	Air Liquide	>99.99%
N,N-Diisopropylaniline	4107-98-6	abcr GmbH	97%
N,N-Dimethylaniline	121-69-7	abcr GmbH	99%
N,N-Dimethyl benzyl amine	103-83-3	abcr GmbH	98%
N,N-Dimethyldecanamide	14433-76-2	abcr GmbH	98%
N,N-Dimethyl hexadecyl amine	112-69-6	TCI Germany	>98%
Dimethyl phthalate	131-11-3	TCI Germany	>99%
4-(Dimethylamino)-1-butanol	13330-96-6	Sigma Aldrich	>97%
2-[2-(Dimethylamino)ethoxy]ethanol	1704-62-7	Sigma Aldrich	98%
Dimethylammonium-dimethylcarbamate	4137-10-4	Acros Organics	n.d.
N,N-Dimethylaniline	121-69-7	abcr GmbH	99%
Dimethyl sulfoxide (Sulfolane)	67-68-5	Carl Roth	>99.8%
Ethylcinnamate	4192-77-2	TCI Germany	>99%
n-Hexane	110-54-3	Carl Roth	>99%
1-Hexanol	111-27-3	Acros Organics	98%
Isopropylalcohol (Isopropanol)	67-63-0	Carl Roth	>99.9%
Mesitylene	108-67-8	abcr GmbH	98%
Methyldiethylamine	4097-88-5	TCI Germany	>98%

Name/Formula	CAS No.	Supplier	Purity
N-Methyldiphenylamine	552-82-9	TCI Germany	>98%
2-Methyl butane (*iso*-pentane)	78-78-4	Supelco	99.8%
2-Methylheptane	592-27-8	Acros Organics	99%
2-Methylpentane (*iso*-hexane)	107-83-5	Sigma Aldrich	>99%
Methyltriphenylphosphonium Bromide ($PPh_3Me^+Br^-$)	1779-49-3	TCI Germany	98%
Nitric Acid	7697-37-2	Baker	>99%
n-Octane	111-65-9	Carl Roth	>99%
1-Octene	111-66-0	Acros Organics	>99%
PEG_{300}	25322-68-3	Sigma Aldrich	n.d.
PEG_{600}-diacid	39927-08-7	Merck Milipore	>95%
1-Pentene	109-67-1	Alfa Aesar	97%
2-Phenoxyethanol	122-99-6	Sigma Aldrich	>99%
3-Phenylpropyl isobutyrate	103-58-2	TCI Germany	98%
Praesodym nitrate hexahydrate	15878-77-0	Sigma Aldrich	99.9%
Propylenecarbonate	108-32-7	Sigma Aldrich	99.7%
Quinuclidine	100-76-5	TCI Germany	>96%
Rhodium (III) chloride hydrate	20765-98-4	abcr GmbH	n.d.
Ruthenium (III) nitrosyl nitrate	34513-98-9	Sigma Aldrich	n.d.
SiC granules 46 grit	409-21-2	Alfa Aesar	n.d.
Sodium Nitrate	7631-99-4	Sigma Aldrich	>99%
SulfoXantphos	215792-51-1	Otto-von-Guericke-University	>95%
Tetradecane	629-59-4	abcr GmbH	99%
Tetraethylammonium chloride ($NEt_4^+Cl^-$)	56-34-8	TCI Germany	98%
Tetraethyleneglycol (TetraEG)	112-60-7	TCI Germany	95%
Tetraethyleneglycol dimethyl ether	143-24-8	TCI Germany	>98%
N,N,N´,N´-tetramethyl-1,4-butanediamine	111-51-3	TCI Germany	>98%
N,N,N´,N´-Tetramethyl ethylene diamine	110-18-9	abcr GmbH	99%
N,N,N´,N´-Tetramethyl-1,3-phenylenediamine	22440-93-3	Sigma Aldrich	97%
Toluene	108-88-3	Carl Roth	>99.8%
Tricyclohexylphosphine	2622-14-2	Acros Organics	97%
Triethylamine	121-44-8	Sigma Aldrich	>99%
Triethyleneglycol (TEG)	112-27-06	Acros Organics	99%
Triethylene Glycol Diacetate	111-21-7	TCI Germany	>98%
Triethylene glycol monobutyl ether	143-22-6	TCI Germany	>98%
Triethylene glycol monomethyl ether	112-35-6	TCI Germany	>98%
Triisobutylamin	1116-40-1	TCI Germany	>98%
Trimethylamine (solution 12% in Acetonitrile)	75-50-3	TCI Germany	n.d.
N,N,N´-Trimethyldiaminoethane	142-25-6	abcr GmbH	98%
Tri-*n*-butylphosphine	998-40-3	abcr GmbH	99%
Triphenylphosphine	603-35-0	Alfa Aesar	99%
Triphenylphosphine, polymer bound	39319-11-4	Sigma Aldrich	n.d.
Tripropylene glycol (TPG)	24800-44-0	Acros Organics	99%
Tripropylene glycol mono butyl ether	55934-93-5	Sigma Aldrich	>95%

7 References

1 M. J. Menne, C. N. Williams, B. E. Gleason, J. J. Rennie and J. H. Lawrimore, *J. Clim.*, 2018, **31**, 9835–9854.

2 NOAA, *State of the Climate: Monthly Global Climate Report for Annual 2021*, 2022.

3 Y. K. Dwivedi, L. Hughes, A. K. Kar, A. M. Baabdullah, P. Grover, R. Abbas, D. Andreini, I. Abumoghli, Y. Barlette, D. Bunker, L. Chandra Kruse, I. Constantiou, R. M. Davison, R. De', R. Dubey, H. Fenby-Taylor, B. Gupta, W. He, M. Kodama, M. Mäntymäki, B. Metri, K. Michael, J. Olaisen, N. Panteli, S. Pekkola, R. Nishant, R. Raman, N. P. Rana, F. Rowe, S. Sarker, B. Scholtz, M. Sein, J. D. Shah, T. S. H. Teo, M. K. Tiwari, M. T. Vendelø and M. Wade, *Int. J. Inf. Manage.*, 2022, **63**, 102456.

4 Atmospheric Carbon Dioxide (CO_2) levels, 1800–present, https://sealevel.info/co2.html, (accessed 12 April 2022).

5 NASA, Global Temperature, https://climate.nasa.gov/vital-signs/global-temperature/, (accessed 12 April 2022).

6 H. Ritchie, Sector by sector: where do global greenhouse gas emissions come from?, https://ourworldindata.org/ghg-emissions-by-sector, (accessed 12 April 2022).

7 K. Handayani, Y. Krozer and T. Filatova, *Energy Policy*, 2019, **127**, 134–146.

8 W. Leitner, J. Klankermayer, S. Pischinger, H. Pitsch and K. Kohse-Höinghaus, *Angew. Chem. Int. Ed.*, 2017, **56**, 5412–5452.

9 B. Ekwurzel, J. Boneham, M. W. Dalton, R. Heede, R. J. Mera, M. R. Allen and P. C. Frumhoff, *Clim. Change*, 2017, **144**, 579–590.

10 D. Gielen, F. Boshell, D. Saygin, M. D. Bazilian, N. Wagner and R. Gorini, *Energy Strategy Rev.*, 2019, **24**, 38–50.

11 European Comission, *Electrification of the Transport System, Studies and Reports*, Bruessels, 2017.

12 European Environment Agency, New registrations of electric vehicles in Europe, https://www.eea.europa.eu/ims/new-registrations-of-electric-vehicles, (accessed 12 April 2022).

13 Z. Navas-Anguita, D. García-Gusano and D. Iribarren, *Renew. Sustainable Energy Rev.*, 2019, **112**, 11–26.

14 R. Schäppi, D. Rutz, F. Dähler, A. Muroyama, P. Haueter, J. Lilliestam, A. Patt, P. Furler and A. Steinfeld, *Nature*, 2022, **601**, 63–68.

15 B. Rego de Vasconcelos and J.-M. Lavoie, *Front. Chem.*, 2019, **7**, 1–24.

16 V. Dieterich, A. Buttler, A. Hanel, H. Spliethoff and S. Fendt, *Energy Environ. Sci.*, 2020, **13**, 3207–3252.

17 R. Daiyan, I. MacGill and R. Amal, *ACS Energy Lett.*, 2020, **5**, 3843–3847.

18 H. Gruber, P. Groß, R. Rauch, A. Reichhold, R. Zweiler, C. Aichernig, S. Müller, N. Ataimisch and H. Hofbauer, *Biomass Convers. Biorefin.*, 2021, **11**, 2281–2292.

19 J. Hu, F. Yu and Y. Lu, *Catalysts*, 2012, **2**, 303–326.

20 D. Neumann, S. Pischinger, M. Zubel, B. Heuser, K. Thenert, W. Leitner, M. Schönen, J. Schaub and C. Jörg in *39. Internationales Wiener Motorensymposium 26.-27. April 2018,* eds. B. Geringer and H. P. Lenz, VDI Verlag, 2018, p. 230.

21 B. Rajesh Kumar and S. Saravanan, *Renew. Sustainable Energy Rev.*, 2016, **60**, 84–115.

22 L. Cai, Y. Uygun, C. Togbé, H. Pitsch, H. Olivier, P. Dagaut and S. M. Sarathy, *Proc. Combust. Inst.*, 2015, **35**, 419–427.

23 B. Kerschgens, L. Cai, H. Pitsch, B. Heuser and S. Pischinger, *Combust. Flame*, 2016, **163**, 66–78.

24 B. Heuser, A. Vorholt, G. Prieto, B. Graziano, S. Schönfeld, M. Messagie, G. Cardellini, S. Tuomi, N. Sittinger and R. Hermanns, in *Transport Research Arena 2020*, Helsinki, Finland, 2020.

25 S. Püschel, S. Störtte, J. Topphoff, A. J. Vorholt and W. Leitner, *ChemSusChem*, 2021, **14**, 5226–5234.

26 A. Behr and P. Neubert, *Applied Homogeneous Catalysis*, Wiley-VCH, 1st edn., 2012.

27 M.-R. Kula, *Enzyme Catalysis in Organic Synthesis*, Wiley, 2nd edn., 2002.

28 W. Ostwald, *Phys. Z.*, 1902, **3**, 313–322.

29 A. Behr, D. Agar and J. Jakob, *Einführung in die technische Chemie*, Spektrum Verlag, 2011.

30 S. Kozuch and J. M. L. Martin, *ACS Catal.*, 2012, **2**, 2787–2794.

31 X. Hu and A. C. K. Yip, *Front. Catal.*, 2021, **1**, 1–3.

32 A. Lazzarini, R. Colaiezzi, F. Gabriele and M. Crucianelli, *Materials*, 2021, **14**, 6796.

33 N. Duyckaerts, M. Bartsch, I.-T. Trotuş, N. Pfänder, A. Lorke, F. Schüth and G. Prieto, *Angew. Chem. Int. Ed.*, 2017, **129**, 11638–11642.

34 Y. G. Shelke, A. Yashmeen, A. V. A. Gholap, S. J. Gharpure and A. R. Kapdi, *Chem. Asian J.*, 2018, **13**, 2991–3013.

35 T. Rösler, T. A. Faßbach, M. Schrimpf, A. J. Vorholt and W. Leitner, *Ind. Eng. Chem. Res.*, 2019, **58**, 2421–2436.

36 D. J. Cole-Hamilton, *Science*, 2003, **299**, 1702–1706.

37 M. Janssen, C. Müller and D. Vogt, *Green Chem.*, 2011, **13**, 2247.

38 I. Vural Gürsel, T. Noël, Q. Wang and V. Hessel, *Green Chem.*, 2015, **17**, 2012–2026.

39 M. J. Muldoon, *Dalton Trans.*, 2010, **39**, 337–348.

40 W. Keim, *Green Chem.*, 2003, **5**, 105–111.

41 J. Bianga, K. U. Künnemann, T. Gaide, A. J. Vorholt, T. Seidensticker, J. M. Dreimann and D. Vogt, *Chem. – A Eur. J.*, 2019, **25**, 11586–11608.

42 V. S. Shende, V. B. Saptal and B. M. Bhanage, *Chem. Rec.*, 2019, **19**, 2022–2043.

43 B. M. L. Dioos, I. F. J. Vankelecom and P. A. Jacobs, *Adv. Synth. Catal.*, 2006, **348**, 1413–1446.

44 K. Zhao, X. Wang, D. He, H. Wang, B. Qian and F. Shi, *Cata. Sci. Technol.*, 2022, **12**, 4962–4982.

45 C. P. Mehnert, R. A. Cook, N. C. Dispenziere and M. Afeworki, *J. Am. Chem. Soc.*, 2002, **124**, 12932–12933.

46 E. Janssen, A. Bösmann, G. Francio, M. Solinas, W. Leitner and P. Wasserscheid, *Angew. Chem. Int. Ed.*, 2001, **2**, 2697–2699.

47 G. Franciò, U. Hintermair and W. Leitner, *Philos. Trans. R. Soc. London, Ser. A*, 2015,

373, 20150005.

48 F. Zaera, *Coord. Chem. Rev.*, 2021, **448**, 214179.

49 S. Hübner, J. G. de Vries and V. Farina, *Adv. Synth. Catal.*, 2016, **358**, 3–25.

50 W. Keim, *Angew. Chem. Int. Ed.*, 2013, **52**, 12492–12496.

51 P. Kuhn, D. Sémeril, D. Matt, M. J. Chetcuti and P. Lutz, *Dalton Trans.*, 2007, 515–528.

52 C. W. Kohlpaintner, R. W. Fischer and B. Cornils, *Appl. Catal. A*, 2001, **221**, 219–225.

53 G. La Sorella, G. Strukul and A. Scarso, *Green Chem.*, 2015, **17**, 644–683.

54 M. Ferreira, B. Le and H. Bricout, *ACS Sustainable Chem. Eng.*, 2017, **5**, 3598–3606.

55 E. Monflier, E. Blouet, Y. Barbaux and A. Mortreux, *Angew. Chem. Int. Ed.*, 1994, **33**, 2100–2102.

56 E. Monflier, G. Fremy, Y. Castanet and A. Mortreux, *Angew. Chem. Int. Ed.*, 1995, **34**, 2269–2271.

57 E. Monflier, S. Tilloy, G. Fremy, Y. Castanet and A. Mortreux, *Tetrahedron Lett.*, 1995, **36**, 9481–9484.

58 Y. Brunsch and A. Behr, *Angew. Chem. Int. Ed.*, 2013, **52**, 1586–1589.

59 M. Terhorst, C. Heider, A. Vorholt, D. Vogt and T. Seidensticker, *ACS Sustainable Chem. Eng.*, 2020, **8**, 9962–9967.

60 W. Leitner, *Acc. Chem. Res.*, 2002, **35**, 746–756.

61 U. Hintermair, G. Franciò and W. Leitner, *Chem. Commun.*, 2011, **47**, 3691.

62 G. L. Zabot, in *Green Sustainable Process for Chemical and Environmental Engineering and Science*, eds. Inamuddin, A. M. Asiri and A. M. Isloor, Elsevier, 2020, pp. 255–278.

63 J. M. del Valle, *J. Supercrit. Fluids*, 2015, **96**, 180–199.

64 G. B. Jacobson, C. T. Lee, K. P. Johnston and W. Tumas, *J. Am. Chem. Soc.*, 1999, **121**, 11902–11903.

65 K. Burgemeister, G. Franciò, V. H. Gego, L. Greiner, H. Hugl and W. Leitner, *Chem. Eur. J.*, 2007, **13**, 2798–2804.

66 D. J. Heldebrant and P. G. Jessop, *J. Am. Chem. Soc.*, 2003, **125**, 5600–5601.

67 D. J. Heldebrant, H. N. Witt, S. M. Walsh, T. Ellis, J. Rauscher and P. G. Jessop, *Green Chem.*, 2006, **8**, 807.

68 R. A. Brown, P. Pollet, E. McKoon, C. A. Eckert, C. L. Liotta and P. G. Jessop, *J. Am. Chem. Soc.*, 2001, **123**, 1254–1255.

69 M. Schmitkamp, D. Chen, W. Leitner, J. Klankermayer and G. Franciò, *Chem. Commun.*, 2007, 4012.

70 U. Hintermair, T. Höfener, T. Pullmann, G. Franciò and W. Leitner, *ChemCatChem*, 2010, **2**, 150–154.

71 J. Theuerkauf, G. Franciò and W. Leitner, *Adv. Synth. Catal.*, 2013, **355**, 209–219.

72 U. Hintermair, G. Franciò and W. Leitner, *Chem. Eur. J.*, 2013, **19**, 4538–4547.

73 Z. Hou, B. Han, L. Gao, T. Jiang, Z. Liu, Y. Chang, X. Zhang and J. He, *Nouv. J. Chim.*, 2002, **26**, 1246–1248.

74 A. Fürstner, D. Koch, K. Langemann, W. Leitner and C. Six, *Angew. Chem. Int. Ed.*, 1997,

36, 2466–2469.

75 R. Duque, E. Öchsner, H. Clavier, F. Caijo, S. P. Nolan, M. Mauduit and D. J. Cole-Hamilton, *Green Chem.*, 2011, **13**, 1187.

76 M. F. Sellin, P. B. Webb and D. J. Cole-Hamilton, *Chem. Commun.*, 2001, 781–782.

77 P. B. Webb, T. E. Kunene and D. J. Cole-Hamilton, *Green Chem.*, 2005, **7**, 373.

78 M. Solinas, J. Jiang, O. Stelzer and W. Leitner, *Angew. Chem. Int. Ed.*, 2005, **44**, 2291–2295.

79 T. E. Kunene, P. B. Webb and D. J. Cole-Hamilton, *Green Chem.*, 2011, **13**, 1476.

80 U. Hintermair, G. Zhao, C. C. Santini, M. J. Muldoon and D. J. Cole-Hamilton, *Chem. Commun.*, 2007, 1462.

81 D. Koch and W. Leitner, *J. Am. Chem. Soc.*, 1998, **120**, 13398–13404.

82 E. Ramsey, Q. Sun, Z. Zhang, C. Zhang and W. Gou, *J. Environ. Sci.*, 2009, **21**, 720–726.

83 M. Arai, S. Fujita and M. Shirai, *J. Supercrit. Fluids*, 2009, **47**, 351–356.

84 P. G. Jessop, S. Trakhtenberg and J. Warner, *ACS Symp. Ser.*, 2009, 401–436.

85 D. E. Fogg and E. N. Dos Santos, *Coord. Chem. Rev.*, 2004, **248**, 2365–2379.

86 M. Strohmann, J. T. Vossen, A. J. Vorholt and W. Leitner, *Green Chem.*, 2020, **22**, 8444–8451.

87 G. D. Frey, *J. Organomet. Chem.*, 2014, **754**, 5–7.

88 B. Zhang, C. Kubis and R. Franke, *Science*, 2022, **377**, 1223–1227.

89 I. Piras, R. Jennerjahn, R. Jackstell, A. Spannenberg, R. Franke and M. Beller, *Angew. Chem. Int. Ed.*, 2011, **50**, 280–284.

90 R. Crabtree, *Acc. Chem. Res.*, 1979, **12**, 331–337.

91 A. Kämper, S. Jenny, K. Reiswich, R. Kuhlmann, R. Franke and A. Behr, *Chem. Eng. Sci.*, 2016, **144**, 364–371.

92 D. Evans, J. A. Osborn, F. H. Jardine and G. Wilkinson, *Nature*, 1965, **208**, 1203–1204.

93 T. Mitsudo, N. Suzuki, T. Kondo and Y. Watanabe, *J. Mol. Catal. A: Chem.*, 1996, **109**, 219–225.

94 K. Takahashi, M. Yamashita, Y. Tanaka and K. Nozaki, *Angew. Chem. Int. Ed.*, 2012, **51**, 4383–4387.

95 I. Fleischer, L. Wu, I. Profir, R. Jackstell, R. Franke and M. Beller, *Chem. Eur. J.*, 2013, **19**, 10589–10594.

96 J. Pospech, I. Fleischer, R. Franke, S. Buchholz and M. Beller, *Angew. Chem. Int. Ed.*, 2013, **52**, 2852–2872.

97 S. Pandey, K. V. Raj, D. R. Shinde, K. Vanka, V. Kashyap, S. Kurungot, C. P. Vinod and S. H. Chikkali, *J. Am. Chem. Soc.*, 2018, **140**, 4430–4439.

98 R. Franke, D. Selent and A. Börner, *Chem. Rev.*, 2012, **112**, 5675–5732.

99 B. D. Evans, A. Osborn and W. Wilkinson, *Inorg. Phys. Theor.*, 1968, **566**, 3133.3142.

100 G. M. Torres, R. Frauenlob, R. Franke and A. Börner, *Cata. Sci. Technol.*, 2015, **5**, 34–54.

101 J. L. Van Winkle, S. Lorenzo, R. C. Morris, R. F. Mason and M. Valley, *'Single Stage Hydroformylation of Olefins to Alcohols',* US3420898A, 1969.

102 L. H. Slaugh and R. D. Mullineaux, *J. Organomet. Chem.*, 1968, **13**, 469–477.

103 F. E. Paulik, *Catal. Rev.*, 1972, **6**, 49–84.

104 O. Diebolt, C. Müller and D. Vogt, *Cata. Sci. Technol.*, 2012, **2**, 773.

105 F. M. S. Rodrigues, P. K. Kucmierczyk, M. Pineiro, R. Jackstell, R. Franke, M. M. Pereira and M. Beller, *ChemSusChem*, 2018, **11**, 2310–2314.

106 M. R. L. Furst, V. Korkmaz, T. Gaide, T. Seidensticker, A. Behr and A. J. Vorholt, *ChemCatChem*, 2017, **9**, 4319–4323.

107 K. Takahashi, M. Yamashita and K. Nozaki, *J. Am. Chem. Soc.*, 2012, **134**, 18746–18757.

108 R. H. Crabtree, *Chem. Rev.*, 2015, **115**, 127–150.

109 B. Fell and A. Geurts, *Chem. Ing. Tech.*, 1972, **44**, 708–712.

110 A. T. Jurewicz, L. D. Rollmann and D. D. Whitehurst, in *Homogeneous Catalysis - II*, eds. D. Forster and J. F. Roth, American Chemical Society, Washington DC, 1974, pp. 240–251.

111 K. Kaneda, M. Yasumura, M. Hiraki, T. Imanaka and S. Teranishi, *Chem. Lett.*, 1981, **10**, 1763–1766.

112 L. L. W. Cheung, G. Vasapollo and H. Alper, *Adv. Synth. Catal.*, 2012, **354**, 2019–2022.

113 T. Vanbésien, E. Monflier and F. Hapiot, *Green Chem.*, 2016, **18**, 6687–6694.

114 S. Fuchs, D. Lichte, M. Dittmar, G. Meier, H. Strutz, A. Behr and A. J. Vorholt, *ChemCatChem*, 2017, **9**, 1436–1441.

115 H. Schulz, *Appl. Catal. A*, 1999, **186**, 3–12.

116 R. Steiner, *Chemierohstoffe aus Kohle*, Georg Thieme Verlag, Stuttgart, 1st edn., 1978.

117 M. E. Dry, *Catal. Today*, 2002, **71**, 227–241.

118 K. Jeske, A. C. Kizilkaya, I. López-Luque, N. Pfänder, M. Bartsch, P. Concepción and G. Prieto, *ACS Catal.*, 2021, **11**, 4784–4798.

119 O. R. Inderwildi, D. A. King and S. J. Jenkins, *Phys. Chem. Chem. Phys.*, 2009, **11**, 11110.

120 Web of Science, https://www.webofscience.com/wos/woscc/basic-search, (accessed 12 April 2022).

121 H. Mahmoudi, M. Mahmoudi, O. Doustdar, H. Jahangiri, A. Tsolakis, S. Gu and M. LechWyszynski, *Biofuels Eng.*, 2017, **2**, 11–31.

122 E. Iglesia, *Appl. Catal. A*, 1997, **161**, 59–78.

123 T. Ishida, T. Yanagihara, X. Liu, H. Ohashi, A. Hamasaki, T. Honma, H. Oji, T. Yokoyama and M. Tokunaga, *Appl. Catal. A*, 2013, **458**, 145–154.

124 W. Shafer, M. Gnanamani, U. Graham, J. Yang, C. Masuku, G. Jacobs and B. Davis, *Catalysts*, 2019, **9**, 259.

125 Y. Huang, Q. Chu, Q. Yi, J. Feng, W. Li, K. Xie and Q. Sun, *Energy Procedia*, 2017, **142**, 3049–3054.

126 C.-I. Ahn, Y. M. Park, J. M. Cho, D. H. Lee, C.-H. Chung, B. G. Cho and J. W. Bae, *Catal. Surv. from Asia*, 2016, **20**, 210–230.

127 M. E. Dry, in *Encyclopedia of Catalysis*, ed. I. Horváth, Wiley, Hoboken, NJ, USA, 2010.

128 J. van de Loosdrecht, F. G. Botes, I. M. Ciobica, A. Ferreira, P. Gibson, D. J. Moodley, A. M. Saib, J. L. Visagie, C. J. Weststrate and J. W. Niemantsverdriet, in *Comprehensive*

Inorganic Chemistry II, Elsevier, 2013, pp. 525–557.

129 B. Shi and B. H. Davis, *Catal. Today*, 2005, **106**, 129–131.

130 T. Agapie, *Coord. Chem. Rev.*, 2011, **255**, 861–880.

131 Z. Gholami, F. Gholami, Z. Tišler, J. Hubáček, M. Tomas, M. Bačiak and M. Vakili, *Catalysts*, 2022, **12**, 174.

132 H. M. Torres Galvis and K. P. de Jong, *ACS Catal.*, 2013, **3**, 2130–2149.

133 A. Steynberg and M. Dry, *Fischer-Tropsch Technology*, Elsevier, 1st edn., 2004.

134 J. Kim, V. Nese, J. Joos, K. Jeske, N. Duyckaerts, N. Pfänder and G. Prieto, *J. Mater. Chem. A*, 2018, **6**, 21978–21989.

135 W. Linghu, X. Liu, X. Li and K. Fujimoto, *Catal. Letters*, 2006, **108**, 11–13.

136 L. Zhong, F. Yu, Y. An, Y. Zhao, Y. Sun, Z. Li, T. Lin, Y. Lin, X. Qi, Y. Dai, L. Gu, J. Hu, S. Jin, Q. Shen and H. Wang, *Nature*, 2016, **538**, 84–87.

137 Z. Zhao, W. Lu, R. Yang, H. Zhu, W. Dong, F. Sun, Z. Jiang, Y. Lyu, T. Liu, H. Du and Y. Ding, *ACS Catal.*, 2018, **8**, 228–241.

138 A. P. Amrute, K. Jeske, Z. Łodziana, G. Prieto and F. Schüth, *Chem. Mater.*, 2020, **32**, 4369–4374.

139 H. T. Luk, C. Mondelli, D. C. Ferré, J. A. Stewart and J. Pérez-Ramírez, *Chem. Soc. Rev.*, 2017, **46**, 1358–1426.

140 J. Barrault, A. Guilleminot, J. C. Achard, V. Paul-Boncour and A. Percheron-Guegan, *Appl. Catal.*, 1986, **21**, 307–312.

141 G. Jiao, Y. Ding, H. Zhu, X. Li, J. Li, R. Lin, W. Dong, L. Gong, Y. Pei and Y. Lu, *Appl. Catal. A*, 2009, **364**, 137–142.

142 G. . Volkova, T. . Yurieva, L. . Plyasova, M. . Naumova and V. . Zaikovskii, *J. Mol. Catal. A: Chem.*, 2000, **158**, 389–393.

143 V. M. Lebarbier, D. Mei, D. H. Kim, A. Andersen, J. L. Male, J. E. Holladay, R. Rousseau and Y. Wang, *J. Phys. Chem. C*, 2011, **115**, 17440–17451.

144 K. Jeske, T. Rösler, M. Belleflamme, T. Rodenas, N. Fischer, M. Claeys, W. Leitner, A. J. Vorholt and G. Prieto, *Angew. Chem. Int. Ed.*, , DOI:10.1002/anie.202201004.

145 M. L. Clarke and J. J. R. Frew, in *Organometallic Chemistry*, Royal Society of Chemistry, Cambridge, pp. 19–46.

146 J. A. Bilbrey, A. H. Kazez, J. Locklin and W. D. Allen, *J. Comput. Chem.*, 2013, **34**, 1189–1197.

147 D. M. P. Mingos and T. E. Müller, *Transit. Met. Chem.*, 1995, **20**, 533–539.

148 C. A. Tolman, *Chem. Rev.*, 1977, **77**, 313–348.

149 C. A. Tolman, *J. Am. Chem. Soc.*, 1970, **92**, 2956–2965.

150 A. L. Seligson and W. C. Trogler, *J. Am. Chem. Soc.*, 1991, **113**, 2520–2527.

151 T. Rösler, K. R. Ehmann, K. Köhnke, M. Leutzsch, N. Wessel, A. J. Vorholt and W. Leitner, *J. Catal.*, 2021, **400**, 234–243.

152 B. T. Heaton, A. D. C. Towl, P. Chini, A. Fumagalli, D. J. A. McCaffrey and S. Martinego, *J. Chem. Soc. Chem. Commmunications*, 1975, **6**, 523–524.

153 C. Brown, B. T. Heaton, L. Longhetti, W. T. Povey and D. O. Smith, *J. Organomet. Chem.*, 1980, **192**, 93–99.

154 B. T. Heaton, A. D. C. Towl, P. Chini, A. Fumagalli, D. J. A. McCaffrey and S. Martinengo, *J. Chem. Soc. Chem. Commun.*, 1975, **6**, 523.

155 J. D. S. Newman and G. J. Blanchard, *Langmuir*, 2006, **22**, 5882–5887.

156 T. Ayvalı, M. Zahmakıran and S. Özkar, *Dalton Trans.*, 2011, **40**, 3584.

157 L. Xu, D. Liu, D. Chen, H. Liu and J. Yang, *Heliyon*, 2019, **5**, e01165.

158 S. Püschel, J. Sadowski, T. Rösler, K. R. Ehmann, A. J. Vorholt and W. Leitner, *ACS Sustainable Chem. Eng.*, 2022, **10**, 3749–3756.

159 S. Püschel, E. Hammami, T. Rösler, K. R. Ehmann, A. J. Vorholt and W. Leitner, *Cata. Sci. Technol.*, 2022, **12**, 728–736.

160 S. K. Brayshaw, M. J. Ingleson, J. C. Green, P. R. Raithby, G. Kociok-Köhn, J. S. McIndoe and A. S. Weller, *Angew. Chem. Int. Ed.*, 2005, **44**, 6875–6878.

161 S. K. Brayshaw, M. J. Ingleson, J. C. Green, J. S. McIndoe, P. R. Raithby, G. Kociok-Köhn and A. S. Weller, *J. Am. Chem. Soc.*, 2006, **128**, 6247–6263.

162 C. Allevi, B. T. Heaton, C. Seregni, L. Strona, R. J. Goodfellow, P. Chini and S. Martinengo, *J. Chem. Soc., Dalt. Trans.*, 1986, **4**, 1375.

163 A. B. Koudriavtsev, A. T. Teleshev, A. A. Zhdanov, E. E. Nifant'ev and W. Linert, *Monatsh. Chem.*, 2001, **132**, 1001–1012.

164 S. C. van der Slot, P. C. J. Kamer and P. W. N. M. van Leeuwen, *Organometallics*, 2001, **20**, 1079–1086.

165 F. Doro, J. N. H. Reek and P. W. N. M. Van Leeuwen, *Organometallics*, 2010, **29**, 4440–4447.

166 A. Jörke, A. Seidel-Morgenstern and C. Hamel, *J. Mol. Catal. A: Chem.*, 2017, **426**, 10–14.

167 K. Wang, G. J. Kennedy and R. A. Cook, *J. Mol. Catal. A: Chem.*, 2009, **298**, 88–93.

168 M. Garland and G. Bor, *Inorg. Chem.*, 1989, **28**, 410–413.

169 E. Watanabe, K. Murayama, Y. Hara, Y. Kobayashi, K. Wada and T. Onoda, *J. Chem. Soc., Chem. Commun.*, 1986, 227–228.

170 S. Martinengo, A. Fumagalli, P. Chini, V. G. Albano and G. Clani, *J. Organomet. Chem.*, 1976, **116**, 333–342.

171 J. L. Vidal and R. C. Schoening, *Inorg. Chem.*, 1982, **21**, 438–441.

172 J. L. Vidal and R. C. Schoening, *J. Organomet. Chem.*, 1983, **241**, 395–416.

173 M. Garland and P. Pino, *Organometallics*, 1991, **10**, 1693–1704.

174 R. Lazzaroni, R. Settambolo and A. Caiazzo, in *Rhodium Catalyzed Hydroformylation*, eds. P. W. N. M. van Leeuwen and C. Claver, Kluwer Academics Publisher, New York, 2000, pp. 15–33.

175 G. Liu, R. Volken and M. Garland, *Organometallics*, 1999, **18**, 3429–3436.

176 S. Kandasamy, S. P. Samudrala and S. Bhattacharya, *Cata. Sci. Technol.*, 2019, **9**, 567–577.

177 C. M. Hansen, *Hansen Solubility Parameters A User's Handbook*, CRC Press, 2nd edn., 2007.

178 A.-F.-M. Barton, *CRC Handbook of Solubility Parameters and Other Cohesion Parameters, Second Edition*, CRC Press, 2nd edn., 1991.

179 T. Rösler, J. Betting, S. Püschel, A. J. Vorholt and W. Leitner, *Green Chem.*, 2022, **24**, 6578–6588.

180 M. H. S. A. Hamid, C. L. Allen, G. W. Lamb, A. C. Maxwell, H. C. Maytum, A. J. A. Watson and J. M. J. Williams, *J. Am. Chem. Soc.*, 2009, **131**, 1766–1774.

181 A. J. A. Watson, A. C. Maxwell and J. M. J. Williams, *J. Org. Chem.*, 2011, **76**, 2328–2331.

182 M. E. Dry, *J. Chem. Technol. Biotechnol.*, 2002, **77**, 43–50.

183 F. Hebrard and P. Kalck, *Chem. Rev.*, 2009, **109**, 4272–4282.

184 D. M. Hood, R. A. Johnson, A. E. Carpenter, J. M. Younker, D. J. Vinyard and G. G. Stanley, *Science*, 2020, **367**, 542–548.

185 C. Dwyer, H. Assumption, J. Coetzee, C. Crause, L. Damoense and M. Kirk, *Coord. Chem. Rev.*, 2004, **248**, 653–669.

186 C. D. Wood and P. E. Garrou, *Organometallics*, 1984, **3**, 170–174.

187 R. J. Klingler, M. J. Chen, J. W. Rathke and K. W. Kramarz, *Organometallics*, 2007, **26**, 352–357.

188 K. W. Kramarz, R. J. Klingler, D. E. Fremgen and J. W. Rathke, *Catal. Today*, 1999, **49**, 339–352.

189 M. Absi-Halabi, J. D. Atwood, N. P. Forbus and T. L. Brown, *J. Am. Chem. Soc.*, 1980, **102**, 6248–6254.

190 Y. Zhao and D. G. Truhlar, *Theor. Chem. Acc.*, 2008, **120**, 215–241.

191 F. Weigend and R. Ahlrichs, *Phys. Chem. Chem. Phys.*, 2005, **7**, 3297.

192 F. Weigend, *Phys. Chem. Chem. Phys.*, 2006, **8**, 1057.

193 I. Kaljurand, R. Lilleorg, A. Murumaa, M. Mishima, P. Burk, I. Koppel, I. A. Koppel and I. Leito, *J. Phys. Org. Chem.*, 2013, **26**, 171–181.

194 V. Barone and M. Cossi, *J. Phys. Chem. A*, 1998, **102**, 1995–2001.

195 A. J. Hoefnagel, M. A. Hoefnagel and B. M. Wepster, *J. Org. Chem.*, 1981, **46**, 4209–4211.

196 J. P. Mészáros, O. Dömötör, C. M. Hackl, A. Roller, B. K. Keppler, W. Kandioller and É. A. Enyedy, *Nouv. J. Chim.*, 2018, **42**, 11174–11184.

197 S. Grimme, *Chem. Eur. J.*, 2012, **18**, 9955–9964.

198 G. J. Tawa, R. L. Martin, L. R. Pratt and T. V. Russo, *J. Phys. Chem.*, 1996, **100**, 1515–1523.

199 N. Sieffert and M. Bühl, *Inorg. Chem.*, 2009, **48**, 4622–4624.

200 D. Christopher Roe, *J. Magn. Reson.*, 1985, **63**, 388–391.

201 I. T. Ibrahim and A. Williams, *J. Chem. Soc. Perkin Trans. 2*, 1982, 1459.

202 V. Frenna, N. Vivona, G. Consiglio and D. Spinelli, *J. Chem. Soc. Perkin Trans. 2*, 1985, 1865–1868.

203 J. F. King, J. H. Hillhouse and S. Skonieczny, *Can. J. Chem.*, 1984, **62**, 1977–1995.

204 V. K. Aggarwal, I. Emme and S. Y. Fulford, *J. Org. Chem.*, 2003, **68**, 692–700.

205 B. van de Graaf, A. J. Hoefnagel and B. M. Wepster, *J. Org. Chem.*, 1981, **46**, 653–657.

206 M. P. Vlasenko and V. A. Ozeryanskii, *J. Phys. Org. Chem.*, 2017, **30**, e3609.

8 List of Figures

9 List of Tables

10 Appendix

10.1 List of Publications

1) T. Rösler; K. R. Ehmann; K. Köhnke; M. Leutzsch; N. Wessel; A. J. Vorholt; W. Leitner, “Reductive Hydroformylation with a Selective and Highly Active Rhodium Amine System”, *J. Catal.* **2021**, *400*, 234–243.

2) T. Rösler; J. Betting; S. Püschel; A. J. Vorholt; W. Leitner, “Solvent Design for Catalyst Recycling of Rhodium/Amine Catalysts via $scCO_2$ Extraction in the Reductive Hydroformylation of Alpha Olefins”, *Green Chem.*, **2022**, 24 (17), 6578–6588.

3) K. Jeske; T. Rösler; M. Belleflamme; T. Rodenas; N. Fischer; M. Claeys; W. Leitner; A. J. Vorholt; G. Prieto, “Direct Conversion of Syngas to Higher Alcohols via Tandem Integration of Fischer-Tropsch Synthesis and Reductive Hydroformylation”, *Angew. Chem. Int. Ed.*, **2022**, 61, e20220100.

4) T. Rösler; T. A. Faßbach; M. Schrimpf; A. J. Vorholt; W. Leitner, “Toward Water-Based Recycling Techniques: Methodologies for Homogeneous Catalyst Recycling in Liquid/Liquid Multiphase Media and Their Implementation In Continuous Processes”, *Ind. Eng. Chem. Res.*, **2019**, 58, 7, 2421–2436

10.2 Tabularized Data for Experiments in Chapter 4.1 to 4.2

Table A 1: Corresponding data to Figure 21 in the results section; Screening of rhodium und ruthenium precursors in combination with triethylamine for the reductive hydroformylation of 1-octene. **Reaction conditions:** 1-Octene (2.0 mmol), catalyst precursor (40 µmol, 2 mol% Rh), triethylamine (0.2 mmol), MeCN (2.34 g), CO/H_2 (30 bar, 1:1), 60 °C, 8 h, 700 rpm.

Catalyst Precursor	$X_{1\text{-octene}}$	$Y_{n\text{-nonanol}}$	$Y_{iso\text{-nonanol}}$	$Y_{n\text{-nonanal}}$	$Y_{iso\text{-nonanal}}$	Y_{octane}	$Y_{octene\ isomers}$	$\sum Y$	***n/iso***
	[%]	[%]	[%]	[%]	[%]	[%]	[%]	[%]	[-]
$[Rh(COD)Cl]_2$	91	44	20	6	6	1	9	86	2.2
$[RhCl(nbd)]_2$	97	53	28	0	0	1	9	91	1.9
$[Rh(COD)]_2SbF_6$	98	50	27	0	0	4	10	91	1.9
$[Rh(acac(CO)_2]$	98	53	27	0	0	1	10	91	2.0
$[Rh(C_2H_4)_2Cl]_2$	98	20	15	0	0	35	21	91	1.3
$[Rh(CO)_2Cl]_2$	73	0	0	5	4	30	28	67	1.3
$RhCl_3 \times 3H_2O$	98	54	31	0	0	0	8	93	1.7
$[Ru(C_6H_6)Cl_2]_2$	25	0	0	1	0	0	17	18	-
$[Ru(p\text{-Cymol})Cl_2]_2$	27	0	0	1	0	0	27	28	-

Table A 2: Corresponding data to Figure 22 in the results section; investigation of the metal-to-amine ratio for the [Rh]/tertiary amine catalyzed reductive hydroformylation of 1-octene. [a] Triethylamine as neat solvent. **Reaction conditions:** 1-Octene (2.0 mmol), $[Rh(acac)(CO)_2]$ (30 µmol, 1.5 mol% Rh), triethylamine (concentration given), MeCN (2.59 g - $m_{triethylamine}$), CO/H_2 (30 bar, 1:1), 60 °C, 8 h, 700 rpm.

Rh:N ratio	$X_{1\text{-octene}}$	$Y_{n\text{-nonanol}}$	$Y_{iso\text{-nonanol}}$	$Y_{n\text{-nonanal}}$	$Y_{iso\text{-nonanal}}$	Y_{octane}	$Y_{octene\ isomers}$	$\sum Y$	***n/iso***
[-]	[%]	[%]	[%]	[%]	[%]	[%]	[%]	[%]	[-]
1:2	73	1	0	10	5	1	46	63	2.0
1:5	84	38	16	7	6	0	10	77	2.0
1:10	79	37	17	5	5	0	9	73	1.9
1:20	78	32	14	9	8	0	9	72	1.9
1:50	83	41	20	4	4	0	9	78	2.0
1:100	77	39	20	2	2	0	8	71	1.9
1:200	98	54	28	0	0	0	11	93	1.9
1:400	96	52	30	0	0	0	10	92	1.7
1:776[a]	49	15	9	1	1	0	7	33	1.6

Table A 3: Corresponding data to Figure 23 in the results section; Yield-time plot for the reductive hydroformylation of 1-octene at high amine concentrations. **Reaction conditions:** 1-Octene (2.0 mmol), [Rh(acac)$(CO)_2$] (30 µmol, 1.5 mol% Rh), triethylamine (11.2 mmol), MeCN (1.14 g), CO/H_2 (30 bar, 1:1), 60 °C, 700 rpm.

Reaction time	$X_{1\text{-octene}}$	$Y_{n\text{-nonanol}}$	$Y_{iso\text{-nonanol}}$	$Y_{n\text{-nonanal}}$	$Y_{iso\text{-nonanal}}$	Y_{octane}	$Y_{octene\ isomers}$	$\sum Y$	***n/iso***
[h]	[%]	[%]	[%]	[%]	[%]	[%]	[%]	[%]	[-]
1	54	28	15	0	0	0	6	49	1.9
1.5	52	27	15	0	0	0	6	48	1.8
2	80	43	23	0	0	0	9	75	1.9
3	90	48	25	0	0	0	11	84	1.9
4	90	49	27	0	0	0	10	86	1.8
6	98	54	29	0	0	0	10	93	1.9
8	96	52	30	0	0	0	10	92	1.7

Table A 4: Corresponding data to Figure 24 in the results section; Influence of the variation of the carbon monoxide and hydrogen pressure on the reductive hydroformylation of 1-octene using rhodium/tertiary amine catalysts. **Reaction conditions:** 1-Octene (2.0 mmol), [Rh(acac)$(CO)_2$] (30 μmol, 1.5 mol% Rh), triethylamine (11.2 mmol), MeCN (1.14 g), 60 °C, 8 h, 700 rpm.

p_{CO}	$CO:H_2$	***Pressure***	$X_{1\text{-octene}}$	$Y_{n\text{-nonanol}}$	$Y_{iso\text{-nonanol}}$	$Y_{n\text{-nonanal}}$	$Y_{iso\text{-nonanal}}$	Y_{octane}	$Y_{octene\ isomers}$	$\sum Y$	***n/iso***
[bar]	[-]	[bar]	[%]	[%]	[%]	[%]	[%]	[%]	[%]	[%]	[-]
20	2:1	30	32	14	8	1	1	0	3	27	1.7
15	1:1	30	52	27	15	0	0	0	6	48	1.8
10	1:2	30	65	32	15	1	0	0	9	57	2.2
5	1:5	30	74	9	2	25	5	1	27	69	4.9
10	1:4	50	64	34	18	1	1	0	8	62	2.0
5	1:2	15	70	11	2	17	4	0	19	53	4.7
15	1:2	45	50	25	15	1	1	0	5	47	1.6
20	1:2	60	38	10	7	1	1	0	3	22	1.4

Table A 5: Corresponding data to Figure 26; Catalytic activity of different amines in the reductive hydroformylation of 1-octene plotted against their electronic and steric properties. **Reaction conditions:** 1-Octene (2.0 mmol), [Rh(acac)(CO)$_2$] (20 μmol, 1 mol% Rh), amine (11.2 mmol), MeCN (1.54 g), CO/H$_2$ (30 bar, 1:2), 100 °C, 1.5 h, 700 rpm.

Amine ligand	$X_{1\text{-octene}}$ [%]	$Y_{n\text{-nonanol}}$ [%]	$Y_{iso\text{-nonanol}}$ [%]	$Y_{n\text{-nonanal}}$ [%]	$Y_{iso\text{-nonanal}}$ [%]	Y_{octane} [%]	$Y_{octene\ isomers}$ [%]	∑*Y* [%]	*n/iso* [-]
Trimethylamine	98	23	5	31	15	1	21	96	2.7
Dimethylbenzylamine	98	39	11	4	4	1	28	87	3.0
Dimethylethylamine	98	42	11	12	7	1	23	96	2.9
Dimethylaniline	98	0	0	8	6	0	71	84	1.2
Methyldiethylamine	98	52	16	0	0	1	27	96	3.2
Triethylamine	98	40	8	7	4	1	30	90	3.4
Quinuclidine	98	28	13	3	2	2	44	92	2.7
Methyldiphenylamine	99	0	0	15	16	1	51	83	0.9
Diisopropylethylamine	98	23	5	31	15	1	21	96	4.0
Diisopropylaniline	96	0	0	13	4	2	71	90	3.0
Tetramethylethylenediamine	98	5	1	39	15	1	4	64	2.8
Tetramethyl-1,4-butandiamine	98	6	1	46	17	1	22	93	2.9
Tetramethyl-1,3-phenylenediamine	98	1	0	18	9	1	58	87	2.1

Table A 6: Corresponding data to Figure 40; Performance of aminated solvents in the reductive hydroformylation of 1-pentene. **Reaction conditions:** 1-Pentene (2.0 mmol), [Rh(acac)(CO)$_2$] (10 μmol, 0.5 mol%), amine/solvent (2.54 g), CO/H$_2$ (60 bar, 1:2), 100 °C, 1.5 h, 700 rpm.

Aminated solvent	$X_{1\text{-octene}}$ [%]	$Y_{n\text{-nonanol}}$ [%]	$Y_{iso\text{-nonanol}}$ [%]	$Y_{n\text{-nonanal}}$ [%]	$Y_{iso\text{-nonanal}}$ [%]	Y_{octane} [%]	$Y_{octene\ isomers}$ [%]	∑*Y* [%]	*n/iso* [-]
Hexadecyldimethylamine	97	6	1	20	6	1	56	90	3.7
Dimethylaminobutanol	98	21	5	14	9	3	44	96	2.5
Dimethylaminoethanol	98	41	10	4	4	2	34	95	3.2
4,4-Diethoxydimethyl butanamine	98	45	12	2	2	1	29	91	3.4
Dimethylamino ethoxyethanol	98	33	15	2	2	2	37	91	2.2

Table A 7: Corresponding data to Figure 37; Tabularized results for the full solvent screening and Hansen-Solubility-Parameters in the reductive hydroformylation of 1-hexene.

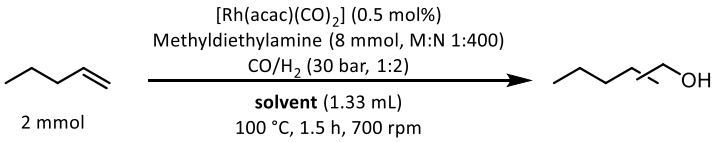

Solvent:

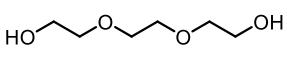

1
Triethylene glycol

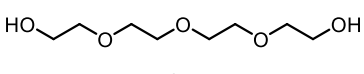

2
Tetraethylene glycol

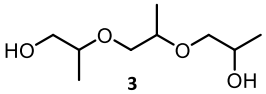

3
Tripropyleneglycol

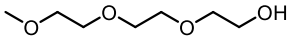

4
Triethylene glycol monomethy ether

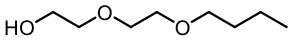

5
Diethylene glycol monobutyl ether

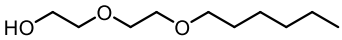

6
Diethylene glycol monohexyl ether

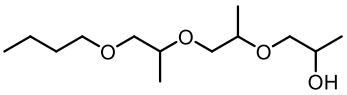

7
Tripropylene glycol monobutyl ether

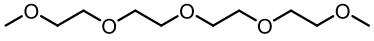

8
Tetraethylene glycol dimethyl ether

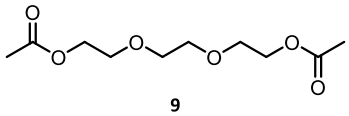

9
Triethylene glycol diacetate

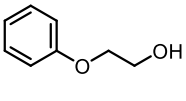

10
2-Phenoxyethanol

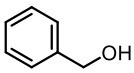

11
Benzylalcohol

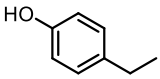

12
4-Ethylphenol

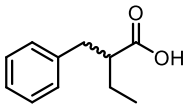

13
Ethylcinnamate

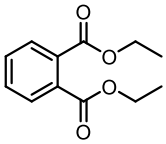

14
Diethyl phthalate

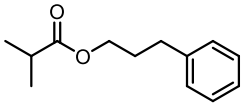

15
3-Phenylpropyl isobutyrat

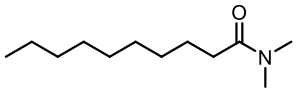

16
N,N-Dimethyldecanamide

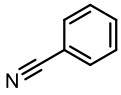

17
Benzonitrile

18
Acetonitrile

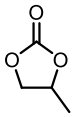

19
Propylene carbonate

20
Sulfolan

21
Toluene

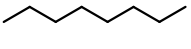

22
Octane

Solvent No.	$Y_{n\text{-Hexanol}}$	$Y_{iso\text{-Hexanol}}$	$Y_{n\text{-Hexanal}}$	$Y_{iso\text{-Hexanal}}$	$Y_{Pentane}$	$Y_{Pentene\ Isomers}$	δ_D	δ_P	δ_H
1	46.8	16.0	1.1	1.4	0.5	11.0	16.0	12.5	18.6
2	49.2	18.6	0.0	0.0	0.0	13.6	18.0	9.8	17.5
3	37.0	10.8	1.0	1.0	2.3	30.9	16.9	7.4	16.3
4	43.0	13.9	0.0	0.0	1.6	34.1	16.2	7.6	12.5
5	42.4	15.3	0.0	0.0	2.2	32.3	16.0	7.0	10.6

6	30.3	8.3	3.7	2.4	2.6	45.8	16.0	6.0	10.0
7	18.5	5.7	5.1	2.9	1.1	56.6	16.3	5.2	10.8
8	39.3	13.7	0.0	0.0	1.0	39.0	16.6	6.2	5.8
9	40.3	14.2	0.0	0.0	1.0	37.3	17.0	9.9	8.1
10	38.2	18.0	1.8	2.0	1.9	37.5	17.8	5.7	14.3
11	36.3	11.5	0.9	1.2	1.6	36.6	18.4	6.3	13.7
12	25.3	8.6	0.0	1.0	1.9	49.5	19.2	5.3	12.8
13	12.2	2.6	8.8	2.7	0.8	50.3	18.4	8.2	4.1
14	45.8	17.7	0.0	0.0	1.8	28.6	17.6	9.6	4.5
15	8.4	2.1	10.5	4.5	1.0	64.3	17.7	4.4	5.0
16	45.9	14.6	2.1	2.2	1.6	27.0	15.8	4.7	5.4
17	52.8	21.6	0.0	0.7	1.3	16.7	17.4	9.0	3.3
18	40.4	10.8	10.7	8.0	1.5	19.1	15.3	18.0	6.1
19	0.4	0.0	35.0	11.1	0.0	16.9	20.0	18.0	4.1
20	1.2	0.00	29.4	8.9	0.4	19.6	20.3	18.2	10.9
21	3.8	0.9	13.8	6.2	1.3	67.0	18.0	1.4	2.0
22	0.8	0.7	12.6	5.7	0.9	69.5	15.5	0.0	0.0

Table A 8: Corresponding data to Figure 41; Increasing substrate concentration when using DEG-amine as the solvent and ligand in the reductive hydroformylation of 1-octene. **Reaction conditions:** 1-Octene (concentration as displayed in table), [Rh(acac)$(CO)_2$] (10 μmol, 0.5 mol%), DEG-amine (remaining w%), CO/H_2 (60 bar, 1:2), 100 °C, 1.5 h, 700 rpm.

Substrate conc. [w%]	$X_{1\text{-octene}}$ [%]	$Y_{n\text{-nonanol}}$ [%]	$Y_{iso\text{-nonanol}}$ [%]	$Y_{n\text{-nonanal}}$ [%]	$Y_{iso\text{-nonanal}}$ [%]	Y_{octane} [%]	$Y_{octene\ isomers}$ [%]	$\sum Y$ [%]	***n/iso*** [-]
10	99	52	24	2	2	1	11	92	2.1
15	99	57	29	0	1	1	9	97	1.9
20	99	56	28	0	0	1	8	93	2.0
25	99	56	30	0	0	1	7	94	1.9
30	99	56	30	0	0	1	7	94	1.9
35	99	56	28	0	0	2	10	96	2.0
40	99	56	30	0	0	1	9	96	1.9
45	99	52	19	1	2	2	19	95	2.5
50	99	52	22	0	2	2	15	93	2.4
55	99	46	18	1	3	2	26	96	2.2
60	99	43	17	1	4	2	29	96	2.1
70	84	15	3	23	8	0	46	95	3.5
80	75	13	2	19	7	0	44	85	3.6

Table A 9: Corresponding data to Figure 42; Yield-time plot for the reductive hydroformylation of 1-octene using 2,2-dimethylaminoethoxyethanol (DEG-amine) as solvent/ligand. **Reaction conditions:** 1-Octene (40 w%), [Rh(acac)(CO)$_2$] (10 μmol, 0.5 mol%), DEG-amine (60 w%), CO/H$_2$ (60 bar, 1:2), 100 °C, 700 rpm.

Reaction time [min]	$X_{1\text{-octene}}$ [%]	$Y_{n\text{-nonanol}}$ [%]	$Y_{iso\text{-nonanol}}$ [%]	$Y_{n\text{-nonanal}}$ [%]	$Y_{iso\text{-nonanal}}$ [%]	Y_{octane} [%]	$Y_{octene\ isomers}$ [%]	***∑Y*** [%]	***n/iso*** [-]
10	15	3	0	12	5	0	5	21	3.0
20	88	34	9	20	9	1	24	97	3.0
30	>99	54	19	0	0	3	20	93	2.8
60	99	53	23	0	00	2	18	96	2.3
90	99	56	30	0	0	1	9	96	1.9
120	>99	56	26	0	0	2	13	97	2.2
180	>99	57	35	0	0	1	4	97	1.6

Table A 10: Corresponding data to Figure 47; Application of several aminated high molecular weight solvents for the reductive hydroformylation of 1-octene. **Reaction conditions:** 1-Octene (40 w%), [Rh(acac)(CO)$_2$] (10 μmol, 0.5 mol%), aminated solvent (60 w%), CO/H$_2$ (60 bar, 1:2), 100 °C, 1.5 h, 700 rpm.

Aminated solvent	$X_{1\text{-octene}}$ [%]	$Y_{n\text{-nonanol}}$ [%]	$Y_{iso\text{-nonanol}}$ [%]	$Y_{n\text{-nonanal}}$ [%]	$Y_{iso\text{-nonanal}}$ [%]	Y_{octane} [%]	$Y_{octene\ isomers}$ [%]	***∑Y*** [%]	***n/iso*** [-]
PEG$_{300}$-diamine	>99	12	5	40	25	2	14	98	1.7
PEG300-diamine + PEG$_{300}$ 50:50	99	51	27	2	2	4	6	92	1.8
PEG$_{300}$-mixture (30% amination)	99	55	27	3	11	3	5	105	1.5
PEG600-diamine	98	47	28	0	0	1	7	83	1.7
DEG-amine	99	55	29	0	1	2	4	90	1.9

Table A 11: Corresponding data to Figure 48; Catalyst recycling of a rhodium catalyst in a PEG$_{300}$ mixture by extraction of product alcohols with *sc*CO$_2$. **Reaction conditions:** 1-Pentene (40 w%), [Rh(acac)(CO)$_2$] (10 μmol, 0.5 mol%), PEG$_{300}$-amine mixture with 30% amination (60 w%, 8.4 g), CO/H$_2$ (60 bar, 1:2), 100 °C, 1.5 h, 700 rpm. Stationary phase = PEG$_{300}$ amine mixture with an amination degree of 30%.

Recycling Run No.	$extract_{\Sigma Hexanol}$ [g]	$extract_{\Sigma Hexanal}$ [g]	$extract_{stationary\ Phase}$ [g]	***Rh leaching*** [ppm]	***Rh leaching*** [%Rh]
1	2.737	0.055	0.238	1.8	0.01
2	1.397	0.351	1.025	15.3	0.11
3	1.294	0.636	0.652	15.9	0.11
4	0.305	0.373	0.587	18.3	0.06
5	0.366	0.377	0.697	16.3	0.06
6	0.222	0.351	0.509	34.9	0.10
7	0.375	0.489	0.587	20.4	0.08
8	0.414	0.409	0.545	30.7	0.11
9	0.275	0.571	0.521	23.8	0.09

Table A 12: Corresponding data to Figure 50; Catalyst recycling of a rhodium catalyst in diaminated $PEG6_{00}$ by extraction of product alcohols with *sc*CO_2. **Reaction conditions:** 1-Pentene (30 w%), [$Rh(acac)(CO)_2$] (10 µmol, 0.5 mol%), diaminated PEG_{600} (70 w%, 9.8 g), CO/H_2 (60 bar, 1:2), 100 °C, 1.5 h, 700 rpm. Stationary phase = diaminated PEG_{600}.

Recycling Run No.	$extract_{\sum Hexanol}$ [g]	$extract_{\sum Hexanal}$ [g]	$extract_{stationary\ Phase}$ [g]	***Rh leaching*** [ppm]	***Rh leaching*** [%Rh]
1	1.374	0.202	0.044	2.4	0.005
2	1.786	0.344	0.030	3.4	0.009
3	2.122	0.176	0.012	3.5	0.010
4	1.929	0.510	0.011	3.8	0.012
5	2.066	0.188	0.006	12.6	0.036
6	1.931	0.333	0.004	5.5	0.016
7	2.328	0.743	0.017	2.0	0.008
8	1.953	0.477	0.000	1.8	0.005
9	2.359	0.611	0.000	1.0	0.004

10.3 Tabularized Data for Experiments in Chapter 4.3.1

Table A 13: Corresponding data to Figure 55. Variation of synthesis gas pressure and synthesis gas ratio during the Co/PCy_3 catalyzed reductive hydroformylation of 1-octene. **Reaction conditions:** 1-Octene (9 mmol), [Co_2CO_8] (7.3 µmol, 1.5 mol%), PCy_3 (13.5 µmol), *n*-hexane (1.8 g), CO/H_2, 195 °C, 3 h, 700 rpm.

Synthesis Gas Pressure; H_2:CO ratio	$X_{1\text{-octene}}$ [%]	$Y_{n\text{-nonanol}}$ [%]	$Y_{iso\text{-nonanol}}$ [%]	$Y_{n\text{-nonanal}}$ [%]	$Y_{iso\text{-nonanal}}$ [%]	Y_{octane} [%]	$Y_{octene\ isomers}$ [%]	$\sum Y$ [%]	***n/iso*** [-]
30 bar; 1:1	>99	23	26	1	1	14	35	100	0.9
60 bar; 1:1	88	29	23	1	1	12	10	75	1.3
90 bar; 1:1	>99	34	43	0	0	9	0	86	0.8
120 bar; 1:1	>99	44	41	0	0	5	0	91	1.1
120 bar; 1:2	>99	44	40	0	0	8	0	92	1.1

Table A 14: Corresponding data to Figure 56. Variation of metal to ligand ratio ratio during the Co/PCy_3 catalyzed reductive hydroformylation of 1-octene. **Reaction conditions:** 1-Octene (9 mmol), [Co_2CO_8] (7.3 µmol, 1.5 mol%), PCy_3 (13.5 µmol times the M:L ratio), *n*-hexane (1.8 g), CO/H_2 (120 bar, 1:2), 195 °C, 3 h, 700 rpm.

Metal to Ligand Ratio [-]	$X_{1\text{-octene}}$ [%]	$Y_{n\text{-nonanol}}$ [%]	$Y_{iso\text{-nonanol}}$ [%]	$Y_{n\text{-nonanal}}$ [%]	$Y_{iso\text{-nonanal}}$ [%]	Y_{octane} [%]	$Y_{octene\ isomers}$ [%]	$\sum Y$ [%]	***n/iso*** [-]
1:1	>99	44	40	0	0	8	0	92	1.1
1:2	99	63	21	0	0	8	0	96	3.0
1:4	99	61	14	1	0	10	3	91	4.3
1:10	99	56	10	1	0	11	12	92	5.5

Table A 15: Corresponding data to Figure 57. Variation of catalyst concentration during the Co/PCy_3 catalyzed reductive hydroformylation of 1-octene. **Reaction conditions:** 1-Octene (9 mmol), [Co_2CO_8], PCy_3 (M:L = 1:1), *n*-hexane (1.8 g), CO/H_2 (120 bar, 1:2), 195 °C, 3 h, 700 rpm.

Cobalt Catalyst Concentration [mol%]	$X_{1\text{-octene}}$ [%]	$Y_{n\text{-nonanol}}$ [%]	$Y_{iso\text{-nonanol}}$ [%]	$Y_{n\text{-nonanal}}$ [%]	$Y_{iso\text{-nonanal}}$ [%]	Y_{octane} [%]	$Y_{octene\ isomers}$ [%]	$\sum Y$ [%]	*n/iso* [-]
1.50	>99	44	40	0	0	8	0	92	0.9
0.75	>99	45	41	0	0	11	0	98	0.9
0.38	>99	42	43	0	0	12	0	98	1.0
0.19	>99	38	36	2	0	11	1	90	1.0
0.10	>99	24	24	19	19	7	0	93	1.0

10.4 Supporting Experimental Data

Table A 16: Effect of decreasing the catalyst concentration at low amine concentrations in the rhodium catalyzed reductive hydroformylation of 1-octene. **Reaction conditions:** 1-Octene (2.0 mmol), [$Rh(acac)(CO)_2$] (concentration given), triethylamine (Rh/N 1:5), MeCN (2.34 g), CO/H_2 (30 bar, 1:1), 60 °C, 8 h, 700 U/min

c_{Rh} [mol%]	*Rh:N* [-]	$X_{1\text{-octene}}$ [%]	$Y_{n\text{-nonanol}}$ [%]	$Y_{iso\text{-nonanol}}$ [%]	$Y_{n\text{-nonanal}}$ [%]	$Y_{iso\text{-nonanal}}$ [%]	Y_{octane} [%]	$Y_{octene\ isomers}$ [%]	$\sum Y$ [%]	*n/iso* [-]
2	1:5	92	46	21	3	4	1	11	86	2.0
1.5	1:5	83	34	14	8	6	< 1	11	73	2.1
1	1:5	63	7	2	22	12	1	8	51	2.1
1	1:400	85	40	20	0	0	1	13	74	2.0

Table A 17: Temperature dependency of the rhodium/tertiary amine catalyzed reductive hydroformylation of 1-octene. **Reaction conditions:** 1-Octene (2.0 mmol), [$Rh(acac)(CO)_2$] (30 µmol, 1.5 mol% Rh), triethylamine (12.0 mmol), MeCN (1.14 g), CO/H_2 (30 bar, 1:2), 1.5 h, 700 rpm.

T [°C]	$X_{1\text{-octene}}$ [%]	$Y_{n\text{-nonanol}}$ [%]	$Y_{iso\text{-nonanol}}$ [%]	$Y_{n\text{-nonanal}}$ [%]	$Y_{iso\text{-nonanal}}$ [%]	Y_{octane} [%]	$Y_{octene\ isomers}$ [%]	$\sum Y$ [%]	*n/iso* [-]
50	39	6	3	1	1	< 1	2	13	1.7
60	65	32	15	1	< 1	< 1	9	57	2.1
80	98	51	14	< 1	< 1	< 1	25	90	3.6
100	99	51	18	< 1	< 1	1	17	87	2.8
120	98	40	11	< 1	< 1	1	37	89	3.8

Table A 18: Different cationic and basic additives instead of tertiary amines in the rhodium catalyzed reductive hydroformylation of 1-octene. **Reaction conditions:** 1-Octene (2.0 mmol), [$Rh(acac)(CO)_2$] (10 µmol, 0.5 mol% Rh), additive (cation or base), TEG (1.5 g), CO/H_2 (30 bar, 1:2), 1.5 h, 100 °C, 700 rpm.

Additive [-]	$m_{Additive}$ [g]	$X_{1\text{-octene}}$ [%]	$Y_{n+\ iso\text{-nonanol}}$ [%]	$Y_{n+iso\text{-nonanal}}$ [%]	Y_{octane} [%]	$Y_{octene\ isomers}$ [%]	$\sum Y$ [%]
NEt_2Me (reference)	0.7	99	70	0	1	22	93
$PPh_3Me^+Br^-$	0.7	68	0	6	0	15	21
$NEt_4^+Cl^-$	0.7	59	0	5	0	12	17
PNP^+Cl^-	0.7	3	0	0	0	0	0
KOH	0.3	5	0	0	4	2	6
$NEt_4^+Cl^-$ + KOH	0.7 + 0.3	13	0	0	0	1	1

Table A 19: Small screening of solvents in the rhodium/tertiary amine catalyzed reductive hydroformylation of 1-octene. [a] Mixture biphasic after reaction, [b] no evaluation of octane by product possible. TEG = Triethelyene glycol, cPC = cyclopropanecarbonate, MeCN = acetonitrile. **Reaction conditions:** 1-Octene (2.0 mmol), [Rh(acac)(CO)$_2$] (30 µmol, 1.5 mol% Rh), triethylamine (12.0 mmol), solvent (1.14 g), CO/H$_2$ (30 bar, 1:2), 1.5 h, 60 °C 700 rpm.

Solvent	$X_{1\text{-octene}}$	$Y_{n\text{-nonanol}}$	$Y_{iso\text{-nonanol}}$	$Y_{n\text{-nonanal}}$	$Y_{iso\text{-nonanal}}$	Y_{octane}	$Y_{octene\ isomers}$	$\sum Y$	n/iso
[-]	[%]	[%]	[%]	[%]	[%]	[%]	[%]	[%]	[-]
H$_2$O[a]	48	16	6	3	< 1	2	14	41	2.7
MeOH	56	30	10	< 1	< 1	< 1	11	51	3.1
TEG[a]	72	25	11	3	< 1	2	22	64	2.4
cPC[a]	16	< 1	< 1	1	1	1	4	7	1.4
MeCN	65	32	15	1	< 1	< 1	9	57	2.1
Toluene	-8	4	2	1	1	< 1	4	12	2.4
Octane[b]	26	< 1	< 1	1	1	-	4	5	1.9

Table A 20: Combination of trialkylamine ligands and phosphorus ligands in deficit for the reductive hydroformylation of 1-octene. **Reaction conditions:** 1-Octene (2.0 mmol), [Rh(acac)(CO)$_2$] (10 µmol, 0.5 mol% Rh), diethylmethylamine (4.0 mmol), phosphorus ligand (0.2 mol% for monodentate ligands, 0.1 mol% for bidentate ligands), triethyleneglycole (0.92 g), CO/H$_2$ (30 bar, 1:2), 1.5 h, 100 °C 700 rpm.

Phosphorus Ligand	$X_{1\text{-octene}}$	$Y_{n\text{-nonanol}}$	$Y_{iso\text{-nonanol}}$	$Y_{n\text{-nonanal}}$	$Y_{iso\text{-nonanal}}$	Y_{octane}	$Y_{octene\ isomers}$	$\sum Y$	n/iso
(+ NEt$_2$Me)	[%]	[%]	[%]	[%]	[%]	[%]	[%]	[%]	[-]
-	>99	40	11	1	2	1	30	85	3.2
TPP	>99	0	0	55	18	4	12	89	3.1
XantPhos	>99	37	8	11	5	2	24	87	3.7
dppe	>99	21	4	23	8	1	27	84	3.7
dppb	>99	30	8	14	7	2	24	85	2.9
DPEphos	>99	32	7	13	7	5	19	83	3.2
BiphePhos	>99	42	6	4	3	16	13	84	5.1

Table A 21: Combination of trialkylamine and phosphorus ligands in different concentrations for the reductive hydroformylation of 1-octene. **Reaction conditions:** 1-Octene (2.0 mmol), [Rh(acac)(CO)$_2$] (10 µmol, 0.5 mol% Rh), diethylmethylamine (4.0 mmol), phosphorus ligand (concentration given), triethyleneglycole (0.92 g), CO/H$_2$ (30 bar, 1:2), 1.5 h, 100 °C 700 rpm.

P-Ligand	*conc.*	$X_{1\text{-octene}}$	$Y_{n\text{-nonanol}}$	$Y_{iso\text{-nonanol}}$	$Y_{n\text{-nonanal}}$	$Y_{iso\text{-nonanal}}$	Y_{octane}	$Y_{octene\ isomers}$	n/iso
(+ NEt$_2$Me)	[mol%]	[%]	[%]	[%]	[%]	[%]	[%]	[%]	[-]
TPP	0.13	98	1	0	36	15	12	15	2.5
TPP	0.20	99	23	5	19	8	8	23	3.2
TPP	0.50	99	34	9	2	2	9	23	3.3
XantPhos	0.03	99	43	12	1	1	4	28	3.3
XantPhos	0.12	99	42	11	1	1	3	29	3.6
XantPhos	0.23	99	38	8	2	2	3	17	4.0
XantPhos	0.45	99	13	0	51	2	10	11	32.0
BiphePhos	0.05	100	41	6	2	1	17	11	6.1
BiphePhos	0.20	100	23	6	2	2	24	7	3.1
BiphePhos	0.40	100	0	0	2	3	50	11	0.7

Table A 22: Phenanthrolin poisoning experiments to test for nanoparticles in the reductive hydroformylation of 1-octene. Phenanthroline acts as poison for nanoparticles and molecular catalysts. Under assumption of strong binding phenanthroline equivalents <<1 are needed to completely poison nanoparticles (usually around 0.1 eq.-0.2 eq.). Around 0.4 eq. phenanthroline are needed which hints towards multinuclear species as reported in chapter 4.1.5. [a] The relative catalytic activity is based on the total amount of catalytic products (aldehydes +alcohols) whereas alcohols are factored x2 because two catalytic steps are needed for their formation. **Reaction conditions:** 1-Octene (2.0 mmol), [Rh(acac)$(CO)_2$] (10 µmol, 0.5 mol% Rh), triethylamine (4 mmol), 1,10-phenanthroline (concentration given), MeCN (1.4 g), CO/H_2 (30 bar, 1:2), 1.5 h, 100 °C, 700 rpm.

Phenanthroline to [Rh] equivalents	$X_{1\text{-octene}}$	$Y_{\sum Alcohol}$	$Y_{\sum Aldehyde}$	Y_{Alkane}	$Y_{Alkane\ Isomers}$	***n/iso***	**∑catalytic products**	**Relative catalytic activity[a]**
[-]	[%]	[%]	[%]	[%]	[%]	[-]	[%]	[-]
-	98	13	45	0	33	4.6	57.3	1.00
0.10	98	13	46	0	30	3.7	58.8	1.00
0.20	96	3	57	0	34	4.2	60.1	0.88
0.25	70	0	40	0	29	4.8	40.0	0.56
0.30	58	0	29	0	25	4.7	29.5	0.41
0.35	35	0	13	0	14	4.2	13.2	0.18

Table A 23: Mercury drop poisoning test for nanoparticles in the reductive hydroformylation of 1-octene. **Reaction conditions:** 1-Octene (2.0 mmol), [Rh(acac)$(CO)_2$] (20 µmol, 1 mol% Rh), methyldiethylamine (4 mmol), MeCN (1.4 g), CO/H_2 (30 bar, 1:2), 1.5 h, 100 °C, 700 rpm.

Mercury Drop	$X_{1\text{-octene}}$	$Y_{n\text{-nonanol}}$	$Y_{iso\text{-nonanol}}$	$Y_{n\text{-nonanal}}$	$Y_{iso\text{-nonanal}}$	Y_{octane}	$Y_{octene\ isomers}$	$\sum Y$	***n/iso***
	[%]	[%]	[%]	[%]	[%]	[%]	[%]	[%]	[-]
-	98	40	12	0	0	11	27	90	3.3
Yes (≈ 0.2 g)	98	48	16	0	1	3	25	93	2.8

Table A 24: Comparison of tricyclohexylphosphine and polymer bound triphenylphosphine on the catalytic acticity and selectivity of the cobalt catalyzed reductive hydroformylation of 1-octene. **Reaction conditions:** 1-Octene (9.0 mmol), [Rh(acac)$(CO)_2$] (1.5 mol%), phosphorus ligand (1.5 mol%), *n*-hexane (1.8 g), CO/H_2 (120 bar, 1:2), 3 h, 195 °C, 700 rpm.

Phosphorus ligand	$X_{1\text{-octene}}$	$Y_{n\text{-nonanol}}$	$Y_{iso\text{-nonanol}}$	$Y_{n\text{-nonanal}}$	$Y_{iso\text{-nonanal}}$	Y_{octane}	$Y_{octene\ isomers}$	$\sum Y$	***n/iso***
	[%]	[%]	[%]	[%]	[%]	[%]	[%]	[%]	[-]
PCy_3	>99	44	40	0	0	8	0	92	1.1
TPP-Polymer bound	>99	38	34	2	3	2	11	90	1.1

Table A 25: Cone-angles and pKa values for 13 different tertiary amines. pKa values for most amines are found in literatre. [a] pKa has been determined by titration with HCl.

Amine		pK_a	Cone angle [°]	
Trimethylamine		10.0[201]	132	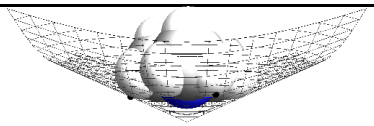
Dimethylethylamine	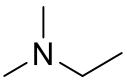	10.12[202]	136	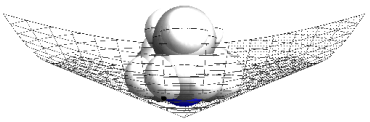
Methyldiethylamine	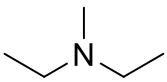	10.37[202]	142	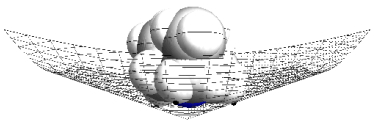
Triethylamine	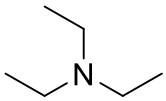	10.68[202]	149	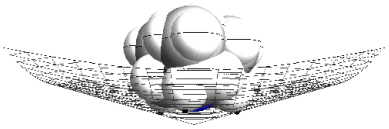
Diisopropylethylamine	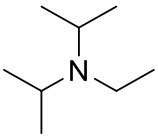	11.51[203]	164	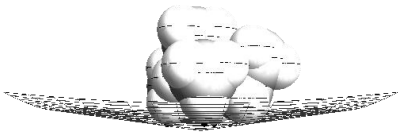
Quinuclidine	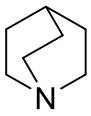	11.3[204]	137	
N,*N*-Dimethyl-benzylamine	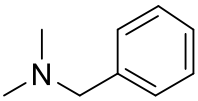	9.03[202]	135	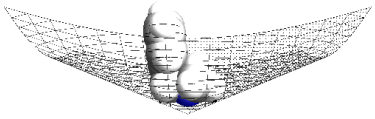
N,*N*-Dimethylaniline	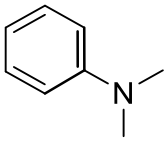	5.10[193]	142	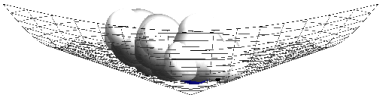
N,*N*-Diisopropylaniline	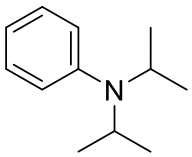	8.25[205]	173	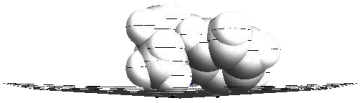
N-Methyl-diphenylamine	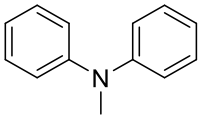	0.86[195]	162	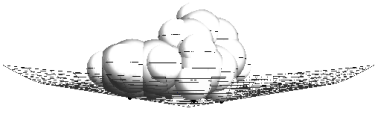
N,*N*,*N*',*N*'-Tetramethyl-ethylendiamine	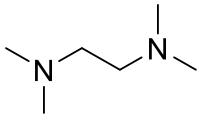	5.95[196]	210	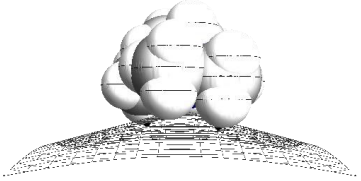

Amine		*p*K$_a$	Cone angle [°]	
N,*N*,*N*',*N*'-Tetramethyl-1,4-butandiamine	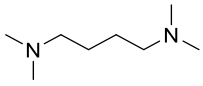	9.65[a]	238	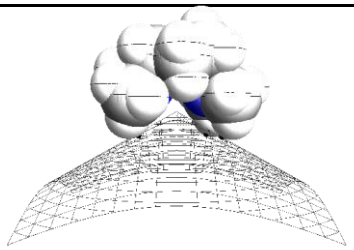
N,*N*,*N*',*N*'-Tetramethyl-1,3-phenylendiamine[b]	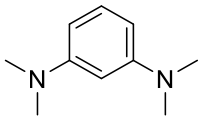	5.38[206]	162[a]	

Table A 26: Coordinates of the optimized structure of the $Ni(CO)_3L$ complex with L = trimethylamine.

Ligand L	**Trimethylamine**		
Atom	**x**	**y**	**z**
Ni	0.05050029809986	-0.20531076952419	-0.96873219287556
C	-0.52548511385768	1.49579299925818	-0.94398207444305
C	-0.42186896262722	-1.06439046437827	-2.47295862160086
C	-0.42346014535073	-1.11134737921579	0.50742135505072
O	-0.81402928963056	-1.60702069615888	-3.41286894371538
O	-0.98931663914361	2.55241057654689	-0.93009021584338
O	-0.81816768362985	-1.68443360125910	1.42796376546280
N	2.19518898394040	-0.13169780242880	-0.96887747404632
C	2.71456604961152	-1.49708115967830	-0.98922728508549
C	2.64317142340300	0.55764625234535	0.23876371337809
C	2.64199928342037	0.59278844377302	-2.15620970001202
H	2.28580888907473	0.08607634925354	-3.06204043638686
H	2.23262562827226	1.61084838116081	-2.15189800054055
H	2.35908921367306	-2.02153858694506	-1.88516380193903
H	2.35991373373734	-2.04770105290631	-0.10880820644806
H	2.28756133036785	0.02471869992991	1.12963718526769
H	2.23398296892051	1.57546167059334	0.26457888857332
H	3.74744634592608	0.62262916341317	0.28701538714384
H	3.82168786640746	-1.51351018356505	-0.99002201974562
H	3.74622181938521	0.65938115978555	-2.20348132219430

Table A 27: Coordinates of the optimized structure of the $Ni(CO)_3L$ complex with L = dimethylethylamine.

Ligand L	**Dimethylethylamine**		
Atom	**x**	**y**	**z**
Ni	0.07960395315473	-0.22675070611551	-0.97728801876445
C	-0.48636546634547	1.47679691843528	-1.02982671261926
C	-0.34706546067094	-1.13307925328223	-2.46731350235931
C	-0.45410197528950	-1.07273739620428	0.51393842200985
O	-0.71208488915491	-1.70359641315226	-3.40171416165743
O	-0.94590919665232	2.53477458954175	-1.06659491179606
O	-0.89023784345016	-1.60374539350579	1.44113153103415
N	2.23144864987410	-0.16218536538172	-0.90481427778702
C	2.70521380330539	-1.56294315625040	-0.87387318032581
C	2.61860010096527	0.56690169280684	0.30071114003434
C	2.70188372109425	0.54195782709662	-2.09547852772252
H	2.41141803620883	-0.01207396369816	-2.99771630889357
H	2.23975513779450	1.53618221124445	-2.14554960302800
H	2.29016793791294	-2.05920471873557	-1.76483267119140
H	2.21993252431634	-2.04449666845400	-0.01069214603135
C	4.20456740155355	-1.76829260267607	-0.81220431485255
H	2.26838522113627	0.03006049927468	1.19208161419008
H	2.15222766744001	1.56041524924443	0.29908972694677
H	4.72576927621042	-1.34475653950025	-1.68203767238774
H	4.42846477760356	-2.84269092750456	-0.79892109874264
H	4.65353149394451	-1.33787143495909	0.09376380715618
H	3.79927281729656	0.67804708610654	-2.10392880710728
H	3.71268831175206	0.70631246566932	0.38094467389502

Table A 28: Coordinates of the optimized structure of the $Ni(CO)_3L$ complex with L = methyldiethylamine

Ligand L	**Methyldiethylamine**		
Atom	**x**	**y**	**z**
Ni	0.11958106928802	-0.21425404463921	-0.97051792554372
C	-0.44911387170420	1.47041809306785	-1.22755845808697
C	-0.32944946351342	-1.28484268668440	-2.34114380799507
C	-0.40870855262269	-0.88164125500962	0.61122324491278
O	-0.72668683878907	-1.95315490277725	-3.19407289911251
O	-0.91865957394739	2.51120074472027	-1.39508281934753
O	-0.84864926023662	-1.30160179104927	1.59198343907054
N	2.28865254822507	-0.12807981446040	-0.89736285105434
C	2.73111649819280	-1.53658847119303	-0.96433510741536
C	2.62276854728627	0.54505145455713	0.37991867407917
C	2.72554048865202	0.63701871064064	-2.06118708894613
H	2.31210944236580	0.18816446270786	-2.97391362128882
H	2.34689500976707	1.66577047065261	-1.99350105589046
H	2.37116318872378	-1.92625398925771	-1.92941368037994
H	2.16733251534853	-2.08899757562274	-0.19633995126094
C	4.21190233504674	-1.82289386180677	-0.81738510143573
H	2.46561064270256	-0.19840581416952	1.17750896754995
H	1.85738670474934	1.31948695821785	0.54850091811664
C	3.99092669586272	1.18873962738562	0.50182962629541
H	4.82527142396276	0.49628132336497	0.33663996642823
H	4.10643445884828	1.60302213690886	1.51225365872424
H	4.11318636528500	2.02768709950071	-0.19705037047411
H	4.83000279881309	-1.24129110617056	-1.51630913046074
H	4.40187840492994	-2.88354991642137	-1.02953722112158
H	4.57693272914068	-1.63336096125671	0.20100918026039
H	3.82433969362295	0.68686510879419	-2.16897858562339

Table A 29: Coordinates of the optimized structure of the $Ni(CO)_3L$ complex with L = triethylamine.

Ligand L		**Triethylamine**	
Atom	**x**	**y**	**z**
Ni	0.15616286037952	-0.22308869906508	-0.96910811397138
C	-0.45234349255533	1.44024520853115	-1.27224255332046
C	-0.30292394820098	-1.35664622394053	-2.28565229452049
C	-0.32876944868992	-0.83651840428469	0.64897626836997
O	-0.71503787281315	-2.06458313641551	-3.09835075603781
O	-0.95493992082741	2.46131108519053	-1.46291690485386
O	-0.75533667871838	-1.22154233447729	1.64966876141552
N	2.35006628774080	-0.10266540001271	-0.97104833118610
C	2.78115600477359	-1.51107572633565	-1.08858313844774
C	2.67113202592785	0.52903279737320	0.32548941598888
C	2.65932914236174	0.73191306290244	-2.15052550771598
H	1.94478255002964	0.45310048074916	-2.94197705357339
C	4.05818605901796	0.67618469747119	-2.73459021855747
H	2.39559303703477	1.76687322402502	-1.87878391642303
H	2.58778905921798	-1.81094699832502	-2.13126007364384
H	2.08531563930727	-2.11494022637450	-0.48373207684751
C	4.19754978736230	-1.87462902306336	-0.68518182692723
H	2.50446178504420	-0.23955238177804	1.09748819099135
H	1.90061368270301	1.29446052084271	0.51315195599172
C	4.03250476111265	1.17424025553995	0.50261484755973
H	4.87288721539655	0.48770087323359	0.33900037836456
H	4.11923214080242	1.55880883185251	1.52820365086666
H	4.16479599941614	2.03654444841178	-0.16587928553811
H	4.97039338176092	-1.32350485112364	-1.23588431794383
H	4.36268382943959	-2.94461454601184	-0.87251024729813
H	4.36912321406490	-1.71603602298156	0.38873078349402
H	4.29093229025145	-0.31798227398333	-3.14123579181238
H	4.84766143430900	0.94234361654222	-2.02029604031673
H	4.12660517435092	1.38056314550731	-3.57509280410695

Table A 30: Coordinates of the optimized structure of the $Ni(CO)_3L$ complex with L = diisopropylethylamine.

Ligand L	**Diisopropylethylamine**		
Atom	**x**	**y**	**z**
Ni	4.87688603795981	-1.30181478759543	-2.86603087445110
C	5.50727576408618	-1.81517224515309	-4.47096959670884
C	5.42970330680037	0.35485276713138	-2.43803822573443
C	5.37153339541858	-2.46314101808756	-1.58316568038380
O	5.92397915027441	1.36173116340249	-2.16802252183823
O	5.83977468257423	-3.16304316994002	-0.79457995523679
O	6.01743920415232	-2.13888246045250	-5.45385422560737
N	2.59834920519123	-1.24511176613102	-2.97946326083094
C	2.19404192196448	-1.68367265611482	-1.62466111843958
C	2.23027349889400	-2.17521945159001	-4.08966355843900
C	2.30178582160480	0.20482666249631	-3.22168443028818
C	0.88893710925922	0.69689222395595	-2.91575214639639
C	2.75069300987901	0.64643142293250	-4.60238772017433
H	2.94842104403099	0.72630241632551	-2.49537257297878
H	2.49684681012674	-0.86814872978680	-0.94772946750106
C	0.75697392857950	-2.09411407944692	-1.33758923505200
H	2.86934817367202	-1.86446842636920	-4.93376946132296
C	2.61934146609807	-3.60438980406898	-3.75213742957363
C	0.79184396943871	-2.11803477936248	-4.59871212291602
H	0.53556112356496	-1.14529184030169	-5.03530698167203
H	0.04487276684905	-2.34893773817085	-3.82904574647030
H	0.66821895395641	-2.86177380602921	-5.39893088418851
H	2.76536058515746	1.74333139174809	-4.65193063331583
H	2.08133969322007	0.29955378526688	-5.40253761639090
H	3.76620636338892	0.29283922367762	-4.82684690886787
H	0.49491178233078	-3.04764001089073	-1.81476642493834
H	0.00139643757541	-1.35846193424885	-1.63482671214573
H	0.64832162989979	-2.25012544290984	-0.25482466142650
H	0.82889823251255	1.76588571570557	-3.16485808304465
H	0.64502428859303	0.61520120691556	-1.84915226119769
H	0.10091846854725	0.18909208909429	-3.48612446800533
H	1.95458526046499	-4.05974795012091	-3.00421437020807
H	3.64855528116420	-3.66411720108241	-3.37401961501001
H	2.55950017909841	-4.22842525472463	-4.65366013015635
H	2.83472545367203	-2.53211151607420	-1.34369289908849

Table A 31: Coordinates of the optimized structure of the $Ni(CO)_3L$ complex with L = *N,N*-dimethylaniline.

Ligand L		***N,N*-Dimethylaniline**	
Atom	**x**	**y**	**z**
Ni	-0.44470678304504	0.09589600342233	-2.18286266776691
C	0.53625614797018	0.16834190305809	-0.68189218707673
C	-0.29841619112174	1.59042129073891	-3.16973978466260
C	-2.15174286782149	-0.39466717793525	-1.86931728298356
O	-0.25450018707059	2.61244156915610	-3.70334030701443
O	-3.24602908879364	-0.65040139329812	-1.61713425186850
O	1.11158127634949	0.27503313901124	0.31246894594734
N	0.38622904433650	-1.54447301974058	-3.39818573805776
C	0.33414546469150	-3.11280844436392	-1.50400670505934
C	-0.21821137501106	-4.20237788026786	-0.84436787803966
C	-1.73030079248220	-4.55400510599267	-2.67071561627818
C	-1.17608897842723	-3.46673428068531	-3.34603629954424
C	-0.09435359295360	-1.31166747773480	-4.75764106648046
H	1.12429024088769	-2.54417756029238	-1.01154284191250
H	0.16623501838523	-4.47628993347265	0.14049392455016
H	-2.54303547889497	-5.11075063039566	-3.14233208943951
H	-1.57374245518121	-3.20287327711366	-4.32510132704656
H	0.35760347579297	-0.38837970458987	-5.13843891430172
H	0.16852554227496	-2.13831078494862	-5.44284281507495
H	-1.18170506622199	-1.17411684918410	-4.76699839990538
C	-1.25928928254227	-4.93128112655357	-1.41927723376069
H	-1.69697031268275	-5.78170089013885	-0.89370490961566
C	-0.14270795586356	-2.72173871330627	-2.76525820228459
C	1.84802389432354	-1.44078730354088	-3.36221389609128
H	2.32831943804578	-2.22716526942770	-3.97143035073147
H	2.14464463921020	-0.45965474430727	-3.75280123484275
H	2.22781887784529	-1.51131482009669	-2.33879715265800

Table A 32: Coordinates of the optimized structure of the $Ni(CO)_3L$ complex with L = diisopropylaniline.

Ligand L		***N,N*-Diisopropylaniline**	
Atom	**x**	**y**	**z**
Ni	4.85402049405382	-1.57791418844778	-2.85164135308273
C	5.33475248593562	-2.19962520501750	-4.46973969998664
C	5.59869430496149	0.01628054692238	-2.49179389518576
C	5.15651910940146	-2.77387517273321	-1.52903850947986
O	6.19639883885070	0.97851611252048	-2.27172061537883
O	5.44290839549364	-3.51595720781001	-0.69685117087235
O	5.74650904014594	-2.61021793865656	-5.46620333327085
N	2.56311807479937	-1.25012586170767	-2.86716666809554
C	2.09837336361038	-2.09518630582781	-4.01469896996408
C	2.39256255787858	0.23606621831526	-3.08056610807545
C	1.01146101353010	0.77455271808915	-2.72853470087356
C	2.83906938286311	0.67877902202437	-4.45918197810499
H	3.09417887286318	0.69534543324728	-2.36868648139186
H	2.69871507153506	-1.71308669422150	-4.85419570816724
C	2.47195490756769	-3.57242944042729	-3.86781048369860
C	0.63640705246712	-1.93751645396369	-4.42495852129794
H	0.42772929125304	-0.95933024749059	-4.87455178145382
H	-0.06590107193263	-2.07543895885407	-3.59152561632725
H	0.39340728397130	-2.69133041571090	-5.18713684785033
H	2.91564843698788	1.77417081573702	-4.47925159097887
H	2.13269965157388	0.39498580026333	-5.25230359896538
H	3.82815276602545	0.27361956213551	-4.71470897340653
H	1.04975594708472	1.87254229966479	-2.70370904508538
H	0.68101957438198	0.44075779944014	-1.73569547117045
H	0.23669881829912	0.49806236579377	-3.45397906126145
H	1.61989063959200	-4.20653156893899	-3.59064617746003
H	3.26205699569073	-3.73397776806634	-3.12476977116625
H	2.84876990016639	-3.95636328047835	-4.82596131238174
C	2.78158612857310	-0.97377319418359	-0.44500227917099
C	2.50236997991833	-1.34088303725881	0.86317488632440
C	1.02897393286936	-3.05246996526519	0.07078351120808
C	1.29388696031888	-2.67699169775620	-1.24761448813328
H	3.50107172682457	-0.17345651966712	-0.62519826506080
H	2.99050868611992	-0.80529089348469	1.68051814203483
H	0.33223515857798	-3.87350313894159	0.25492617999471
H	0.78594599457214	-3.21123135240828	-2.04568279065928
C	1.62779317725612	-2.39331402158920	1.13592032061357
H	1.41881533088093	-2.69090821897331	2.16498480166827
C	2.19401572503754	-1.64405994627326	-1.53471657438573

Table A 33: Coordinates of the optimized structure of the $Ni(CO)_3L$ complex with L = *N,N*-methyldiphenylamine.

Ligand L	***N,N*-Methyldiphenylamine**		
Atom	**x**	**y**	**z**
Ni	-0.25351379551430	-0.11298241990967	-1.76266330126457
C	1.00620534757355	-0.33480070900708	-0.49775318647910
C	-0.31412269130883	1.56305485330745	-2.40865317982670
C	-1.87583370802897	-0.72454963308692	-1.25531478549340
O	-0.40274041419873	2.68230529973008	-2.67462889149103
O	-2.90416129555850	-1.05962568378330	-0.86126042095774
O	1.76951911594607	-0.43191380438070	0.35979766874898
N	0.33821112423171	-1.53398422861615	-3.44451587654564
C	0.15483496124349	-3.37955854385136	-1.85312021823277
C	-0.52492148349737	-4.46561366966450	-1.32318941182890
C	-2.19978407888220	-4.26322998518778	-3.03184078295582
C	-1.51698556874848	-3.17592386149101	-3.58100625899010
C	-0.24404283895583	-0.89686071243496	-4.63064512434575
H	1.07483938632822	-3.02514251384238	-1.38166096129903
H	-0.12647281284006	-4.96304006988835	-0.43625266448397
H	-3.12552147407476	-4.60037994789646	-3.50325930408872
H	-1.92562302805111	-2.68829003038483	-4.46565711925044
H	0.31699301143307	0.01740934957311	-4.85341890321181
H	-0.20386070456088	-1.55426978733650	-5.51757167958838
H	-1.28617966686850	-0.61482416811864	-4.43677479928566
C	-1.71466918080179	-4.91208752695475	-1.90383744046075
H	-2.25471048490604	-5.75863332128274	-1.47617725325447
C	-0.34155279256024	-2.71188986567323	-2.98468408781013
C	1.77564442717322	-1.66340429156784	-3.59113488654928
C	2.35710095479354	-2.86918262682573	-3.99119808531118
H	1.72809082017141	-3.74760385516001	-4.15199536228976
C	3.73548209218592	-2.95018902879017	-4.17578070491736
H	4.18082859397196	-3.89931192384901	-4.48192089234412
C	4.54070978297531	-1.83047135405889	-3.98141743390598
H	5.62088311479880	-1.89801052542504	-4.12518793030875
C	3.95736562356123	-0.62264859101014	-3.60299767218124
C	2.58267802155724	-0.53859736895804	-3.40616333697122
H	2.11938340320511	0.40187863758954	-3.09757327647980
H	4.57729123820673	0.26284790823600	-3.44741843634542

Table A 34: Coordinates of the optimized structure of the $Ni(CO)_3L$ complex with L = *N,N*-dimethylbenzylamine.

Ligand L	***N,N*-Dimethylbenzylamine**		
Atom	**x**	**y**	**z**
Ni	-0.95040136141317	0.25177743611963	-2.23523626542866
C	-0.70478153565964	0.15279234195742	-0.45923698225142
C	-0.32232291622306	1.78770349807853	-2.92300465509583
C	-2.65014587892983	-0.07087107995272	-2.71583912117266
O	0.01472534828404	2.82116716843415	-3.30993503411426
O	-3.76684712720193	-0.20260681701336	-2.97518916142026
O	-0.60218076232135	0.16424087327005	0.69011905063065
N	0.23166513890813	-1.32880851832555	-3.09575456978491
C	2.21936353153073	-5.47241683437039	-2.74515300835891
C	1.78107873091428	-6.14080625089641	-3.88678946176329
C	-0.00591850756914	-4.53728433597970	-4.12754811524028
C	0.42798029852240	-3.84960400262244	-2.98806549159395
C	0.06858704435674	-1.28452536696729	-4.54776236799325
H	3.08722666618413	-5.84079988039592	-2.19363557789636
H	2.30585137620557	-7.03304066149675	-4.23505576072447
H	-0.89018669477285	-4.17976967351842	-4.66424211721779
H	0.36315163816971	-0.29456071866434	-4.91908248168534
H	0.68257612340935	-2.04486581175729	-5.06522367846070
H	-0.98523185612459	-1.44585250632781	-4.81162833664238
C	0.66389924916733	-5.67279859073401	-4.57591480087463
H	0.30791847528500	-6.19895620713367	-5.46443724074117
C	1.54585218839671	-4.33753376486430	-2.30101281312329
C	1.63045755214375	-1.09565958195065	-2.74059340835389
H	1.93844623185487	-0.10487870349145	-3.09851450877294
H	2.30941761281212	-1.84917958819905	-3.18105761198061
H	1.74810207500195	-1.11362675463321	-1.64879546181082
C	-0.27512049158874	-2.60349101557259	-2.52491667612477
H	-1.34683176427226	-2.65590446649601	-2.76916132569015
H	1.88574086433890	-3.82183067092015	-1.39747081399194
H	-0.20478024940915	-2.51073351557632	-1.43067620232171

Table A 35: Coordinates of the optimized structure of the $Ni(CO)_2(L\cap L)$ complex with L∩L = N,N,N',N'-tetramethylethylenediamine.

Ligand L	***N,N,N',N'*-Tetramethylethylenediamine**		
Atom	**x**	**y**	**z**
N	-1.32009324992436	4.70508718623381	12.24702216686040
N	-2.30336246483597	4.49594706637579	9.51589714770622
C	-0.02149028261020	4.56120149114497	12.89345806501400
H	0.22456092729499	5.42728569799576	13.54000246148220
H	0.76343731516464	4.44897429325541	12.13503251528390
C	-1.33781488821192	5.84724490973978	11.32980373577390
H	-1.43165383295686	6.80878278560890	11.87514702939730
H	-0.36308049457955	5.88093572420410	10.81927901996560
C	-2.44800833859175	5.71826350709441	10.31022001888970
H	-2.48172254047364	6.62226804555964	9.66793421019122
C	-1.26702062131774	4.63150251236879	8.49826296240562
H	-1.51426612088168	5.41831130042434	7.75693946237525
H	-0.29989452943993	4.87117295576592	8.95642158067663
H	-1.14510340220137	3.67825436364214	7.96940473228236
H	-0.01813071773837	3.65550976076532	13.51283530540840
O	0.62145207140146	1.40273234536123	10.25509790491670
C	-0.25796636204379	2.12194164775965	10.51373305848520
Ni	-1.70709362038878	2.99475269678838	10.96661796695720
C	-3.03224251902838	1.99170213950248	11.51875572594910
O	-3.81150270758283	1.19432544645586	11.85717294610200
H	-3.42206218789879	5.67135651206949	10.82107582794110
C	-2.36853112133633	4.80561036066565	13.25622654715260
C	-3.56398510497882	4.11425797949215	8.89130393225362
H	-3.35730853142961	4.86666430056060	12.78578752410450
H	-2.36432518681238	3.90394531555137	13.88089439116300
H	-2.23068184757488	5.69018593412035	13.91064027152260
H	-3.43938656270114	3.15806132948289	8.36778509278314
H	-3.91620434590680	4.86920203715767	8.16006022760815
H	-4.33528873241521	3.97564435485313	9.65924816934758

Table A 36: Coordinates of the optimized structure of the $Ni(CO)_2(L \cap L)$ complex with L∩L = N,N,N',N'-tetramethylbutanediamine

Ligand L	***N,N,N',N'*-Tetramethylbutanediamine**		
Atom	**x**	**y**	**z**
Ni	0.96480299966071	0.62634476386664	0.55880159471258
C	0.46019854305941	2.30533479072763	0.66901403254929
C	0.98821836818556	-0.19519377623589	2.11002106458177
O	0.15455415793512	3.39660745749517	0.94111591830873
O	0.89941589325693	-0.58666672204953	3.20397835550901
N	2.91183496780904	0.55317980297062	-0.46614460594927
C	3.79577569957104	-0.05214248652576	0.52889257691128
C	3.33835679866664	1.92842009342374	-0.70981204450324
H	2.62867116610847	2.44935488468103	-1.36411121563348
H	3.36360544885099	2.47494462059430	0.24086693078502
H	3.47673505959339	-1.08151862281030	0.73650999548323
H	3.74359415613779	0.51159589149196	1.46817482983571
H	4.84928647609668	-0.07247625136106	0.18126272173450
H	4.34726780132538	1.97320054486916	-1.16893441725896
N	-0.35768304712270	-0.61840995383694	-0.72502070754747
C	-0.51079454876301	-1.94669304787596	-0.14198916626241
C	-1.61516601037326	0.11778829326141	-0.59329142785876
H	-1.52931465041109	1.10395123063951	-1.06732014113349
H	-2.45684072104568	-0.42785454929513	-1.06778353229456
H	0.45330952298465	-2.47367083333878	-0.14591272976174
H	-1.25060796051578	-2.56094504932216	-0.69369903670322
H	-0.84028361857666	-1.86374229333750	0.90129253037878
H	-1.84445365290474	0.27747727242938	0.46767986412947
C	2.97510888693255	-0.25118233992475	-1.69113760773128
C	0.00077271957181	-0.72624845897348	-2.14927908274161
H	2.61254848165537	-1.25976167494044	-1.42796126347107
H	4.03803302299305	-0.38573968506525	-1.98849920371197
H	-0.91022115960288	-0.94907440645035	-2.74055198742691
H	0.64202659389158	-1.61463552843759	-2.26610189037335
C	2.21080353491696	0.29339816814944	-2.88189496230786
C	0.71859458584983	0.51184431665355	-2.67188072538816
H	2.67835198113210	1.22546574093630	-3.23727130760806
H	2.36021410437568	-0.42671659614317	-3.70394858175261
H	0.27433082486097	0.84928771023993	-3.62040183099463
H	0.55805257389412	1.33251069349429	-1.95001094650526

Table A 37: Coordinates of the optimized structure of the $Ni(CO)_2(L\cap L)$ complex with L∩L = N,N,N',N'-tetramethylphenylenediamine.

Ligand L	***N.N.N'.N'*-Tetramethylphenylenediamine**		
Atom	**x**	**y**	**z**
N	-0.27701515650929	6.10520071637968	12.49275677884020
N	-2.58990240496709	3.94454433259595	8.79561567873403
C	0.93485709069590	6.39135488715350	13.21284726495180
H	1.62675639702692	7.01446213393777	12.62291898268820
H	1.48546573148493	5.48010227402983	13.51003370153030
C	-2.44351368339047	3.32874763661689	7.47897012228010
H	-1.99534387903397	4.01887775140511	6.74097867646296
H	-1.82567225417468	2.42565759921330	7.53949414898100
H	-3.43381156950810	3.02864259278652	7.11657868844214
H	0.69541137357995	6.94667697619263	14.12564956607580
O	-0.99243929282287	0.61284719116155	10.66045571281600
C	-1.87181883892745	1.31531208317265	10.41548476825100
Ni	-3.31927610056160	2.34974307844479	10.11807712353890
C	-4.62678139982287	1.50262191339886	9.22326080810715
O	-5.48394579861720	0.88967092959455	8.75251708425741
C	-1.55135189174538	6.31979710094089	13.12633877437690
C	-3.61720384476137	4.98883078746680	8.73674186727366
H	-2.07910428586142	5.37800402355283	13.36011476393730
H	-1.40703220751198	6.86287527366713	14.06597004166710
H	-2.22698164741991	6.92582670071850	12.49956486623970
H	-4.54856967509786	4.55174865274734	8.35578319008971
H	-3.31654976657450	5.81992212605351	8.07375530741827
H	-3.83136861577476	5.39588894252149	9.72929507782637
C	-0.11389438490277	4.05018924304007	8.82672116428192
C	1.05291251274283	4.41459743751677	9.49937538219338
H	2.01845608027247	4.15590501144529	9.05842246419971
H	1.96364567234521	5.34635385335407	11.19974312203360
C	1.02629797790593	5.09116214236547	10.70691895769700
C	-0.21452977159081	5.43403813053587	11.29157696207760
H	-2.35383412633272	5.27269769126504	11.07140234237370
C	-1.38996868363768	5.05701866738479	10.61584635424170
C	-1.34961984400674	4.36701706212609	9.39990210959932
H	-0.03937116219824	3.51758470790565	7.88102184890183
C	-3.90380377173408	3.15133580287406	11.61015842277550
O	-4.28144377856834	3.60083054643478	12.60510987483780

Table A 38: Coordinates of the optimized structure of the $Ni(CO)_3L$ complex with L = quinuclidine

Ligand L	**Quinuclidine**		
Atom	**x**	**y**	**z**
N	2.89903525258083	-0.06742839017635	-1.09657649035994
C	2.15748448299779	-1.34476986295008	-1.17760478558715
C	2.74577391987424	0.48987308745405	0.26489090658791
C	2.32088128581810	0.88362946356041	-2.07084594354614
C	0.64295625133368	-1.12044751566392	-1.02692885456093
H	2.55726001460656	-1.99935194201541	-0.38847836547068
H	2.41364430151937	-1.82401777000048	-2.13352717937793
C	1.26284594335524	0.58720656461678	0.66347759311226
H	3.23793726927943	1.47414976693350	0.26657687239467
H	3.32128302052764	-0.14302924347084	0.95571651479357
C	0.41334460861109	0.32218936759094	-0.57870513022409
H	0.2103468590352	-1.82548661798700	-0.29861324387187
H	0.11989829873521	-1.30515313837969	-1.97851644783861
H	1.03616167635222	1.57835461301531	1.08400452622404
H	1.01664009502257	-0.14462271998069	1.44901084999993
C	0.87677308335761	1.25805231752659	-1.69422606614216
H	-0.65118848697046	0.48890320691842	-0.35697949849460
H	2.37688108442661	0.40478486716915	-3.06008605513148
H	2.98005143350154	1.76250272605993	-2.11712071431889
H	0.81576102768263	2.30423953992185	-1.35506826108437
H	0.21277539489456	1.17850696191015	-2.56795243928826
O	5.89847017079784	-2.62162649516089	0.16014407279607
C	5.47977255754482	-1.75098259028592	-0.47163992454252
Ni	4.95146814078851	-0.39268262092524	-1.52135091555291
C	5.04714225327649	-0.80828544688901	-3.26596389474834
O	5.19653638015841	-1.08670942535439	-4.37613603270206
C	5.80547487051445	1.14053718448896	-1.13800547759786
O	6.43457007750947	2.08247179707390	-0.91606316146768

10.5 Supporting Figures

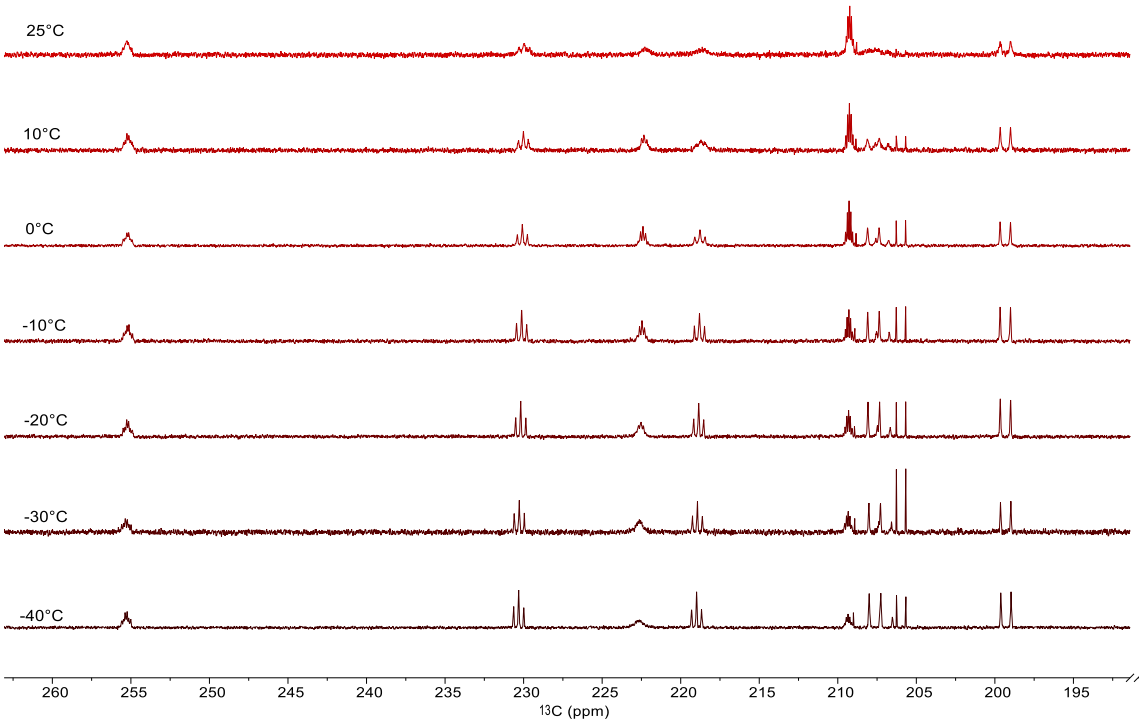

Figure A 1: Temperature dependent carbonyl region in the ^{13}C NMR (126 MHz, d_3-acetonitrile, 21 °C) spectrum of a ^{13}CO enriched catalyst solution (40 mg $[Rh(acac)(CO)_2]$ in 0.33 mL NE_{t3} and 0.66 mL d_3-acetonitrile) measured at 25 °C.

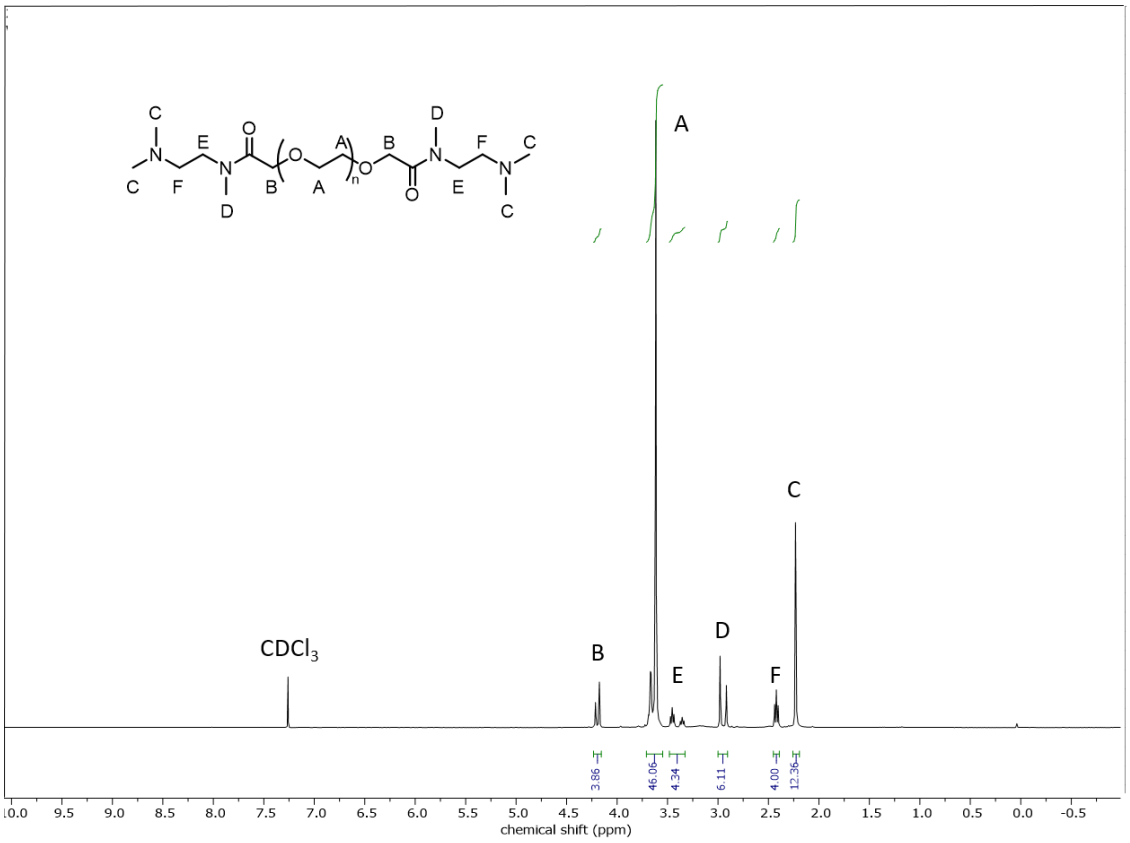

Figure A 2: ^{1}H-NMR (400 MHz, $CDCl_3$, room temperature) spectrum of diamine functionalized PEG_{600} synthesized via amide condensation as described in chapter 6.2.5.

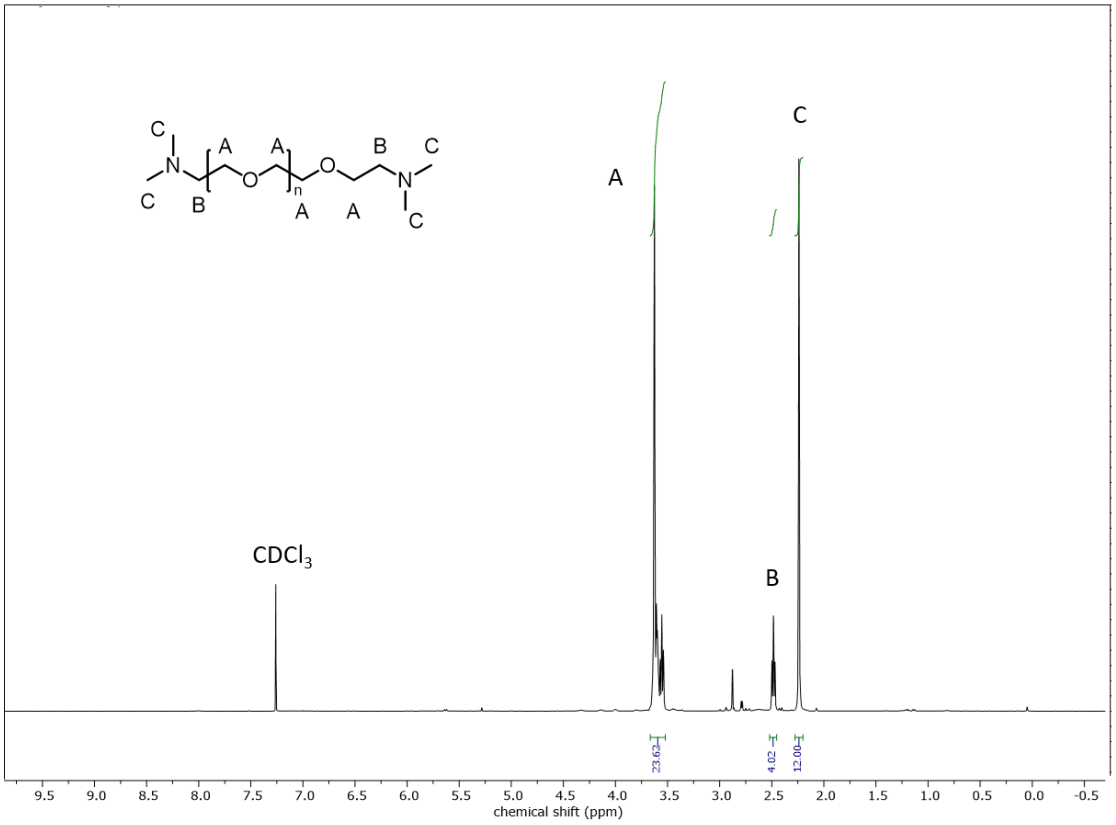

Figure A 3: ^{1}H-NMR (400 MHz, $CDCl_3$, room temperature) spectrum of diamine functionalized PEG_{300} synthesized via alcohol amination as described in chapter 6.2.4.

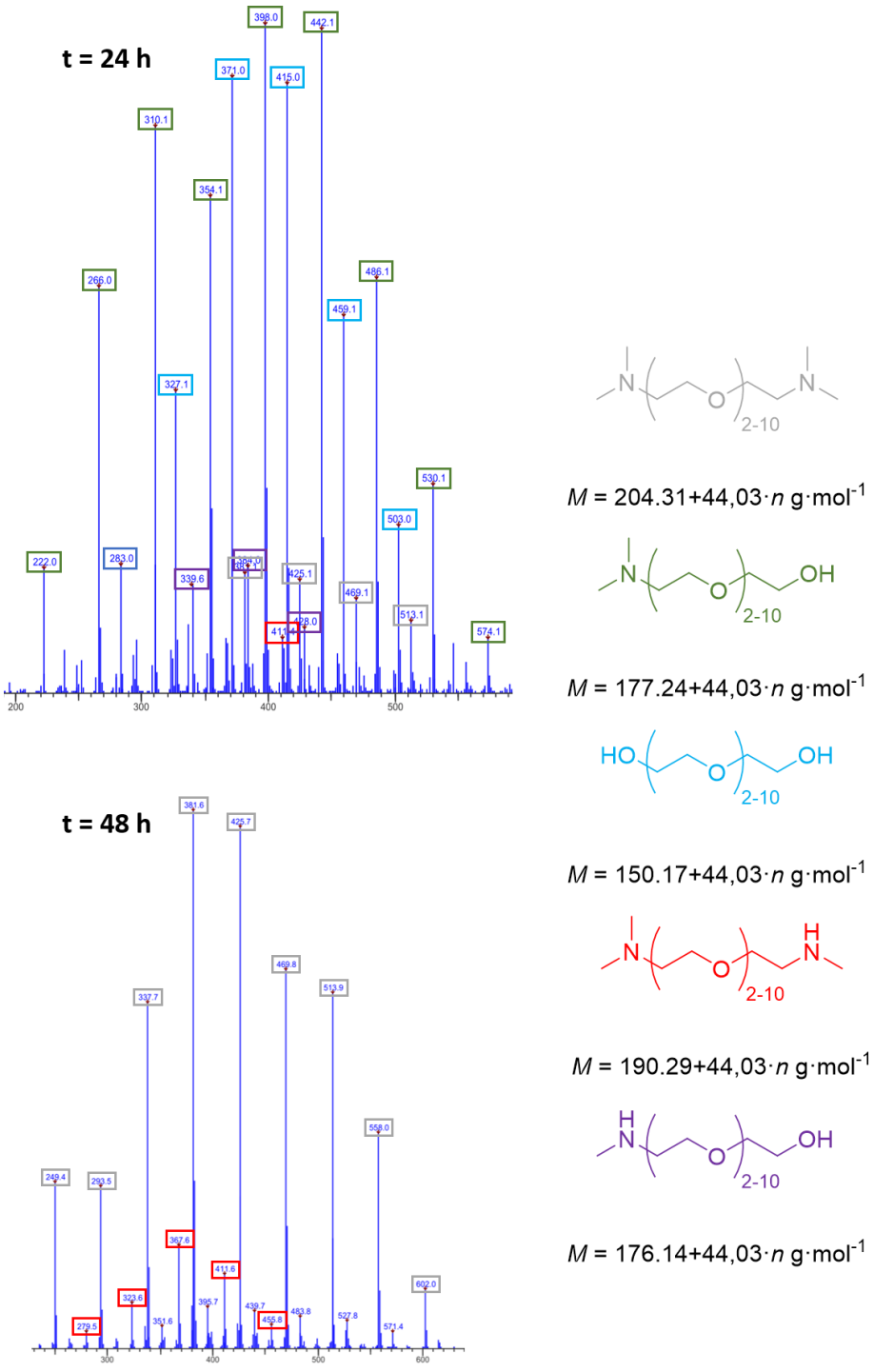

Figure A 4: APCI spectra of the purificated product mixture after 24 h (top) and 48 h (bottom) for the alcohol amination of PEG_{300} using dimethylcarbamate as amination agent. Representative excerpts of the mass distribution for the product mixtures are shown.

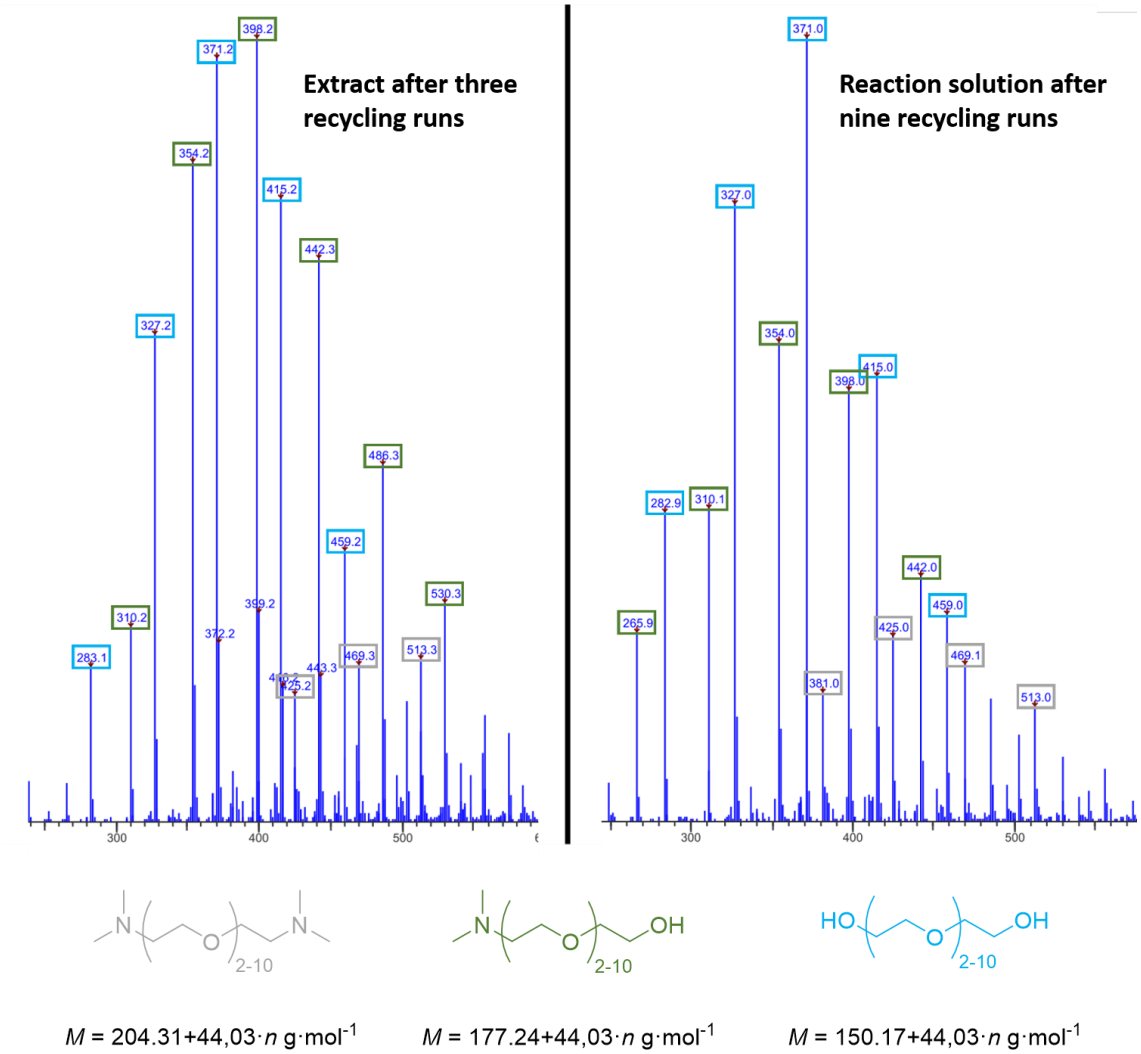

Figure A 5: APCI spectra of the extracted solution after the third recycling run (left) and the catalyst solution after nine recycling runs (right) measured during recycling experiments using a PEG_{300}-amine mixture.

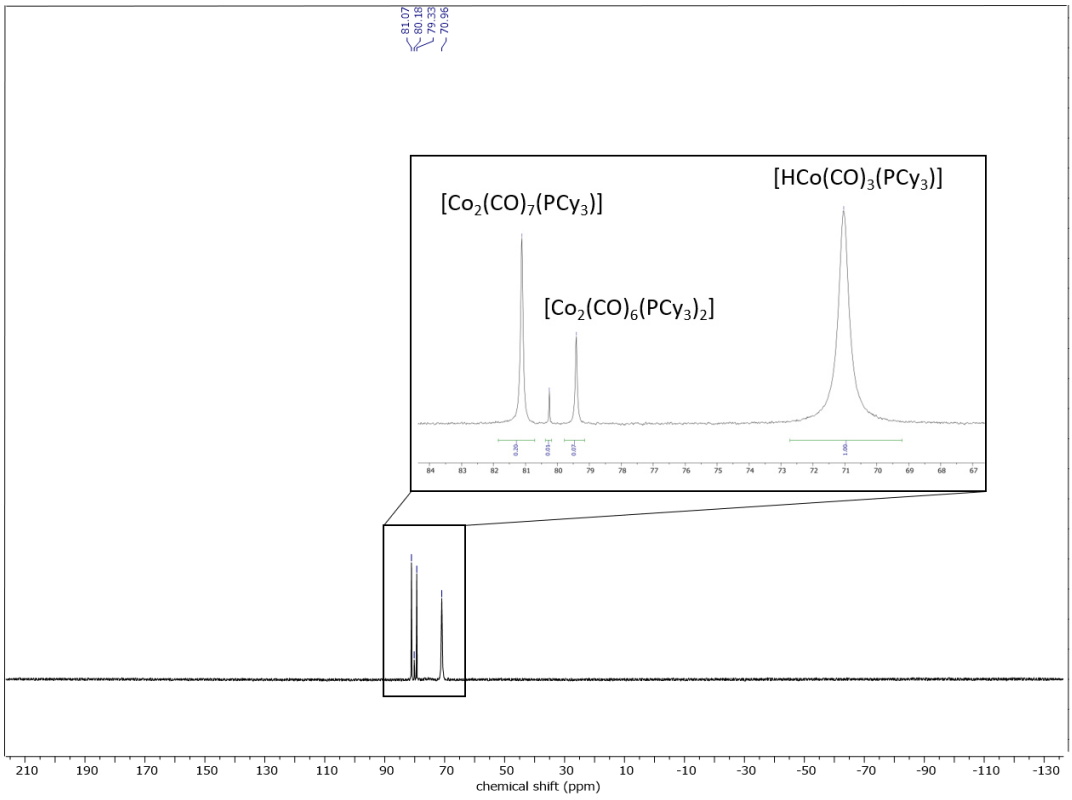

Figure A 6: Full ^{31}P-NMR (202 MHz, $CDCl_3$, room temperature) spectrum of a post reaction solution after the reductive hydroformylation of 1-octene using a homogeneous $[Co_2(CO)_8]/PCy_3$ catalyst. Reaction conditions: **Reaction conditions**: 1-Octene (9 mmol), $[Co_2CO_8]$, PCy_3 (1,5 mol%, M:L = 1:1), *n*-hexane (1.8 g), CO/H_2 (120 bar, 1:2), 195 °C, 3 h, 700 rpm.

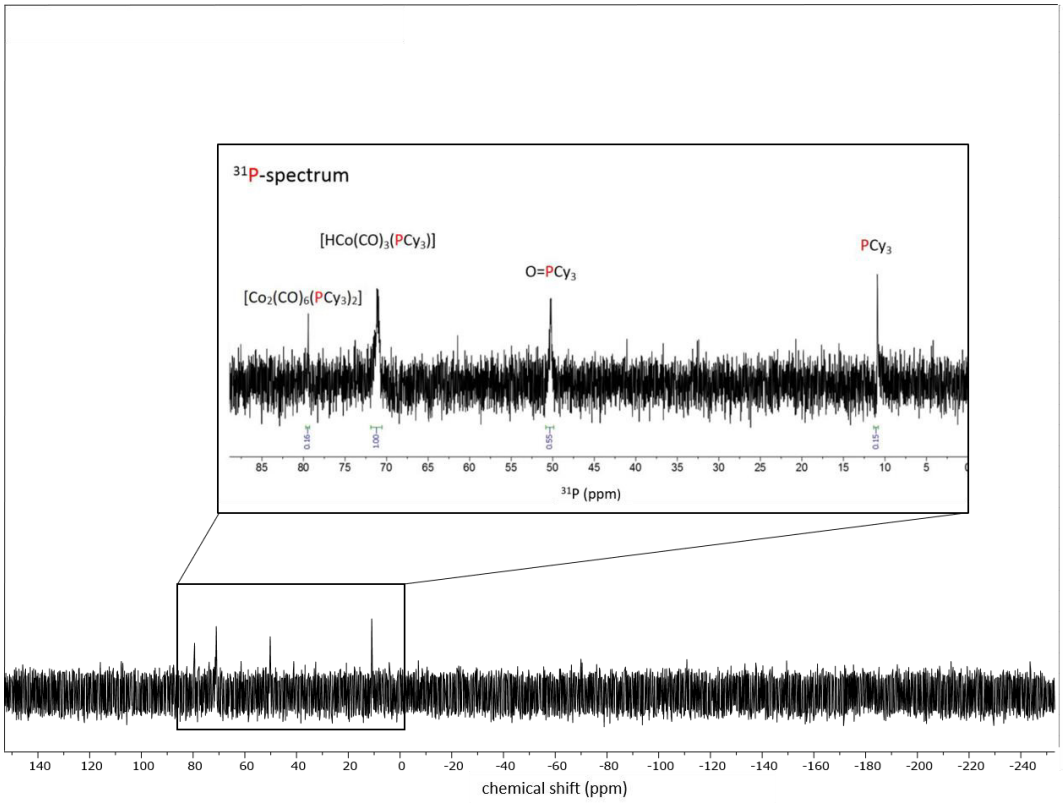

Figure A 7: ^{31}P-NMR (202 MHz, $CDCl_3$, room temperature) spectrum of the post reaction catalyst solution in the combined Fischer-Tropsch/hydroformylation approach proving the presence of catalytically hydride species in solution. Oxygenated tricyclohexylphosphine likely originates from oxygen exposition during handling of the NMR-tube. **Reaction conditions:** NaPr-CoRu@AOmM 40 mg, $Co_2(CO)_8$ 12 mg, PCy_3 20 mg, *iso*-hexane 0.9 g, 195 °C, $CO:H_2$ 1:1, 120 bar (at RT), 24 h, 700 rpm.

11 Eidesstaatiche Erklärung

Ich Thorsten Rösler

erklärt hiermit, dass diese Dissertation und die darin dargelegten Inhalte die eigenen sind und selbstständig, als Ergebnis der eigenen originären Forschung, generiert wurden.

Hiermit erkläre ich an Eides statt

1. Diese Arbeit wurde vollständig oder größtenteils in der Phase als Doktorand dieser Fakultät und Universität angefertigt;
2. Sofern irgendein Bestandteil dieser Dissertation zuvor für einen akademischen Abschluss oder eine andere Qualifikation an dieser oder einer anderen Institution verwendet wurde, wurde dies klar angezeigt;
3. Wenn immer andere eigene- oder Veröffentlichungen Dritter herangezogen wurden, wurden diese klar benannt:
4. Wenn aus anderen eigenen- oder Veröffentlichungen Dritter zitiert wurde, wurde stets die Quelle hierfür angegeben. Diese Dissertation ist vollständig meine eigene Arbeit, mit der Ausnahme solcher Zitate:
5. Alle wesentlichen Quellen von Unterstützung wurden benannt;
6. Wenn immer ein Teil dieser Dissertation auf der Zusammenarbeit mit anderen basiert, wurde von mir klar gekennzeichnet, was von anderen und was von mir selbst erarbeitet wurde;
7. Ein Teil oder Teile dieser Arbeit wurden zuvor veröffentlicht und zwar in:

Rösler, T.; Ehmann, K. R.; Köhnke, K.; Leutzsch, M.; Wessel, N.; Vorholt, A. J.; Leitner, W. Reductive Hydroformylation with a Selective and Highly Active Rhodium Amine System. *J. Catal.* **2021**, *400*, 234–243.

Rösler, T.; Betting, J.; Püschel, S.; Vorholt, A. J.; Leitner, W. Solvent Design for Catalyst Recycling of Rhodium/Amine Catalysts via $scCO_2$ Extraction in the Reductive Hydroformylation of Alpha Olefins. *Green Chem.*, **2022**, 24 (17), 6578–6588.

Jeske, K.; Rösler, T.; Belleflamme, M.; Rodenas, T.; Fischer, N.; Claeys, M.; Leitner, W.; Vorholt, A. J.; Prieto, G. Direct Conversion of Syngas to Higher Alcohols via Tandem Integration of Fischer–Tropsch Synthesis and Reductive Hydroformylation. *Angew. Chemie Int. Ed.*, **2022**, *61* (31).